D-228

MEGAWATT SOLAR POWER SYSTEMS FOR LUNAR SURFACE OPERATIONS

FINAL REPORT

Space Systems Design, AA420/421
NASA/USRA University Advanced Design Program

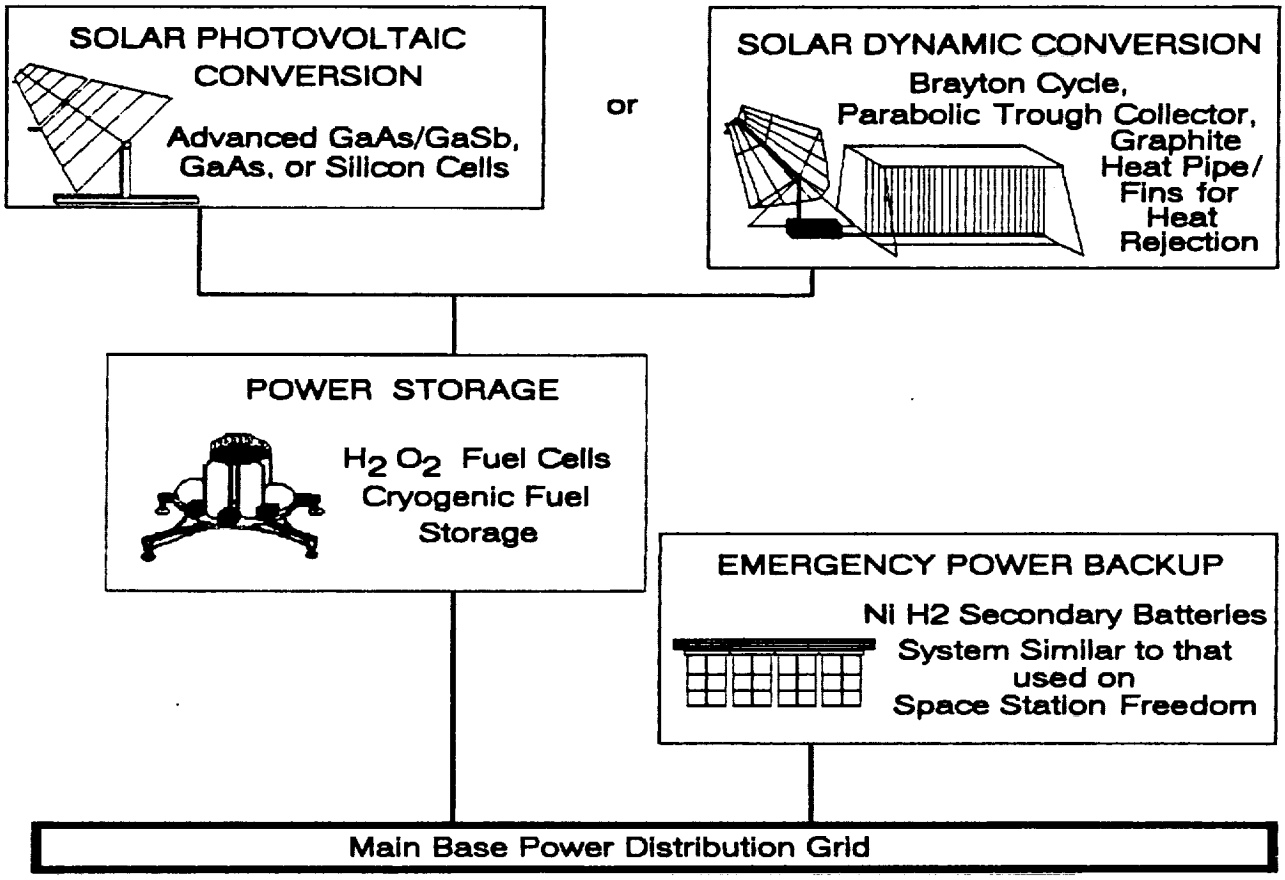

Department of Aeronautics and Astronautics
University of Washington
Seattle, Washington 98195

June 21, 1990

MEGAWATT SOLAR POWER SYSTEMS FOR LUNAR SURFACE OPERATIONS

FINAL REPORT

Space Systems Design, AA420/421
NASA/USRA University Advanced Design Program

Prepared By

Brian Adams
Sam Alhadeff
Shawn Beard
David Carlile
David Cook
Craig Douglas
Don Garcia
David Gillespie
Raymond Golingo
Drew Gonzalez
Peter Gurevich
Christine Hansen
Wendy Hopkins
John Iacometti
Matt Jardin
Tad Lipscomb
Stan Love
Thomas Montague
John Nelson
Darren Ritter

Faculty Advisors

Adam P. Bruckner

Abraham Hertzberg

Department of Aeronautics and Astronautics
University of Washington
Seattle, Washington 98195

June 21, 1990

ABSTRACT

Lunar surface operations require habitation, transportation, life support, scientific, and manufacturing systems, all of which require some form of power. Nuclear thermal power is often considered to be the only type of power system which can provide a lunar base with power on the megawatt level, but political and technological obstacles may severely limit the application of nuclear power in space. As an alternative to nuclear power, this report focuses on the development of a modular one megawatt solar power system, examining both photovoltaic and dynamic cycle conversion methods, along with energy storage, heat rejection, and power backup subsystems.

For photovoltaic power conversion, two systems are examined. First, a substantial increase in photovoltaic conversion efficiency is realized with the use of new GaAs/GaSb tandem photovoltaic cells, offering an impressive overall array efficiency of 23.5%. Since these new cells are still in the experimental phase of development, a currently available GaAs cell providing 18% efficiency is examined as an alternate to the experimental cells. Both Brayton and Stirling cycles, powered by linear parabolic solar concentrators, are examined for dynamic cycle power conversion. The Brayton cycle is studied in depth since it is already well developed and can provide high power levels fairly efficiently in a compact, low mass system. The dynamic conversion system requires large scale waste heat rejection capability. To provide this heat rejection, a comparison is made between a heat pipe/radiative fin system using advanced composites, and a potentially less massive liquid droplet radiator system. To supply power through the lunar night, both a low temperature alkaline fuel cell system and an experimental high temperature monolithic solid-oxide fuel cell system are considered. The reactants for the fuel cells are stored cryogenically in order to avoid the high tankage mass required by conventional gaseous storage. In addition, it is proposed that the propellant tanks from a spent, prototype lunar excursion vehicle be used for this purpose, therefore resulting in

a significant overall reduction in effective storage system mass. Emergency backup power is supplied by a nickel-hydrogen battery system derived from the energy storage system to be used on Space Station Freedom, in order to save on development costs and to provide one of the most reliable systems available. Structural elements for the entire power system are made of composites and aluminum, keeping system mass to a minimum. All components of the system are designed for transport to low Earth orbit in modular units aboard the Shuttle-C launch vehicle.

PREFACE

The Department of Aeronautics and Astronautics at the University of Washington has been a participant in the NASA/USRA Advanced Design Program since its inception in January 1985. Our instructional program in space systems design developed from ongoing activities in space engineering, particularly as related to space power and propulsion. From the beginning, student participation in this program has been integrated as much as possible with our faculty's NASA-funded research in these areas. The student response has been excellent and the synergism with our research program has proven highly beneficial to both the teaching and the research.

The structure of our space design course is aimed at exposing the students to a design situation which is "real world" as much as possible within the University framework. In addition, the course undertakes the responsibility of teaching the students those aspects of space engineering and science which are needed for a general capability in the field of space systems. Students are taught the fundamentals of reentry physics, nuclear and solar power systems, space structures and thermal management, as well as selected topics on advanced propulsion systems and orbital mechanics. The design problems are selected to expose the students to situations in which they must understand the complete systems dependence of structural components, thermal components, and environmental constraints particular to space.

The current course offering consists of two 10-week academic quarters (Winter and Spring). The Winter Quarter course has a typical enrollment of 35-45 students and is initially structured as a formal lecture/discussion series which meets 5 hrs/week. Lectures by the instructors and presentations by guest lecturers from industry and NASA provide the students with the fundamental background they need to carry out their design studies. By the second week of the quarter, the students are divided into design teams whose responsibility is to address specific subsystems of the overall design. As the design progresses, more and more

time is devoted to in-class discussions of the students' work. A teaching assistant supported by the NASA/USRA funds works with the students and helps the instructors with project management. The results of the design study are presented at the end of the quarter in the form of formal written reports, one by each of the design groups.

The Spring Quarter offering is intended to refine and advance the design developed during the Winter Quarter and to address key unresolved problem areas. Participation in this class has been elective; typically, those students who sign up for this offering are usually the most capable and motivated students in the department. The class meets formally three hours a week in group discussion format. Early in the quarter the students are encouraged to submit papers on their projects to the AIAA Region VI Student Conference. Since the inception of the NASA/USRA program our students have garnered several awards in the undergraduate division of that competition. At the end of the Spring Quarter the students submit a single final report on the overall design to NASA and USRA, and make an oral presentation at the annual NASA/USRA Advanced Design Program Summer Conference. The results of the design study are typically also submitted as papers to professional meetings or archival journals.

Although the work load is very heavy for this program, the students are virtually unanimous in agreeing that it provides them with a quality introduction to the world of design. A general competitive atmosphere is maintained wherever possible, as an additional simulation of the real world. The feedback from the students also has proved effective in stimulating the instructors. In addition, the basic research program carried out by the University has benefitted by the recognition of the practical problems of design as they reflect back through the program.

Under the NASA/USRA program our students have examined various problems relating to the critical needs of space prime power and propulsion. For example, in 1985 the problem of providing space prime power for the post-space station era was explored, and a unique solar dynamic power module capable of powering either roving or orbital space factories was designed. In 1986 the design of a multimegawatt nuclear space power system for lunar base applications was undertaken. In 1987 and 1988 an engineering design study of a

mass launcher system based on the ram accelerator concept developed at the University was carried out. The design topic chosen for the 1988-89 academic year was advanced solar propulsion of a cargo-carrying spacecraft to Mars in support of a manned mission to that planet. Beginning with the 1986 project, each of the design studies enumerated above has been presented at professional society meetings and/or published in archival journals.

The design study selected for the current academic year - a megawatt level solar power system for lunar surface operations - was motivated by the need to explore alternatives to nuclear power for the initial phases of a lunar base of the type being envisioned under the lunar/Mars initiative by NASA. Both photovoltaic (advanced and state of the art) and dynamic power systems were considered. The students have responded to the design challenges with enthusiasm and creativity, and have paved the way for follow-up studies of the concepts presented here.

A.P Bruckner
Research Professor

A. Hertzberg
Professor

June 21, 1990

ACKNOWLEDGEMENTS

This year's AA420/421 design team could not have completed this report without the advice and guidance of some very helpful persons. First of all, we would like to thank our professors, Adam Bruckner and Abraham Hertzberg, whose vast libraries of personal knowledge were always available for us to draw upon. Special thanks goes to Professor Hertzberg and Northlake Tavern for supplying the pizza for the final exam, but that's another story. Professor Tom Mattick, also from the University of Washington Department of Aeronautics, was a great help in the design of the thermal management systems for this report.

As for helpful information from industry professionals, the solar photovoltaic cells group would like to begin by thanking Lou Fraas of the Boeing Corporation for developing the new highly efficient tandem cells used in this report, and for making a special trip to the University of Washington to present his developments. Information regarding the cover slides and concentrating lenses for the Boeing cells was generously provided by M. O'Neill of Entech, Inc. Additionally, M. Kruer of TRW supplied the necessary information on the GaAs cells which were examined as a state-of-the-art comparison to the Boeing cells.

From the NASA Lewis Research Center, Lisa Kohout and Pat O'Donnell were of great assistance for their information on current fuel cell systems and cryogenic reactant storage, and deserve our thanks. Mike Zernic, also from NASA Lewis, generously supplied reports on the Space Station Freedom power system, from which information was used in the design of the emergency lunar power backup subsystem presented in this report.

International thanks goes to the Shimizu Corporation in Tokyo, Japan, for providing information on their innovative lunar concrete forming methods. We hope to hear more about lunar concrete developments in the future.

The class would especially like to thank Dave Carlile, John Iacometti, and, Matt Jardin for their post-graduation effort in compiling the summary report, and in preparing and presenting the final report at the 1990 NASA/USRA Summer Conference in Cleveland,

Ohio. Extra special thanks go to the chief editors, Dave Carlile and Matt Jardin for just being swell guys , and for compiling this final report. Terri Schmitt, the class teaching assistant, should also be thanked for her help throughout the project design.

Finally, the entire AA420/421 class extends their gratitude to NASA/USRA for the support, funding, and resources necessary for the existence of this program. Without them, this report could not have been possible.

TABLE OF CONTENTS

SECTION 4: WASTE HEAT RADIATORS

SECTION 5: ENERGY STORAGE

SECTION 6: POWER TRANSMISSION AND CONDITIONING

SECTION 7: STRUCTURAL DESIGNS

SECTION 8: EMERGENCY BACKUP POWER SYSTEM

1.0 INTRODUCTION

David Carlile
Matt Jardin

Plans for a permanent lunar base and subsequent lunar development will require a large power system to support all of the planned activities. Nuclear energy has usually been the assumed power source due to the relatively high power densities offered, yet nuclear power is far from ideal. There are many problems, including the startup of the plant, the large amounts of radiation produced and the need for a large area set aside permanently as a result, and the impossibility of maintenance. The Space Systems Design Course at the University of Washington has, therefore, performed this design study on the harnessing of solar power for use on the Moon as a cleaner, safer alternative to nuclear power.

Initially, the class researched some less traditional ideas for supplying power to the Moon. Placing a large power generating station at one of the Moon's poles was one of the seemingly more promising ideas because it offered the possibility of continuous solar power generation, since areas of the lunar poles are always in sunlight. Solar power generating satellites were another consideration, for a series of satellites placed in well selected orbits could also supply continuous power to the lunar surface. Although these, and other ideas initially looked promising, the transmission of the power to places on the lunar surface where the power would be used proved to be a major operational problem. Since most lunar bases will likely lie near the lunar equator, transmitting power from the poles makes such a power system quite inefficient. Microwave relay towers, orbiting relay satellites, long transmission lines, and even physical transport of charged fuel cells were looked into for the polar power station, but all required a large infrastructure, and were incredibly costly in terms of initial mass. Ideally, many of the systems could be built using lunar materials, but this would require a well developed lunar infrastructure as well, and to create the infrastructure would require some less ambitious power system to be available first. The same problems exist for the power generating satellites since a large power system would necessarily have to be in place before the

main system could be built. For these reasons, power systems were examined which could be used immediately upon the resumption of manned missions to the Moon, and which could be used to create the lunar infrastructure. After this has happened, then some of the more ambitious power generation schemes may become sufficiently attractive to be re-examined.

This report considers two basic methods of converting solar energy into electrical power, with the objective of providing one megawatt of electrical power. The first method is the use of direct electrical conversion of solar energy using a new, highly efficient solar cell developed by the Boeing Corporation. The second method is the use of a dynamic cycle operating on energy supplied by a solar concentrator system. The Brayton cycle was chosen for this study for its relatively high efficiency and its availability in the time frame of the lunar base as a proven and reliable unit. This cycle requires an extensive heat rejection capability provided by one of two systems examined in this study: an advanced technology heat pipe radiator or a liquid droplet radiator.

Of course, neither of these power sources will provide power during the lunar night and thus energy is stored using a fuel cell system. Fuel cells similar to those used on the Space Shuttle, along with cryogenic hydrogen and oxygen stored in the tanks of a spent lunar lander, are employed as the energy storage system. Energy storage is relatively massive, so in order to keep the overall mass of the lunar power system from becoming excessively large, the nighttime energy storage system is designed to provide just 50 kW rather than a full megawatt. This nighttime power reduction may be compensated for by adding more daytime power generating units which are far less massive.

The entire power system is designed to be modular, configured in such a way that no single point failures are possible. In the rare event of catastrophic failure, however, emergency power for repair and evacuation procedures is provided. For development, cost, and reliability reasons, the energy storage system from the Space Station Freedom was reconfigured to provide the required emergency backup power.

2.0 PHOTOVOLTAIC ARRAY

Chris Hanson
Wendi Hopkins
Peter Gurevich

2.1 INTRODUCTION

This chapter outlines the design for a solar array capable of producing 1.0 MW_e of electricity for use during the lunar day, with enough additional capacity to charge a storage facility which provides 50 kW_e during the night. This array will operate at full capacity during the 336-hour lunar day, tracking the sun continuously, and will lie dormant during the lunar night while users are supplied from the energy storage facility.

To design an appropriate solar array, the choice of a photovoltaic cell is crucial. Typical cells currently in use for space and terrestrial applications rely heavily on thin, single cells of Silicon (Si) or Gallium Arsenide (GaAs). These cells generally offer an unconcentrated efficiency of 14 to 22% respectively. Boeing Aerospace Company, however, is developing a tandem Gallium Arsenide/Gallium Antimonide(GaSb) cell for space applications, offering a concentrated target cell efficiency of 28% [1].

Two alternative arrays are proposed here. The first uses the Boeing concentrated tandem cell, which has the advantage of high efficiency and therefore reduced array size. This array has a total efficiency of 23.5% at an operating temperature of 80°C when wiring and concentration losses are included. The tandem cell has not yet been completely tested, and thus, is not available in large quantities. The second alternative uses advanced GaAs cells, developed by TRW, with an array efficiency of 18% [2]. This design has the advantage of being fully tested and currently available, however, the lower efficiency results in more cells required to produce the same quantity of power, at increased cost.

The details of an array using the Boeing tandem cell are presented in this chapter. Specifically, the properties of the cell materials, the concentrating lenses, and the housing are

discussed, along with final configuration numbers for the entire array. The TRW cell array is presented as an available alternative, and the benefits of both arrays are compared.

2.2 HIGH EFFICIENCY TANDEM CELL

Current state of the art GaAs cells have obtained efficiencies as high as 22% under ideal conditions, however, these cells cannot absorb solar energy which falls in the infrared region below the band gap of GaAs (1.42 eV) [3]. (The bandgap is the lowest energy photon that will be absorbed and converted to electricity.) Boeing has introduced a two-junction solar cell, designed for satellite applications, which converts more of the energy available in solar radiation to electricity by making use of an infrared sensitive booster cell. By mechanically stacking a GaAs cell on top of a GaSb cell, Boeing has achieved efficiencies of over 31% under ideal air mass zero conditions (AM0: no air or convective gasses). This represents an increase of nearly 8% over previous maximum efficiency cells. Practical cell efficiencies, under non-ideal conditions, of 28% are projected for the near future [1].

Solar arrays can be made more efficient when the sunlight is concentrated. Individual dome lenses mounted on an aluminum honeycomb structure are used to focus sunlight onto the active portion of the cell [3]. The cells are mounted on ceramic printed circuit boards which provide electrical connections from cell to cell and transfer heat to a radiative backing (see Fig. 2.1). To further increase efficiency, cover slides designed by Entech, Inc. deflect light around gridlines thus avoiding losses due to shading by the gridlines. When completely assembled, total array efficiency is 23.5% [1].

2.2.1 TANDEM CELL

Traditional solar cells absorb energy in a limited spectrum. The concept of a tandem cell introduces the usage of two cells of different materials whose absorption spectra

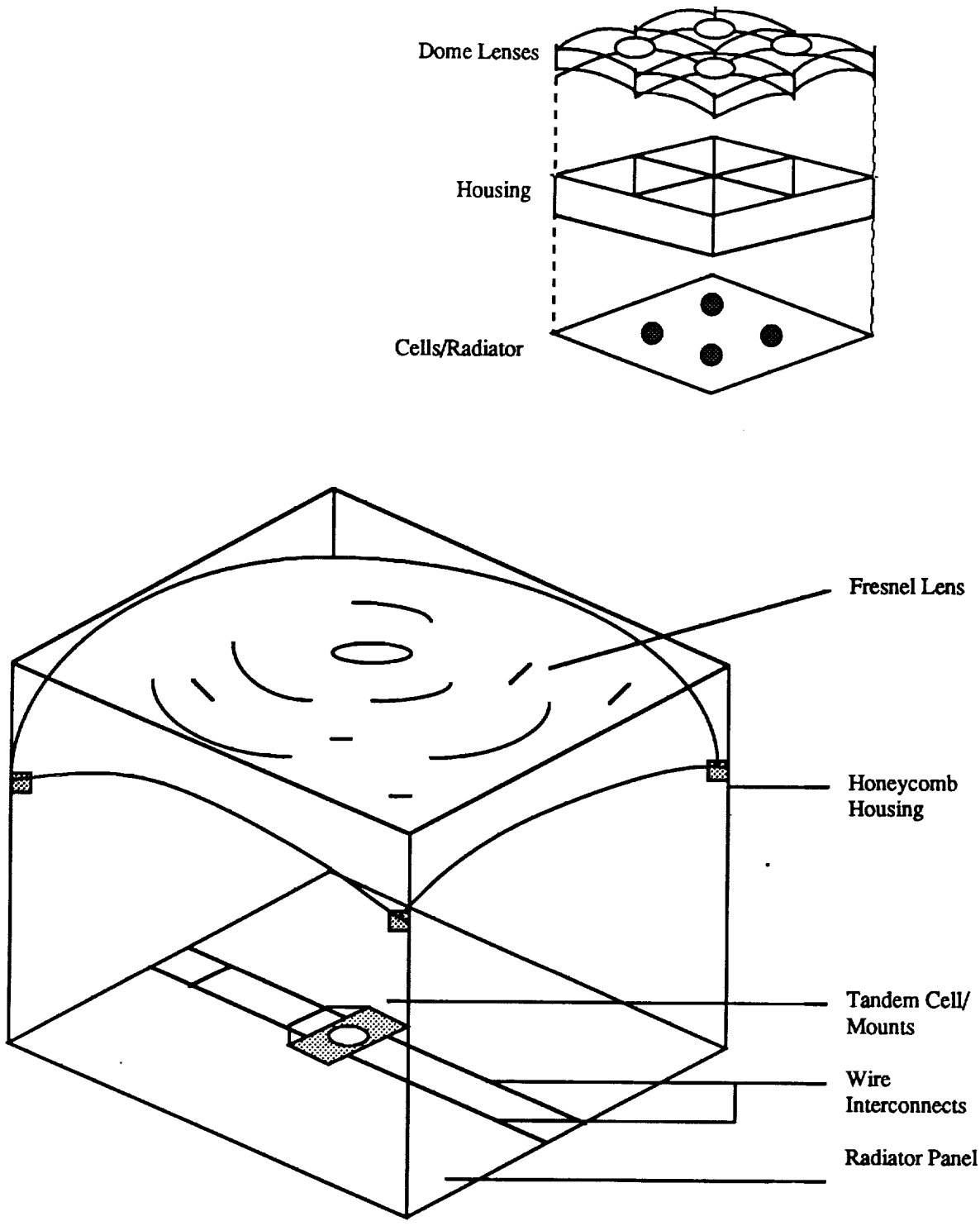

Fig. 2.1. Boeing Cell/Lens Configuration.

complement each other. That is, the two cells are stacked such that the lower cell absorbs light not absorbed by the upper cell.

Two materials must be chosen which exhibit the above properties. To date, GaAs cells are the most energy efficient single junction devices available. The properties of single GaAs cells are shown in Fig. 2.2. Note that the maximum efficiency is 24.1% at 99 suns (AM0) i.e. when the sunlight is concentrated by lenses 99 times. It will be shown later that these cells can be made transparent to infrared radiation. Therefore, a booster cell material must be chosen which absorbs well in the infrared spectrum [4]. GaSb was selected as the infrared sensitive booster cell for the following reasons:

1. GaSb has a bandgap of 0.72 eV, which is significantly lower than that of GaAs, allowing it to absorb a large portion of the spectrum not absorbed by GaAs.
2. GaSb is a direct band gap material (high absorption coefficient) which generates larger currents, and thus higher efficiencies.
3. The voltage produced by each GaSb cell is nearly one-third that of the upper GaAs cell, allowing the two to be wired in a voltage matched configuration.
4. GaSb is a simple, binary compound that is easy to manufacture.

Properties of the single GaSb cell are shown in Fig. 2.2. Note that the maximum efficiency is 8.2% at 84 suns (AM0) [3].

The two cells are mechanically stacked, with the GaAs cell placed above the GaSb cell. In order for light to pass through to the lower cell, the normal solid metal backing on the GaAs cell is replaced by a fine metal grid. The light thus passes through the upper cell, through the grid, and onto the lower cell. Shading effects from this grid can be neglected since the back grid requires fewer lines than the top grid (due to different layer properties within the cell) [3].

To increase the amount of infrared radiation transmitted through the GaAs cell, the wafer thickness is reduced, and the n-type doping density is decreased. In addition, an anti-reflection coating on top of the cell is modified to enhance transparency to wavelengths below the band gap of GaSb. Performance data on the stacked cell are shown in Fig. 2.2. Note that the total tested efficiency is 30.8%. When wired together and arranged inside the housing,

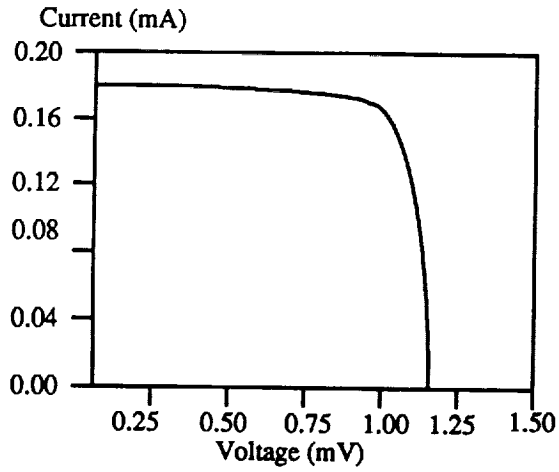

Isolated GaAs Cell Performance

Efficiency..... .24.1%
Concentration.....99 Suns
Volatge Max.....971 mV

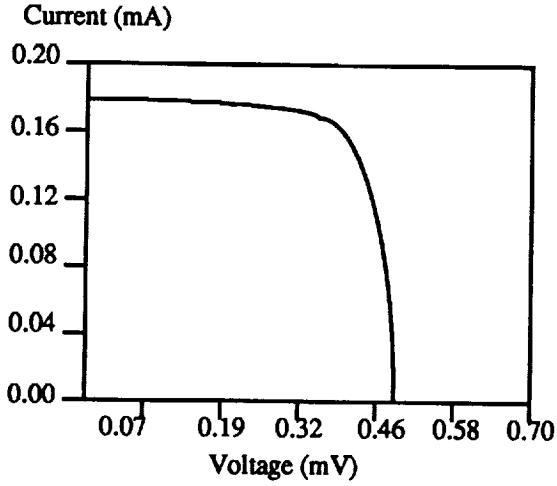

Isolated GaSb Cell Performance

Efficiency.....8.2%
Concentration.....84 Suns
Voltage Max.....380 mV

Stacked Tandem Cell Performance
(Concentration 100 Suns AM0)

	Efficiency (%)	Voltage Max (V)
GaAs	23.9	.987
GaSb	6.9	.367
Total	30.8	-----
Matched Triplet	-----	1.0

Fig. 2.2. Individual and Stacked Cell Performance [4].

losses will occur due to packing density, voltage mismatching, and lens inefficiency, though the target cell efficiency is still 28%, distinctly higher than any single cell efficiency [1].

2.2.2 CELL ASSEMBLY

Transparent GaAs cells are mounted over holes on the front side of a ceramic double-sided printed wiring card, and GaSb cells are mounted on the back side of the same card. As can be seen from Fig. 2.3, cells are first bonded to thin metal disks which have center holes slightly larger than the cell active areas. The metal disks, or heat spreaders, then conduct heat away from the active area of the cell to the back radiating panel. The two cells are interconnected with separate wiring patterns on the front and back of the card, connected through holes at the corners of the card [5].

Because the maximum voltage of a GaAs cell is approximately three times that of a GaSb cell, wiring the cells in a series-parallel arrangement as shown in Fig. 2.3 produces a coordinated one volt triplet. Three GaAs cells are wired in parallel on the top of the circuit board and three GaSb cells are wired in series on the bottom. This triplet forms the smallest voltage unit, and any number of triplets can then be connected in series to obtain the desired voltage [1]. This array will be wired to produce electricity at a relatively low potential of 200 V to reduce the risk of arcing damage.

2.2.3 ENTECH COVER SLIDES

To avoid losses in efficiency caused by reflection off the metal gridlines of both cells, the Boeing cell uses a prismatic cover slide made by Entech, Inc., laid over each semiconductor surface. The cover bends incoming sunlight that might normally hit gridlines toward the active portion of the cell (see Fig. 2.4). Cover slides are used on both upper and lower cells, increasing efficiency by about 10% in each [4].

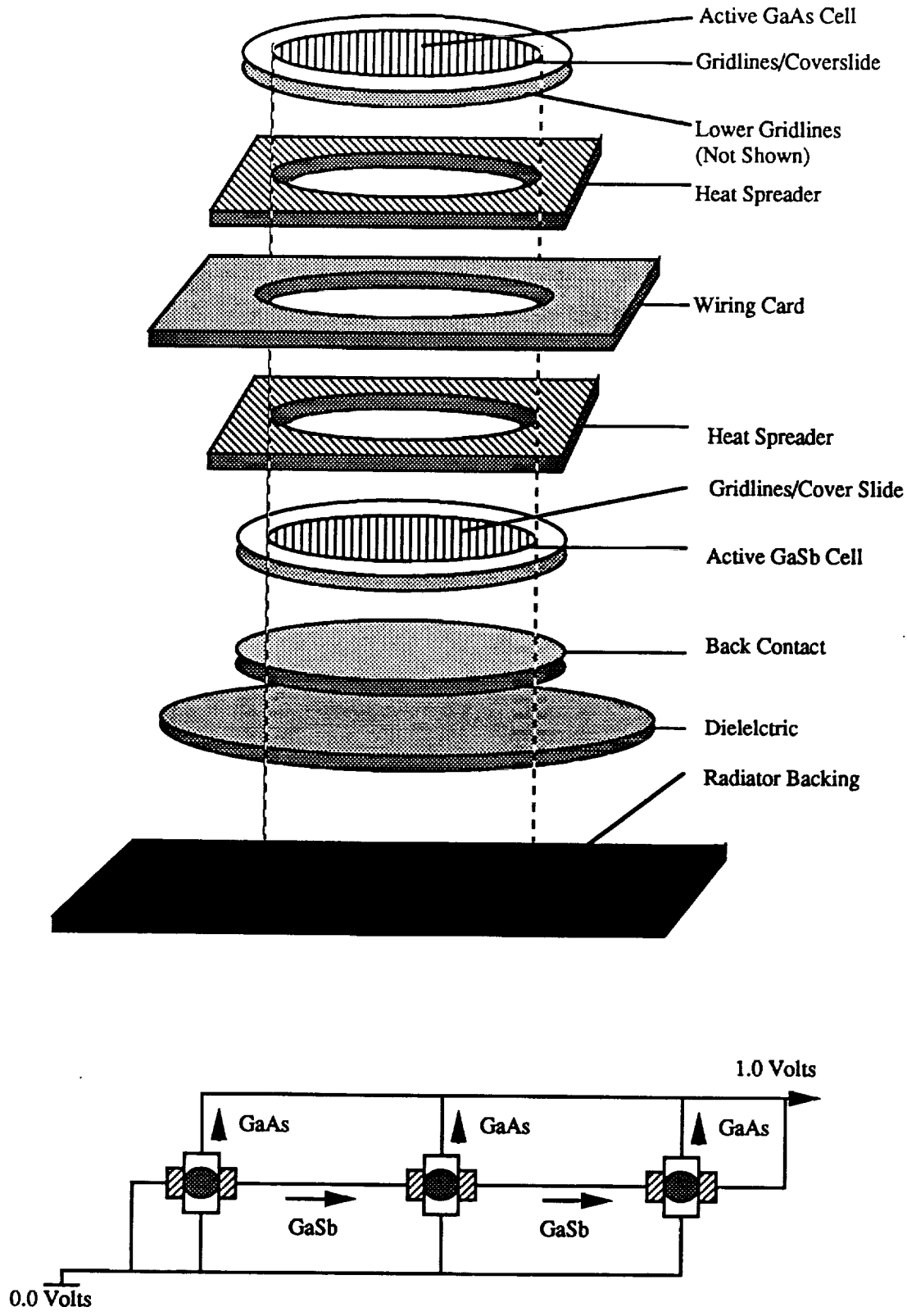

Fig. 2.3. Cell Assembly and Triplet Formation [1].

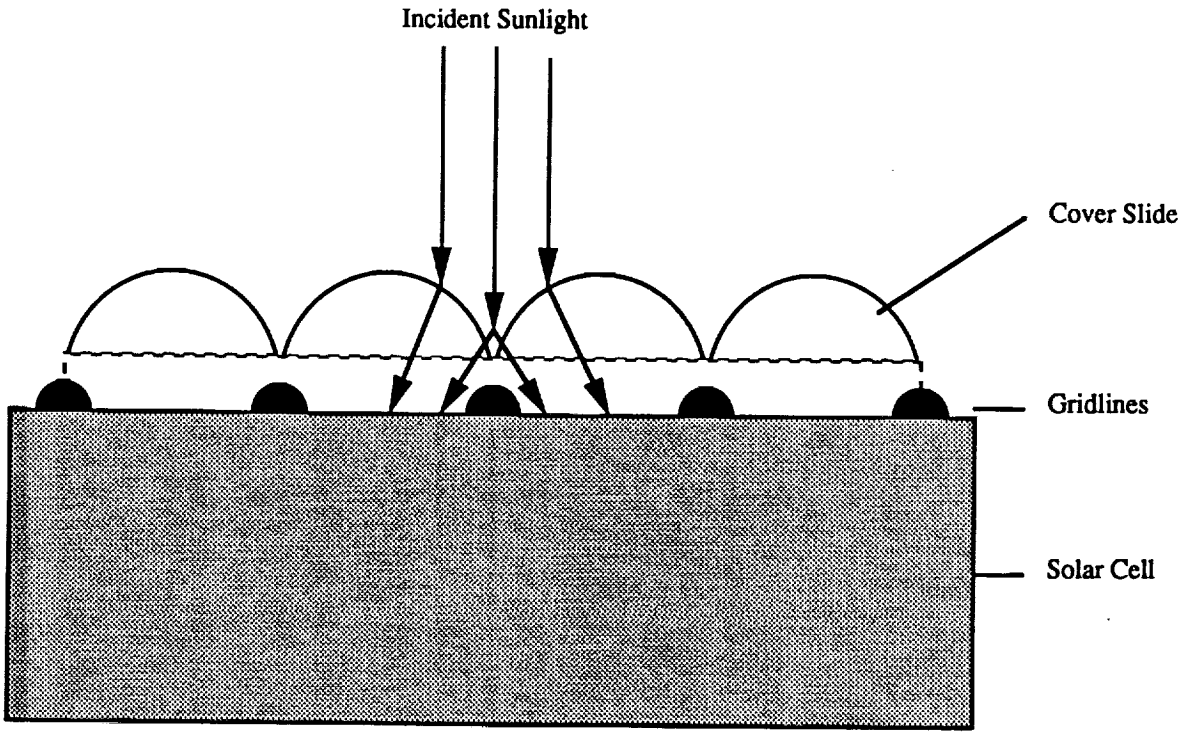

Fig. 2.4. Cover Slide Over Gridlines [3].

2.3 CONCENTRATING LENSES

To increase the efficiency of the tandem cells it is necessary to concentrate incident sunlight through lenses. Domed Fresnel lenses, developed by Entech, Inc., are supported 4.0 cm above the cells and concentrate light to 100 suns, focused on the center of the cell (Fig. 2.1). Prototype lenses have been shown to transmit 90% of incoming sunlight, averaged over all wavelengths [6]. The lenses are supported by a honeycomb structure, and together the lenses and honeycomb comprise 65% of the total panel mass. Masses for all components of the array are given in Table 2.1 below.

Table 2.1: Panel Component Masses [7].

Component	Material	Thickness (mm)	Mass/Area (kg/m^2)	Total Mass %
Lens Superstrate	Microglass	0.15	0.49	20
Lens Prisms	Silicone	0.15	0.19	7.8
Radiator	Aluminum	0.20	0.55	22.5
Cell/Cover/Mount	-----	0.46	0.05	2.0
Honeycomb	Aluminum	0.15	0.91	37.3
Radiator Coating	Alumina	0.01	0.08	3.3
Miscellaneous	-----	-----	0.17	7.0
Total	-----	-----	2.44	100

2.3.1 LENS STRUCTURE

The lens is composed of two layers; a 0.15 mm microglass superstrate, and a 0.15 mm thick Fresnel dome lens made of polymeric silicone. As parallel light strikes the lens, it is refracted through the two layers toward the active area of the cell [3].

The microglass shielding is designed to protect against solar proton flares, so the panels will not require additional protection on the moon. The microglass density is 2.5 g/cm^3, and the ratio of curved surface area to the panel area is 1.3, giving a mass per unit area of 0.49 kg/m^2 [6].

The flexible silicone (aka. rubber silicone) lens is laminated to the underside of the shield, and consists of a 0.1 mm thick base and 0.1 mm high prisms which focus emerging light (see Fig. 2.5). The density of the silicone is 1.0 g/cm^3, and has an effective thickness of 0.15 mm, giving a total mass per unit area of 0.19 kg/m^2. Thus, the total lens mass is 0.68 kg/m^2, or 28% of the total panel mass.

2.3.2 HONEYCOMB SUPPORT STRUCTURE

The rigid dome lenses described above are fitted into an aluminum honeycomb structure designed to hold the lenses in precise alignment above the photovoltaic cells. The lenses focus light onto the center of the active cell, leaving a one-degree margin for lens-placement error or tracking error. This means that any deformation due to transportation or installation must be taken into account.

The honeycomb housing itself has a square cross-section, 3.75 cm on a side, with a 0.15 mm wall thickness (see Fig. 2.6) [1]. The lenses rest inside the housing on four supports extending from the corners and are secured with silicone adhesive. This places the active portion of the cell 4.0 cm away from the top of the lens. The sides of the honeycomb extend 0.5 mm past the top of each lens allowing the panels to be stacked and protecting the lenses from breakage.

Of all the panel components, the aluminum housing contributes the largest mass percentage. At a density of 2.77 g/cm^3 and a surface area to panel area ratio of 2.2, the housing has a mass per unit area of 0.91 kg/m^2, which is 37% of total panel mass [7].

2.4 RADIATOR AND THERMAL CONTROL

During the daytime as the array is illuminated by sunlight it produces electricity with an efficiency of 23.5%, which means a large percentage of incoming energy is converted to heat.

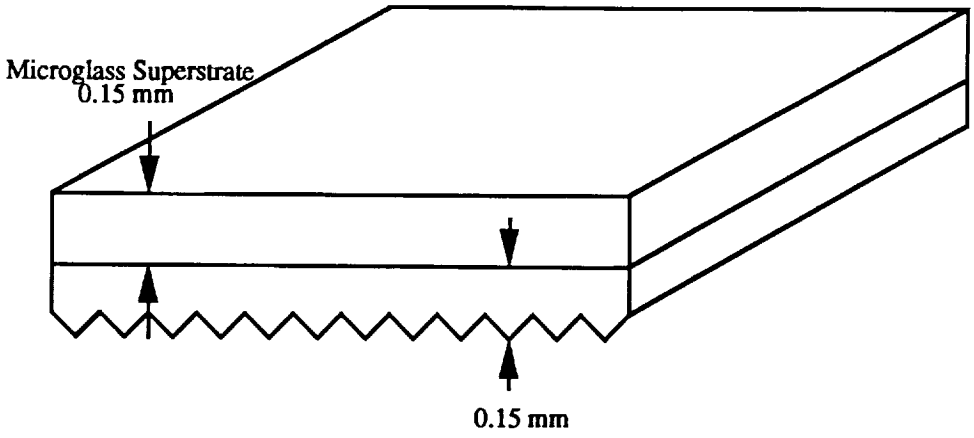

Detail of Lens Structure

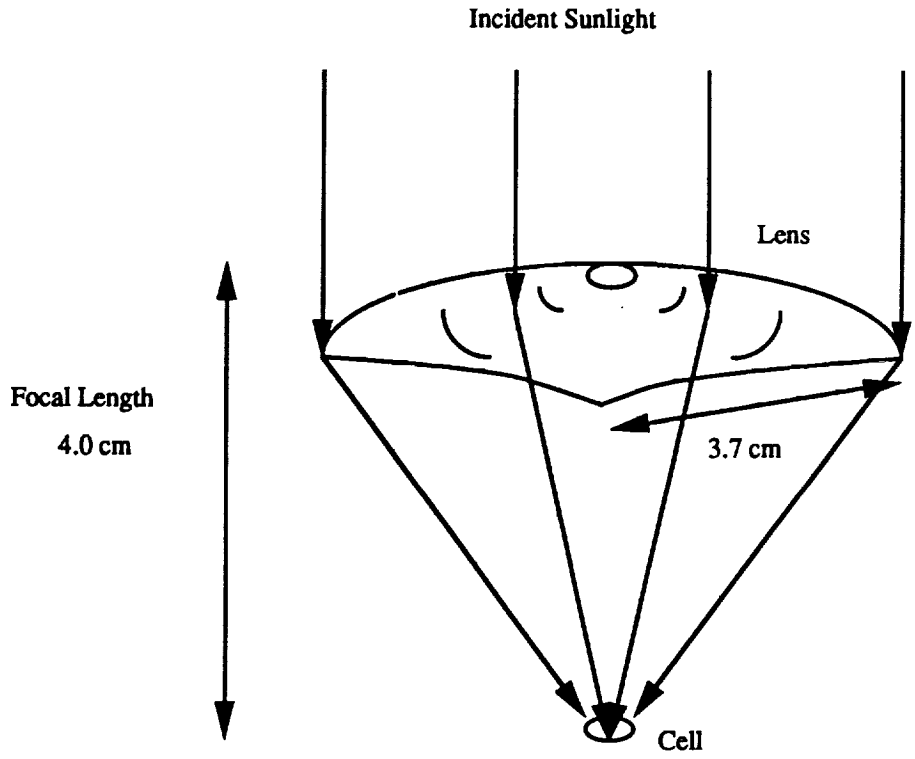

Fig. 2.5. Domed Fresnel Lens [7].

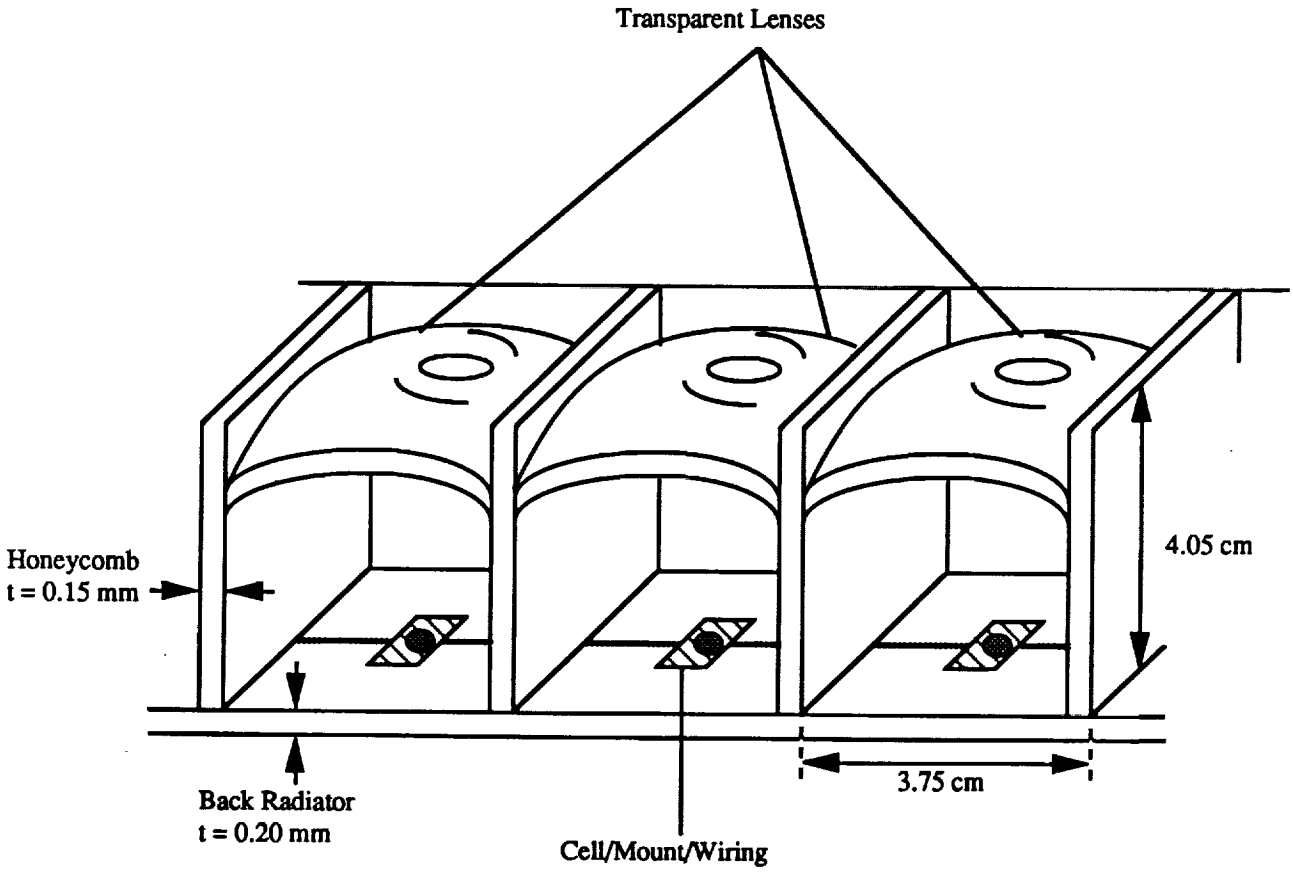

Fig. 2.6. Honeycomb Section Dimensions [7].

Since photovoltaic cells operate more efficiently at lower temperatures, it is desirable to radiate away unused energy to keep the temperature down. Boeing's tandem cell has shown an efficiency of 32% at 25°C, but only 28% at 100°C [6]. Conveniently, the backing, to which the cells and honeycomb are attached, provides a large surface area which is used to reject excess heat.

2.4.1 RADIATOR AND COATING

The radiator backing is simply a 0.2 mm thick aluminum sheet to which the cells and interconnecting wiring are attached. The cells are spaced at 3.75 cm intervals on the backing, underneath the honeycomb structure and lenses. At a density of 2.77 g/cm^3, this gives the radiator a mass per unit area of 0.55 kg/m^2, or 23% of total panel mass [6]. Heat is conducted through the active cell into the heat spreader, and from there to the aluminum backing, which radiates heat to the surroundings.

2.4.2 OPERATING TEMPERATURE

To determine an equilibrium temperature of the solar panels it is first necessary to find the amount of heat rejected by applying an energy balance to the panel. The necessary temperature for heat rejection can then be found through radiation heat transfer analysis. Since the array produces power with 23.5% efficiency, 76.5% of incoming solar radiation must be converted to heat. Efficiency is defined as the percentage of incoming sunlight that is converted to electricity.

The following assumptions are made in the analysis below:

1. Temperature is constant throughout the panel.
2. No heat transfer occurs between the radiator and the supporting structure.
3. Lunar regolith has poor thermal conductivity, therefore the shaded regions of the lunar surface are assumed to be at the nighttime temperature of the moon (116 K), and the illuminated regions are assumed to be at the daytime temperature (390 K).
4. The front of the radiator absorbs nearly all radiation not converted to electricity.

The equilibrium temperature of the panel can be determined from the amount of radiation absorbed by the panel and the amount re-radiated through the front and back surfaces. The back of the radiator is coated with alumina, which has an emissivity of 0.8 between 70 and 100°C, and an absorptivity of 0.5 (mean spectral absorptance over the solar spectrum) [8]. The front of the radiator, on which the housing and cells are mounted, is also coated with alumina, but its emissive area is reduced by 15% due to coverage by the cells and wiring and an additional 5% emissivity is lost due to reflection from the inside of the lens [8]. The radiation absorbed is then all the radiation incident on the front of the panel that is not converted to electricity plus half of the radiation incident on the back of the panel. The former value is 76.5% of the solar constant (1035 W/m^2). The latter value is a function of tilt angle, θ.

As shown in Fig. 2.7, radiation incident on the back of the panel originates from areas 4, 5, and 6. View factors for areas 4, 5, and 6 to area 2 were calculated as a function of θ. Radiation flux to the back of the panel was calculated using these variable view factors, and the night and day surface temperatures of the moon, i.e.,

$$T_e = \left[\frac{Q_i + \alpha_b \left(Q_4(\theta) + Q_5(\theta) + Q_6(\theta) \right)}{\sigma(\varepsilon_f + \varepsilon_b)} \right]^{\frac{1}{4}} \tag{2.1}$$

where T_e is the equilibrium temperature, Q_i is the solar radiation not converted to electricity, $Q_4(\theta)$, $Q_5(\theta)$, and $Q_6(\theta)$ are radiation from areas 4, 5, and 6, σ is the Stefan-Boltzmann constant, and ε_f and ε_b are the emissivities of the front and back of the panel, respectively.

This gives a temperature range between 337 K and 361 K over the entire day and an average operating temperature of approximately 353 K, at which the tandem cell array has an efficiency of 23.5%.

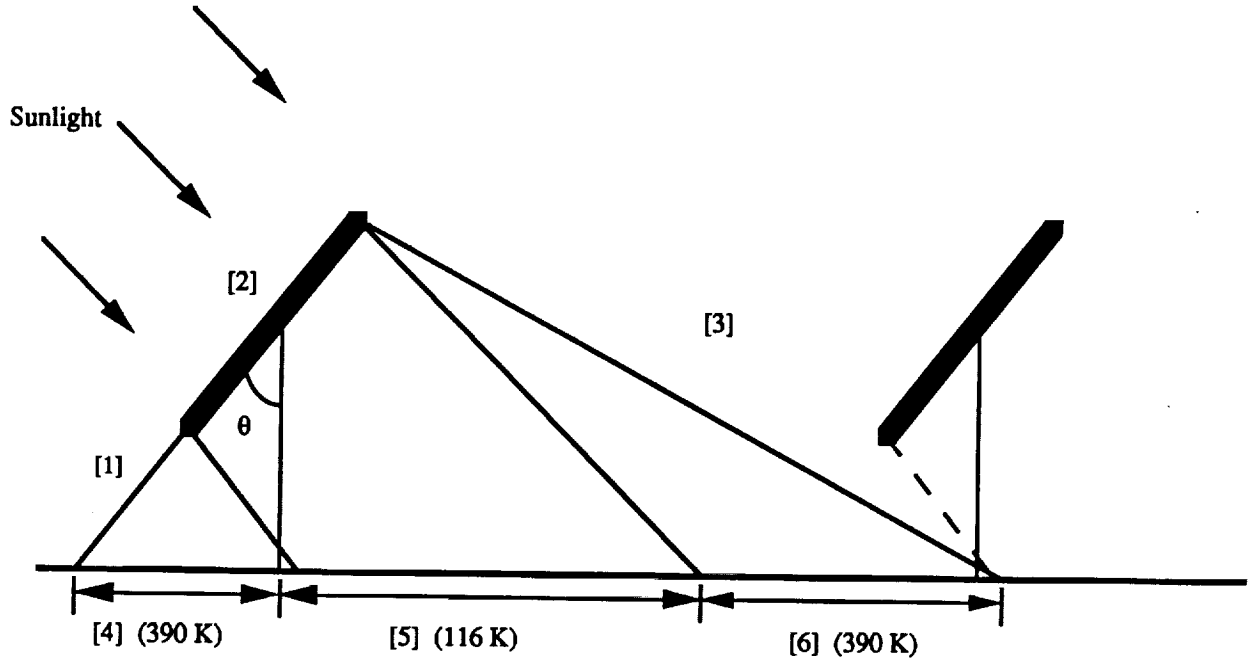

Fig. 2.7. Equilibrium Temperature Diagram.

2.5 ARRAY SIZING AND CONFIGURATION

Total array area is determined by the power requirement, including compensation for all inefficiencies, and by the efficiency of the cells. One megawatt is the baseline design parameter needed for the user during the daytime. Fifty kilowatts will be provided initially during the nighttime through the use of an energy storage unit. Due to subsystem losses shown in Fig. 2.8, the total power required is calculated by dividing the day and night power needed by their respective efficiencies (Eq. 2.2)

$$P_T = \frac{P_D}{\eta_D} + \frac{P_N}{\eta_N} \tag{2.2}$$

where P_T is the total power required from the array, P_D and P_N are the day and night power requirements of the user, and η_D and η_N are the day and night transmission and storage efficiencies. Thus, the total power required from the array is 1.175 MW_e.

Given that incident solar radiation is 1,400 W/m^2 and array efficiency is 23.5%, the total collection area can be determined by

$$A_c = \frac{P_T}{(\eta_A)(S)} \tag{2.3}$$

where A_c is the total collection area, η_A is the array efficiency, and S is the solar constant. This gives a total array area of 3,750 m^2.

2.5.1 PANEL SIZING

Individual panel dimensions are determined by structural limitations and ease of maintenance. For ideal power production, the panels would be wide and long to provide the most exposed area. In the event of a breakdown however, the cells will need to be easily accessible, therefore a width of 3.0 m was chosen to facilitate repair by an astronaut in a spacesuit in lunar gravity. The panels are rotated about a central axis, 1.7 m above the ground,

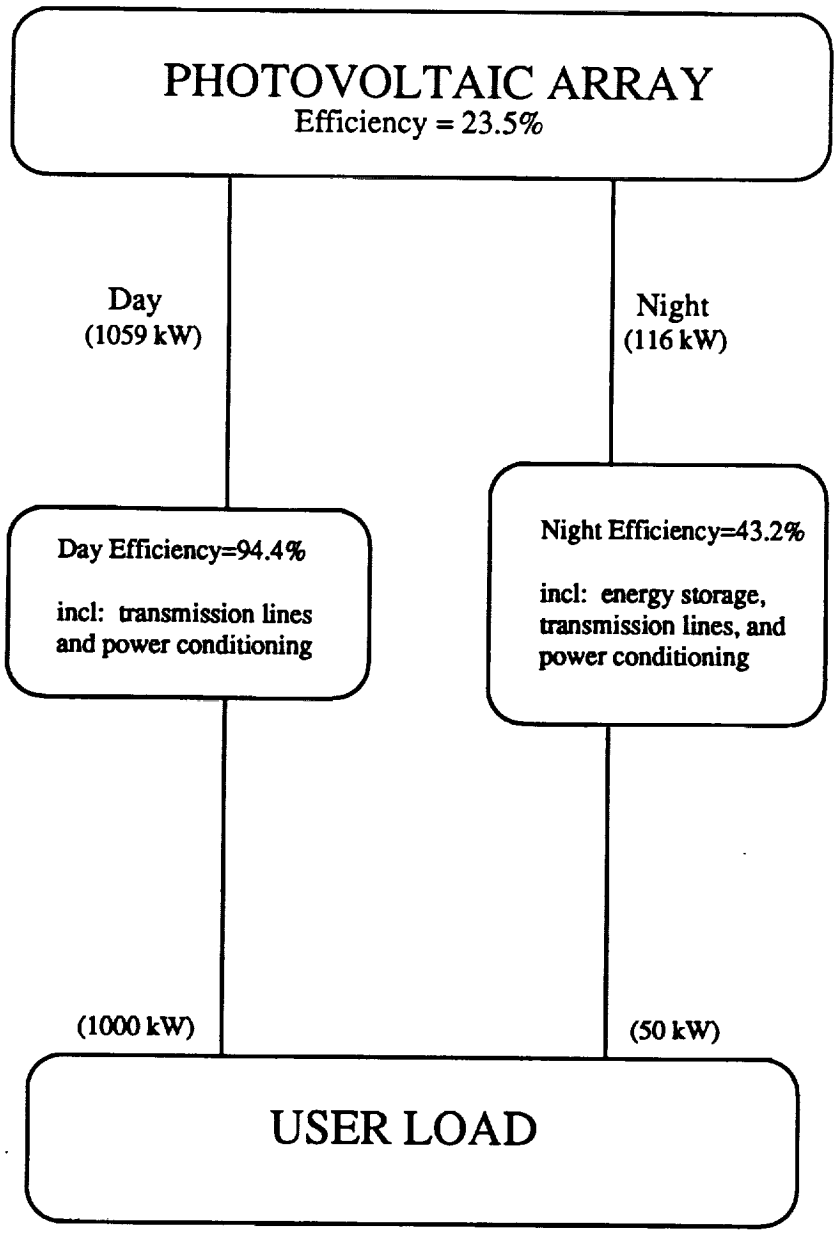

Fig. 2.8. Day and Night Efficiencies for Total Power Calculation. .
(Does not represent actual power paths.)

making each half of the panel accessible with no mechanical assistance. The length, L, of each panel was chosen to be 12.5 m to minimize structural weight (Fig. 2.9).

With panel dimensions defined, the array can be sized and row spacing determined by considering shading effects. The closer the rows are together, the more they shade each other, but excessive spacing would be an impractical use of real-estate and would require longer transmission lines which would add mass.

The loss in system power due to mutual shadowing is calculated assuming that the amount of power produced by a panel is proportional to the area of the panel that is illuminated. The amount of shadowing experienced by an individual panel is a function of the ratio of panel width, W, to the distance between rows, D. The effective shadowing that the system receives will also be a function of the number of rows, N.

In Fig. 2.10, two panels are shown with sunlight radiating from the left. When the sun is at a low angle, a significant portion of the rear panel is shaded. When the sun reaches the critical angle above the horizon, θ_c, shadowing is eliminated. It can be seen that this critical angle is equal to

$$\theta_c = \sin^{-1}\left(\frac{W}{D}\right) \tag{2.4}$$

Before the critical angle has been reached, the area illuminated on the rear panel is

$$A_i = LD\sin\theta \tag{2.5}$$

and the total area illuminated at a given angle for N rows is

$$A = L[W + D(N-1)\sin\theta] \tag{2.6}$$

To shorten the time that the energy storage facility must provide power, it is desirable to arrange the panels such that there are many sets per row, with few rows. This gives the greatest frontal area to be illuminated as soon as the sun rises. Since 50 panel sets are required

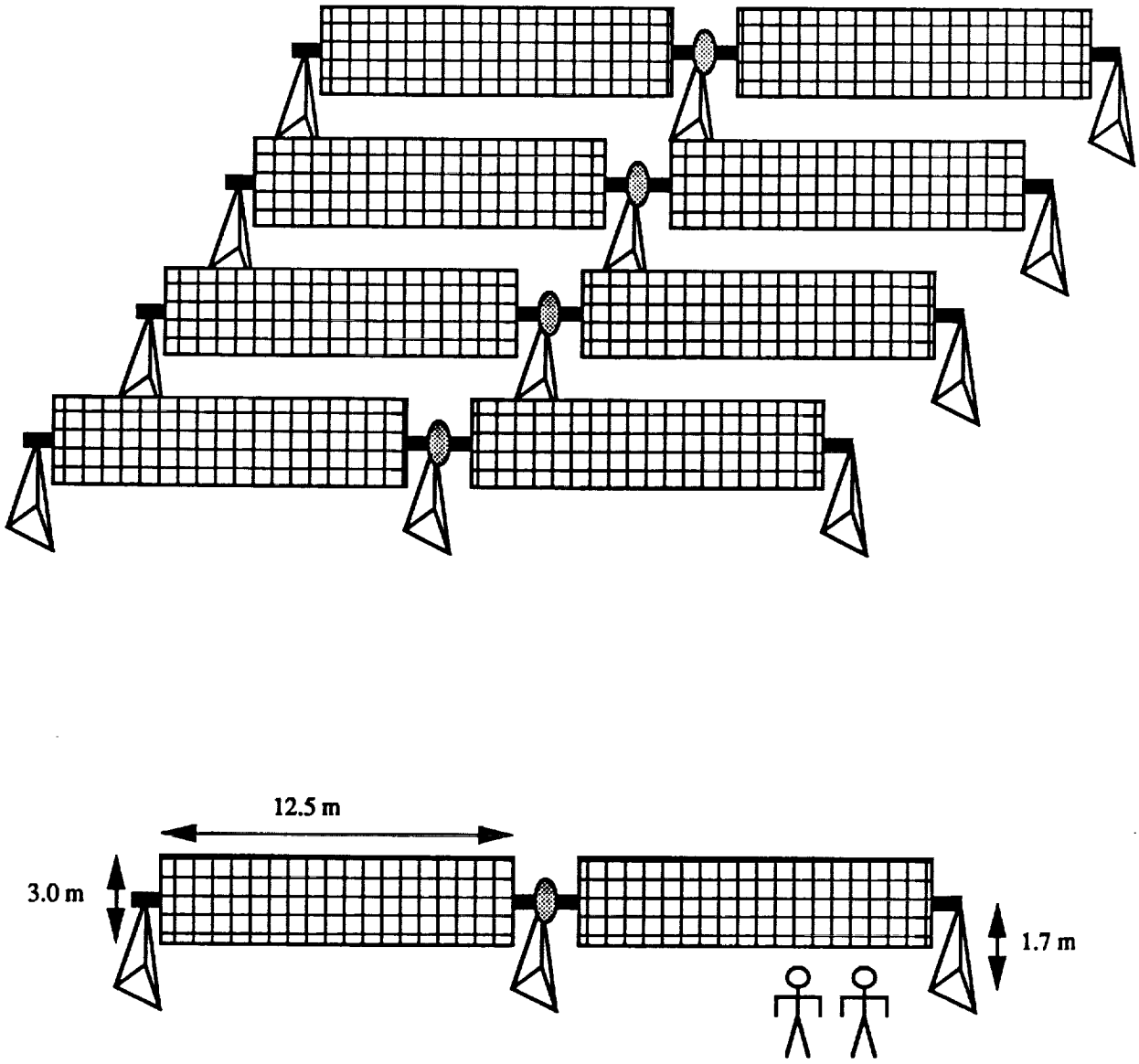

Fig. 2.9. Panel Set Dimensions.
(Structural Elements Represented)

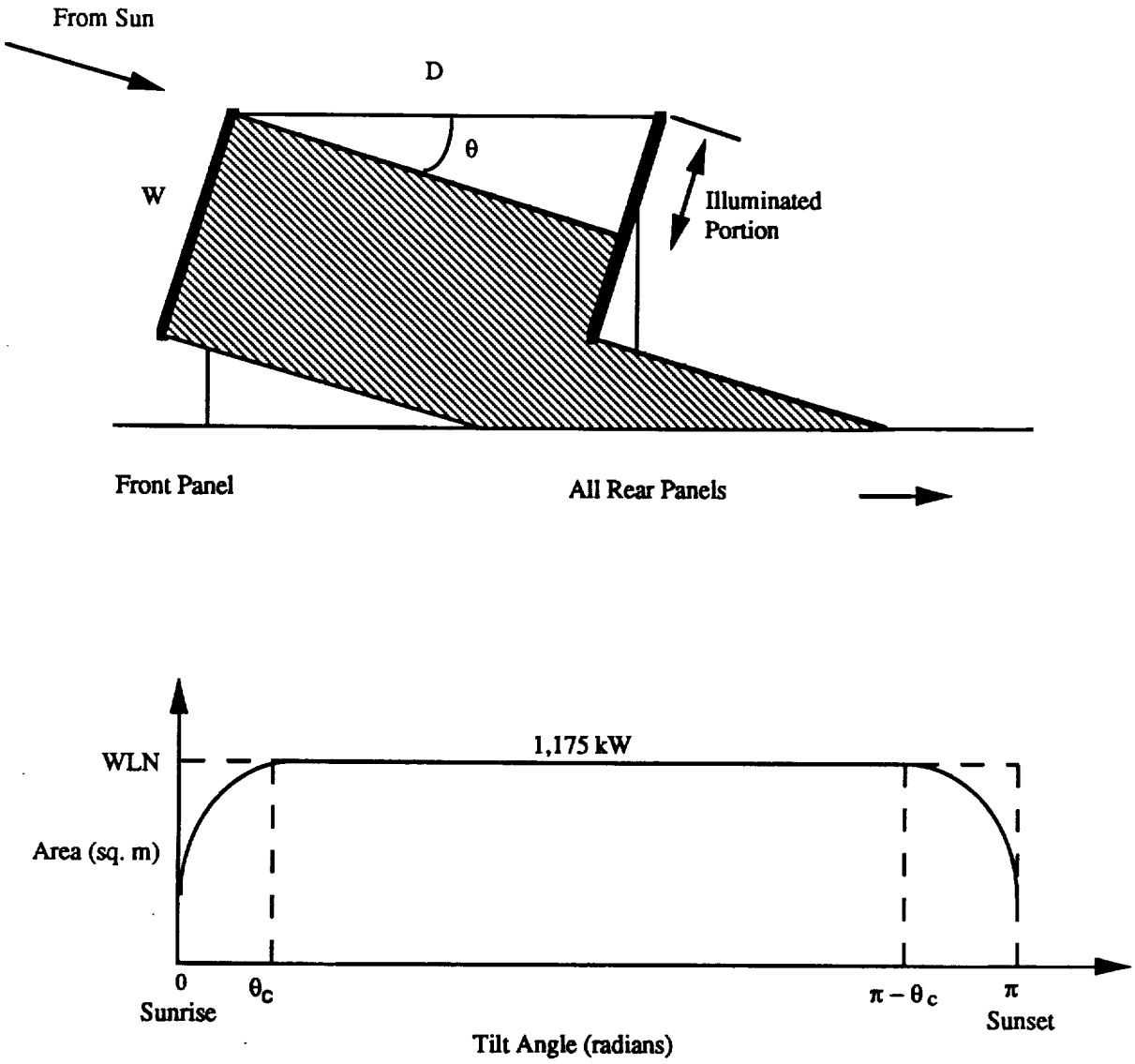

Fig. 2.10. Fraction of Array Illuminated.

for the baseline array, this lends itself easily to 5 rows of 10 panel sets each, which will provide 239 kW_e immediately.

As spacing between rows is increased, the critical angle approaches zero and total daily power produced approaches a maximum

$$A_{max} = NWL\pi \tag{2.7}$$

as shown in Fig. 2.10.

Ninety-five percent of the maximum power was chosen as a value above which further spacing gained little advantage. Integrating Eq. 2.6 and setting it equal to 95% of A_{max} gives the row spacing.

$$\int_0^{\theta_c} A d\theta + \int_{\theta_c}^{\pi-\theta_c} A d\theta + \int_{\pi-\theta_c}^{\theta_c} A d\theta = .95A_{max} \tag{2.8}$$

$$2L[W\theta_c + D(N-1)(1 - \cos\theta_c)] + WN(\pi - 2\theta_c) = .95(LWN\pi) \tag{2.9}$$

Since N is equal to 5 and W is set at 3 m, Eq. 2.9 gives a row spacing of 15 m.

Figure 2.11 shows a plan view of the final configuration. The entire array consists of 5 rows of 10 panel sets spaced at 15 m intervals. In this configuration all panels are fully illuminated when the sun is 11.5 degrees above the horizon, or 21.3 hours after sunrise. The total array uses a land area of 17,199 m^2 (4.3 acres).

2.5.2 TRACKING

Two concepts for panel tracking were originally considered. The first was to simply lay the panels flat on the ground, with no tracking. This had the advantage of eliminating the need for motors and support structures. It was rejected, however, because power produced would depend on sun angle, so total power production would gradually increase as the sun rose, then decrease again, providing an unsteady supply to users. Also, to compensate for

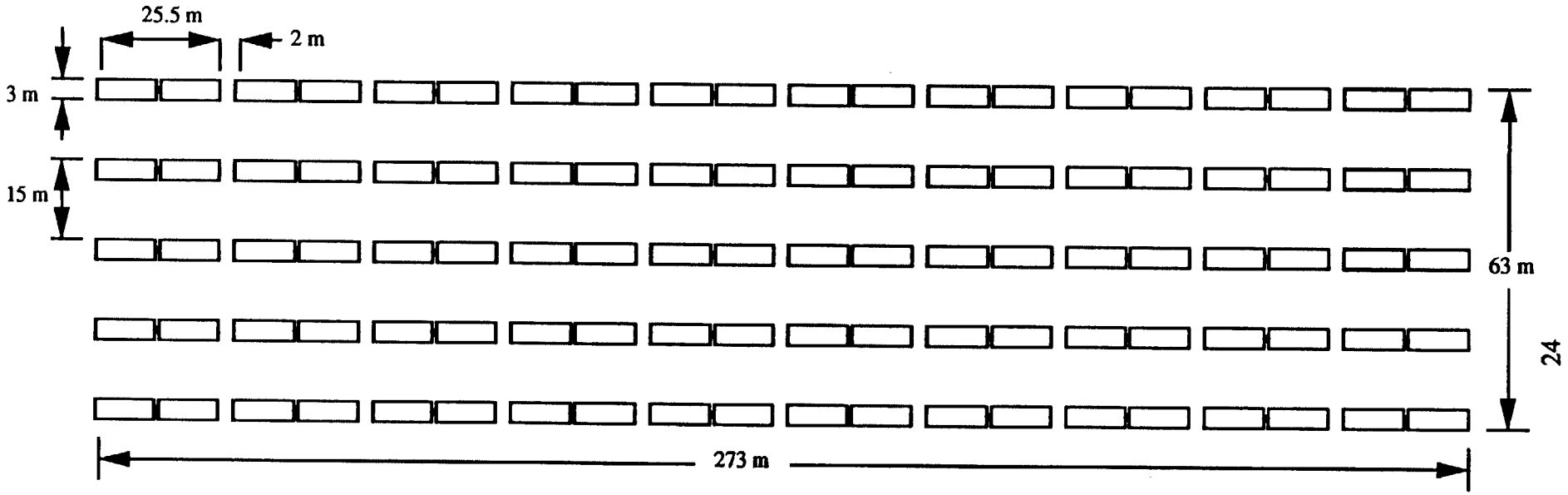

Total Land Area: 17,199 sq. m (4.3 acres)

Fig. 2.11. Final Configuration.

power lost due to extreme sun angle, total array area would have to be increased by 50%. For these reasons, an untracked configuration was rejected.

Since this array system will be located close to the equator, a single-axis system is sufficient to correctly position the panels. They will be rotated 180 degrees during the lunar day and repositioned at the beginning of lunar night.

The concentrating lenses focus incoming solar radiation within a one-degree range onto the active area of the cell, making exact alignment with the sun critical. Since the lunar day is 336 hours long, the sun only moves 0.54 degrees/hr, making continuous tracking unnecessary. For optimum performance, the cell/lens system should maintain directional accuracy to within 0.5 degrees, thus a DC stepper motor is used to rotate the panels in 0.54 degree increments, one motion every hour.

The motor will be regulated by an open loop control system; i.e. the array will be directed to a calculated position, instead of relying on the sun to generate a signal. The motor, gears, and controller will be encased in an insulated, tightly sealed housing to prevent evaporation of the lubricant. Each tracking motor will have a mass of approximately 5 kg [9].

2.5.3 MODULARITY

The fact that every piece of equipment must first be launched to LEO and then to the moon for installation, makes it desirable to launch a complete modular power package, ready to be set up immediately. This modularity would provide: 1) instant power--rather than waiting for many launches to assemble the entire plant, 2) failure protection--individual breakdown of one or more modules would leave enough power for survival, and 3) location flexibility--panels could either be centralized or placed close to load areas. As can be seen from Fig. 2.8, of the total 1.175 MW_e array, 90% of the total power produced (1,059 kW_e) goes directly to the user, while 10% (116 kW_e) goes to the energy storage facility for nighttime use.

2.6 ALTERNATIVE PHOTOVOLTAIC CELL

A proposed alternative to the Boeing tandem cell is a GaAs cell manufactured by TRW [2]. These cells, unlike the Boeing cells, have been thoroughly developed and tested and are currently available off- the- shelf. However, they have a lower conversion efficiency which necessitates an increase in the number of panel sets required and thus an increase in mass.

Although the GaAs array could be made slightly more efficient through the use of concentrating lenses, the additional mass required for the lenses and lens housings would negate this effect. The GaAs cells are mounted on a radiative aluminum backing, as are the Boeing tandem cells.

2.6.1 GaAs CELL

TRW produces solar cells of GaAs deposited on a Germanium substrate and covered with an anti-reflection coating (Fig. 2.12). These cells have an unconcentrated efficiency of 18% while operating within the lunar temperature range [2]. The cells are wired in series and total array efficiency is also 18%, as losses due to resistances in the wiring are insignificant. Each cell is rectangular, with dimensions of 2.0 cm x 4.0 cm x 0.2 mm thick. The average array lifetime is 5 to 10 years with minimum cell replacement and maintenance [2].

GaAs cells have superior radiation hardness compared to that of conventional silicon solar cells [10]. Even so, a thin (0.15 mm) glass cover is used for protection against solar proton flares. The GaAs cells will be mounted on a 0.2 mm thick aluminum backing, which will be mounted directly onto the tracking structure. Excess heat will be removed from the cells via radiation from the backing. The extreme night and day lunar temperature variation will not present problems for the operation or durability of the GaAs cells [2].

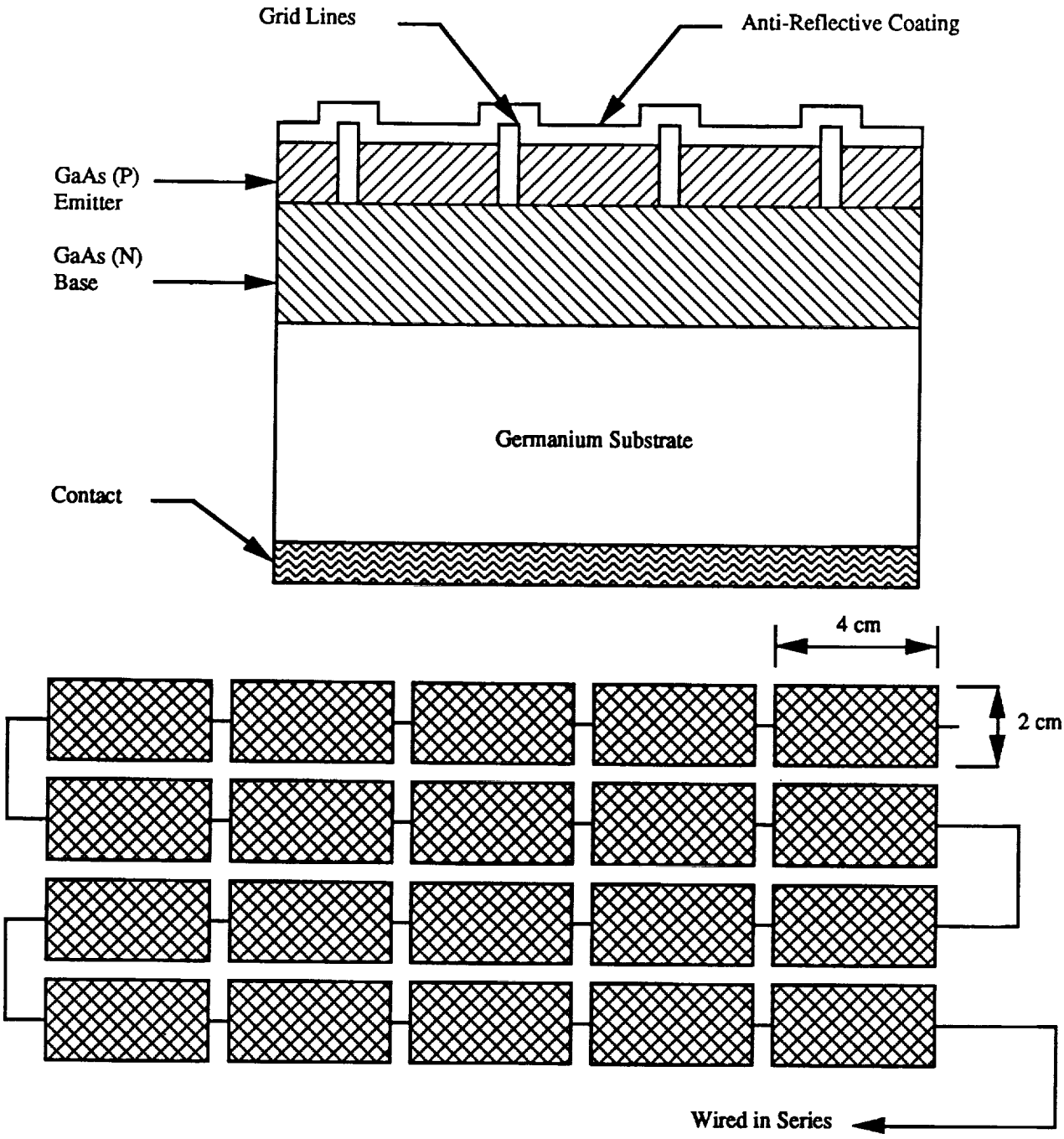

Fig. 2.12. GaAs Solar Cell.

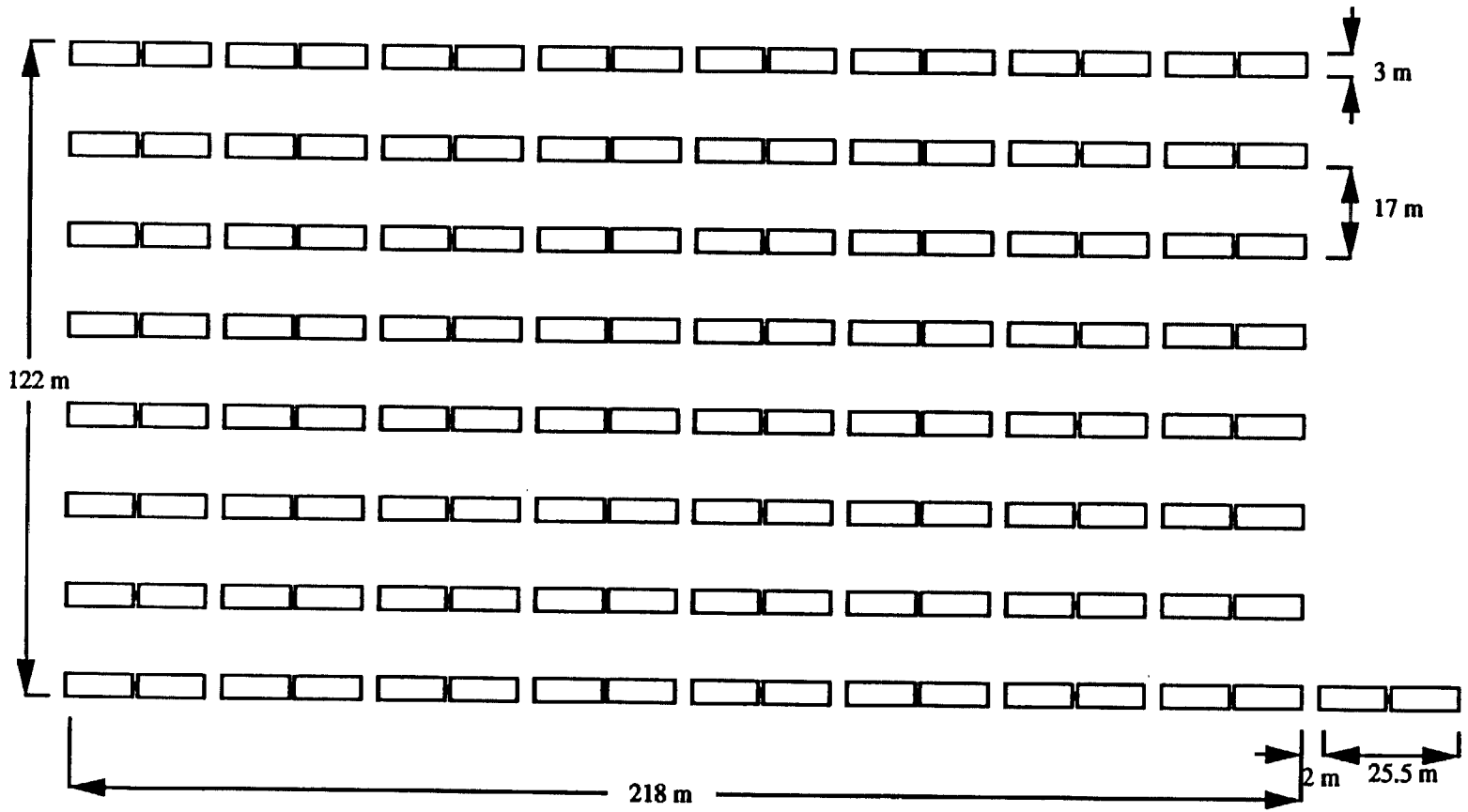

Total Land Area: 26,679 sq. m (6.6 acres)

Fig. 2.13. GaAs Array Configuration.

2.6.2 ARRAY SIZING AND CONFIGURATION

In order to obtain 1 MW_e of continuous usable power during the day and a subsistence level of 50 kW_e during the lunar night, 1.175 MW_e of power needs to be produced to account for the inefficiencies in power transmission and energy storage facilities. The total required array area is 4,825 m^2 with a mass of 11 metric tons (excluding structural elements); approximately 10 tons for daytime power, and 1 ton for the nighttime power.

As before, each panel is 12.5 m long by 3.0 m wide, with a central tracking motor shared by two panels. The total array consists of 65 panel sets arranged in 1 row of 9 sets and 7 rows of 8 sets with a row spacing of 17 m (Eq. 2.9). The array uses a total land area of 26,679 m^2 (6.6 acres).

2.7 CONCLUSION

The overall characteristics of both the GaAs/GaSb tandem cell and the GaAs single cell arrays are summarized in Table 2.2. These numbers represent a baseline array providing 1.0 MW_e during the day and 50 kW_e during the night to the user load. Each GaAs/GaSb panel set provides 23.85 kW_e at a mass cost of 183 kg. Masses given do not include tracking structures.

Table 2.2: Cell Comparison Summary.

	Tandem Cell	GaAs Cell
Array Efficiency	23.5%	18.0%
Concentration Ratio	100	1.0
Power/Area (W_e/m^2)	318	243.3
Total Required Area (m^2)	3,750	4,875
# Panel Sets	50	65
Cell Mass (kg/m^2)	2.44	2.27
Total Array Mass (kg/m^2)	9,150	11,066
Mass/Panel Set (kg)	183	170
Power/Panel Set (kW_e)	23.85	18.26
Power Density (W_e/kg)	130.3	107.3

One panel set is the smallest unit into which the array may be divided. If it is desired to launch a fraction of the total array, thus building up the power supply in a series of installations, the array may be divided into modules of any size. For example, a group of four panel sets would provide 95 kW for a mass cost of less than ton, or about 1.5 tons including structural mass. With the entire array in place, 50 panel sets are required at a total mass of 9,150 kg.

The GaAs cell has approximately the same mass per panel as the tandem cell, but its lower efficiency makes the entire array much heavier. Fifteen additional panels are required, adding 1,900 kg to the total system mass, or an increase of 21% over the tandem array. This is a considerable cost increase when launching from Earth.

The TRW cell however, is much less complex and is currently available for sale, at a cost of about $130 per cell [2]. These cells use existing technology that would require few changes. The Boeing cells are still in development and prototypes have been only partially tested. However, much lower cost of $5 per cell assembly has been suggested as a future manufacturing cost [1].

Another advantage of the GaAs array is that the system is simple. The entire system consists of cells and wiring mounted on a flat radiator backing. The GaAs/GaSb system requires lenses that may break or be misaligned over the cell, and an aluminum housing structure. These factors will necessitate an additional degree of caution during transportation and installation.

The GaAs cell has the advantage of being currently available and well tested. It also carries less risk during installation due to simplicity. The tandem cell array however, requires significantly fewer panels and therefore less mass, and is projected to be much cheaper to produce than currently available GaAs cells. If the lunar base is still at least a decade away, then these two factors may outweigh the time it will take to finish testing and begin manufacture of the tandem cell.

2.8 NOMENCLATURE

A	Total illuminated area (m^2)
A_c	Total collection area (m^2)
A_i	Illuminated area on rear panels (m^2)
A_{max}	Area illuminated at infinite spacing (m^2)
D	Spacing between rows (m)
L	Panel length (m)
N	Number of rows
P_D	Day power required by user (W_e)
P_N	Night power required by user (W_e)
P_T	Total power required from array (W_e)
S	Solar constant = 1400 W/m^2
T_e	Equilibrium temperature (K)
Q_i	Solar radiation not converted to electricity (W/m^2)
$Q_4(\theta)$	Radiation from area 4 (W/m^2)
$Q_5(\theta)$	Radiation from area 5 (W/m^2)
$Q_6(\theta)$	Radiation from area 6 (W/m^2)
W	Panel width (m)
α_b	Absorptivity of back of panel
ε_b	Emissivity of back of panel
ε_f	Emissivity of front of panel
η_A	Array efficiency (%)
η_D	Day efficiency (%)
η_N	Night efficiency (%)
θ_c	Critical angle (radians)
σ	Stefan-Boltzmann constant = 5.67×10^{-8} $W \cdot m^{-2} \cdot K^{-4}$

2.9 REFERENCES

1. Fraas, L., "Boeing High Efficiency Solar Cells", Lecture, University of Washington, January 31, 1990.

2. Kruer, M.,TRW, Personal communication, May 7, 1990.

3. Fraas, L., "Tandem Solar Cells with 31% (AM0) and 37% (AM1.5) Energy Conversion Efficiencies", IEEE Aerospace & Electronic Systems Magazine, Volume 4, Number 11, November, 1989, p. 3-9.

4. Henderson, B.W., "Boeing Achieves Major Advance in Space Solar Cell Efficiency", Aviation Week and Space Technology, October 23, 1989, p. 61-63.

5. Avery, J. E., L. M. Fraas, and V. S.Sundaram, "Tandem Concentrator Solar Cells with 30% (AM0) Power Conversion Efficiency", NASA SPRAT, 1989.

6. O'Neill, M., Entech, Inc., Personal communication, April 25, 1990.

7. O'Neill, M. J. and M. F. Piszczar, "Development of a Dome Fresnel Lens/Gallium Arsenide Photovoltaic Concentrator for Space Applications", Entech, Inc., 1987.

8. Rauschenbach, H. S., Solar Array Design Handbook, Litton Educational Publishing, Inc., 1980.

9. Maish, A.B., "Development of an Array Tracking Controller Using a Single Chip Computer", Sandia National Laboratories, SAND-87-0147C, 1987.

10. Anspaugh, B. and R. Kachare, "Photon Degradation of AlGaAs/GaAs Solar Cells", Jet Propulsion Laboratory, California Institute of Technology, JPL 88-39, 1988.

3.0 DYNAMIC POWER CONVERSION

Darren Ritter
Thomas Montague
Don Garcia

3.1 INTRODUCTION

The goal of this study is to develop a thermodynamic power system for the conversion of solar energy to electrical power for use in lunar based applications. The objective is to produce the required 1 MW of electrical power (MW_e) using a number of lower power modular units. The nominal power output for each modular unit was chosen as 250 kW_e, which makes for a system that is sufficiently small and reasonably easy to transport and construct, but still of a useful power output. This requires a total of 5 units to produce the power required for the nighttime storage in addition to the 1 MW_e for daytime use. These units each contain solar collection, power conversion, and radiator components, as shown in Fig. 3.1. The 250 kW_e size provides a high level of redundancy for the system and allows an entire unit to be launched from Earth in one Shuttle-C flight.

The solar collection unit selected is a linear parabolic trough collector composed of a polished aluminum reflector and a central receiver tube. The receiver tube is coated with cobalt oxide which provides a spectrally selective surface and limits the energy loss through radiation from the tube's surface. Gaseous helium is pumped through the receiver tube from the heat engine and is heated by solar radiation to power the system.

To meet the design requirements of low unit mass and size, a trade study was conducted between a Stirling cycle and a Brayton cycle. As a result of this study a regenerative Brayton cycle was chosen as the power conversion unit. This section summarizes the results of this trade study and describes the analytical methods used in designing the Brayton cycle and the solar collector.

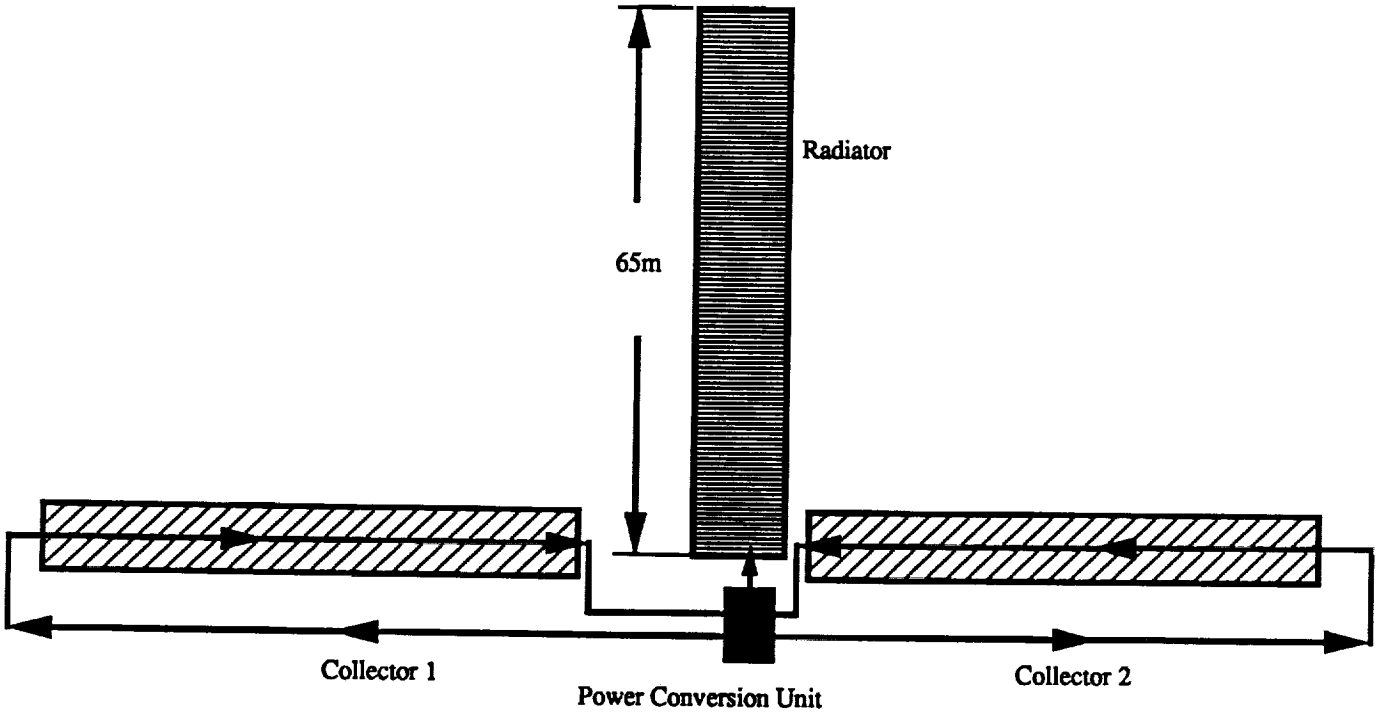

Fig. 3.1: Dynamic Conversion System Layout.

3.2 SYSTEM COMPONENT SELECTION

The selection of the thermodynamic power cycle was based on several factors including the mass, complexity, and ease of integration with the rest of the system. Two cycles were investigated: The Stirling cycle and the Brayton cycle. The collector layout and the working fluid were also selected based on structural and thermodynamic requirements and the operational environment.

The cycle selection was based on the use of separate modular systems each capable of producing 250 kW_e of electrical power. The chosen cycle results in a system that has a relatively low level of complexity to provide for ease of installation and maintenance on the Moon. The system was designed to have a minimum size and mass, allowing each complete module to be launched in a single Shuttle-C flight. Also, the system yields a high level of reliability and a long operational lifetime.

3.2.1 SOLAR RECEIVER SELECTION

Because the solar radiation flux at the moon stays very near 1.34 kW/m^2, a concentrating collector is required to achieve the needed operating temperatures for the system. The need for a large collector area to produce 250kW_e of power and the transportability of the system are the basis for the choice of solar receiver geometry. A parabolic dish collector would require a very large diameter and would pose significant structural problems for construction and breakdown to fit into the Shuttle-C bay. For this reason a linear collection unit is used, which can be broken down into sections for transportation to the lunar surface. The linear system requires a working fluid to be pumped through a duct at the focus of the reflector; this can be easily integrated into a power conversion cycle with a circulating fluid without a large loss in efficiency.

3.2.2 WORKING FLUID SELECTION

Several factors affect the choice of the working fluid: the extreme cold experienced during the two week lunar night, the need for a noncorrosive gas to limit erosion and breakdown of system components, and the need for a high specific heat to minimize the mass flow rate. The working fluid cannot be allowed to condense during lunar night or the droplets still in the system during startup will damage the rotating machinery in the dynamic conversion unit. Helium was chosen as the working fluid because it does not become liquid at the temperatures reached during lunar night and has a high specific heat. Heat engines have higher component efficiencies using working fluids of higher molecular weight, but any gases other than helium will condense out of the mixture at the low temperature of 116 K reached during lunar night.

3.2.3 POWER CYCLE SELECTION

The free piston Stirling engine (FPSE) was initially considered for this study because of several potentially favorable characteristics [1]. The FPSE is a self-contained unit which could be installed easily on the moon with a high level of reliability, and has an expected operational lifetime of 60,000 hours. After investigating the current research being done in the application of Stirling engine power systems, a design developed by Mechanical Technologies Incorporated (MTI) was chosen for this study [2]. Although MTI has developed a method for scaling a system up to the 175 kW_e level, it is not certain that a system in the 250 kW_e range would be practical.

The system being developed by MTI has its initial application as a power conversion unit for the SP-100 space reactor system. The latter employs heat pipes as the method for importing heat into the engine and a pumped loop liquid metal system for heat rejection. Because of the cool-down encountered during the two week lunar night, such approaches present a substantial problem for a solar power system. Great difficulties have been encountered while trying to start a heat pipe from a cold solid state. The Stirling Technologies

Company is developing a system which employs a liquid metal boiler which appears to alleviate these problems [3].

Because the Stirling engine is a closed system, the addition of a pumped loop and heat exchanger for energy transfer from the solar collector to the engine is required. This significantly increases the system mass and complexity, as well as reducing its overall efficiency. Based on these problems, as well as the uncertainty in Stirling technology, it was determined that the Stirling conversion unit is not suitable for a lunar based system and, therefore, was not selected for the present design.

The Brayton cycle has many features that make it a favorable system for our proposed application. Its proven technology is currently being used for power production with output levels significantly greater than 250 kW_e. The Brayton cycle is well suited for integration with a linear solar collector unit because its working fluid is pumped through the collector without additional pumping equipment or the need for an additional heat exchanger to transfer the thermal energy from the collector fluid to the cycle fluid. The addition of a regenerator to the Brayton cycle increases the mass, but the increase in efficiency can significantly reduce the masses of the other components of the system. Because the Brayton cycle is of proven design and is easily integrated with the solar collector unit, without increasing the system complexity or mass, it was chosen for this design study.

3.3 SOLAR COLLECTOR UNIT

The purpose of the Solar Collector Unit is to provide the required energy through heat addition to the cycle working fluid prior to expansion through the turbine. Because of the high temperatures needed to get reasonable efficiencies in the Brayton cycle, a concentrating collector must be used.

3.3.1 SYSTEM DESCRIPTION

The solar collector consists of a linear parabolic trough reflector and a central receiver tube coated with a spectrally selective surface (see Fig. 3.2). Precise orientation of the collector to track the sun is required to ensure that all of the solar radiation incident on the reflector is focused on the central receiver tube. Because the Moon's axial tilt is very small, the collector can be placed with a north south orientation on or near the lunar equator, requiring only a single degree of freedom of motion to track the sun.

The reflector has a parabolic surface with a focal length of 1.0 m and an aperture of 7.0 m. The reflective surface is provided by a thin aluminum foil which is laminated to a rigid substrate that provides the desired parabolic shape, in a manner similar to that planned for the Space Station. Aluminum is used for the reflective surface because it is light in weight and will reflect a large fraction of the radiation incident upon it. Aluminum foil has a reflectivity of 86% for solar radiation [4].

The receiver is a 5.4 cm O.D. metal alloy tube which has a spectrally selective surface. The selective surface is necessary to minimize the losses due to reradiation from the receiver surface. Because the reradiation varies as T^4, these losses can be quite significant. The selective coating is a thin layer of cobalt oxide, deposited on the tube by electroplating [5]. The function of the coating is to minimize the surface emissivity in the thermal range, reducing the losses due to reradiation, and maximize the emissivity, and therefore the absorption, over the solar spectrum.

The selective surface spectral emissivity (ε_λ) was modeled as having a value of 0.95 for wavelengths from 0 to 3 μm and 0.07 for wavelengths greater than 3 μm (see Fig. 3.3). This appears to be a reasonable approximation for the spectral characteristics for the cobalt oxide surface. Thus, the effective emissivity and absorptivity of the surface are given by:

$$\varepsilon_S = 0.07f(\lambda T)+0.95(1-f(\lambda T)) \tag{3.1}$$

$$\alpha_S = 0.07f(\lambda T)+0.95(1-f(\lambda T)) \tag{3.2}$$

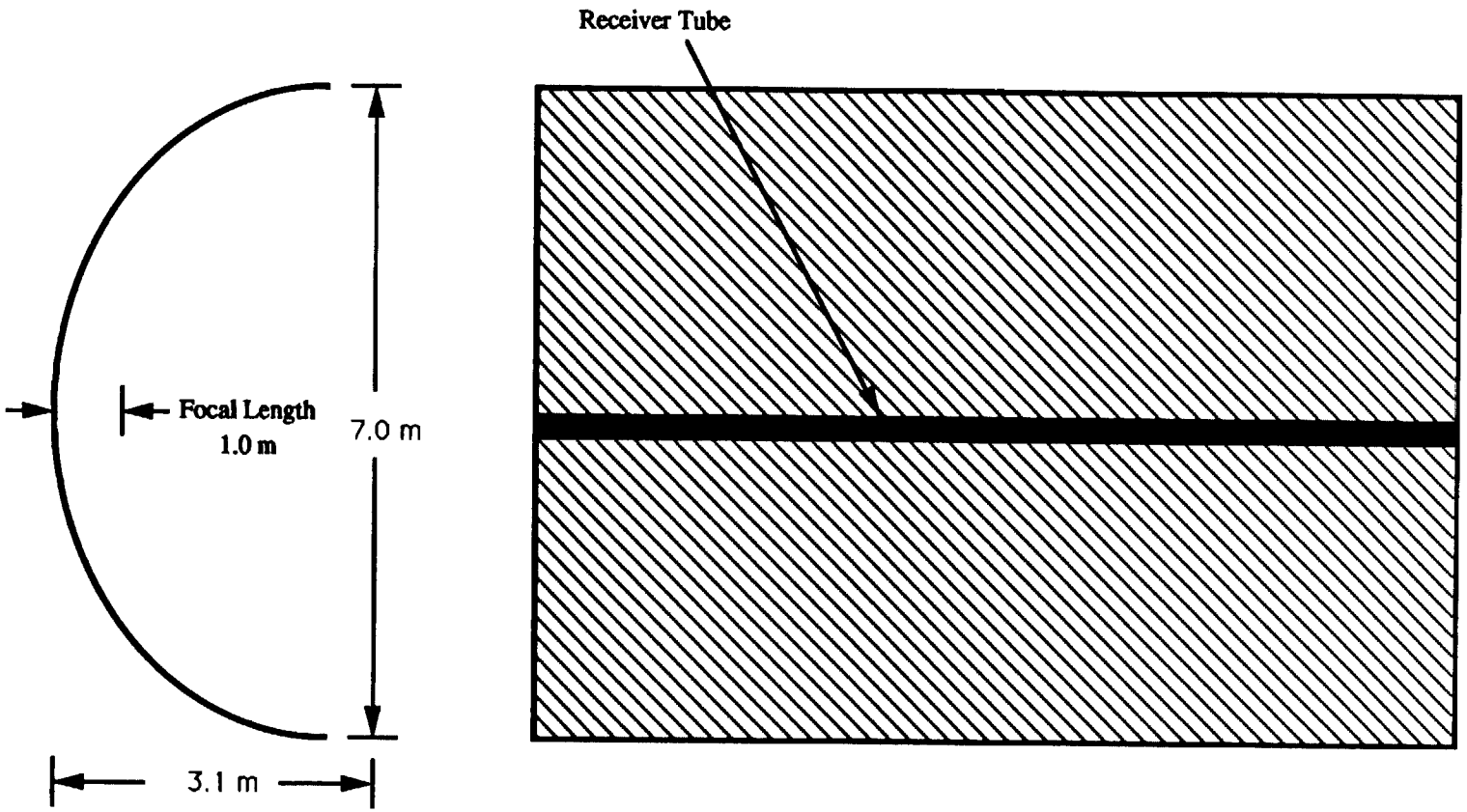

Fig. 3.2: Schematic of Solar Concentrator.

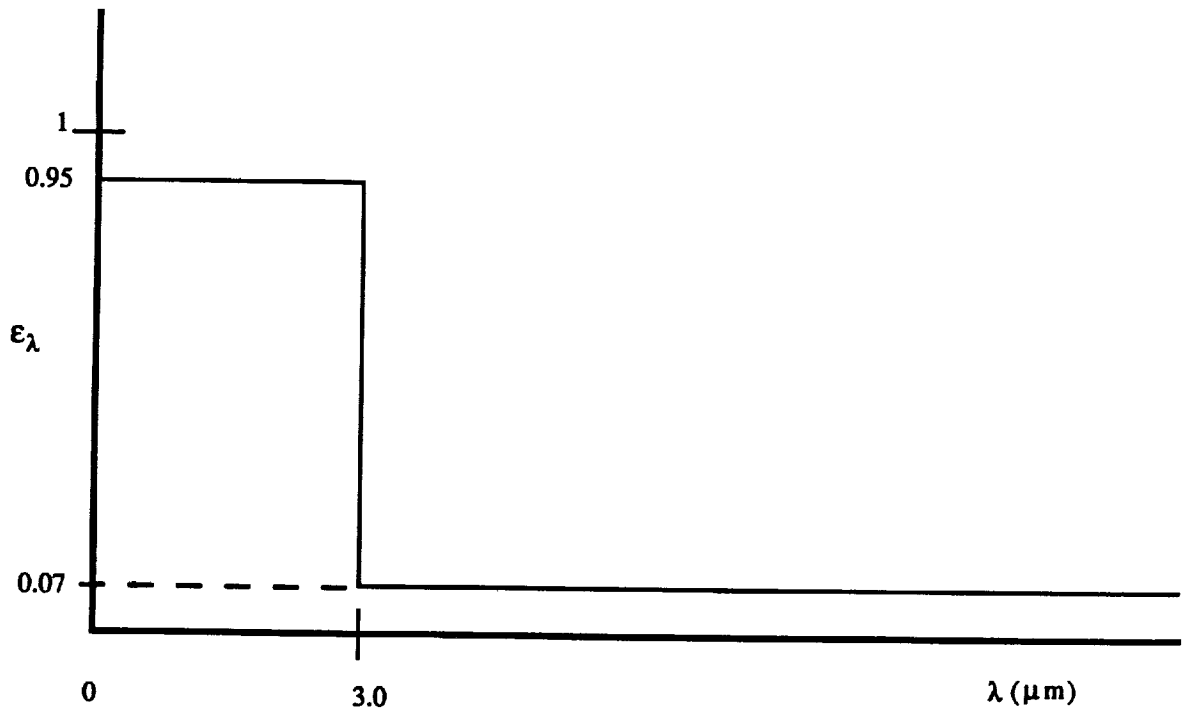

Fig. 3.3: Approximation to Spectral Emissivity of Cobalt Oxide Coating.

where $f(\lambda T)$ is the fraction of total blackbody radiation from 0 to 3 μm for the surface temperature. This gives an effective emissivity of from 0.18 to 0.32 for the operating temperatures and an absorptivity for solar radiation of 0.95. For the solar absorptivity $f(\lambda T)$ is taken at T=5800 K, which is the effective radiant temperature of the sun. Although test results for this coating material operating at a temperature of 1000 K were not found, cobalt oxide on nickel plate has been tested up to about 700 K in a vacuum with no degradation in its effectiveness [5]. No data for its reliability in ultraviolet radiation was available, however, tests have been done on other metallic oxides, such as iron and zinc oxides, with no apparent degradation [5].

The duct must be made of an alloy which has a high strength at high temperatures. Because the efficiency of the dynamic cycle rises with increasing high temperature, the duct walls should be constructed of a material able to withstand temperatures of up to ~1100 K. The duct wall thickness must be sufficient to contain approximately 46 atm of internal pressure. There is also a requirement that the duct be sufficiently stiff to avoid displacement from the reflector line of focus. The material selected for the duct is a nickel based superalloy designated UDI MET 700. This alloy, at 1100 K, has a 1% creep strength of 29,000 psi for 1000 hours [6]. For present purposes, a tensile strength of 10,000 psi is assumed.

3.3.2 SYSTEM ANALYSIS

The analysis used to size the collector is based on the assumption that an incremental length of the receiver duct receives a heat flux that is constant over that length (see Fig. 3.4). This constant flux, q_U, is the incident solar radiation, S, less the heat radiated to space from the tube, q_L:

$$q_U = S - q_L \tag{3.3}$$

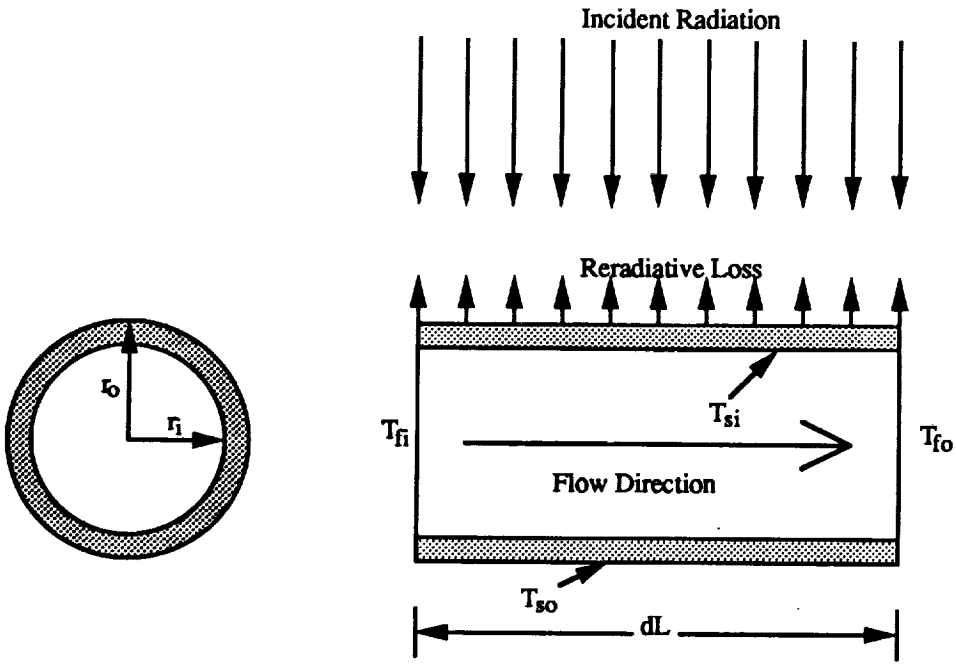

Fig. 3.4: Receiver Tube Element.

where $S = \alpha_S \rho C_R I_C$, and α_s is the solar absorptivity, ρ is the reflectivity of the reflector, C_R is the collector concentration ratio, and Ic is the solar constant (1340 W/m^2). The concentration ratio is the ratio of the reflector area to the illuminated receiver area. The collector chosen has a concentration ratio of 41. The reradiative loss, q_L, is given by

$$q_L = \varepsilon_s \sigma T_{so}^4 \tag{3.4}$$

where ε_s is the effective emissivity of the receiver surface, σ is the Stephan-Boltzman constant (5.67×10^{-8} W/m^2K^4), and T_{so} is the outer surface temperature of the receiver.

It is assumed that an incremental length dL of the receiver provides an increase in the fluid temperature of increment δT (see Fig. 3.4). If δT is small, the variation of the outer surface temperature of the length dL will also be small. A δT of 2 K was chosen and the numerical analysis was begun with the inlet temperature, T_{fi}, of the first element set equal to the collector inlet temperature, T_o. For subsequent elements T_{fi} was set equal to the outlet temperature of the previous element, T_{fo}. For each element, the temperature difference, ΔT, between the bulk mean fluid temperature, T_{fm}, and the outer surface temperature, T_{so}, of the receiver was assumed, i.e.

$$\Delta T = T_{so} - T_{fm} \tag{3.5}$$

where the bulk mean fluid temperature is defined as

$$T_{fm} = \frac{(T_{fi} + T_{fo})}{2} \tag{3.6}$$

With this assumption, T_{so}, can be estimated and therefore, the heat flux radiated from the tube q_L can be calculated by Eq. 3.4. Using the properties of the working fluid, the length dL required to give the temperature rise δT can be calculated

$$dL = \frac{\dot{m} C_P}{\pi D}(T_{fo} - T_{fi}) \tag{3.7}$$

Using the turbulent flow approximation, the Nusselt number based on the flow Reynolds number can be estimated

$$Nu_D = 0.023 Re_D^{0.8} Pr^{0.4} \tag{3.8}$$

where Re_D is the Reynolds number based on the inner diameter of the receiver and Pr is the Prandtl number of the working fluid [7]. The film coefficient, h_f, is then obtained from

$$h_f = \frac{Nu_D k}{D} \tag{3.9}$$

where k is the thermal conductivity of the working fluid. The temperature of the inside surface of the tube, T_{si}, can be calculated from:

$$T_{si} = \frac{q_U}{h_f} + T_{fm} \tag{3.10}$$

Using the equation for heat conduction through a circular cylinder, and the estimated heat flux through the receiver wall, a new outside surface temperature, T'_{so}, can be calculated.

$$T'_{so} = \frac{\left(T_{si} + q_L(D_o)\ln\left|\frac{r_o}{r_i}\right|\right)}{2k} \tag{3.11}$$

The difference between T_{fm} and T'_{so} can be substituted for the original ΔT. After only a few iterations the solution converges and the true T_{so} is obtained. Later, in section 3.4.2, the entire

dynamic conversion system is optimized to achieve the lowest mass possible, and the result is a collector length of approximately 50 m and a collector outlet temperature of 1000 K. Figure 3.5 shows the receiver tube outside surface temperature distribution along the collector length. Note that the outside temperature distribution is slightly higher than what the inside temperature distribution will be.

3.4 DYNAMIC CONVERSION UNIT

The Brayton cycle (Fig 3.5) is the power producing section of the system. It converts a portion of the thermal energy collected in the solar collector into electrical energy. The unit consists of a compressor, turbine, regenerator, and a heat exchanger to transfer the waste heat from the working fluid to the radiator. The rotational energy is converted to electrical energy with an alternator connected to the compressor and turbine shaft. The system design of the dynamic conversion unit is a scaled down version of a system designed in an earlier study [8].

3.4.1 CYCLE ANALYSIS

The specific heat at constant pressure, C_P, for helium is constant and, therefore, the analysis can be conducted by assuming that the enthalpy per unit mass, h, of the working fluid at temperature T is given by:

$$h = C_P T \tag{3.12}$$

This allows for the cycle to be determined by the compressor inlet conditions T_1 and P_1 , (see Fig. 3.6) the turbine inlet conditions T_4 and P_4, and the component efficiencies.

The compressor outlet temperature,T_2, is given by

$$T_2 = T_1 + \frac{1}{\eta_C}(T_{2S} - T_1) \tag{3.13}$$

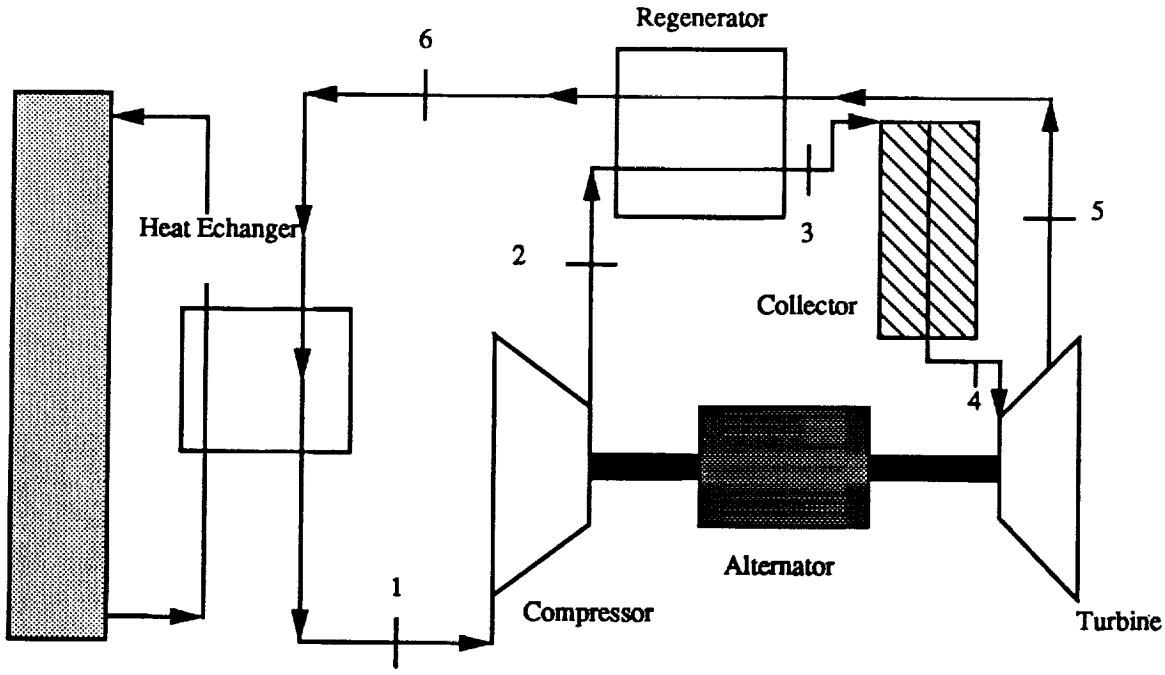

Fig. 3.5: Brayton Cycle Diagram

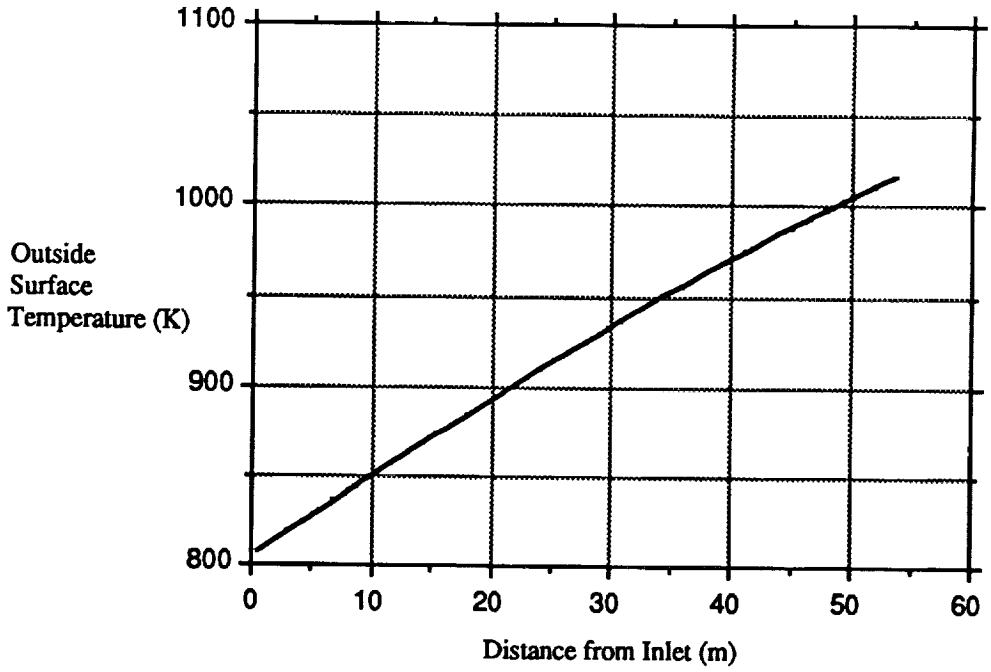

Fig. 3.6: Outside Surface Temperature Distribution Along Receiver Tube.

where η_C is the compressor efficiency and T_{2S} is the temperature that would be obtained through an isentropic compression of the working fluid from P_1 to P_2, i.e.,

$$T_{2S} = T_1\left(\frac{P_2}{P_1}\right)^{\frac{(\gamma-1)}{\gamma}} \tag{3.14}$$

where γ is the specific heat ratio. The temperature at the turbine outlet, T_5, is given by

$$T_5 = T_4+\eta_T(T_4-T_{5S}) \tag{3.15}$$

where η_T is the turbine efficiency and T_{5S} is the temperature that would be obtained through isentropic expansion of the working fluid through the turbine from P_4 to P_5, i.e.,

$$T_{5S} = T_4\left(\frac{P_5}{P_4}\right)^{\frac{(\gamma-1)}{\gamma}} \tag{3.16}$$

The temperature at the exit of the cold side of the regenerator, T_3 , is calculated from

$$T_3 = T_2+\eta_{REG}(T_5-T_2) \tag{3.17}$$

where η_{REG} is the regenerator effectiveness. The temperature at the exit of the hot side of the regenerator, T_6 is calculated by conducting an energy balance on the regenerator. This is done by noting that there is no heat transferred across a control volume around the regenerator. This gives an equation for T_6:

$$T_6 = T_5+T_2-T_3 \tag{3.18}$$

The principal losses, other than the inefficiencies of the components, are pressure losses in the regenerator, the heat rejection heat exchanger, and the piping for the collector. These losses can be minimized by selecting an operating pressure sufficiently high to give a high density of the working fluid and thereby reduce the flow velocities required.

3.4.2 OPTIMIZATION OF CYCLE OPERATING RANGE

To produce a system with the least mass for the 250 kW_e power output of each module, all of the components must be considered. The Brayton cycle efficiency increases with increasing range between the turbine inlet and compressor inlet temperatures . However, the efficiency of the solar collector decreases with rising turbine inlet temperature and the radiator efficiency decreases with decreasing low end temperature. Because the optimal temperatures for the radiator and collector run opposite to the Brayton cycle a balance is needed to obtain the maximum overall system efficiency. The optimum system design takes into account the component masses as well as the relation of the system pressures to Brayton cycle efficiency and power losses due to pressure losses in the collector, heat exchangers and piping.

By varying the compressor inlet temperature and turbine inlet temperature it was found that the overall system size was driven by the Brayton cycle efficiency and the turbine inlet temperature, provided that the compressor inlet temperature does not become too small. This is due to the fact that the radiator mass is affected more by the cycle efficiency than by the temperature at which the radiator operates. This implies that the cycle low end temperature should be chosen as low as possible without causing the radiator mass to become to great in proportion to the rest of the system. Below temperatures of 300 K, the radiator mass increases rapidly; above 350 K, the system mass increases due to the decrease in Brayton cycle efficiency. The solar collector outlet temperature establishes the turbine inlet temperature and the collector length grows with increased outlet temperature (see Fig. 3.7). Because the collector length is also directly related to the Brayton cycle efficiency, which increases with turbine inlet temperature, a balance was made to reach the minimum collector length. A

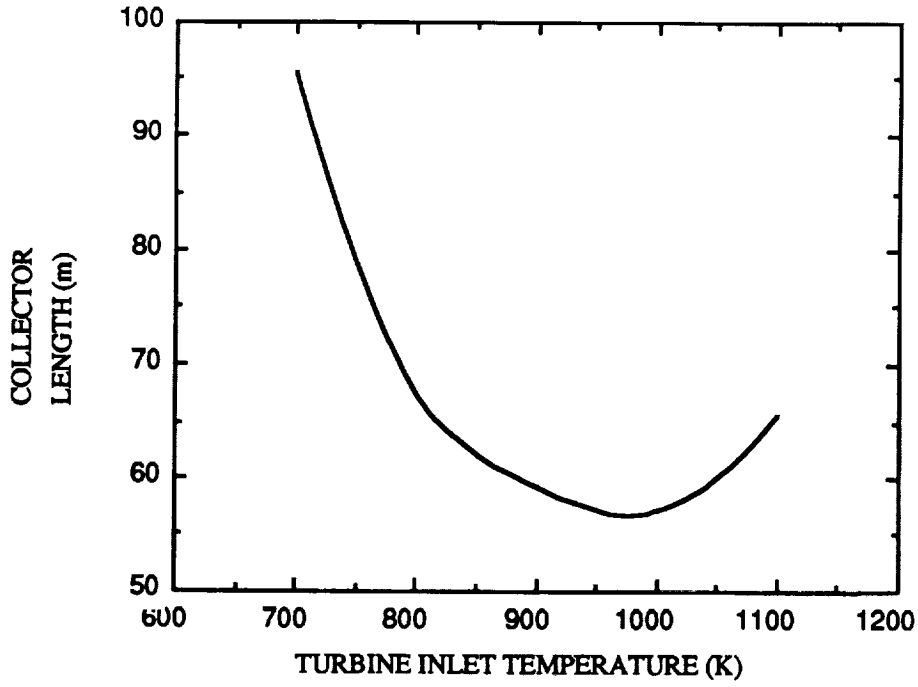

Fig. 3.7: Variation Of Collector Length With Turbine Inlet Temperature.

decrease in the turbine inlet temperature below about 1000 K requires a larger collector because of the decrease in cycle efficiency. Increasing the turbine inlet temperature above 1000 K also increases the collector length, due primarily to the fact that the average temperature at which the receiver radiates is higher. These factors indicate that the optimum cycle operates with a low end temperature of 330 K and a high end temperature of 1000 K.

Once the turbine inlet and the compressor temperatures were determined the compressor pressure ratio at which the Brayton cycle has the maximum efficiency was found. The cycle optimization requires a compressor pressure ratio of 1.85 for the Brayton component efficiencies used (Table 3.1). This gives a maximum cycle efficiency of 36%.

Table 3.1: Cycle Operating Conditions

Station	Pressure (Atm)	Temperature (K)
1 Compressor Inlet	25.0	330
2 Compressor Exit	46.8	437
3 Collector Inlet	45.9	785
4 Turbine Inlet	45.9	1000
5 Turbine Exit	25.8	815
6 Waste Heat Exchanger Inlet	25.8	467
7 Waste Heat Exchanger Exit	25.8	330

COMPONENT EFFICIENCIES	
Turbine Efficiency	90%
Compressor Efficiency	86%
Regenerator Effectiveness	92%
Collector Efficiency	63%

PRESSURE LOSSES	
Heat Exchangers	2%
Regenerator	2%
Solar Collector and Piping	1%

PERFORMANCE	
Electrical Power Output	250 kW_e
Energy Conversion Efficiency	22.7%
Mass Flow Rate	0.62 kg/s

3.4.3 ROTATING MACHINERY

In the dynamic conversion unit the compressor and turbine are mounted on the same shaft along with an alternator to produce the electrical power. Radial compressors and turbines have a lower component efficiency than axial flow components, but have several advantages that make them more reliable. Radial flow components are lighter in weight and more rugged than axial flow components. Also, radial compressors require fewer stages than axial flow compressors to obtain the same pressure increase. For these reasons the rotating machinery consists of a radial compressor and turbine. The compressor and turbine masses are scaled from a previously designed 3.36 MW_e Brayton cycle power conversion unit [8]. For power outputs over 100 kW_e the specific mass of a Brayton system is roughly constant [9].

3.4.4 REGENERATOR

The regenerator is a counterflow heat exchanger that transfers some of the waste heat in the working fluid that has just exited the turbine into the fluid before it enters the solar collector. The geometry of the regenerator is a long slender box to minimize the mass of the inlet and outlet headers (see Fig. 3.8). The size and mass of this device are directly related to the energy transfer required. Although the external surface area to volume ratio increases for a smaller regenerator, the decrease in casing stresses due to internal pressure counteracts this effect and the casing can be thinner for a smaller system.

The regenerator mass is obtained by scaling down the mass from a previous study [8] by the ratio of power outputs. The regenerator is constructed of Mapalloy 754 and a safety factor of three is used in the design [8].

3.4.5 WASTE HEAT EXCHANGERS

Two different radiator systems have been considered for the rejection of the waste heat in the thermodynamic cycle (see section 4). Because the specific properties of the heat rejection fluids for each radiator system are different, two different waste heat exchangers were

Dark Squares Indicate helium inflow,
Light Squares Indicate helium Outflow.

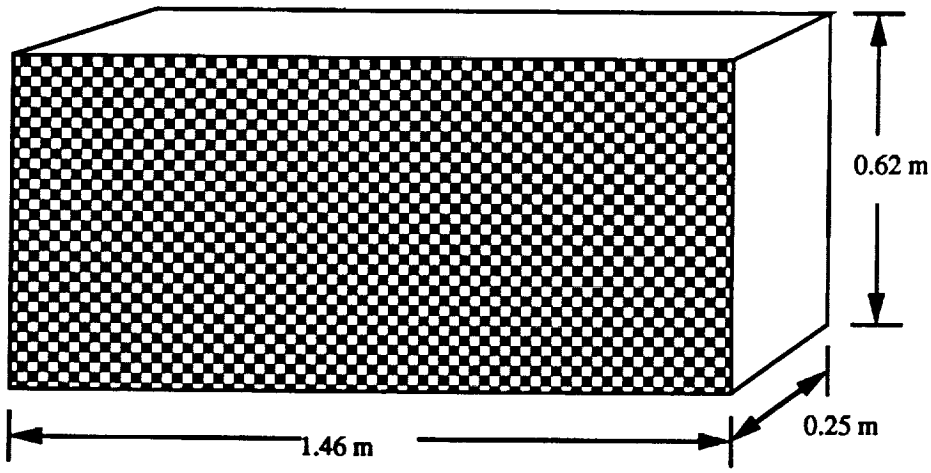

Core Volume: 0.226 m^3
Core Mass: 195 kg
Header Mass: 12 kg
Total Mass: 207 kg

Fig. 3.8: Counterflow Regenerator

designed. Both are compact heat exchangers with the same core design (see Fig. 3.9) which has a density of 497 kg/m^3 when constructed of Hastelloy X [10]. Pressure losses are limited to 2% and the component masses are minimized.Fig. 3.8: Regenerator.

The heat exchanger for the liquid droplet radiator (LDR) is composed of long finned tubes through which DOW 705 fluid flows. The pressurized helium flows over the finned tubes perpendicular to the DOW 705 fluid flow (see Fig. 3.9). Because of the high temperature range and pressure experienced by the heat exchanger make aluminum unsuitable, the core is constructed of Hastelloy X. The shell of the heat exchanger is also constructed of Hastelloy X and has rounded corners to minimize stress concentrations. A schematic showing the dimensions and mass of this heat exchanger is shown in Fig 3.10.

The heat exchanger for the heat pipe radiator (HPR) (Fig. 3.11) has the same core design as the previous heat exchanger. However, the helium flows through the pipes and the heat exchanger is placed inside the fluid reservoir of the main heat pipe. The heat exchanger for the heat pipe radiator is also constructed entirely of Hastelloy X.

3.4.6 BEARINGS AND ALTERNATOR

The choice of bearings for the rotating unit must be highly reliably and there should be no contamination of the helium gas. Gas bearings are used because they are more reliable than oil lubricated bearings and have no possibility of gas contamination. Although gas bearings are quite sensitive to thermal loads, a small portion of the working gas can be routed from the compressor outlet to cool the bearings. This is also necessary to cool the alternator. An estimated 2% flow bypass is needed for both.

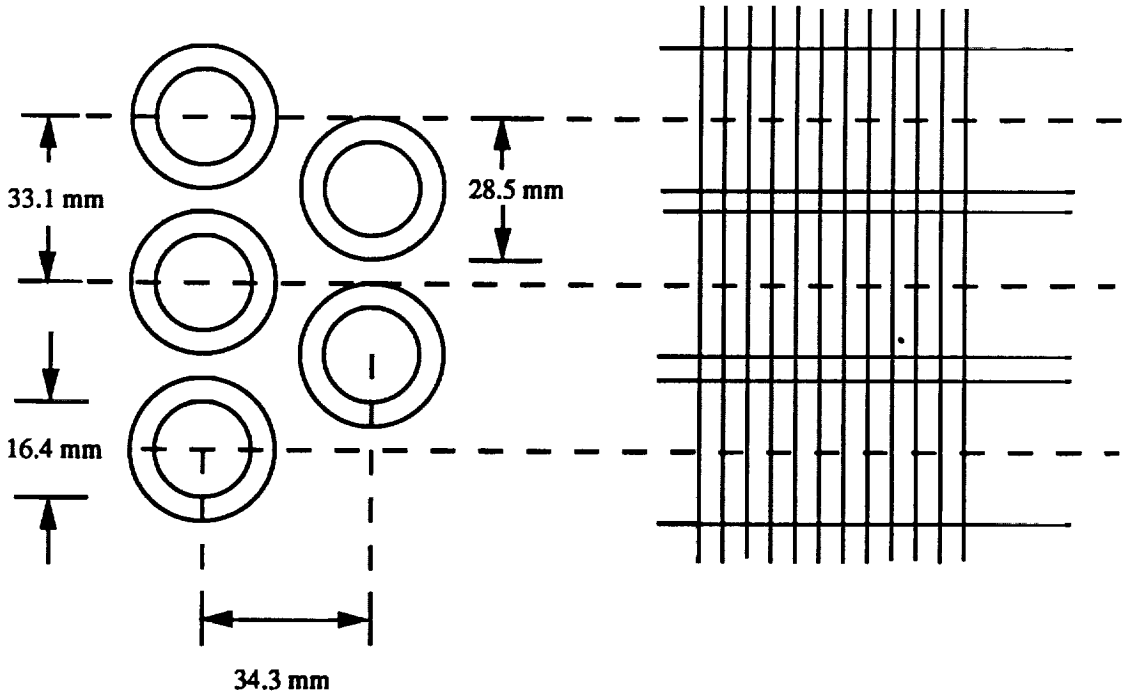

Fig. 3.9: Waste Heat Exchanger Core Geometry.

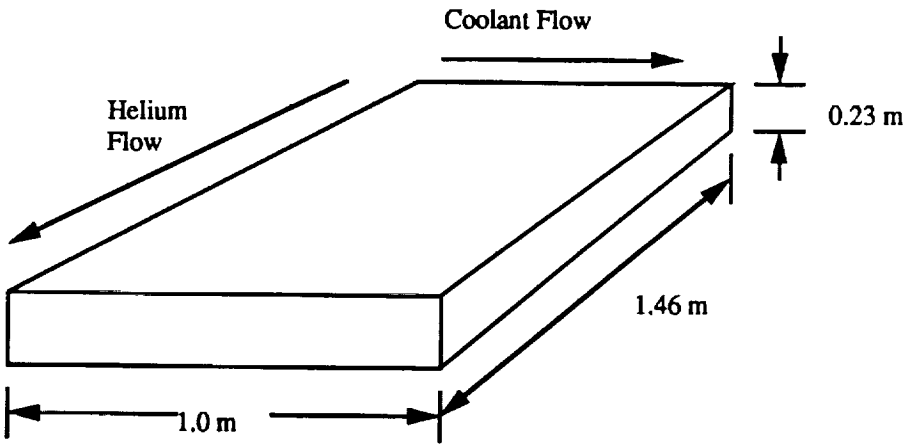

Core Volume:	0.336 m^3
Core Mass:	167 kg
Header Mass:	39 kg
Total Mass:	**206 kg**

Fig. 3.10: LDR Heat Exchanger.

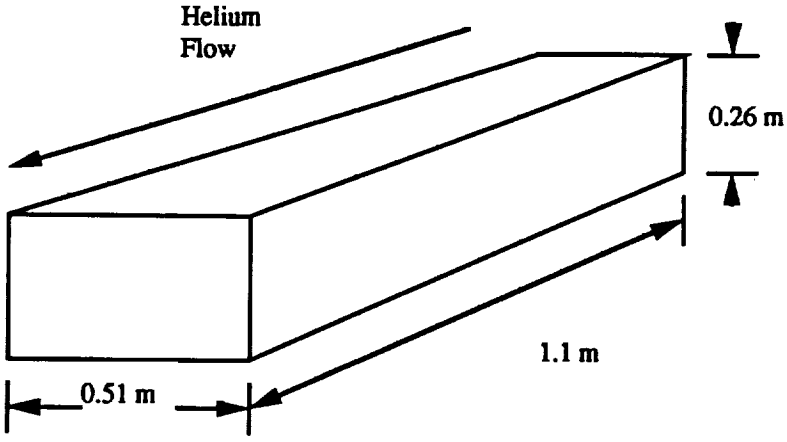

Core Volume:	0.146 m^3
Core Mass:	72 kg
Shell and Header Mass:	76 kg
Total Mass:	**148 kg**

Fig. 3.11: HPR Heat Exchanger

3.5 CONCLUSIONS

The dynamic power conversion unit consists of a solar concentrator that provides thermal energy to a regenerative Brayton cycle which drives an alternator to produce electrical power. Components were selected to increase the reliability and limit the system complexity and total mass. The complete system is composed of five modular units that each produce 250 kW_e in order to provide redundancy in the case of single point failure and to facilitate transportation of the system to the Moon. Helium is used as the working fluid to prevent condensation during the extreme cold of the lunar night which would cause startup problems and erosion of the turbomachinery components. The operating temperatures were selected to produce the system with the maximum specific power output. A high operating pressure was selected to minimize the pressure losses in the solar concentrator and the two heat exchangers. Rejection of the waste heat is accomplished through one of two possible systems, a liquid droplet radiator or a heat pipe radiator, which are discussed in the following chapter. Although the total system mass is quite high, due to the solar collection unit, the dynamic conversion unit uses proven technology. The dynamic power conversion unit has power output of 22 W/kg; component mass breakdown is shown in Table 3.2.

Table 3.2: 250 kW_e Unit Mass Breakdown.

Brayton Conversion Unit

Turbomachinery	234 kg
Regenerator	207 kg
LDR Heat Exchanger	206 kg
HPR Heat Exchanger	148 kg
Gas Supply	8 kg
Total Mass (LDR)	**655 kg**
Total Mass (HPR)	**597 kg**

Solar Collector

Reflector Material	2808 kg
Receiver Tube	15 kg
Piping	105 kg
Support Structure	7977 kg
Total Mass	**10,905 kg**

Dynamic Conversion Unit

Total Mass (LDR)	11560 kg
Total Mass (HPR)	11502 kg
Power Output per module	250 kW_e
Specific Power	**22 W/kg**

3.6 NOMENCLATURE

C_P	Specific heat at constant pressure
C_R	Concentration ratio
dL	Incremental length of receiver duct
$f(\lambda T)$	Fraction of blackbody radiation
FPSE	Free piston Stirling engine
HPR	Heat pipe radiator
h	Specific enthalpy
h_f	Heat transfer film coefficient
I_C	Solar constant
k	Thermal conductivity
LDR	Liquid droplet radiator
MTI	Mechanical Technologies Incorporated
Nu_D	Nusselt number based on flow diameter
P_1	Pressure at compressor inlet
P_2	Pressure at compressor exit
P_4	Pressure at turbine inlet
P_5	Pressure at turbine exit
Pr	Prandtl number
q_L	Reradiative heat loss from receiver
q_U	Useful energy gain of working fluid
Re_D	Reynolds number based on flow diameter
S	Solar radiation incident on receiver
t	Receiver tube wall thickness
T_1	Temperature at compressor inlet
T_2	Temperature at compressor exit

T_{2S}	Temperature at compressor exit, isentropic
T_3	Temperature at regenerator cold side exit
T_4	Temperature at turbine inlet
T_5	Temperature at turbine exit
T_{5S}	Temperature at turbine exit, isentropic
T_6	Temperature at regenerator hot side exit
T_{fi}	Mean fluid temperature entering an incremental length of the receiver tube
T_{fm}	Bulk mean fluid temperature
T_{fo}	Mean fluid temperature exiting an incremental length of the receiver duct
T_o	Fluid temperature entering the solar collector
T_{si}	Temperature of the inside surface of the receiver duct
T_{so}	Temperature of the outside surface of the receiver duct
T'_{so}	Temperature of the outside surface of the receiver duct after one iteration
α_S	Effective solar absorptivity of the receiver surface
γ	Specific heat ratio
ΔT	Temperature difference between T_{so} and T_{fm}
δT	Temperature difference between T_{fo} and T_{fi}
ε_S	The effective emissivity of the receiver surface
ε_λ	Total hemispherical emissivity of the selective surface
η_C	Compressor efficiency
η_{REG}	Regenerator effectiveness
η_T	Turbine efficiency
σ	Stephan-Boltzman constant

3.7 REFERENCES

1. Ritter, D., et.al., "Dynamic Power Conversion," Final Report, AA 420 Space Systems Design Course, Department of Aeronautics and Astronautics, University of Washington, Seattle, WA, March 1990.

2. Mechanical Technologies Incorporated, "Space Power Free Piston Stirling Engine Scaling Study," NASA CR-182218, 1989.

3. Stirling Technology Company, "25 kWe Solar Thermal Stirling Hydraulic Engine System," NASA CR-180889, 1988.

4. Duffie, J.A., W.A. Beckman, Solar Engineering of Thermal Processes, John Wiley & Sons, 1980, p. 168.

5. Van der Leij, M., Spectral-Selective Surfaces for the Thermal Conversion of Solar Energy, Delft University Press, 1979, pp. 64-96.

6. Zumdike, B., University of Washington, Personal communication, May 1990.

7. Incropera, F.P.and D.Dewitt, Fundamentals of Heat and Mass Transfer, John Wiley & Sons, 1985, pp. 394, 501-544.

8. Trueblood, B., Pressentin, R. and Brunkner, A. P., "Multimegawatt Nuclear Power System for Lunar Base Applications", Space Nuclear Power Systems 1987, El-Genk M. S. and Hoover, M. D., Eds., Orbit Book Company, Malabar, FL, 1988.

9. Klann, J.L., "Preliminary Mass Optimization of Solar-Brayton Space Power Systems", ITM-4210-5, Space Power Technology Division, NASA Lewis Research Center, August 1983.

10. Coombs, M. G., Morse, C. J., and Richard, C. E., "Preliminary Design Study of Nuclear Brayton Cycle Heat Exchanger and Duct Assembly," NASA CR-72816, 1971.

4.0 WASTE HEAT RADIATORS

Shawn Beard
Craig Douglas
Raymond Golingo
Drew Gonzalez
Tadd Lipscomb

4.1 INTRODUCTION

In any power generation plant there will be a requirement for the disposal of a certain amount of waste heat. In the design of a lunar base, additional complications arise due to the lunar environment. The only viable method of heat rejection in the lunar environment is radiation, since the lack of an atmosphere precludes the use of convection and evaporation as methods of rejecting the waste energy. Also, the thermal conductivity of the moon is very poor, which prohibits the use of conduction of the waste heat to the lunar regolith. The modules of a lunar base will be well insulated by the vacuum, therefore the lunar base will need a radiator to reject waste thermal energy. The overall amount of waste heat to be rejected by the radiator depends dramatically on whether a dynamic cycle power system or a photovoltaic array power system is selected. The dynamic cycle requires a radiator to radiate away the waste heat. The photovoltaic power system, on the other hand, is able to reject its own waste heat as shown in Chapter 2, therefore it does not require a separate heat rejection system.

The waste heat rejection system must take into account any additional background radiation emitted by the lunar surface, as well as any input from reflected solar radiation (Fig. 4.1). In addition, the radiator must have a high radiated power to mass ratio to minimize the mass of the radiator, since all the material for the lunar base must initially be transported from Earth.

Two possible radiator concepts were considered, the finned Heat Pipe Radiator (HPR) and the Liquid Droplet Radiator (LDR). HPRs have been under development since the late 1960's [1]. The device presented here uses a horizontal mother heat pipe (MHP) from which rise a series of vertical heat pipes (VHP) with fins, as shown in Fig. 4.2. The MHP receives

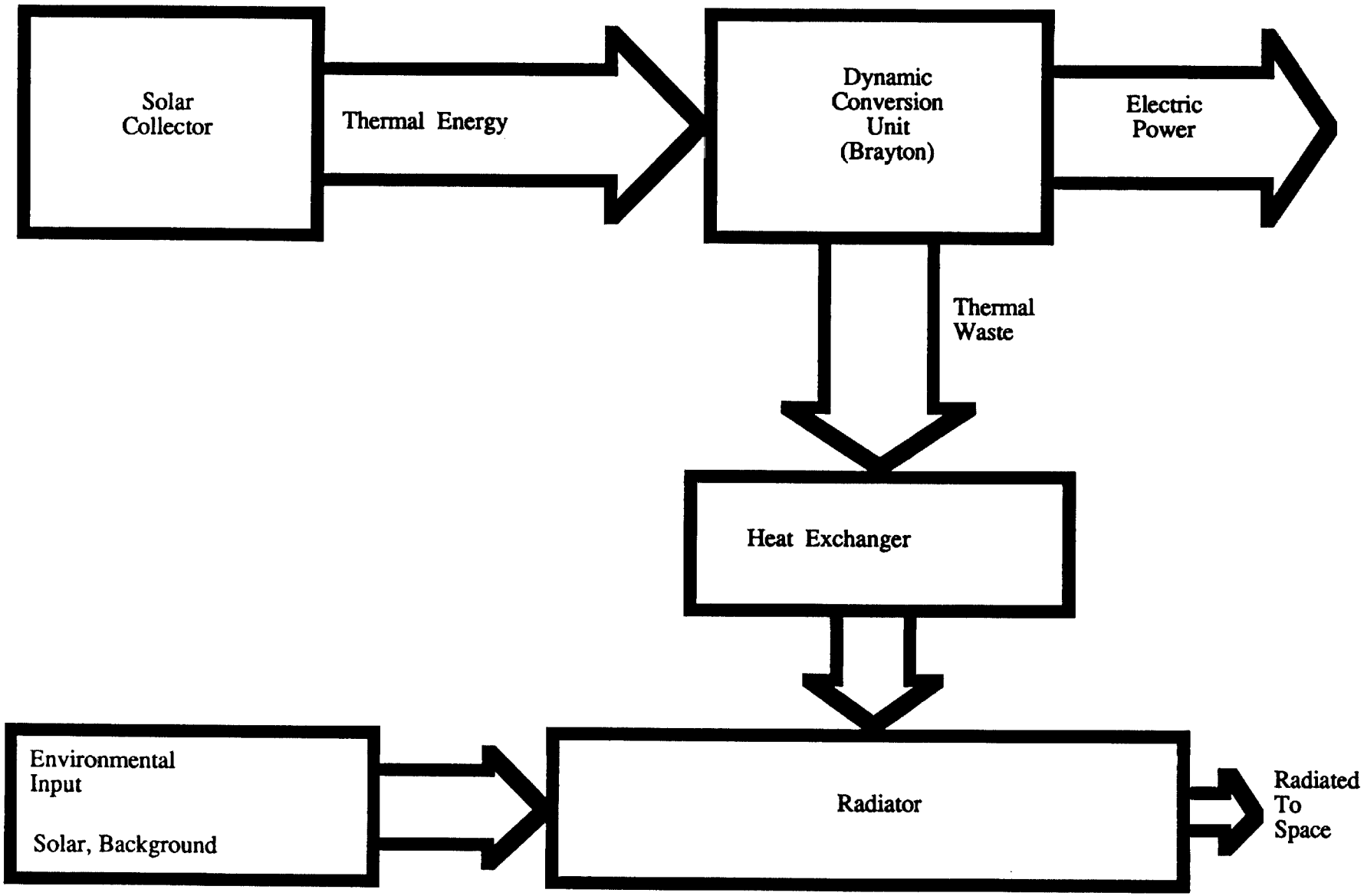

Fig. 4.1: System Integration Schematic.

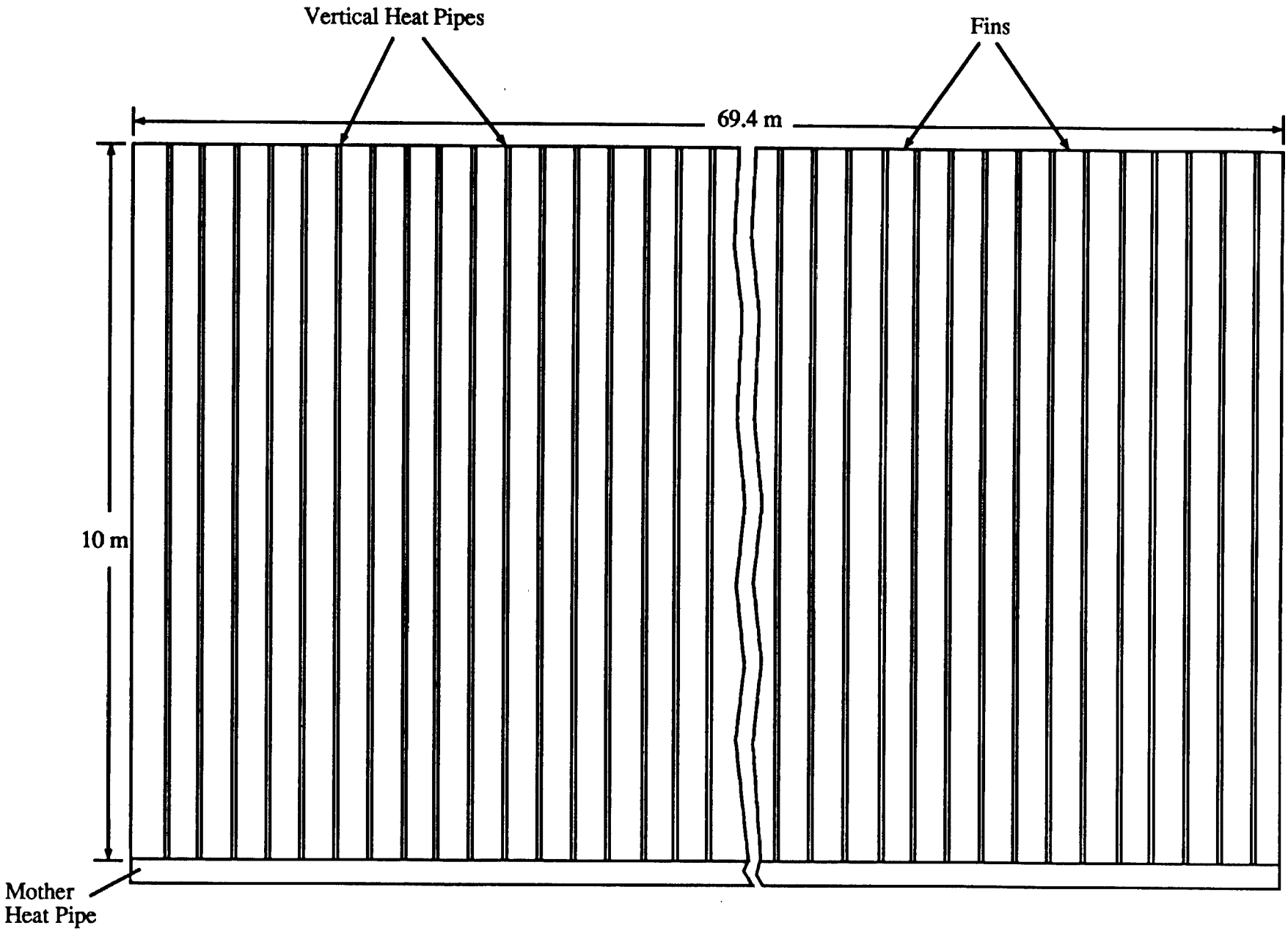

Fig 4.2. Lunar HPR configuration.

waste heat from the Brayton engine, via a heat exchanger, and conducts this heat to the VHP units. The VHP units conduct the thermal energy to fins, which radiate the waste heat into space. Suitable shading and reflecting surfaces are employed to minimize background input to the radiator. The unique design of the HPR utilizes available technology, which reduces the amount of research and development necessary before implementation of the waste heat rejection system.

The LDR, a concept developed at the University of Washington [2,3], utilizes a sheet of freely falling liquid droplets to radiate the waste heat (Fig. 4.3). The working fluid picks up waste heat from the power cycle, via a heat exchanger, and transports this heat to the LDR. At the LDR, the fluid is pumped up through pipes to an emitter, which expels the fluid as a vertical sheet of small spherical droplets. The droplets are then captured by a collector at the bottom of the sheet, and the fluid and is recycled through the system. The dominant factor in the potentially superior performance of the LDR is the high surface area to volume ratio of the small spherical droplets used to radiate heat. Most of the research for the LDR that has been carried out is for space applications, however, additional research is necessary to develop a full-scale working model.

4.2 HEAT PIPE RADIATOR

The Heat Pipe Radiator (HPR) uses a horizontal mother heat pipe (MHP) to which are connected a series of vertical heat pipes (VHP), with fins. The MHP receives waste heat from the Brayton engine, via a heat exchanger, and conducts this heat to the VHP units. The VHP units conduct the thermal energy to the fins, which radiate the waste heat into space.

4.2.1 PRINCIPLES OF HPR OPERATION

Waste heat from the Brayton cycle is transferred to the MHP (evaporator section) by a heat exchanger as shown in Fig 4.4. The thermal energy is transported through the MHP by

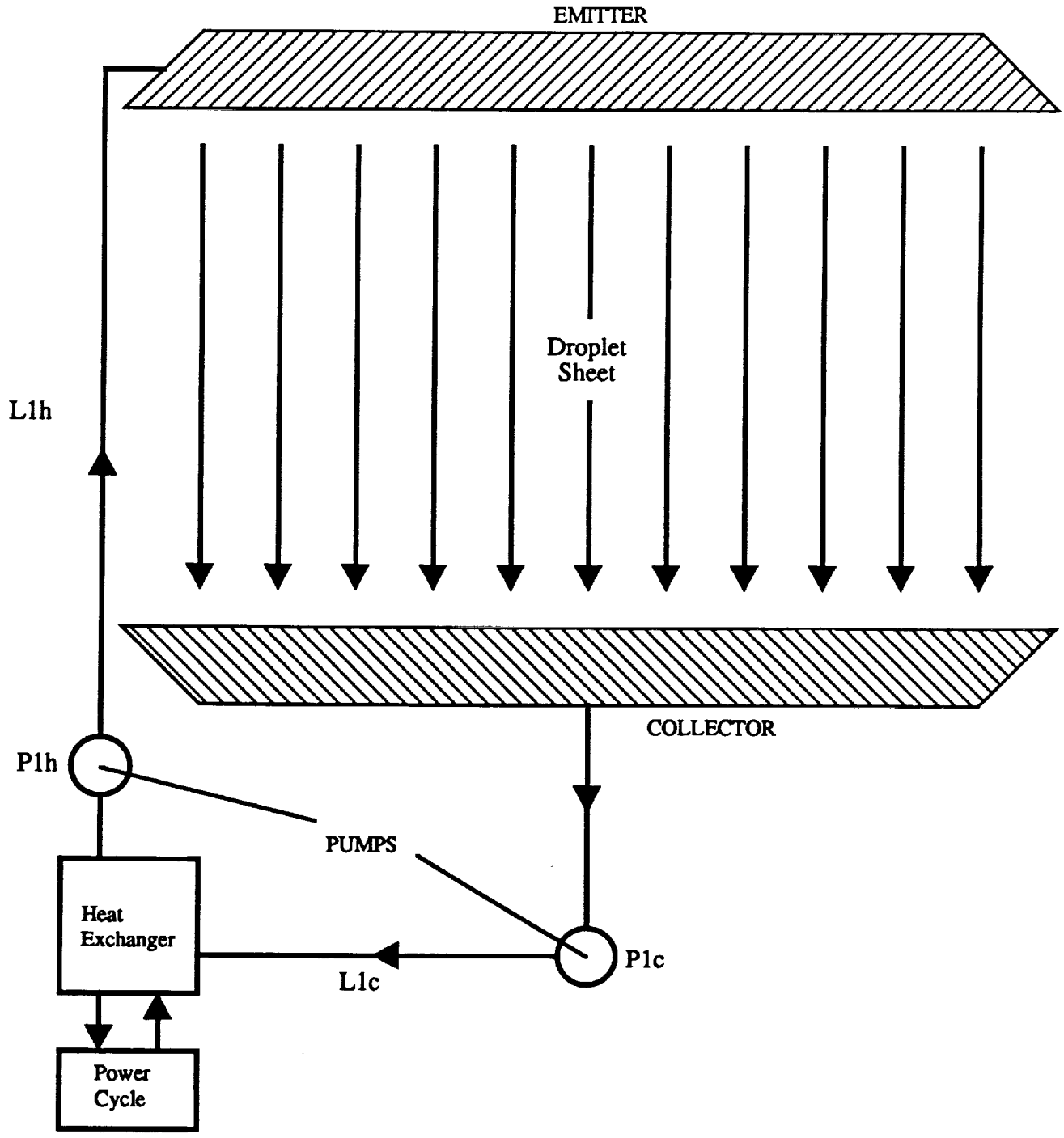

Fig. 4.3. LDR fluid management schematic.

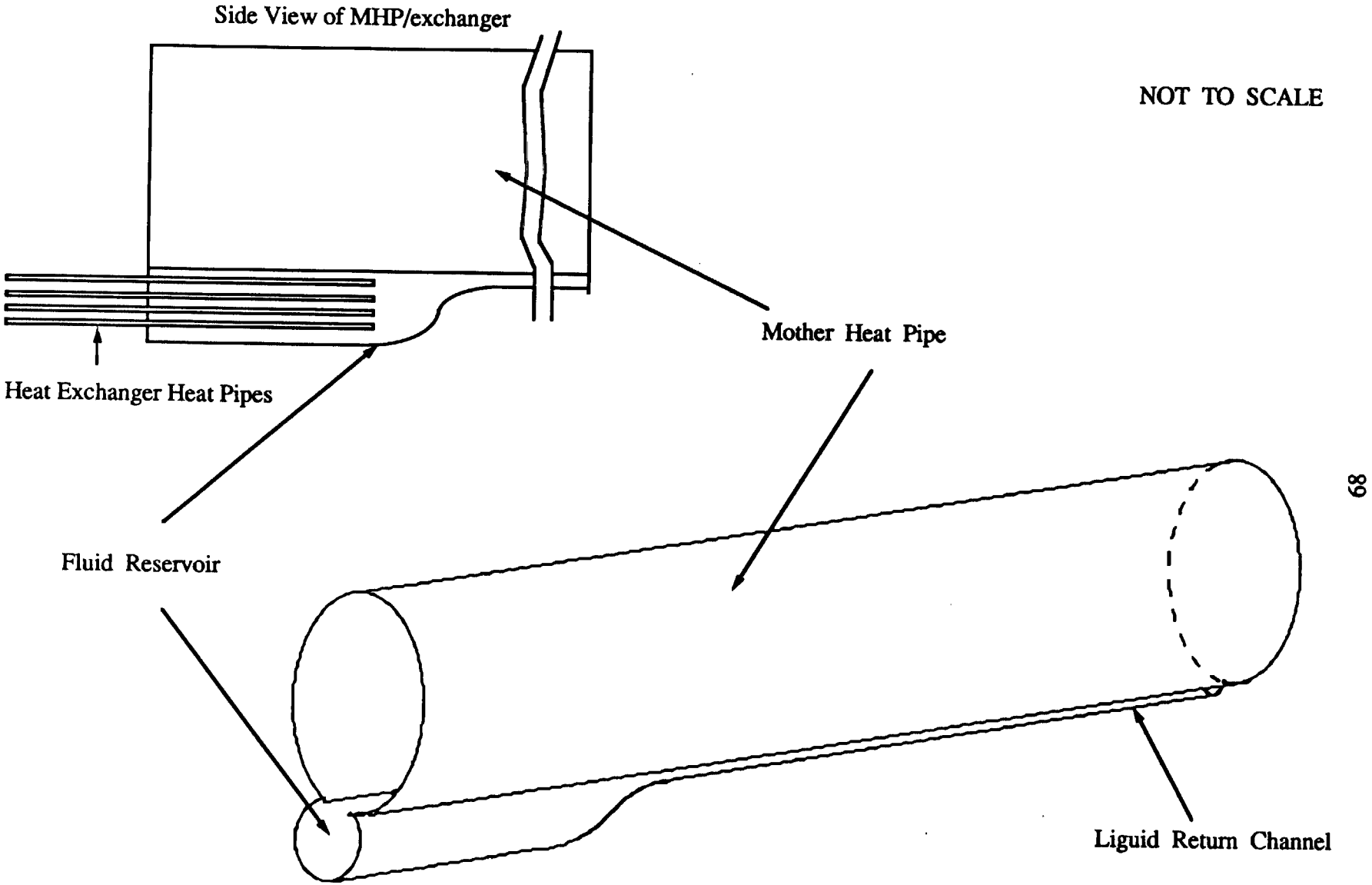

Fig. 4.4. Mother Heat Pipe and Heat Exchanger

vapor flow and conducted to the working fluid of the VHP units embedded throughout the length of the MHP. The waste heat is then transported through the VHP, via vapor flow, and conducted through the fins of the VHP where it is radiated away to space. The dominant factor of the HPR is the lack of moving parts required to transport the waste thermal energy. Additionally, independent VHP sections make the HPR resistant to single point failures. This helps to minimize the overall mass of the heat rejection system, since added components are not necessary to make the system redundant.

The fins will radiate away energy according to the Stefan-Boltzmann law:

$$\text{Power} = (A_{VHP}\varepsilon_{VHP} + A_{fin}\varepsilon_{fin})\sigma(T_{r1}^4 - T_b^4) \tag{4.1}$$

where A_{VHP} is the total radiating surface area of the VHP's, ε_{VHP} is the VHP emissivity, A_{fin} is the total radiating surface area of the fins, ε_{fin} is the fin emissivity, σ is the Stefan-Boltzmann constant, T_{r1} is the effective temperature of the VHP and fins, and T_b is the effective background temperature of space.

At the same time, however, the VHP and fins will absorb heat energy from direct and reflected sunlight, and lunar surface thermal reradiation. Also, additional VHP and fin sections are needed due to possible micrometeorite strikes. For these reasons, the required heat rejection area had to be increased by 9.5% .

The combination of these factors effectively determines the radiating area needed to dissipate the required amount of excess heat. The total planar area, A_1, required to radiate an amount of power, P_r, from a 2-sided VHP and fin section at T is

$$A = \frac{1}{2}\left[\frac{P_r}{\sigma\varepsilon(T_{r1}^4 - T_b^4)}\right] \tag{4.2}$$

The optimum radiating system for a lunar based power plant will have the largest possible radiated power per unit mass of the HPR. Two significant features of the HPR allow the weight to be lower than that of pumped-loop systems [1]. First, energy is transported by vapor flow and released via condensation. This results in heat transport rates exceeding those of any single phase system, and this is accomplished with a very small inventory of working fluid. Second, there is no fluid transfer to or from the heat pipe, therefore each VHP and fin section in a radiator array is independent. The heat pipe radiator may use a large number of heat pipe segments, allowing for a fraction of the pipes to be punctured by micrometeorites over a prescribed period of time. This enables the use of thin vertical heat pipe walls for weight minimization. Although segmentation is also possible with pumped-loop radiators, this requires a very complex system of components to isolate segments which are damaged by micrometeorites and it increases the weight of the entire system substantially [1].

4.2.2 VERTICAL HEAT PIPES & FINS

Waste heat is conducted from the MHP to the working fluid of the VHP sections embedded throughout the length of the MHP. The waste heat is then transported through the VHP, via vapor flow, and conducted through the fins of the VHP where it is rejected away into space.

A single finned VHP section is shown in Fig. 4.5. The choice of low density, high thermal conductivity materials such as pyrolytic graphite, minimizes the mass of the HPR system. The VHP consists of a thin central core sheet of 6-ply epoxy-graphite (for structural integrity), manufactured so that it lies between two pyrolytic graphite fins as shown in Fig 4.6. The fin layers on either side of the core sheet are manufactured to include D-shaped cylindrical heat pipe cavities, also made of pyrolytic graphite.

Pyrolytic graphite was chosen as the VHP material due to its light weight and excellent thermal conductivity in the plane of the fibers (1950 W/m-K). A thin lining of an inert material, such as tungsten, will be flashed on the inner surface of the D-shaped VHP to avoid

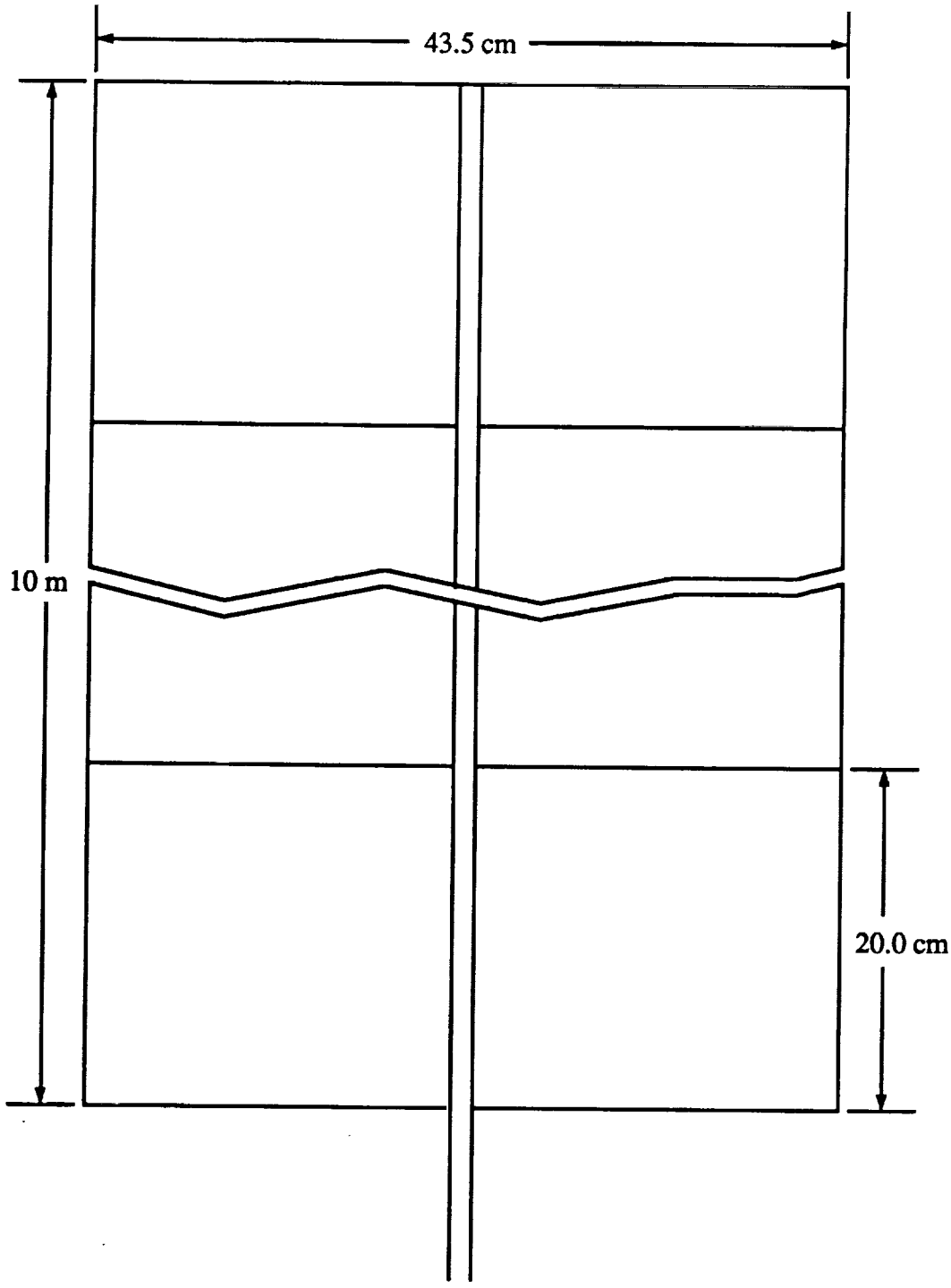

Fig. 4.5. Vertical Heat Pipe and Fin Configuration.

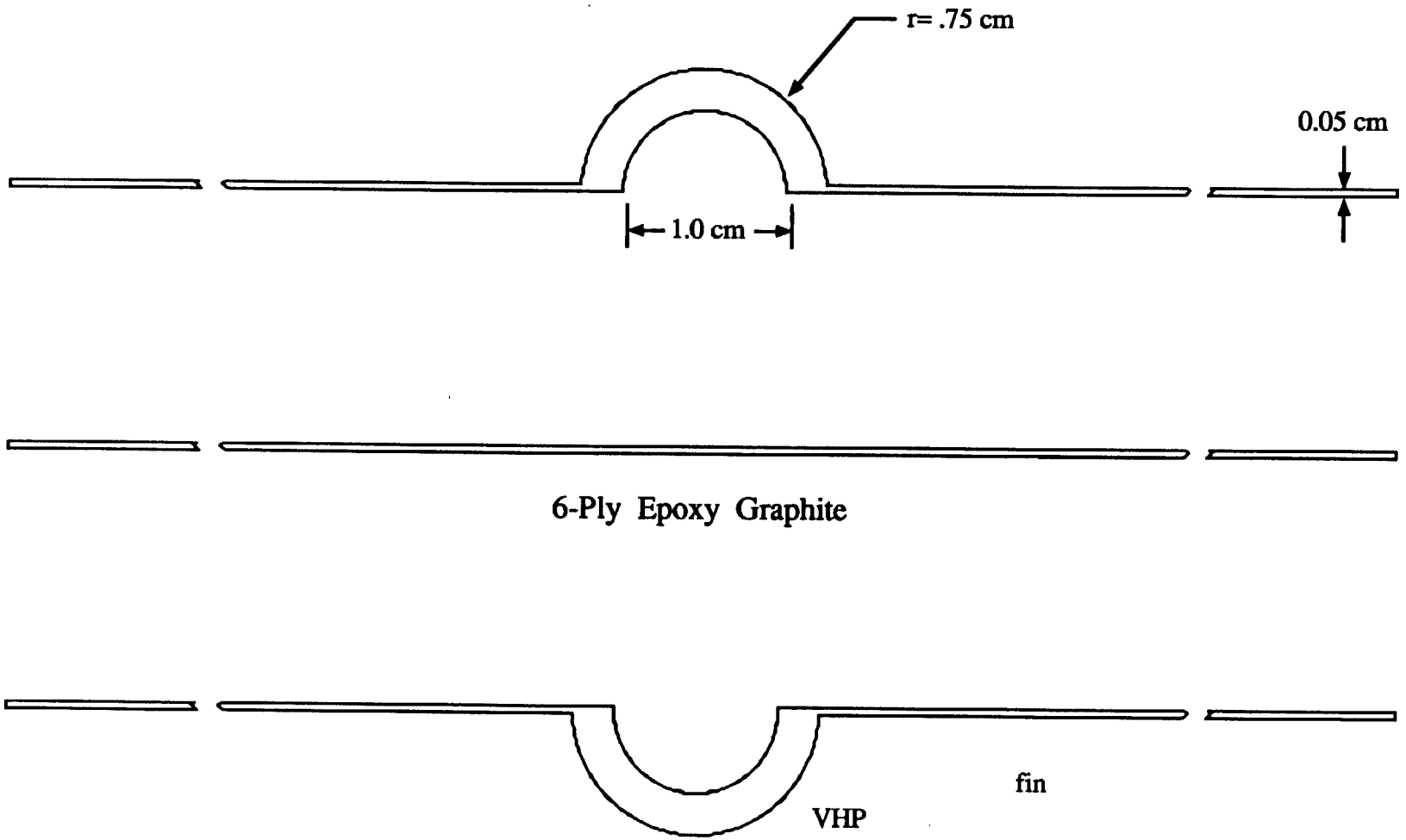

Fig. 4.6. Exploded view of vertical heat pipe and fin.

any reaction of the working fluid with the pyrolytic graphite material. The inner surface area of the D-shaped VHP is grooved to return the condensed working fluid to the evaporator section via capillary action. The presence of gravity also aids in returning the condensed working fluid to the evaporator section of the VHP. It should be noted that the pyrolytic graphite is a highly nonisentropic material in the area of thermal conductivity. The orientation of the fibers in the pyrolytic graphite must be precise in the manufacturing of the D-shaped VHP and fins.

The selection of an appropriate working fluid for the VHP is defined by the heat rejection temperatures and the working fluid freezing point. The fluid must be able to operate over a temperature range of approximately 300 K to 350 K, to coincide with the rejection temperature of the Brayton cycle. The additional requirement for a working fluid with a low freezing point arises due to the low ambient surface temperatures during the lunar night. This situation requires a start-up sequence which avoids the possibility of

damaging the heat pipe walls (see section 4.2.6). The liquid transport factor is the maximum amount of heat that can be transferred over the condensation area required to conduct this heat. A plot of the liquid transport factor of candidate fluids and their operating temperatures is presented in Fig. 4.7. Ammonia, with a temperature range of 200-400 K, was chosen as the working fluid. Its properties are listed in Table 4.1.

TABLE 4.1 Properties of ammonia at 300 K.

Density (vap)	9.041 kg/m^3
Heat of vaporization	1145 kJ/kg
Speed of sound	437.2 m/s
Melting Point	-77.7 C
Heat flux for HP cross sec.	4.525 MW/m^2

The VHP fins, which are an integral part of each VHP, are designed for light weight, structural integrity, and for high thermal conductivity. The materials chosen for the VHP fins are a thin 6-ply epoxy-graphite core sheet with two thin layers of pyrolytic graphite on each

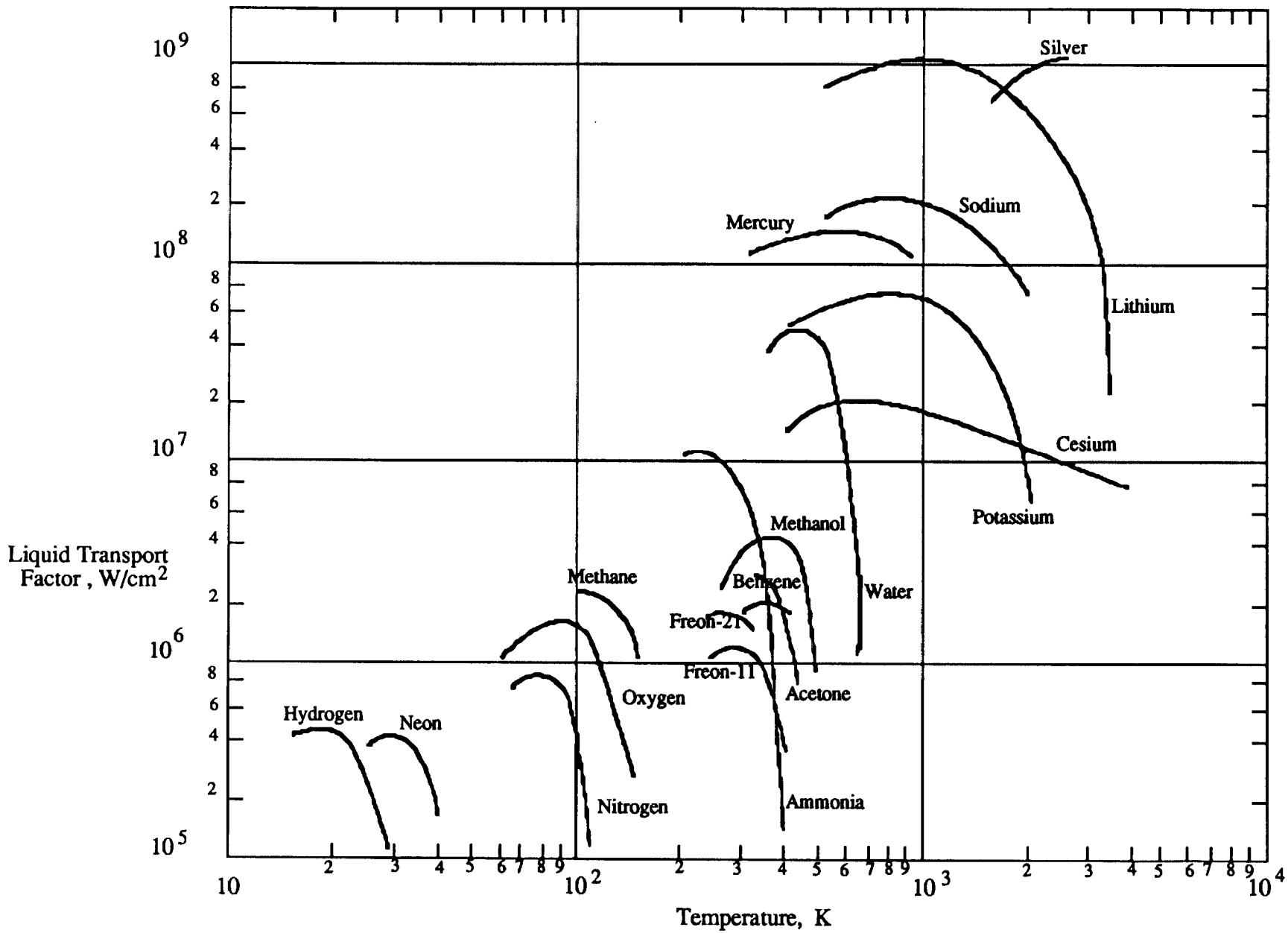

Fig. 4.7. Liquid transport factor vs temperature for various heat pipe working fluids.

side. The 6-ply epoxy-graphite fibers are arranged at 45° angles, which gives the fin the ability to handle any external loading caused by astronauts or micrometeorite strikes. The two thin pyrolytic graphite layers, 0.5 mm thick, in which the fibers are oriented horizontally, are attached to each side of the core sheet. This provides a lightweight fin material with excellent thermal conductivity for heat transfer considerations.

A finite-element program was generated to optimize the radiative power to mass ratio of the HPR for different fin widths. The corresponding temperature drop across the width of the fin is given by

$$\Delta T_i = \frac{q_i - q_{irad}}{R_i} \tag{4.3}$$

where ΔT_i is the change in temperature across each incremental vertical strip of fin as shown in Fig. 4.8, q_i is the amount of heat entering each incremental strip of fin, q_{irad} is the amount of heat radiated by each incremental strip of fin, and R_i is the thermal resistance for each fin increment. The amount of heat radiated by each incremental strip of fin is given by the equation

$$q_{irad} = 2\varepsilon dA_i \sigma T_i^4 \tag{4.4}$$

where ε is the fin emissivity, dA_i is the incremental fin area, σ is the Stefan-Boltzmann constant, and T_i is the incremental fin temperature assumed constant for each successive fin increment. The thermal resistance for each increment is given by the equation

$$R_i = \frac{L_i k}{t_i} \tag{4.5}$$

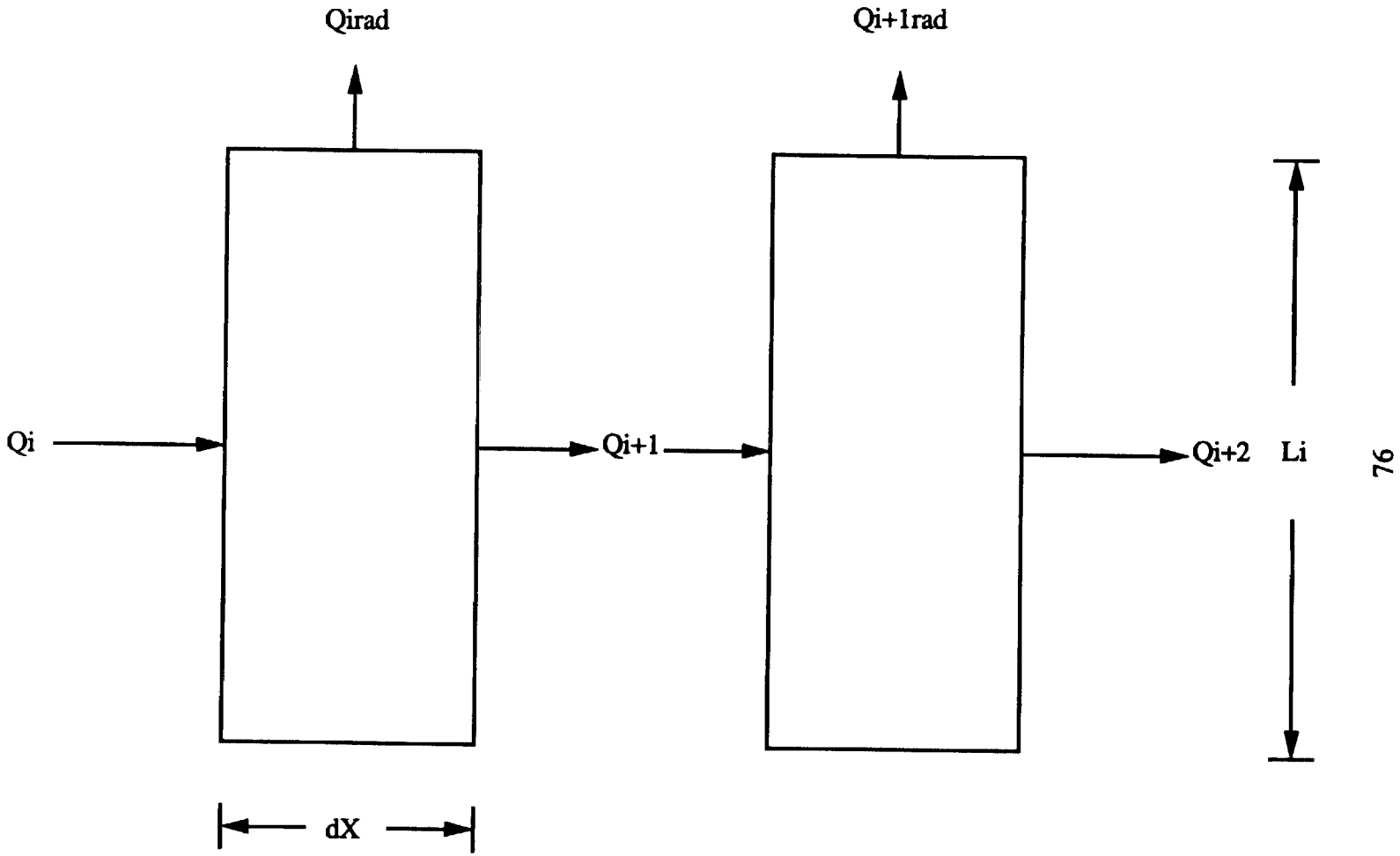

Fig. 4.8. Schematic of Fin Finite Element

where L_i is the height of an incremental strip of fin, k is the thermal conductivity of pyrolytic graphite, and t_i is the thickness of the incremental strip of fin.

The temperature drop in the VHP fins for the Brayton cycle rejection at a temperature of 303 K is only 2%. The extra area and therefore additional weight penalty is smaller than that which would occur if heat pipes without fins were used.

The VHP fins are segmented throughout this height, so that each side of the VHP contains 30 fin sections. A VHP section is shown in Fig. 4.5. The segmentation of each fin will ensure that damage by a micrometeorite strike will not reduce the heat rejection capability of each successive VHP section by a substantial amount. Also, any damaged VHP and fin section can be replaced by astronauts so that its heat rejection capability will be restored to normal.

4.2.3 MOTHER HEAT PIPE

The function of the MHP is to deliver the heat from the Brayton engine to the vertical heat pipes at a constant temperature. The MHP must be able to perform consistently throughout the required temperature ranges. In addition, because it is a single point of transference of heat to the VHP, it must have the structural integrity to withstand micrometeorite damage.

Figure 4.4 shows a schematic of the MHP. It consists of a large pipe with two channels, one for vapor, and a small channel on the bottom which acts as a return path for the condensed working fluid to the reservoir located at the evaporator section of the MHP. The liquid returns by gravity-assisted capillary action to the reservoir, where it is vaporized. The vapor then travels throughout the length of the MHP, condensing on the sockets and the socket annular fins of the MHP. The waste heat is then conducted to the VHP's. The condensed

working fluid falls to the bottom of the MHP, where it is transported back to the evaporator section, and the cycle repeats.

The waste heat from the power cycle is transferred to the evaporator section of the MHP by a heat exchanger consisting of small heat pipes extending directly from the Brayton engine system to the MHP . The number of heat pipes in the heat exchanger, n_x, can be determined from the following equation:

$$n_x = \frac{q'}{UA_x\Delta T_{ln}} \tag{4.6}$$

where q' is the heat flux, U is the overall heat transfer coefficient, A_x is the surface area of each heat pipe, and ΔT_{ln} is the log mean temperature difference of the working fluid in the Brayton engine, or the pumped-loop transfer system, and the constant temperature heat exchanger heat pipes. Because the internal conditions of the Brayton engine have not been completely defined, the overall heat transfer coefficient cannot be determined. Once determined, the number of pipes can be calculated by specifying a desired temperature for the radiator.

The Brayton engine requires that the compressor inlet temperature be 330 K and the regenerator exit be at 400 K. The radiator operating temperature is 303 K, which limits the choices of working fluids for the heat pipes. As in the case of the VHP, the working fluid chosen for the Brayton cycle is ammonia. When sizing the MHP, both the structural integrity to withstand micrometeorite strikes and the flow conditions of the vapor must be considered. Micrometeorite protection is discussed separately, so only the vapor flow requirements are considered here. It is desirable to avoid sonic flow of the vapor due to compressibility effects, therefore the MHP must be large enough to allow the mass flow rate required of the vapor to result in vapor velocities well below sonic. The critical cross sectional area A_{M1}, which results

in sonic velocity of the vapor is computed from

$$A_{M1} = \frac{q''}{\rho_v a h_v} \tag{4.7}$$

where q" is the maximum amount of heat per unit time required to transfer the waste heat, ρ_v is the vapor density, a is the speed of sound in the vapor, and h_v is the heat of vaporization. The same method of finding the sonic cross-sectional area is used in the design of the VHP to reduce the vapor velocity to well below sonic. Exact dimensions and mass for the MHP are included in the summary of the HPR design parameters listed in Table 4.2.

for connecting the VHP and fins to the MHP. The design utilizes the concept of inserting the bottom of the VHP, which extends below the fin sections, into a socket in the MHP, as shown in Fig. 4.9. This socket is lined with a conductive gel to decrease contact resistance between the MHP and VHP. The sockets inside the MHP is manufactured with fins parallel to the vapor flow to improve heat transfer to the VHP.

Fig. 4.9

4.2.4 HPR CONFIGURATION

The final configuration of the HPR is designed for an average heat rejection temperature, T_{rs}, of 303 K for each of the 5 separate engines which generate 443kW of waste heat each. The dynamic cycle HPR dimensions are 10 m high by 69.4 m in length per engine to form a radiating area of 1388 m^2.

The finned vertical heat pipe sections are oriented parallel to the lunar equator. This arrangement reduces the view factor between radiator segments to zero and prevents direct solar energy input to the vertical heat pipes and fins. Table 4.2 provides a summary of the HPR design parameters.

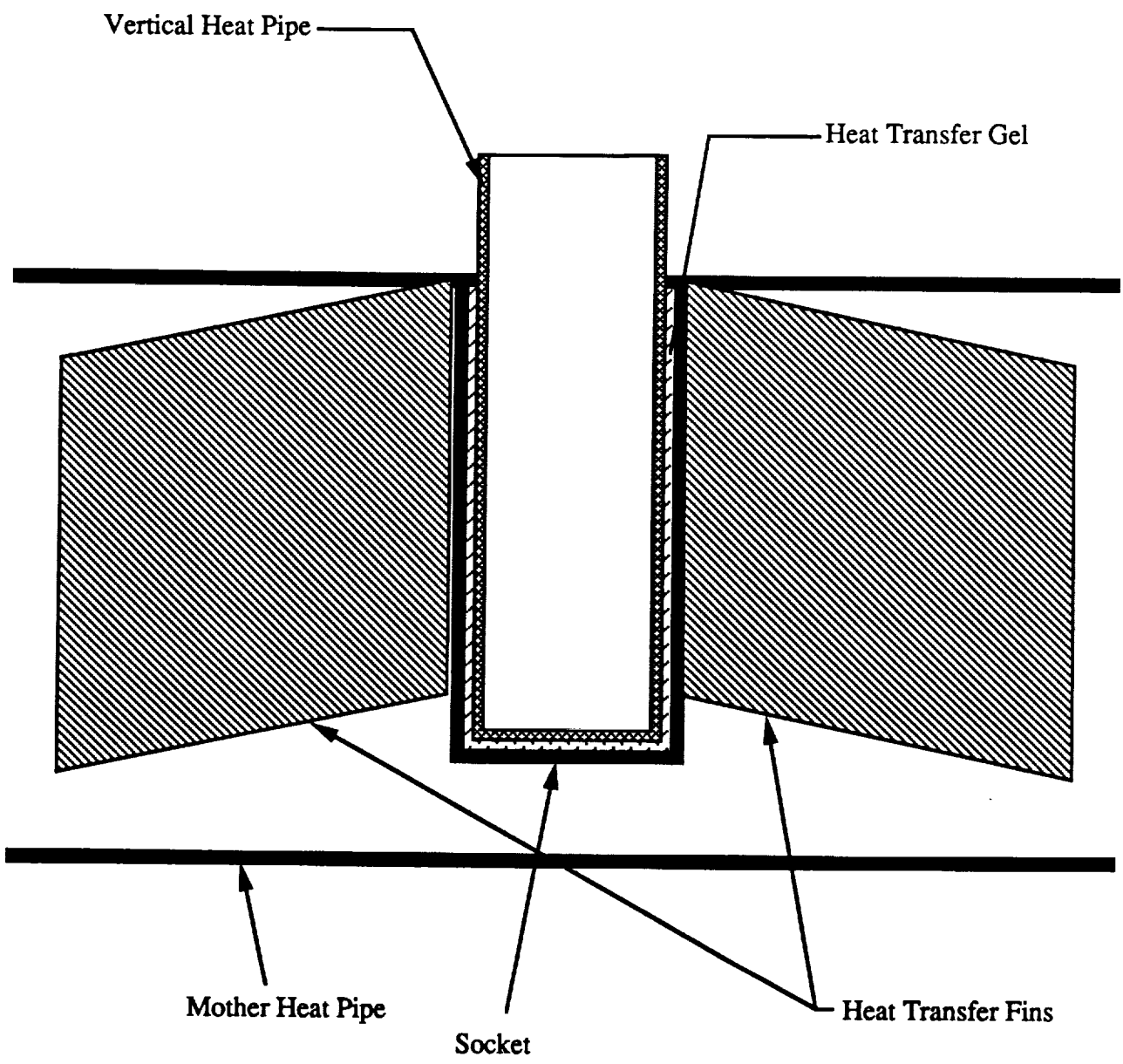

Fig. 4.9. Mother heat pipe and vertical heat pipe connection schematic.

TABLE 4.2: HPR Design Parameters.

MATERIALS:

GRAPHITE, PYROLYTIC:

Melting point	2273 K
Density	2210 kg/m^3
Thermal conductivity to parallel layers	1950 W/m K
Thermal conductivity to perpendicular layers	5.70 W/m K
Emissivity	0.8

GRAPHITE, FIBER EPOXY:

Melting point	450 K
Thermal conductivity	11.1 - 0.87 W/m K

BRAYTON RADIATOR:

Total heat rejected	480 kW/engine
HPR overdesign for peak mid-day solar flux	9.0%
Temperature of VHP	303 K
Working fluid	Ammonia
Outer diameter of VHP	0.015 m
Inner diameter of VHP	0.010 m
Height of VHP	10 m
Width of fin	0.435 m
Thickness of pGraphite layer	0.0005 m
Total fin mass	16.70 kg/fin
Heat rejected	3000 W/fin
Outer diameter of MHP	0.16 m
Inner diameter of MHP	0.14 m
Mass of MHP	10.4 kg/m
Total number of fins	160 fins
Total length	69.6 m
Total mass of fluid	100.0 kg
Total mass	3490 kg/engine

4.2.5 CONTROL SYSTEMS REQUIREMENTS

The control system must be able to deal with variable power demand for the Brayton cycle since the power station output will fluctuate slightly according to the total demand of the station's activities. There will also be the need to deal with start-up dynamics each lunar morning when the Brayton engines are activated.

Heat pipes normally have limited operating temperature when they contain only one working fluid. Their temperature range can be widened by the addition of an inert gas such as nitrogen. It works by changing the pressure in the VHP, thus allowing the working fluid to vaporize at lower temperatures [4]. Using this method, the HPR will be able handle fluctuations in the Brayton cycle without any additional control system.

During the lunar night, the Brayton engines will be turned off, producing no heat. Without any heat to reject, the temperature of the Brayton cycle radiator will drop to approximately that of the nighttime lunar surface (116 K) [5], and the temperature of the Brayton radiator working fluid, ammonia, will fall below its freezing point (175.15 K). This can cause problems when attempting to start-up the heat pipes for the lunar day. The heat pipes must pass through transient states before reaching steady state operation. With a low initial vapor density or a frozen working fluid, the heat pipe transient can be very long (hours) and may result in a frontal start-up as opposed to a uniform start-up. A frontal start-up occurs when the working fluid at the bottom of the vertical heat pipe begins to heat up and the vapor cannot make its way up because of blockage by frozen fluid, or if it does make it up the heat pipe, there is not enough vapor density to allow the condensate to flow down the sides. This results in large localized temperature nonuniformities which may cause the destruction of the heat pipe walls.

The start-up problem can be minimized by the presence of a noncondensable gas in the heat pipe, or by the use of a radiation shield or thermal blanket at night. A design for a radiation shield is shown in Fig 4.10. It consists of two highly reflective panels, one on each side of the HPR, which are opened during the day to reflect the radiated waste heat away from

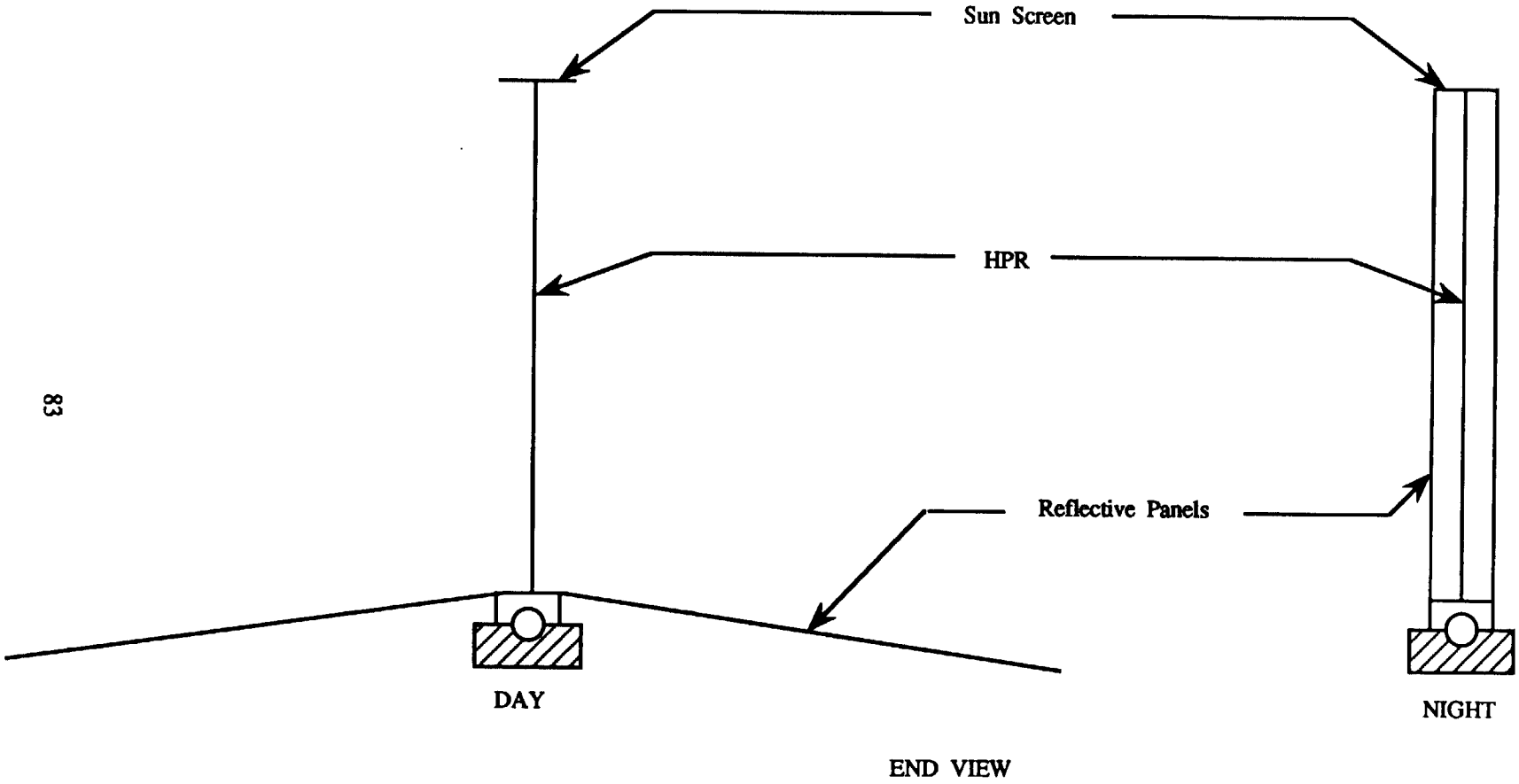

(a) Panels fold down during the day to be used as reflectors.

(b) Panels fold up at night to be used as insulative radiation shields.

Fig. 4.10: HPR side panel configuration for (a) day and (b) night.

the HPR and to reduce heat input from the regolith, and closes during the night to reflect the thermal radiation back to the HPR. During the day, the panels will be folded down, making an obtuse angle with the HPR. This minimizes the view factor to the lunar surface, thus reducing the amount of lunar radiation on the HPR. At night, the panels fold
up parallel to the HPR and reflect the radiation back to the HPR. The panels consist of a lightweight insulator, such as urethane, coated with highly reflective gold or aluminum foil on each sides.

In addition, the lunar HPR control system must be able to deal with the heat input to the HPR vertical heat pipes and fins from the lunar environment. This input varies greatly during the lunar day. The variation of lunar surface temperature throughout the day is shown in Fig. 4.11 [4]. The radiator will radiate excessive heat during the lunar night since the background temperature is very low, and the opposite condition would be experienced during the lunar day.

4.2.6 MICROMETEORITE STRIKES

As referred to earlier in this chapter, the radiators will need to be protected from micrometeorite damage. This can be done by increasing the thickness of the heat pipes or by including redundancies in the system design. Increasing the thickness of each heat pipe rapidly increases the mass of the system, and therefore this is not a viable option for a lunar power plant. However, adding redundancies to the heat rejection system, instead of increasing the thickness, keeps the mass of the radiator to a minimum.

The meteorite flux rate for the moon has, to date, not been established, therefore the Whipple 1963A flux rate was used to calculate meteorite damage [3]. The number of strikes per square meter per second, $F_>$, is given by

$$F_> = \alpha_o m_o^{\beta_o} \tag{4.8}$$

where α_o is the meteoroid flux constant (5.30×10^{-11}), m_o is the meteoroid mass and β_o is a constant (1.34) in the meteoroid equation.

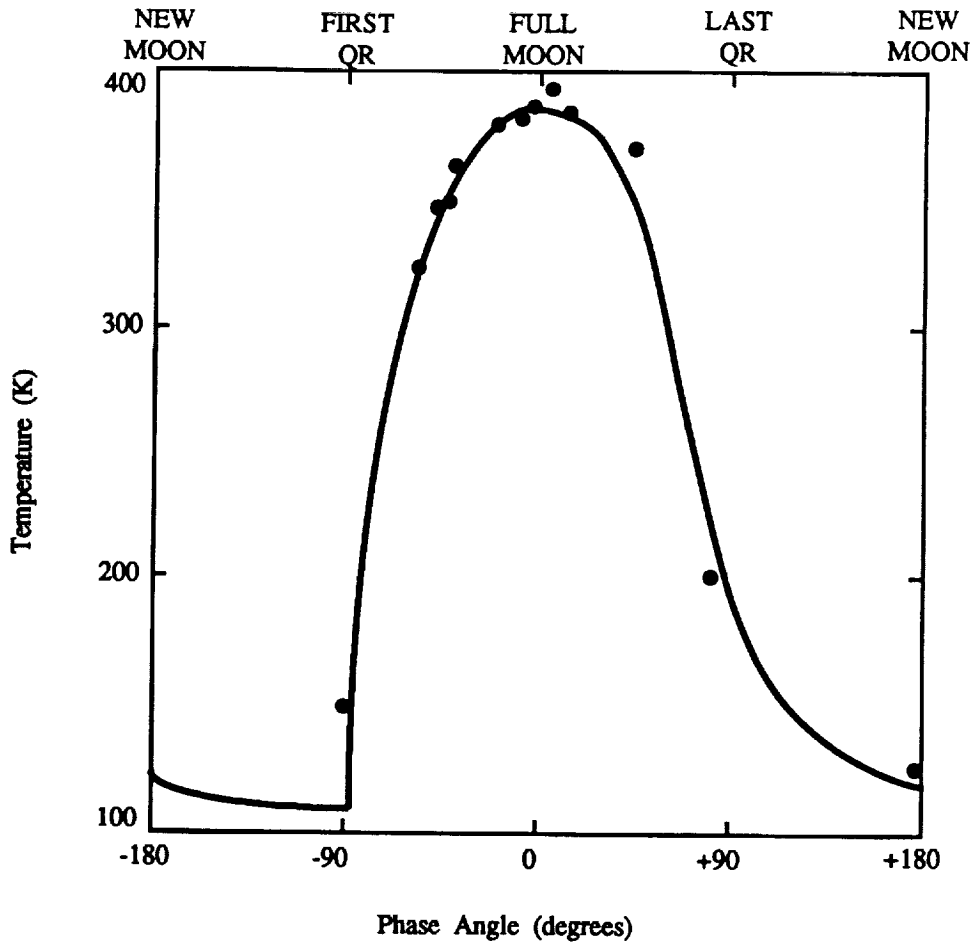

Fig. 4.11: Lunar surface temperature variation.

C-2

On the moon, meteorites travel with a higher velocity than in space because of the gravitational acceleration, and therefore we can expect they will hit the radiator structure with more energy than predicted by the Whipple 1963A flux rate. Their average velocity vector will be oriented at a somewhat smaller angle with the radiator because of the vertical acceleration of the meteorites. This orientation of the meteorites was assumed to cancel the effect of the increased velocity of the meteorites.

With the Whipple 1963A flux rate and penetration equations, it can be shown that

$$H = \left[\frac{6.15\left(\frac{t}{10000}\right)^{.25} A^{.25}}{E^{.33}\rho^{.17}} \right]^4 \tag{4.9}$$

where H is the number of penetrating meteorite strikes, t is the heat pipe thickness, and E is the modulus of elasticity and ρ is the density of the heat pipe material, respectively.

It was assumed that if a meteorite penetrates a VHP, that VHP will no longer be operational. With this assumption, the probability, P, of a VHP surviving is given by

$$P = e^{-H} \tag{4.10}$$

At the end of the design mission period (10 years), the number of operational VHP's, N_{VHP}, is known. The number of VHP's which are needed at the beginning of the mission, N_{VHPO}, is thus given by

$$N_{VHPO} = \frac{N_{fs} + \zeta\sqrt{N_{VHP}P(1 - P)}}{P} \tag{4.11}$$

where ζ is the normal standard deviation, determined from statistical probability tables. The survival probability assumed for each radiator is 0.99, which defines ζ equal to 2.33. To determine the number of heat pipes surviving, N_{fs}, the number of operational VHP's after a 10

year mission period, N_{VHP}, was set equal to the number of heat pipes that were needed in the radiator. N_{VHPO} is then calculated. Numerical iteration was carried out until N_{VHPO} is equal to N_{VHP}.

The mother heat pipe cannot sustain any meteorite damage. Therefore, the MHP wall thickness must be determined. It was assumed that the chance of the MHP failing should be 1/1000 (H = .001) over ten years and the thickness, t, was calculated from Eq.4.9.

The only heat transfer of concern is that which occurs within the MHP itself. Therefore the temperature drop due to the added thickness is irrelevant. A thicker mother heat pipe would benefit the problem of the working fluid freezing during the lunar night by acting as an insulator. The additional weight due to thickness must be tolerated, since the MHP is vital to the lunar radiator system.

4.3 LIQUID DROPLET RADIATOR

The Liquid Droplet Radiator (LDR) utilizes a sheet of freely falling liquid droplets to radiate the waste heat (Fig. 4.3). The working fluid picks up waste heat from the power cycle, via a heat exchanger, and transports this heat to the LDR. At the LDR, the fluid is pumped up through pipes to an emitter, which expels the fluid as a vertical sheet of small spherical droplets. The droplets are then captured by a collector at the bottom of the sheet, and the fluid is recycled through the system.

4.3.1 PRINCIPLES OF LDR OPERATION

The LDR working fluid picks up waste heat from the power cycle at a waste heat exchanger and transports this heat energy to the LDR. At the LDR, the fluid is expelled from the emitter as a multitude of fine droplets which fall freely, radiating the heat away . A collector is positioned at the bottom of the droplet sheet to collect the droplets and pump the fluid back through the system. The dominant factor in the potentially superior performance of the LDR is the high surface area to volume ratio of the small spherical droplets used to radiate

heat. This advantage becomes more pronounced as the magnitude of heat rejection required increases, and hence, the radiating area required increases. The thermal energy, E_1, stored in a droplet at effective temperature T_{eo} is:

$$E_1 = m_d C_p T_{eo} \tag{4.12}$$

where m_d is the droplet mass, and C_p is the specific heat of the droplet fluid.

The droplets will radiate away energy according to the Stefan-Boltzmann law:

$$\text{Power} = A_d \varepsilon_d \sigma T_{eo}^4 \tag{4.13}$$

where A_d is the total effective radiating surface area of the droplet, ε_d is the droplet emissivity, and σ is the Stefan-Boltzmann constant.

At the same time , however, the droplets will absorb heat energy from background radiation (i.e. direct and reflected sunlight and lunar surface thermal reradiation). An energy balance yields a differential equation for the individual droplet temperature with respect to time:

$$S\alpha a_1 - A\varepsilon_s \sigma T_{s1}^4 = m_d C_p \frac{dT}{dt} \tag{4.14}$$

where S is the incoming radiation flux from the environment , α is the droplet absorptivity, a_1 is the projected area of the droplet in the direction of the flux, ε_s is the effective emissivity of the droplet sheet , T_{s1} is the effective radiator temperature, and A is the total radiating area.

The combination of these factors effectively determines the radiating area needed to dissipate the required amount of excess heat. Note that the above equations are for individual droplets in free space. In reality, the properties of the droplet sheet will differ from those of an individual droplet since part of the radiation from any one droplet will irradiate neighboring

droplets. Thus, there will be an optimum droplet spacing, an optimum thickness, t, of the fluid sheet, and a characteristic emissivity, ε_s, for the fluid sheet.

The initial temperature , T_{o1} , and final temperature, T_{b1}, of the LDR operation are determined by the working range of the fluid, as discussed in Section 4.3.2. These two temperatures, T_{o1} and T_{b1}, determine the droplets' time of flight, t_f. This is given by:

$$t_f = \frac{2C_p m_d \tau_o}{3\sigma\varepsilon_s}\left(\frac{1}{T_{b1}^3} - \frac{1}{T_{o1}^3}\right) \tag{4.15}$$

where m_d is the mass of a droplet = $(\pi/3)(D/2)^3$, τ_o is the optical density of the fluid ~ $1/(2\varepsilon_o)^4$, and D is the droplet diameter.

This corresponds to a height for the droplet sheet , h_1, which can be calculated from:

$$h_1 = \frac{1}{2}g_l t_f^2 + v_o t_f \tag{4.16}$$

where v_o is velocity of droplets exiting the emitter and g_l is the lunar gravitational acceleration.

The mass flow of the droplets is determined by the amount of heat rejection required and the two temperature limits of the droplets. The planar area required to radiate an amount of power P_r from a 2 -sided droplet sheet of effective sheet emissivity ε_s operating at an effective temperature, T_{s1}, is

$$A = \frac{P_r}{2\sigma\varepsilon_s\left(T_{s1}^4 - T_b^4\right)} \tag{4.17}$$

where T_b is the effective background temperature.

The optimum radiating system for a lunar based power plant will have the largest power radiating per unit mass. Thus, the high surface area to mass ratio of a spherical droplet, which greatly enhances the effective emissivity of the radiating sheet, is a great advantage for a radiating system.

4.3.2 RADIATING FLUID SELECTION

The LDR operating fluid must be able to withstand the local environment and promote overall system efficiency. The environmental concern for lunar siting is the lack of an ambient pressure, which necessitates a fluid with a very low vapor pressure over the LDR working temperature range.

The system efficiency, or power output per unit mass, is another concern since it will require a radiator that is light , yet effective. Therefore, the fluid of choice should have a high emissivity, high heat capacity, broad heat rejection temperature range and yet have a low density relative to other candidate fluids. A high emissivity increases the rate of heat rejection, thereby lowering the time of flight for the droplets and reducing the height of the radiator. A high heat capacity allows the fluid to carry more thermal energy, lowering the mass flow and the amount of fluid required but increasing the time of flight. A low vapor pressure decreases the need to replace fluid lost due to evaporation. High working temperatures have a powerful influence on the rate of heat rejection since radiated power increases as temperature to the fourth power. Low densities to specific heat ratios decrease the overall mass of the fluid.

There are chemical and physical limits on the degree to which a fluid can be tailored to fit necessary requirements. The fluid must be available "off the shelf" so it will most likely have other characteristics which may affect the LDR design. For example, a viscous fluid will affect pumping and plumbing requirements, and a corrosive material may be particularly harmful to piping and other system components.

Fluid selection begins by determining which fluids have a low enough vapor pressure to prevent excessive evaporation loss of the fluid. Figure 4.12 shows the vapor pressures of candidate fluids versus operating temperature range. The maximum allowable temperature of the fluid can then be determined so that the fluid loss due to evaporation is not excessive. The low end temperature of candidate fluids is limited by excessive viscosity or freezing of the fluid. During the lunar night, the Brayton engines are shut down, and the selected fluid will be

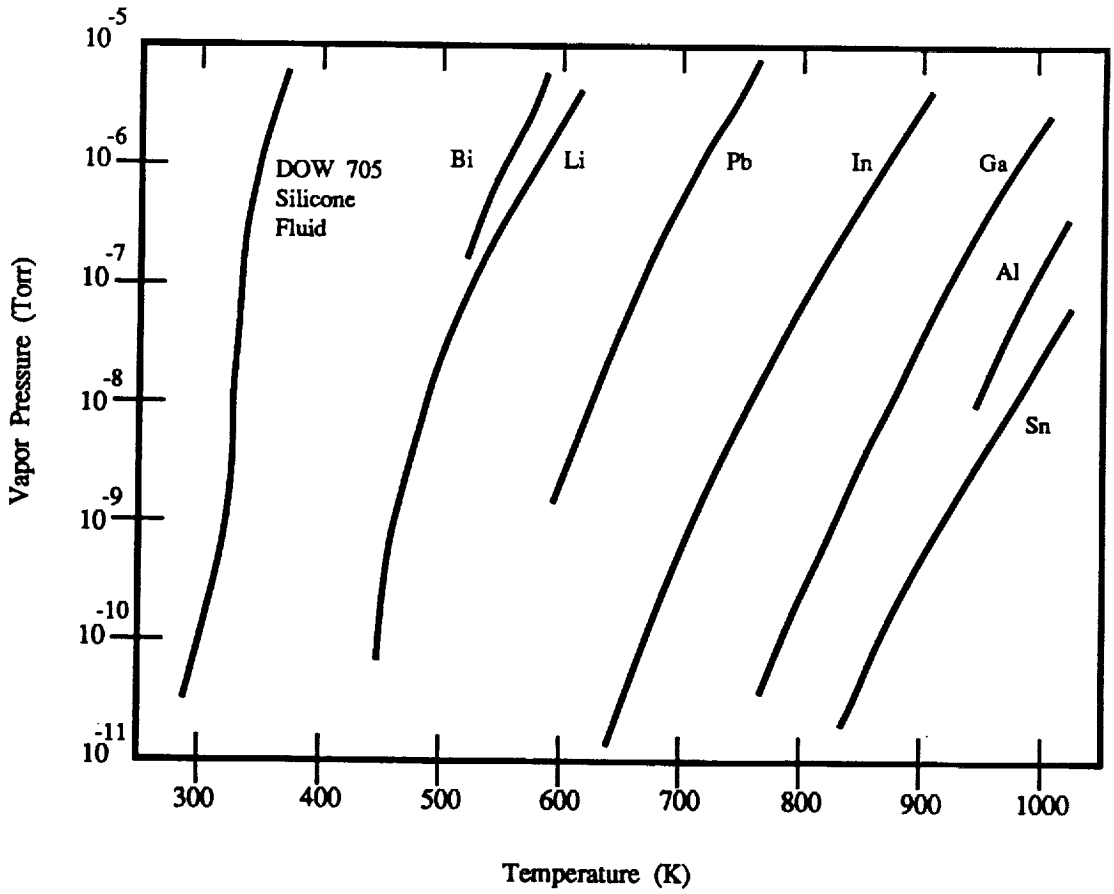

Fig. 4.12: Vapor Pressures Of Candidate Radiator Fluids.

stored in the tank that carried it to the Moon, and will be buried under the insulating regolith.Each of the promising fluids is then given a figure of merit based on its droplet emissivity e_o divided by density ρ. Figure 4.13 shows this figure of merit and the temperature range of the candidate fluids. In addition to the figure of merit, temperature has a strong effect on the power radiated:

$$\frac{\text{Power}}{\text{Mass}} = k_o\left(\frac{\varepsilon_o}{\rho}\right)T_{s1}^4 \tag{4.18}$$

where k_o is a constant of proportionality and ε_o/ρ is the figure of merit.

Plots of constant power per unit mass are also shown in Fig. 4.14. This figure shows clearly that there are three fluids of similar characteristics with a high power to mass ratio: tin, lithium, and DOW 705. Loss of thermal efficiency in the dynamic converter due to a high rejection temperature eliminates tin, leaving only DOW 705 silicone oil and lithium. Analysis of the power conversion cycle showed that the dynamic conversion efficiency rises from ~20% for lithium to ~35% for DOW 705. This substantial increase in conversion efficiency allows for a smaller power converter, thus reducing the heat load to be rejected by the radiator. In addition, DOW 705 is far less corrosive than lithium, does not solidify at the low end temperature expected to be encountered, and its higher emissivity enhances the performance of the radiator. A list of the physical characteristics of DOW 705 is given in Table 4.3.

4.3.3 EMITTER

The radiating droplet sheet is formed by emitting the fluid in the form of droplets from a device appropriately called an emitter. The emitter consists of a tapered manifold filled with the pressurized fluid, which is sprayed out through an orifice plate running along the length of the manifold. The fluid jets emerging from the multitude of orifices are broken up into droplets by

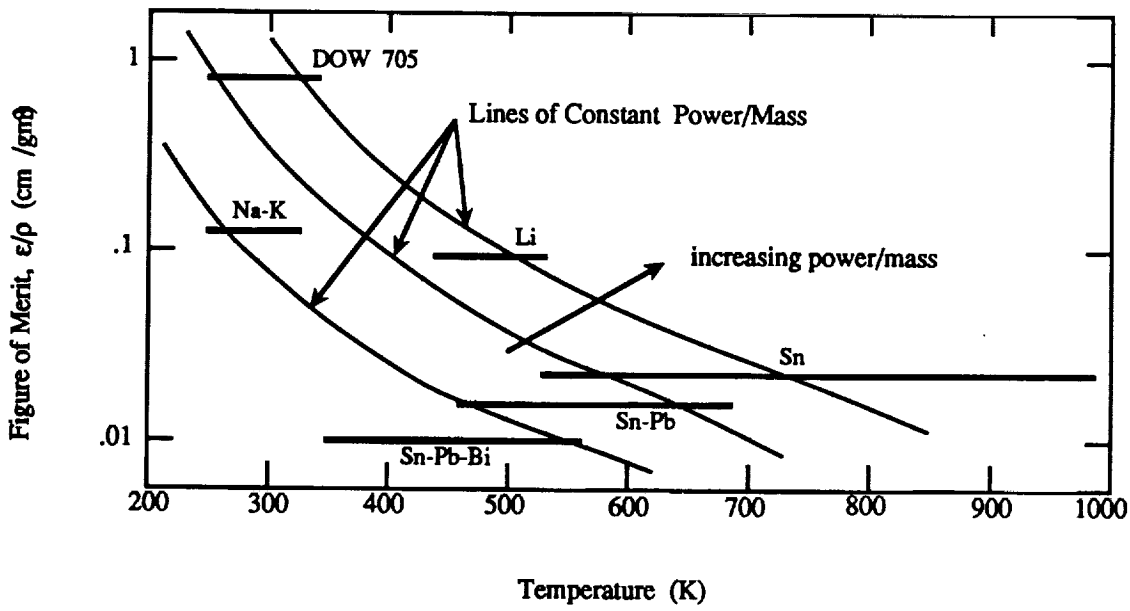

Fig. 4.13: Operating Temperature Ranges Of Candidate LDR Fluids.

{Minimum temperatures correspond to freezing (liquid metals) or high viscosity (DOW 705 silicone oil). High temperatures correspond to evaporation loss of 0.03 kg/m -year. Figure of merit is proportional to power/mass.}

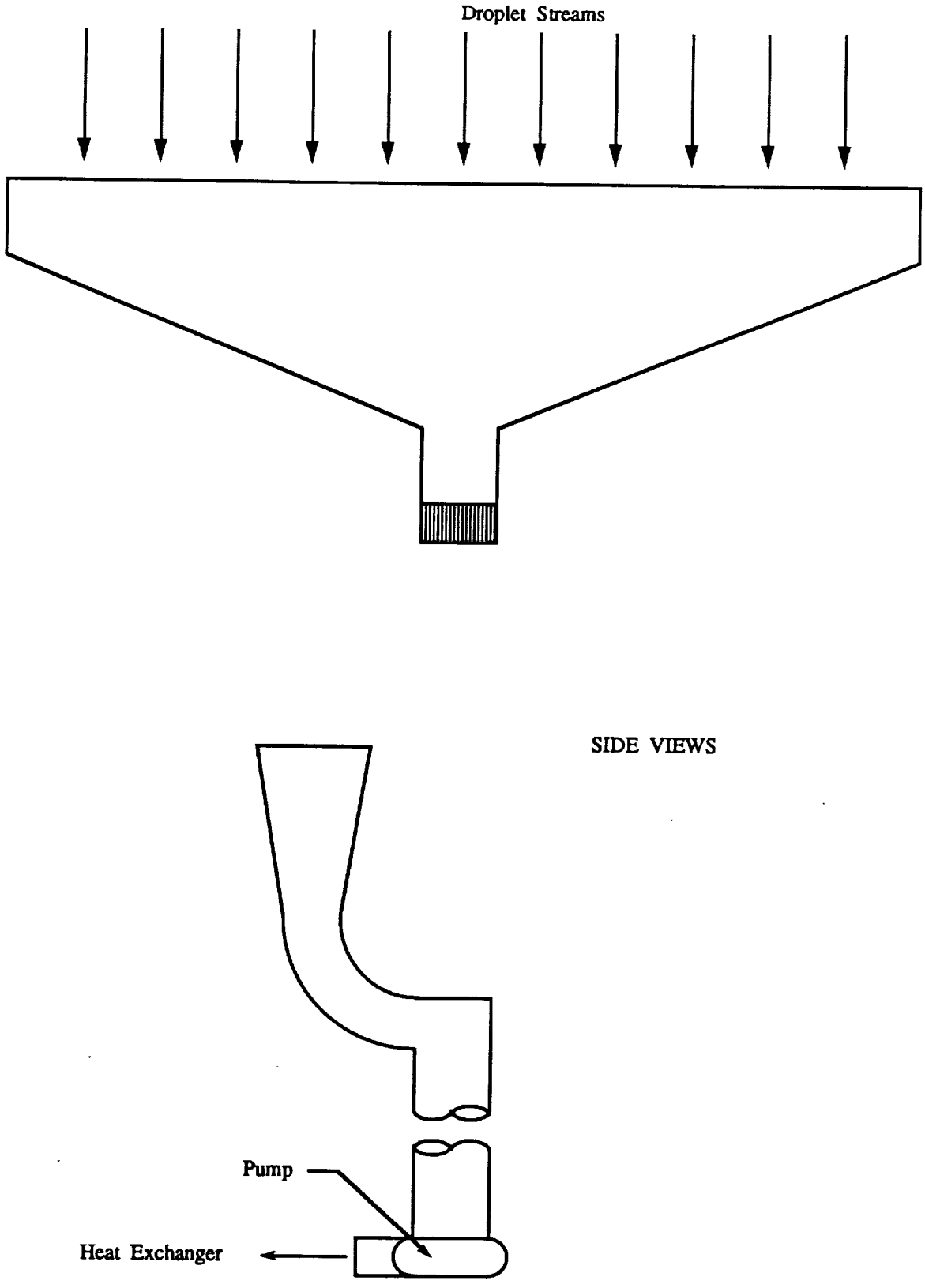

Fig. 4.14: LDR Collector.

TABLE 4.3: Properties of DOW-CORNING 705 Silicone Oil.
(Pentaphenyltrimethyltrisiloxane)

Extrapolated vapor pressure (300 K)	4.0×10^{-8} Pa
Viscosity (330 K)	0.05 Ns/m^2
Viscosity (280 K)	0.63 Ns/m^2
Density (300 K)	1080 kg/m^3
Specific Heat	1465 J/kg K
Emissivity	0.5
Molecular weight	546
Surface tension	3.65 N/m^2

acoustic waves from a piezoelectric driver in the emitter manifold. These acoustic waves enhance the surface tension instabilities which break up the liquid stream into uniform size droplets. In the present design, streams of 100 μm diameter droplets are generated by forcing the liquid through 50 μm orifices and using an excitation frequency of about 105 Hertz [5, 6].

The aiming of the droplets is done with an accuracy of 2 mrad. The driving frequency, f, can be determined from the droplet velocity, v_o,and the droplet spacing, or pitch, p, using the following equation:

$$f = \frac{v_o}{p} \tag{4.19}$$

The pressure, P_i, required to drive droplets at a given velocity, v_o, is given by the Poisseuile-Hagen law which takes into account viscous and inertial effects:

$$P_i = \frac{8\mu L_o v_0}{d_o^2} + \rho_o v_o^2 \tag{4.20}$$

where L_o is the orifice length, d_o in the orifice diameter, μ is the viscosity of the liquid, and ρ_o is the density of the liquid.

The pressure will drop along the length of the manifold, which has a taper ratio (initial diameter/final diameter) of 2. Boost pumps are used along the length of the manifold to

maintain the pressure to within 10% of P_i. The pressure drop in the manifold can be determined from [7]:

$$\delta P = \frac{\gamma L_g m_d^2}{2\rho \pi^2 r_p^5} \int_{z_0}^{z_1} \frac{(1 - Z)^2}{\left(1 - \frac{Z}{2}\right)^5} dZ \tag{4.21}$$

where $Z=x/L_g$, x is the distance along the manifold, L_g is the manifold length, r_p is the average pipe radius, and γ is defined as $16\mu\pi r_d/m_d$.

4.3.4 COLLECTOR

The collector for the lunar LDR, shown in Fig. 4.14, must be wide enough to accommodate the maximum divergence of the droplet paths, yet it must not permit fluid loss due to "splash back". The top meter of the collector utilizes converging sides with a low angle of incidence for incoming droplets. This will eliminate the possibility of splash back in the upper section. The fluid leaves the converging section and flows through a curved duct into the manifold. The curved section is designed to prevent a droplet impact directly on a fluid pool, which would create secondary droplets and the possibility of fluid loss if these escape the collector. The cross-section of the converging section and the curved duct remains constant for the entire length of the collector. The cross-section of the manifold, however, enlarges in width and depth to accommodate increased mass flow and provide for complete drainage during shutdown. The centrifugal pump is located at the lowest point of the manifold, at the center. An estimate for the mass of the collector, m_c, is obtained from:

$$m_c = \rho_{eg}\left[A_c \delta t + 2\pi(0.15)\delta t(5)\right] \tag{4.22}$$

where ρ_{eg} is the density of graphite epoxy (the material of which the collector is made), A_c is the total surface area of the collector, and δt is the thickness of the graphite epoxy sheet.

4.3.5 LDR SYSTEMS INTEGRATION

In the design of a complete power generation system, the limitations of one component will often affect the design parameters of other components. For this system, the LDR imposes limits on low-end heat rejection temperatures due to the temperature constraints of its own working fluid. The radiator upper temperature limit is determined by the loss of radiator fluid due to evaporation. The lower operating limit of the radiator is determined by the acceptable power required to pump the fluid, which may be extremely viscous (silicone oil) or contain frozen solids as the liquid is cooled below its freezing point (liquid metal). These temperature constraints will affect the heat exchanger design, which must allow a high enough mass flow and a large enough area to transfer the required thermal energy from the power cycle to the LDR. Within the low end heat exchanger, the temperature of the working gas will always be higher than the temperature of the radiator fluid. In addition, the low temperature of the radiator determines the compressor inlet temperature. The impact of the liquid droplet radiator operating range is therefore greatest on the dynamic converter and heat exchanger designs.

Dropping the low end temperature of the dynamic conversion unit (DCU) by 15% results in a 17% increase in thermal efficiency on the DCU. Since the LDR's radiative power varies as temperature to the fourth power, in order to achieve the same radiative power with the drop in DCU low-end temperature, the area of the LDR must increase by a factor of two. Thus, with the operating limits of the LDR sensitive to temperature decreases and the LDR working fluid sensitive to temperature increases due to possible evaporation of the fluid, system integration with the DCU is very limited.

The heat exchangers for the power system are designed for specific operating conditions. The recuperator is designed to accommodate the DCU and is essentially fixed by

the temperature constraints imposed by the LDR. Recognizing the sensitivity of the LDR mass to temperature, a mass optimization of the recuperator would cause too great a mass increase in the LDR such that the penalty would far outweigh the benefits.

4.3.6 FLUID MANAGEMENT

The lunar emitter system consists of two long droplet generator pipes (see Table 4.4) which require significant power to keep the generating pressure within 10% of the desired pressure, as dictated by the Hagen-Poiseuille Law (see Section 4.3.3, Eq. 4.20). A pump is required every 2.4 m along its length in order to satisfy this criterion. The following discussion examines the power requirements and pumping considerations.

From the conservation of energy, the power required to pump a fluid through a pipe, w_p, is given by

$$w_p = \dot{m}\left[\frac{g_l dh}{\rho_o dp} + \frac{du}{2}\right] \tag{4.23}$$

$$dh = h_2 - h_1 \tag{4.24}$$

$$dp = p_2 - p_1 \tag{4.25}$$

$$du = u_2^2 - u_1^2 \tag{4.26}$$

where subscripts 1 and 2 refer to the location of the pump and final station, respectively, h is the elevation of the station above some datum, g_l is the local acceleration of gravity, ρ_o is the mass density of the fluid, which is to be considered constant, p is the static pressure of the fluid at the station, and u is the velocity of the fluid at the station. The mass flow rate, m, of

the fluid through the pipe is given by

$$\dot{m} = \frac{\rho_o u \pi d^2}{4} \tag{4.27}$$

where d is the diameter of the pipe. The height term in Eq. 4.23 refers to the power required to elevate the fluid in a gravity field. The pressure term arises from viscous friction encountered by the fluid at the pipe walls, as well as plumbing fittings, such as elbows and tees, and heat exchangers. The velocity term represents the power required to move the fluid at the given mass flow rate.

The pressure term in Eq. 4.23 accounts for the pumping power required to overcome the various viscous friction losses which the flow may encounter. Let δP_t be the total pressure loss which a flow will encounter while moving from station 1 to station 2 in a pipe. That is

$$\delta P_t = P_2 - P_1 = \delta P_r + \delta P_R + \delta P_{Hx} + \delta P_h \tag{4.28}$$

where δP_r, δP_R, δP_{Hx} and δP_h are the pressure drops due to viscous wall friction, pipe fittings, heat exchangers and altitude, respectively.

The pressure drop due to wall friction in a smooth pipe for incompressible flow is given by

$$dP_1 = 0.5 f_f \rho_o u^2 \frac{L}{d} \tag{4.29}$$

where L is the length of the pipe. The friction factor, f_f, for turbulent flows is given by

$$f_f = 0.316 (Re)^{0.25} \tag{4.30}$$

where the Reynolds number is given by

$$Re = \frac{\rho_o u d}{\mu} = \frac{4m}{\mu \pi d} \tag{4.31}$$

The term μ is the dynamic viscosity of the fluid. For DOW 705, μ is a strong function of temperature.

Combining Eq. 4.29, 4.30, and 4.31, a useful form is obtained.

$$\delta P_t = 1.738 \mu \left(\frac{m}{\pi}\right)^7 \left(\frac{L}{p}\right) d^{4.75} \tag{4.32}$$

The pressure losses due to fittings may be obtained from experimental results found in the literature. For example, if a pipe had one elbow and one tee, the corresponding loss coefficients would be 0.9 and 1.8 and empirical relations would be used to obtain the pressure loss. The pressure losses encountered in the heat exchangers must be obtained from the designers or manufacturers of those systems. Tables 4.4-4.6 summarize the fluid management system pipe parameters and the system pump parameters.

4.3.7 CONTROL SYSTEMS REQUIREMENTS

The control system must be able to deal with variable power demand since the power station output will fluctuate slightly according to the total demand of the station's activities. One solution is to keep the power output constant and have a control system to divert any excess power into storage batteries or regenerative fuel cells which must be present in case of emergencies. This method enables the mass flow rates of the dynamic cycle and the LDR to remain constant, which greatly simplifies heat exchanger design.

TABLE 4.4: Lunar Fluid Management System Pipe Parameters.

Pipe material	Graphite-Epoxy
Pipe material density	2210 kg/m^3
Number of pipes	2

Specific pipe parameters	$L1_n$	$L1_c$
Horizontal length	5.0 m	35.0 m
Vertical length	49.0 m	0.0 m
Inner diameter	0.10 m	0.15 m
Wall thickness	0.006 m	0.003 m
Pressure loss within pipe	179.3 kPa	58.5 kPa
Mass	225 kg	109.7 kg
Contained fluid mass	457.5 kg	667.0 kg

TABLE 4.5: Lunar Fluid Management System Pump Parameters.

Specific pump characteristics	$P1_n$	$P1_c$
Mass flow	7.16 kg/s	7.16 kg/s
Operating pressure	276.0 kPa	616.0 kPa
Power requirement	6.0 kW	10.2 kW
Mass	6.0 kg	10.0 kg

TABLE 4.6: Lunar LDR Component and System Mass.

Mass of fluid in radiating sheets	86.85 kg
Mass of fluid in pipes	1124.5 kg
Mass of fluid in emitters	66.34 kg
Mass of collectors	217.31 kg
Mass of pipes	334.7 kg
Mass of pumps	30.88 kg
Total Lunar LDR system mass	1936.72 kg

The fluctuation in power output will cause a fluctuation in the amount of heat rejected. This can be controlled by adjusting the time of flight of the droplets. The control system will need to keep a constant temperature in the collector. By adjusting the pressure in the manifold, the initial velocity of the droplets and the time of flight for each droplet can be controlled to some extent. This will require variable pressure pumps to be used. Since variable amounts of droplets will be forming, the piezo driver must be capable of handling variable frequencies.

4.3.8 LDR CONFIGURATION

The final configuration of the LDR consists of one radiating sheet, 42 m high and 15 m wide to form a total radiating area of 630 m^2 per 250 kW engine, as shown in Fig. 4.15. The sheet is arranged lengthwise to form an array 15 m long and 42 m high oriented parallel to the lunar equator. The arrangement of the sheet parallel with respect to the lunar equator prevents direct solar energy input to the droplet sheet. The plumbing loop for the sheet consists of piping, pumps, and a heat exchanger (Fig. 4.4). The pipes carrying the fluid from the heat exchangers to the LDR and back are buried in the lunar soil to provide protection against micrometeorites. Table 4.7 provides a summary of the LDR design parameters.

4.4 BACKGROUND THERMAL RADIATION CONSIDERATIONS

The input of energy to the HPR or LDR from absorption of direct and reflected sunlight will be prevented by erecting suitable screens and reflectors, fabricated from a lightweight graphite/epoxy composite with a honeycomb core. The overhead screen will run along the length of the HPR or LDR with a small extension of the screen on each end. It will impede a large percentage of the direct incident sunlight. The width of the screen, W_s, for operation near

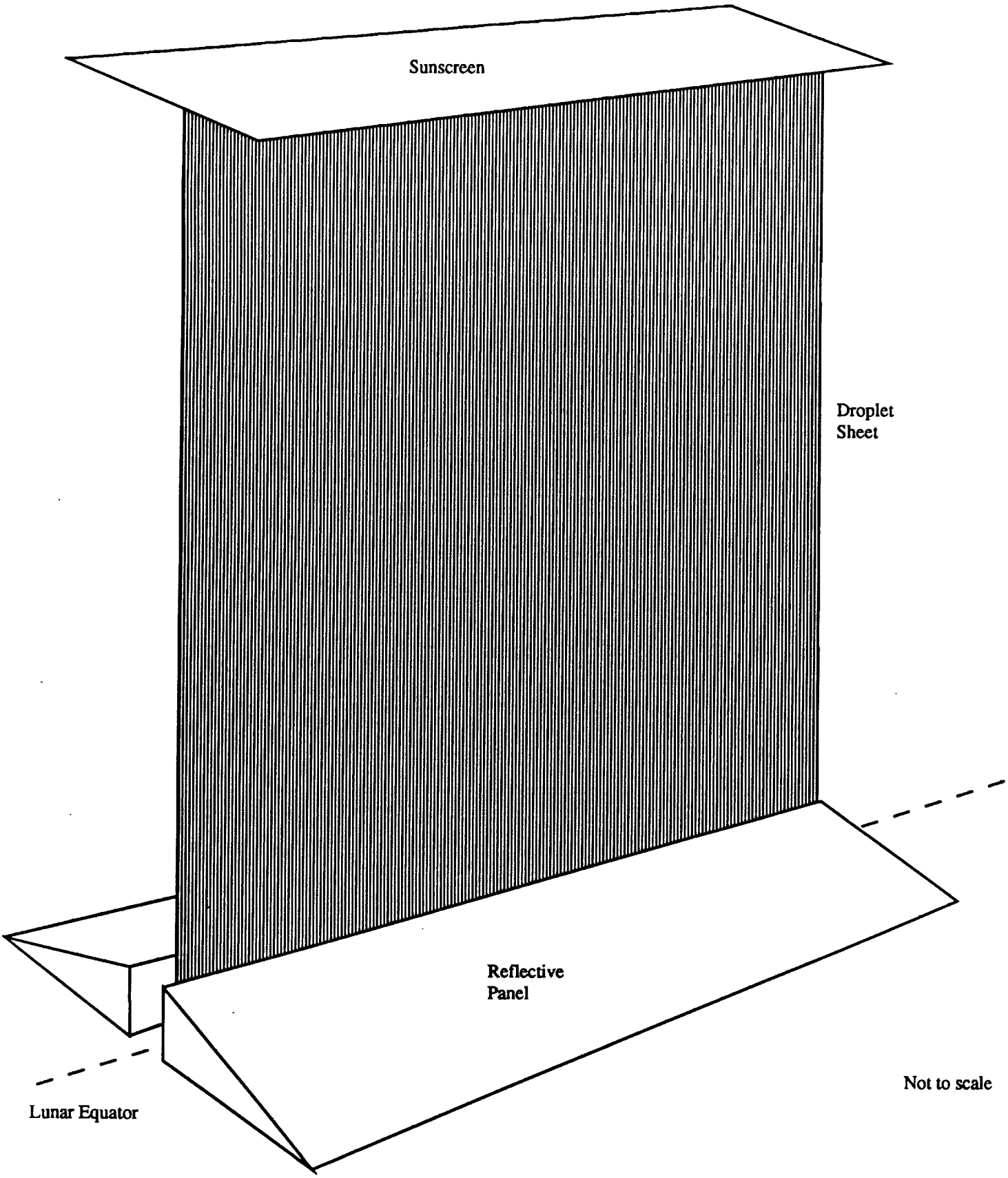

Fig. 4.15: Lunar Liquid Droplet Radiator configuration.

TABLE 4.7: Lunar LDR Design Parameters (for each 250kWe power module)

Power System Parameters

Brayton cycle waste heat output	442 kW
LDR overdesign for peak mid-day solar flux	9.5%

LDR Geometry

Geometric shape	Planar rectangle
Length	15 m
Height	42 m
Total radiating area of LDR per 250 kW	630 m^2

Droplet Sheet Characteristics

Operating fluid	DOW 705
Sheet width at emitter	15 m
Sheet width at collector	15 m
Sheet emissivity	0.80
Thickness	0.03 m
Optical depth	1.0
Droplet diameter	100 μm
Initial droplet (emitter) velocity	1.32 m/s
Mass flow rate of fluid	7.16 kg/s
Droplet time of flight	6.41 s
Emitting temperature	330 K
Collecting temperature	280 K
Effective operating temperature	303.30 K

Emitter

Material	Graphite-Epoxy
Material density	2210 kg/m^3
Number of emitters per sheet	1
Length of emitter	15 m
Depth of emitter	0.10 m
Orifice diameter	50 μm
Orifice separation	300 μm
Number of orifices per emitter	5.00×10^6
Optimum emitter frequency	2.20 kHz
Emitter pump power required	14.88 kW
Pressure at emitter face	33.56 kPa
Emitter mass	76.14 kg
Emitter pump mass	14.88 kg

Collector

Type	Gravity well
Material	Graphite-Epoxy
Material density	2210 kg/m^3
Number of collectors per sheet	1
Length of collector	15 m
Width of collector mouth	0.20 m

the moon's equator is given by [2]

$$W_s = 2h\tan\varphi \tag{4.33}$$

where φ is the angle between the Moon's equatorial plane and the ecliptic plane as shown in Fig 4.16 [4], and h is the height of the radiator. Reflective surfaces, located adjacent to the radiator, on the lunar surface consist of aluminized composite structures slanted at an angle, θ, relative to the horizontal plane [2]. The angle θ is given by

$$\theta = 2\varphi \tag{4.34}$$

This angle is larger than necessary to account for any out of plane areas.

Thermal radiation from the surrounding lunar regolith must also be considered. The lunar surface at the moon's equator on the near side, has an albedo of 0.08. Thus 92% of the sun's energy is absorbed and reradiated diffusely from the surface, which attains a temperature of 390 K during lunar midday [5]. It is possible to determine what fraction of the diffuse thermal radiation from the surrounding lunar soil reaches the vertical plane of the radiator [8]. Treating all surfaces as flat plates, the view factor, F, for the lunar configuration is determined from Fig 4.17 and

$$F_{1\text{-}4} = \frac{1}{A_1}[A_1(F_{1,2\text{-}3,4} - F_{1,2\text{-}3}) + A_2(F_{2\text{-}3} - F_{2\text{-}3,4})] \tag{4.35}$$

where $F_{m\text{-}n}$ is the fraction of thermal radiation leaving surface m which reaches surface n and A_m is the area of surface m. The surfaces for the above equation, in the context of the lunar environment, are defined in Fig 4.18.

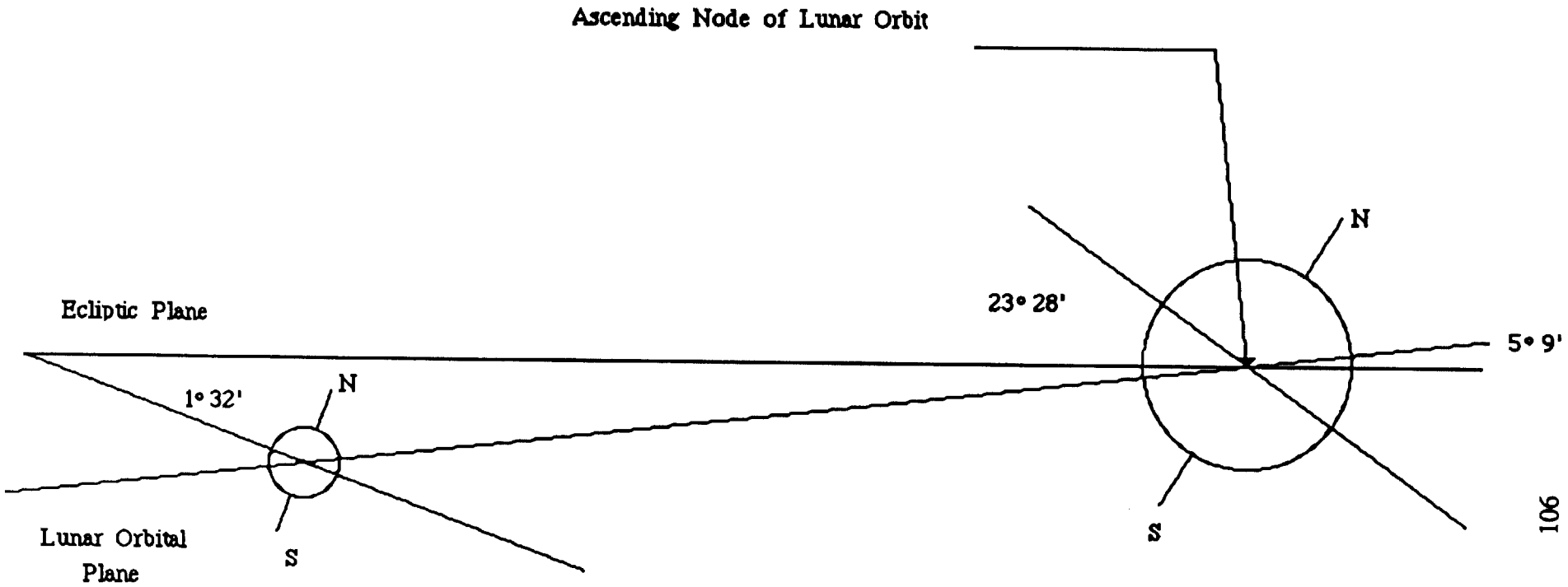

Fig. 4.16. Relative orientation of the lunar plane with the ecliptic plane.

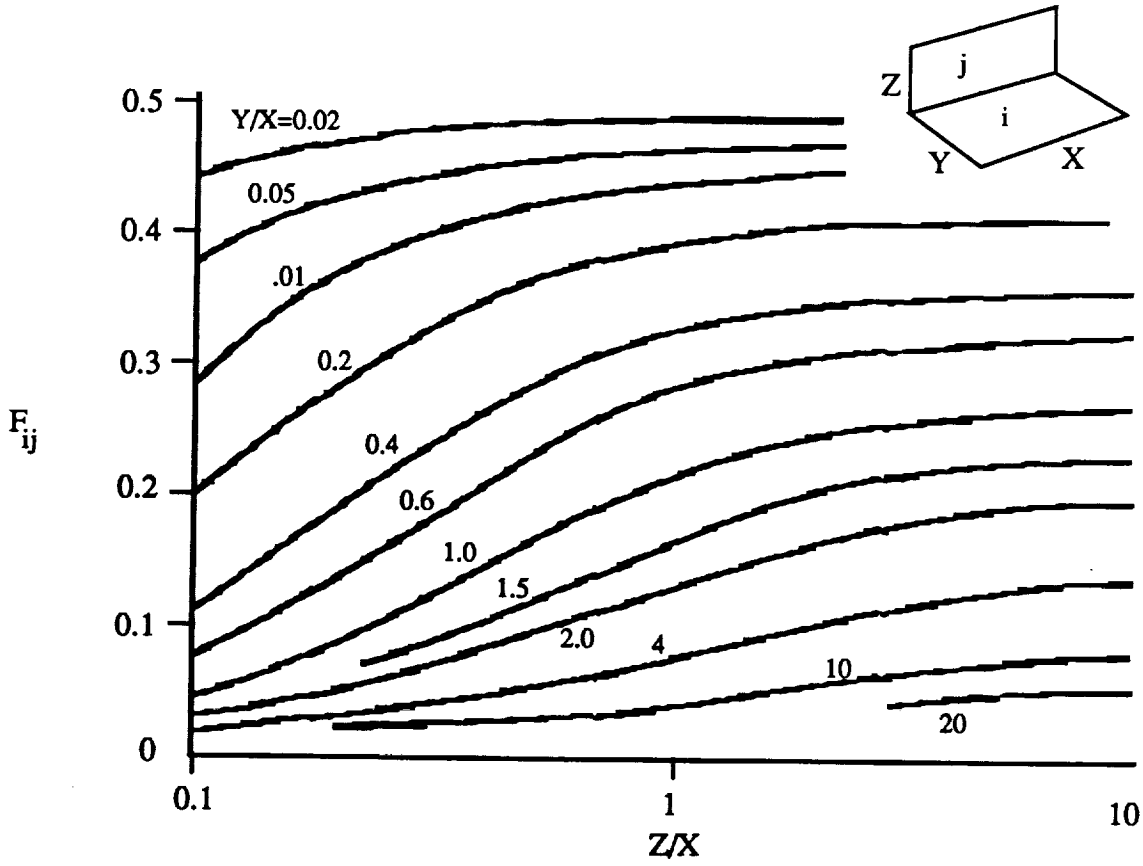

Fig. 4.17. View factor for perpendicular rectangles with a common edge.

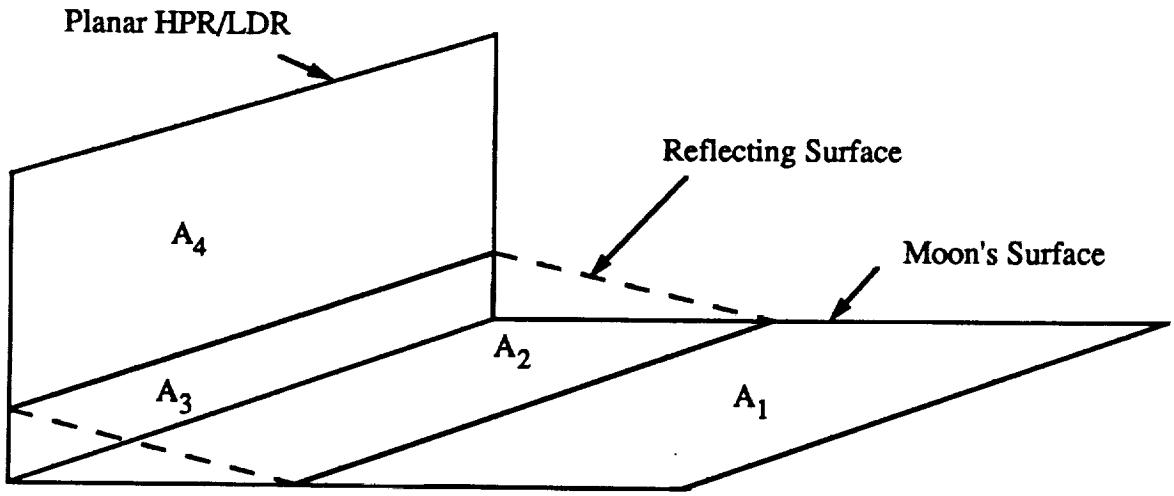

Fig. 4.18. Surfaces used in view factor determination.

The background radiation input, q, from the regolith to the radiator sections is given by

$$q = 2\sigma A_1 F_{1\text{-}4}(\varepsilon_R T_{reg}^4 - \varepsilon_f T_{eff}^4) \tag{4.36}$$

where ε_R is the regolith emissivity and ε_f is radiator emissivity, T_{reg} is the lunar regolith effective temperature, σ is the Stefan-Boltzmann constant, and T_{eff} is the effective temperature of the radiator.

The power that has to be radiated by the radiator, P_r, becomes

$$P_r = \frac{P_o}{\eta_{sc}} + q \tag{4.37}$$

where P_o is the electrical output of the power system and η_{sc} is the Brayton cycle efficiency, including power conditioning. The radiator dimensions may be determined once P_r is known.

4.5 INCREASING THE RADIATING TEMPERATURE USING HEAT PUMPS

The possibility of reducing the mass of the radiator by increasing the temperature at which the waste heat is rejected was considered. The premise for this exercise was that if the rejection temperature is increased sufficiently through the use of a heat pump, it might be possible to reduce the area of the overall system, thus reducing the radiator mass.

The mass of the engines was neglected and the area of radiator, A_o, operating at a temperature, T_o, without a heat pump, needed to reject 1 MW of waste heat was calculated as a baseline. This result was compared to a radiator operating with a heat pump. With a heat pump, the total area of radiator needed for both the heat pump itself and the waste heat generated by the power cycle was determined. An effective area, A, was defined as the sum of

the area of the secondary heat pump , A_r, operating at a temperature T_r and the area of the primary radiator, A_e, operating at a temperature T_e. From this the amount of waste heat to be rejected for the radiator utilizing a heat pump was determined. By assuming the engine and heat pump to be Carnot engines with efficiencies e_e and e_r, A/A_o can be found from [8]

$$\frac{A}{A_0} = \left(\frac{T_0}{T_r}\right)^4 \left(\frac{\frac{T_0}{T_r} - 1}{e_r} + 1\right) + \left(\frac{T_0}{T_r}\right)^4 \left(\frac{\frac{T_r}{T_0} - 1}{e_r}\right) \left[\frac{1 - e_r\left(1 - \frac{T_e}{T_s}\right)}{e_e\left(1 - \frac{T_e}{T_s}\right)}\right] \tag{4.38}$$

Using $T_o/T_s = 3$ and the Brayton cycle efficiency approximately equal to 25%-30%, the area of the radiators would decrease by only 5%-10%.(see Fig. 4.19). Since the heat pump would require energy, the size of the collectors would be increased. This increase in collector size offsets any reduction in the size of the radiators, therefore, the addition of a heat pump is not advantageous.

4.6 CONCLUSIONS

The finned heat pipe radiator (HPR) and the liquid droplet radiator (LDR) are effective thermal management devices for large heat rejection requirements on the lunar surface. Obviously, both systems have benefits and limitations.

Presently, the HPR is the preferred system because it utilizes established technology. Varying heat rejection requirements from the power system and changing radiation input to the HPR from the environment will be easily handled by a suitable control system. The energy input to the HPR from direct, reflected, or reradiated solar radiation is easily prevented by use of lightweight screens and reflecting sheets. The most important factors in favor of the HPR are its lack of moving parts required to transport the waste thermal energy, its resistance to single point failure due to micrometeorite strikes, and its high ratio of heat rejected to mass

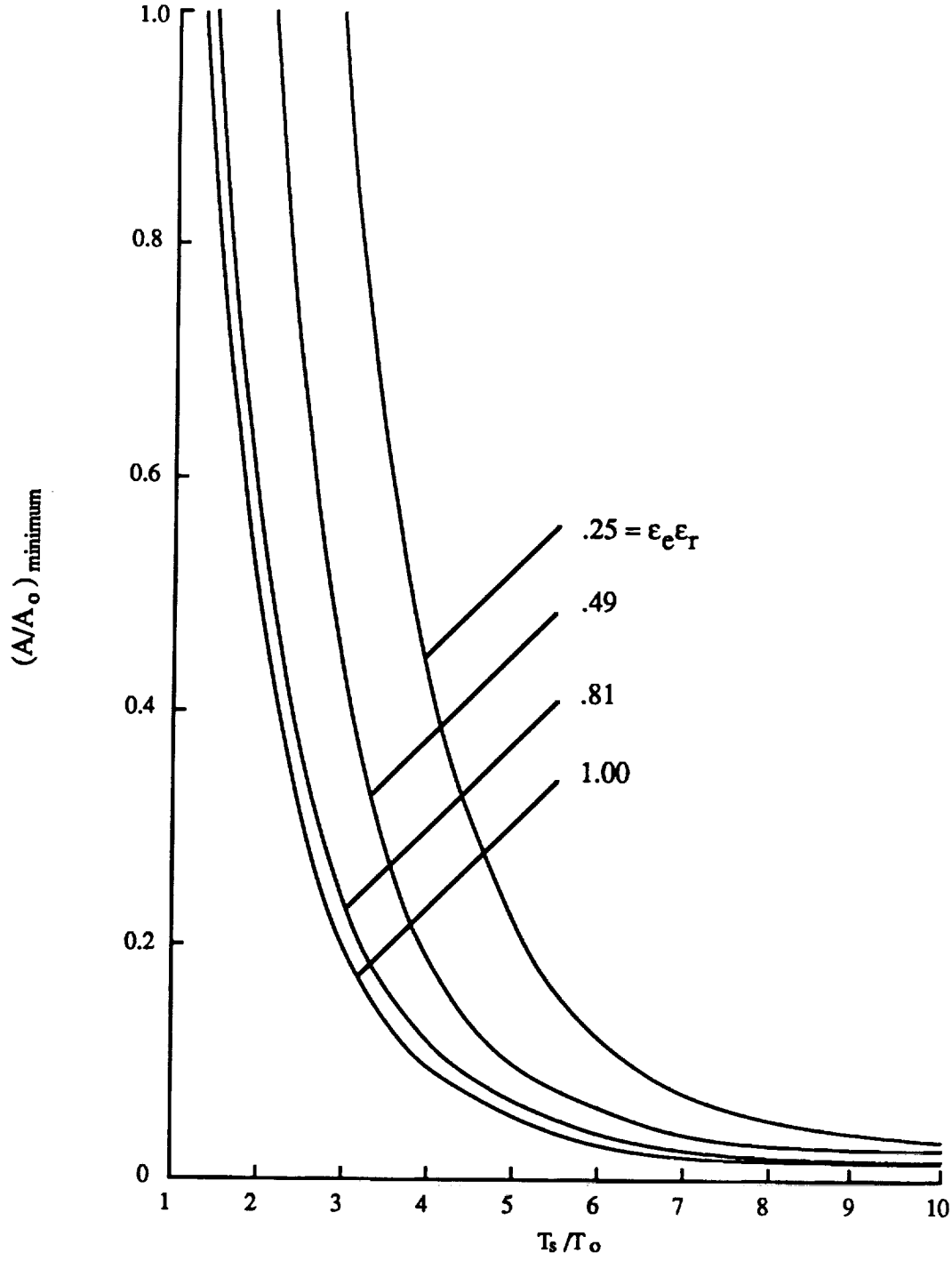

Fig. 4.19: Ratio of minimun radiator area to that for direct heat rejection, as a function of the ratio of the heat engine source temperature and the waste heat source temperature.

(140 W/kg). Additionally, the replaceable independent VHP and fin sections will allow the HPR to be restored to full operational capacity in the event that any VHP or fin section is damaged by a micrometeorite, without shutting down radiator operation. Currently, several corporations have indicated that they are developing similar systems. The lunar heat pipe radiator offers long operational lifetime for relatively low mass, and is well capable of providing thermal management for lunar surface operations.

At first glance, the liquid droplet radiator (LDR) appears to be a very a attractive system, with a radiating power to mass ratio of 250 W/kg. Most of the research that has been done for the LDR is for space applications, however additional research is necessary to develop a full scale working model. Since these radiators rely heavily on small emitter orifices, dust may introduce a problem. Dust from the lunar surface could be kicked up in the proximity of the LDR by lunar landers, lunar surface operations, or even by astronauts walking near the LDR. In order to solve this problem, large areas of the lunar surface would need to be paved and filters would need to be added to the LDR. This not only increases the mass of the system, but also the amount of maintenance required to keep the LDR operational. The LDR is not as resilient to single point failure as the HPR. In the event of a failure the entire radiator must be shut down. Since a working model is still under development, further complications may arise.

For these reasons, the more conservative design of the waste heat rejection system, the HPR, is recommended. Even though the LDR has a power to mass ratio 1.8 times that of the HPR it was decided that the HPR is more reliable and incorporates technology that at the present time is more mature. If and when the LDR is fully developed and tested, it may become the system of choice.

4.7 NOMENCLATURE

a	Speed of sound of vapor in the MHP
a_1	Projected area of droplet in direction of flux
A	Total area of the radiator
A_c	Area of collector
A_d	Area of droplet
A_e	Area of primary radiator
A_{fin}	Total area of each fin
A_i	Area of the finite element of fin
A_{M1}	Critical cross sectional area of MHP
A_r	Area of secondary heat pump radiator
A_o	Area of the radiator without a heat pump
A_{VHP}	Total area of each vertical heat pipe
A_x	Area of individual heat exchanger heat pipes
A_1	Total area of the radiator in the view factor calculation
A_2	Total area of the reradiating surface
C_p	Specific heat of droplet fluid
d	Diameter of pipe
d_o	Emitter orifice diameter
dh	Change in enthalpy
dp	Change in static pressure
du	Change in velocity
E	Modulus of elasticity of the heat pipe material
e_e	Efficiency of Carnot engine for heat pump

e_r	Efficiency of Carnot refrigeration cycle in the heat pump
E_l	Thermal energy stored in a droplet
f	Driving frequency
f_f	Friction factor
F_{m-n}	Fraction of thermal radiation leaving surface m which reaches surface n
$F_>$	Number of hits per unit area per time
g_l	Lunar gravitational constant
h	Height of the heat pipes
h_o	Height of droplet sheet
H	Number of penetrating hits on a given area in a given time
HPR	Heat pipe radiator
h_v	Heat of vaporization
k	Thermal conductivity of pyrolytic graphite
k_o	Constant of proportionality
L	Length of pipe
L_g	Manifold length
L_o	Emitter orifice length
L_i	Length of the finite element of fin
m	Mass
$\dot{m}$	Fluid mass flow rate

m_c	Mass of collector
m_0	meteoroid mass, g
m_d	Droplet mass
MHP	Mother heat pipe
n_x	Number of heat exchanger heat pipes
N_{fs}	Minimum number of heat exchanger heat pipes
N_{VHP}	Same as N_{VHPO} used to solve for N_{VHPO}
N_{VHPO}	Number heat pipes needed at the beginning of a ten year period to ensure adequate end of life performance
p	Droplet spacing
P	Probability of a fin surviving
P_o	Electrical output of power system
P_i	Pressure required to drive droplets at given velocity
P_r	Power to be rejected by the radiator
q	Background radiation input
q'	Heat flux through the heat exchanger
q"	Maximum amount of heat per unit time required to transfer waste heat
q_i	Heat across the finite element
q_{irad}	Heat radiated across the finite element
r_d	Droplet radius
r_p	Average pipe radius
Re	Reynolds number
R_i	Thermal resistance across the finite element
S	Incoming radiation flux
t	Thickness of the heat pipes
T_b	Effective temperature of space

T_{bo}	Low end fluid temperature limit
T_e	Temperature of the engine
T_{eo}	Effective droplet temperature
T_{eff}	Effective temperature of the radiator
t_f	Droplet time of flight
t_i	Thickness of the finite element
T_i	Temperature of the finite element
T_o	Temperature of the radiator without a heat pump
T_{o1}	High end fluid temperature limit
T_r	Temperature of the radiator with a heat pump
T_{reg}	Temperature of the regolith
T_{r1}	Effective temperature of the VHP and fins
T_{ro}	Temperature of the Brayton engine radiator
T_s	Temperature of the engine radiator in the heat pump calculation
T_{s1}	Effective droplet sheet temperature
U	Overall heat transfer coefficient
v_o	Initial droplet velocity
VHP	Vertical heat pipe
w_p	Pump work
W_s	Width of the screen
z	Distance along manifold
α	Droplet absorptivity
α_o	meteoroid flux constant, $g\beta/m^2$-sec
β_o	constant in meteoroid equation

ΔT_i	Incremental temperature change across the finite element of fin
ΔT_{ln}	Log mean temperature difference of the working fluid in the Brayton engine
$\delta\tau$	Thickness of graphite epoxy sheet
δP_h	Pressure drop due to altitude
δP_{Hx}	Pressure drop due to heat exchanger
δP_r	Pressure drop due to wall friction
δP_R	Pressure drop due to pipe fittings
δP_t	Total pressure loss
ε	Effective emissivity of HPR
ε_d	Droplet emissivity
ε_{fin}	Emissivity of the fins
ε_R	Regolith emissivity
ε_s	Effective emissivity of droplet sheet
ε_t	Emissivity of the radiator times the emissivity of the regolith
ε_{VHP}	Emissivity of the vertical heat pipe
γ	Function of m, p, r_d, and m_d
η_{sc}	Brayton cycle efficiency
φ	The angle between the Moon's equatorial plane and the ecliptic plane.
μ	Viscosity of fluid
θ	Angle of aluminized composite relative to the moon's surface
τ	Time before the heat pipes in the radiator will need to be replaced
τ_o	Optical density of LDR fluid
ρ	Density of the heat pipe material

ρ_{eg}	Density of graphite epoxy
ρ_o	Density of LDR liquid
ρ_v	Density of vapor in the MHP
σ	Stefan-Boltzmann constant
ζ	Value of the normal standard deviation

4.8 REFERENCES

1. Mattick, A.T. and Hertzberg, A. , "Advanced Radiator Systems for Space Power",Paper No. IAF-87-230 38th Congress of the International Astronautical Federation, Brighton, United Kingdom, October 10-17, 1987.

2. Mattick, A.T. and Hertzberg, A. "The Liquid Droplet Radiator - An Ultralightweight Heat Rejection System for Efficient Energy Conversion in Space," Acta Astronautica, Vol. 9, No. 165, pp 165-172, 1982.

3. Trueblood, B., Pressentin, R. and Bruckner, A.P., "Multimegawatt Nuclear Power System for Lunar Base Applications", Space Nuclear Power Systems 1987, M.S. El-Genk and M.D. Hoover, eds., Orbit Book Company, Malabar, FL., 1988.

4. Werner, R.W. and Carlson, G.A., "Heat Pipe Radiator for Space Power Plants," IECEC 1968 Record, IEEE, Piscataway, N.J., pp. 487-501 1968.

5. Kopal, Z., The Moon, D.. Rudel Publishing Co., Dordrocht, Holland, 1969, pp. 371-400.

6. Beals,G. et al, "Lightweight Nuclear Powered OTV Utilizing a Liquid Droplet Radiator," Paper No. AIAA-83-1346, AIAA Joint Propulsion Conference, 1983.

7. Kerrebrock, J.L., "Optimization of Heat Rejection in Space," Journal of Propulsion, Vol. 2, No.6, pp562-563, Nov.-Dec. 1986.

8. Incropera, F.P. and DeWitt,D.P, Fundamentals of Heat and Mass Transfer, John Wiley and Sons, New York NY,1985 pp. 501-538 and 623-654.

9. Mattick, A.T. and Hertzberg, A., "Liquid Droplet Radiator Performance Studies," Acta Astronautica, Vol. 12, No. 718, pp. 591-598 1985.

10. Mattick, A.T. and Herzberg, A., "Liquid Droplet Radiator Technology Issues," Space Nuclear Power Systems 1984, M.S. El-Genk and M.D. Hoover, eds., Orbit Book Co., Malabar, FL, 1984.

11. Mattick, A.T. and Taussig, R.T., "New Thermal Management and Heat Rejection Systems for Space Applications," Air Force Rocket Propulsion Laboratory Report No. AFRPL TR-84-039, Edwards Air Force Base , June 1984.

12. Galassi, L. et al., "Liquid Droplet Radiator System," in 150kW$_e$Solar Dynamic Space Power System for Microgravity Processing Station, Final Report, NASA/ University Pilot Program, University of Washington, 1985.

5.0 ENERGY STORAGE

David Cook
Dave Gillespie
John Iacometti
Stan Love

5.1 INTRODUCTION

Using solar energy to power a manned lunar outpost has one major disadvantage: keeping the outpost fully operational at a 1 MW_e level during the long night would require the storage of more than a trillion joules of energy. Since energy storage tends to be extremely heavy, nighttime operation is limited to 50 kW_e for life-support, astronomy, and reduced research activities (see section 1.0).

The lunar mean solar day is 708.7 hours [1]. As a result of shadowing problems with the dynamic cycle and photovoltaic (PV) arrays, the energy storage system will need to provide 50 kW_e from a solar angle of 3° before sunset to 3° after sunrise. At these times, the PV arrays are producing 488 kW_e and the dynamic cycle units are operating at full power, thus 50 kW_e drawn from the energy storage system would be negligible (as well as costly). While the sun is less than 3° above the horizon, the energy storage system takes a considerable amount of the available power for recharging (24% for the PV case, less for solar dynamic, depending on local terrain). The photovoltaic system will be fully operational at 11.5°. This gives an effective lunar night of 366.2 hours and an effective lunar day of 342.5 hours. The storage of 18.3 MWh (6.6×10^{10} J) is necessary to provide a continuous nighttime power level of 50 kW_e.

Recent advances have made the regenerative fuel cell the prime candidate for high power systems and long term storage [2]. Two different fuel cells have been considered for

the present study: the experimental high temperature monolithic solid-oxide fuel cell (MSOFC) [3] and today's alkaline fuel cell that is used on the Space Shuttle [4]. The MSOFC operates at 1273 K and has a round trip efficiency of 40-50%. It has a power density over 10 times that of conventional fuel cells, and its efficiency can increase to 60% if a subsystem is included to utilize the high quality waste heat to produce electric power. Current low temperature fuel cells operate at a round trip efficiency of 55% without the complexity of a low end system.

In systems which require long periods of storage, reactant storage tanks are the predominant mass if the reactants are stored in their gaseous form. New, lightweight composites have reduced this mass, but the tanks still account for 65% of the total system mass (including the photovoltaic array and radiators required by the system) [2]. However, by storing the reactants as cryogenic fluids, the tankage mass can be reduced significantly. In a report by L. Kohout of NASA Lewis Research Center (LeRC), a conceptual design showed that the tankage mass is reduced by a factor of 14, even though it adds the additional mass and energy requirement of a liquefaction plant.

Kohout proposes the construction of special lightweight tanks for storing the cryogenic fluids, but an overview of the lunar development scenario reveals that there may be no need to design and build tanks especially for energy storage, as a variety of such tanks will be already available, i.e., the liquid propellant tanks used on the lunar landers [5]. The energy storage system in this study uses propellant tanks from an expended lunar excursion vehicle (LEV) for its reactant storage. This setup requires no dedicated storage tanks to be shipped from Earth.

5.2 SYSTEM CONFIGURATION

The 50 kW_e storage system is comprised of two 25 kW_e units, each with separate H_2, O_2 and H_20 tanks. If one unit were to malfunction, the other is capable of providing life-support for the 8 astronauts (1.5 kW_e/astronaut) plus 13 kW_e which can be used to repair the

other unit or for further reduced astronomy and research activities. If both units were to fail simultaneously, the backup power system would have to be engaged (see section 8.0).

The H_2 and O_2 propellant tanks remain attached to the LEV, which provides the structural support. All necessary plumbing can be configured before launch from Earth, so that simply turning a few valves makes the propellant tanks operational as reactant storage tanks.

The remaining components of the system (fuel cells, electrolysis units, liquefaction plants, water and water storage tanks) must be transported as cargo on this and/or following LEVs. In addition, the photovoltaic array or solar dynamic cycle that provides the charging power to the system must be transported at least one lunar day in advance of system operation in order for the water to be electrolyzed into the reactants, H_2 and O_2.

A schematic drawing of the 50 kW_e system is shown in Fig. 5.1. During the day, the water is split into its components, H_2 and O_2 and these are liquified for storage. At night, the reactants recombine in the fuel cell to form water and produce electrical power for the lunar outpost.

5.2.1 UPGRADING BEYOND 50 kW_e

Because of the LEV tank sizing, each tank will be less than half full. A single expended LEV has the tanks to support a 100 kW_e energy storage system. To do any upgrading, only the necessary fuel cells, electrolysis units, liquefaction plants, water, and water tanks will need to be transported to the moon. If upgrading beyond the 100 kW_e is desired, as each LEV completes its 5 flight lifetime [5] and goes into retirement, an additional 100 kW_e system can be added.

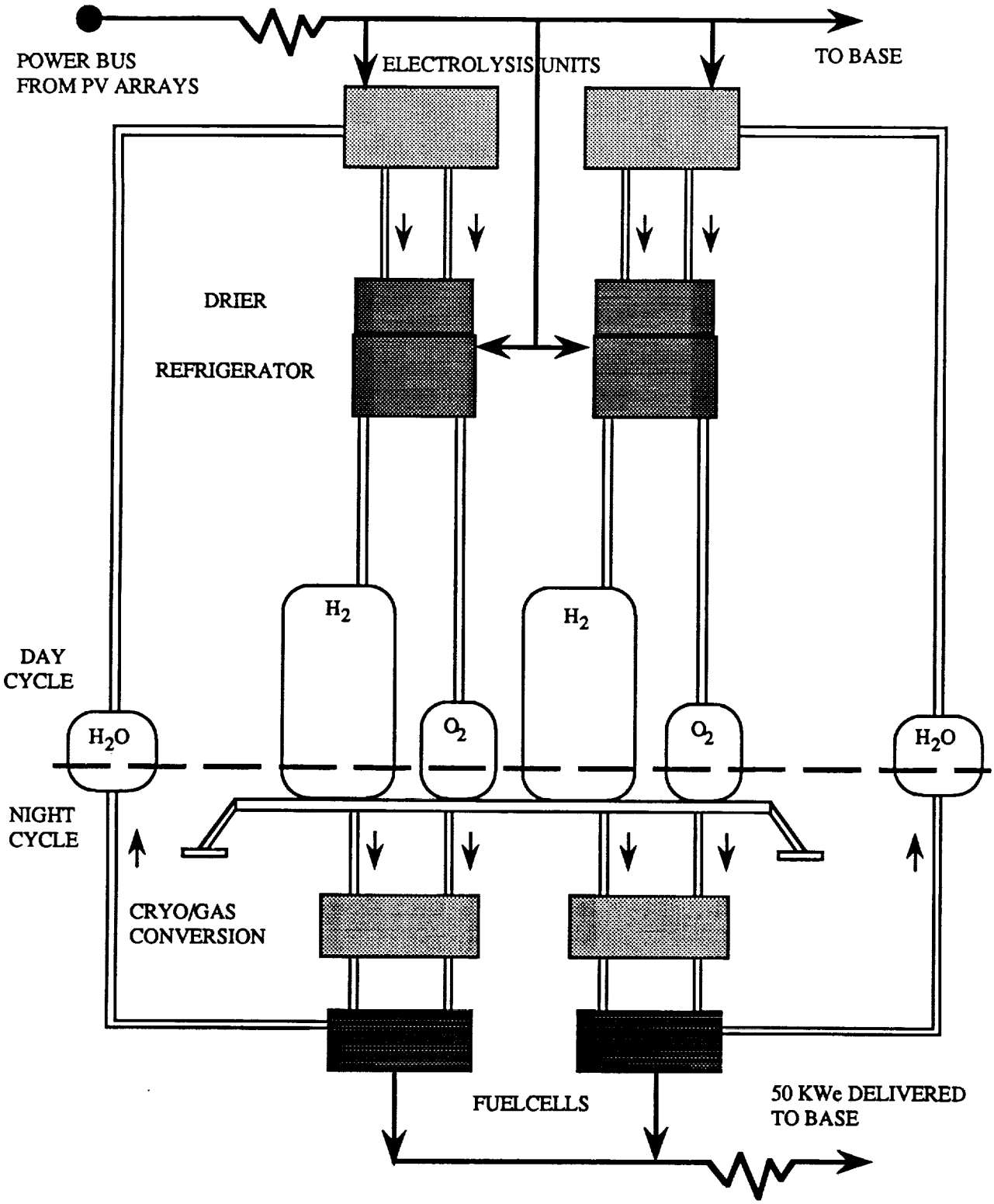

Fig. 5.1. 50 kW_e System Schematic.

5.3 FUEL CELLS

Although both fuel cells and electrolysis units exist, the combination of the two components to create a closed, regenerative system is still under development. Technology for the integration of an alkaline fuel cell with an electrolysis subsystem to form a regenerative fuel cell is being developed under a NASA LeRC program with United Technologies Corp. [6]. The high temperature monolithic solid oxide fuel cell (MSOFC) is currently being developed by Allied Signal AiResearch Division [7].

5.3.1 FUEL CELL/ELECTROLYSIS OPERATION

Though fuel cells can come in a variety of configurations and operate at various temperatures, all have the same basic purpose--to generate electrical power by processing chemical reactants. The chemical reactants, H_2 and O_2, enter the fuel cell where they react to produce electric power and water as a byproduct.

This process of chemical to electrical energy conversion is as follows [3]. The H_2 and O_2 flow on opposite sides of the electrolyte layer (see Fig. 5.2). The oxygen is reduced to oxygen ions when it comes in contact with free electrons supplied by an external circuit. The electric potential difference across the anode and cathode causes the O^{2-} ions to penetrate the electrolyte layer to the fuel side where the following reaction occurs:

$$H_2 + O^{2-} \Rightarrow H_2O + 2e^- \qquad (5.1)$$

These electrons are released to the anode layer which is connected to an external wiring array from which the current can be transmitted to the user grid. Two fuel cell designs, low and high temperature, are considered. Each one has its own special advantages and disadvantages.

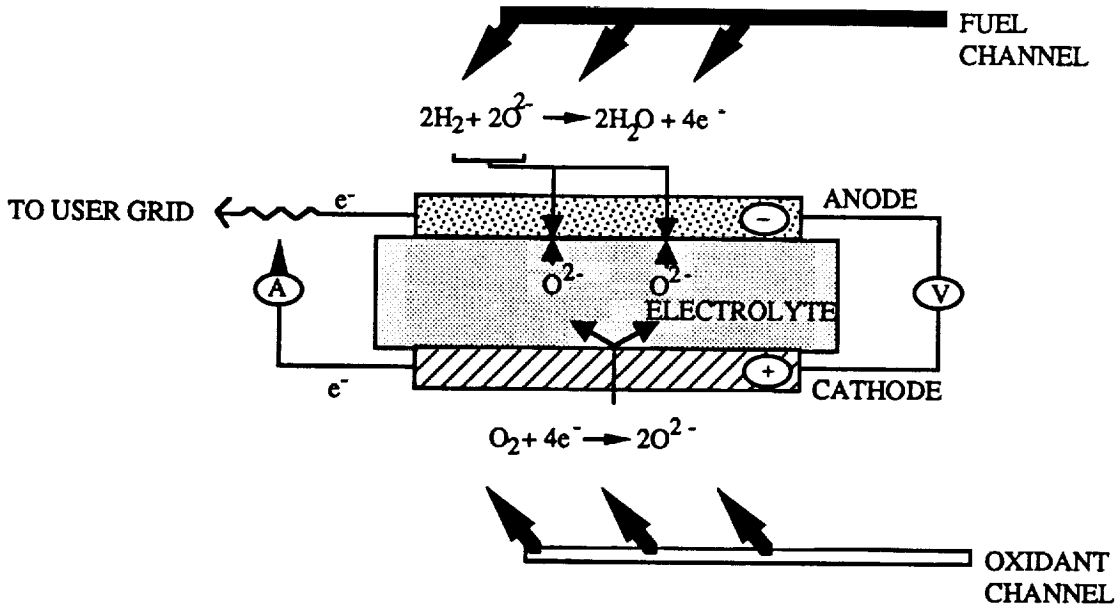

Fig. 5.2. Fuel Cell Operating Principle [8].

During the day, the water produced in the fuel cell is separated back into its components, H_2 and O_2, through a process called electrolysis, which is basically the fuel cell reaction run in reverse. This requires an external energy source (in this study, the PV array or solar-dynamic cycle) to supply the power needed for dissociation of the H_2O.

5.3.2 MONOLITHIC SOLID OXIDE FUEL CELLS

The cell under consideration utilizes a co-flow design in which the hydrogen and oxygen flow in parallel channels. The honeycomb structure depicted in Fig. 5.3 is both lightweight and strong, and has a chemical to electrical efficiency of 60%. The voltage across each cell is 0.65 V, and the cells can be stacked in series to accept or provide power at almost any voltage. For this study, 200 volts is chosen, which is consistent with the voltage produced by the solar PV arrays. The Brayton engines under consideration can be easily configured to produce electricity at 200 V.

For the MSOFC, the same cell is used as an electrolysis unit and fuel cell, operating at 1273 K for both processes. For the electrolysis process, liquid water at approximately 300 K must be converted to high temperature steam. To accomplish this phase change, the water is directed through tubing surrounding the electrolysis unit. There are two main reasons for using the same MSOFC stack as both fuel cell and electrolysis unit. The first is to eliminate an unnecessary secondary system, thus reducing the system mass and avoiding additional complexity. The second reason is to keep the fuel cell at its operating temperature of 1273 K during the lunar night, eliminating the problem of preheating the fuel cell every two weeks. It has been verified by Allied-Signal AiResearch Corporation using the same stack for both operations does not increase degradation of the material in the fuel cell [9].

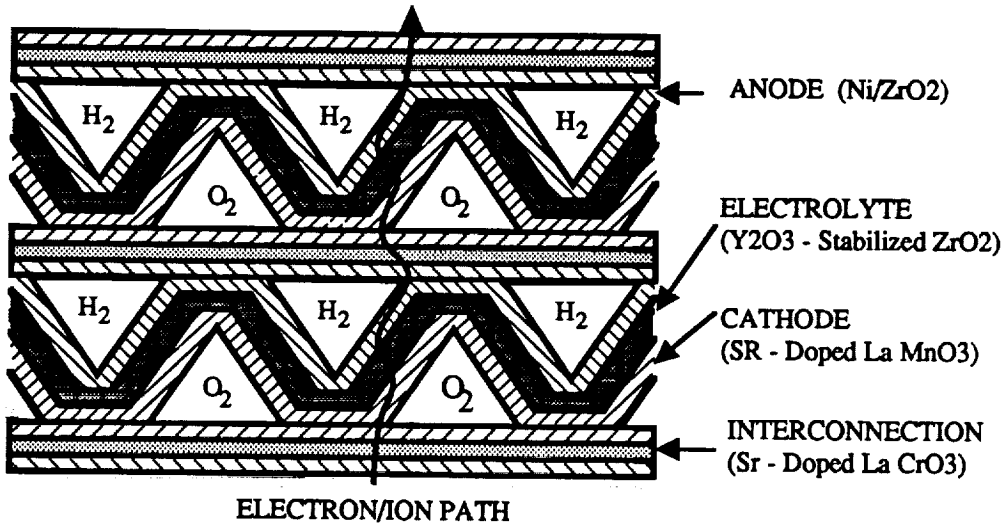

Fig. 5.3. MSOFC Configuration [9].

As stated above, the fuel cell/electrolysis unit operates continuously at a high temperature, eliminating the need to preheat the cell every cycle; however, it must undergo a preheat operation once for the energy system to be functional. This initial startup procedure will take place during the first lunar day that the energy source (solar photovoltaic cells or solar dynamic cycle) is operational.

It is necessary to preheat the fuel cells slowly before operation to prevent thermal shock from damaging the ceramic components. A temperature increase of 5 K/min has been proposed by AiResearch as a safe gradient to achieving the cell's final operating temperature of 1273 K [9]. To accomplish this requirement, the reactants can slowly be burned in the cell (providing internal heating) or resistive heating can be placed on the external surface of the unit. Once preheat of the fuel cell is completed, operation and processing of the reactants can begin.

The properties of the MSOFC are listed in Table 5.1 [7].

Table 5.1: Cell Properties

Cell thickness	2 mm
Specific power	8 kW_e/kg
Volumetric power density	4 kW_e/liter
Voltage	0.65 V/cell
Current density	1 A/cm^2
Component layer thickness	25-100 microns

The cells are composed of ceramic-based materials. The electrolyte is yttria-stabilized zirconia. The cathode is strontium-doped lanthanum. The anode is yttria-stabilized zirconia-nickel. The interconnection is doped lanthanum chromite [9]. These materials were chosen because they have similar coefficients of thermal expansion, so heating the cells will not cause the cell joints to separate [7].

5.3.3 ALKALINE FUEL CELLS

This option utilizes standard Space Shuttle orbiter system hardware rather than the advanced cell components currently under development. This is done to provide a system that incorporates as much current off-the-shelf technology as possible. Although the current fuel cell system aboard the space shuttle is a primary fuel cell (no electrolysis), the alkaline cell has been proven reliable for space operations [6]. These cells, like the MSOFCs, can be stacked in series to produce power at 200V.

The alkaline fuel cell boasts a chemical to electrical efficiency of 70%, and has been estimated to have a round trip system efficiency (fuel cell and electrolysis unit) of 55% [4]. The specific power and volumetric power density given in the low power design are given as 0.147 kW_e/kg and 0.118 kW_e/l respectively. This cell operates at a temperature of 330 K and a current density of 0.323 A/cm^2 (low power design). High power fuel cells (2.15 A/cm^2) offer a higher power density, but the actual life time of the fuel cell system will decrease [6].

5.3.4 COMPARISON OF FUEL CELLS

The above specifications detail each of the fuel cell design characteristics; however, to optimize the operation of energy storage, a careful examination of their advantages and disadvantages must be carried out.

While the efficiency of the high temperature version can be increased to 60% if its waste heat is collected and utilized, this would undoubtedly require a more complex system that could be prone to problems. Its requirement of a preheat phase prior to operation also increases its complexity. For larger systems the high energy density of the MSOFC might overcome these problems of complexity but for a 50 kW_e system it becomes a considerable disadvantage.

The reaction carried out as hydrogen and oxygen combine in a fuel cell is [1]:

$$H_2 + \frac{1}{2}O_2 \Rightarrow H_2O + 238.1 \frac{kJ}{mol} \tag{5.2}$$

This means that, at 100% fuel cell chemical to electric efficiency, the system would require 2.77×10^5 moles of water (4.99 metric tons). However, the chemical to electrical efficiency is much lower, and the reactant mass scales inversely with the efficiency of the fuel cell.

Table 5.2 summarizes the system properties associated with each type of fuel cell design, using PV arrays as the daytime power source. These system masses include the PV array and its structures, the reactants, and the associated fuel cells/electrolysis units. Because the power transmission and the cryogenic system do not scale significantly with fuel cell efficiency, their masses have not been included.

Table 5.2: Mass Summary for a 50 kW_e System

	Alkaline Cell	MSOFC
Chem to Electrical efficiency	70%	60%
Round Trip efficiency	55%	40%
PV Array	1,750 kg	2,410 kg
Reactant Mass	7,125 kg	8,315 kg
Fuel Cell/Electrolysis Units	748 kg	6 kg
Total Mass	**9,623 kg**	**10,731 kg**

This table shows that the MSOFC does not have an advantage over the alkaline cell. If an attached subsystem to convert the high quality waste heat into electric energy were to be included, the MSOFC would have an improved performance, but not without the increased complexity.

The primary advantage of the alkaline fuel cell is the fact that it is currently in use and has been proven to be reliable. The MSOFC is still experiencing problems with the formation

and processing of this sophisticated unit (the interconnector sinters at a different temperature than the rest of the cell components [10]). Due to the availability and reliability of the alkaline fuel cell with current technology, along with an adequate efficiency, this cell was selected for the storage of energy on the Moon in the present design.

5.4 CRYOGENIC REACTANT STORAGE

Kohout [2] has shown that the cryogenic storage of the reactants can decrease the fuel cell energy storage subsystem mass by roughly 50% due to the lower volume and mass of the reactant storage tanks. The study presented here stemmed from this concept with the aim of eliminating as much mass as possible.

5.4.1 ADVANTAGES OF CRYOGENIC REACTANT STORAGE

In conventional energy storage systems, reactants are stored as gases in heavy pressurized tanks. Common materials used to construct these tanks are Inconel (a nickel-based alloy) and lightweight filament-wound materials such as Kevlar/epoxy.

Satellites in low Earth orbit require storage periods of approximately 40 minutes. In these systems, using Inconel tanks, the tankage mass only accounts for 5.5% of the total system mass (Kohout's total system is defined as the electrolysis units, fuel cells, storage tanks, photovoltaic array, radiators, etc. necessary to provide 250 kW_e nighttime power). Lunar missions, however, require storage for approximately 366 hours. For gaseous storage on the moon, the Inconel tanks would account for 82.5% of the total system mass. Substituting light weight filament-wound Kevlar/epoxy tanks, this number can be reduced to 64.6%.

Even though storing the reactants as cryogenic fluids requires additional energy (increase of PV array or Brayton units) and a drying/liquefaction processing plant, the total system mass is reduced by 50%. The tanks recommended by Kohout have a mass only 7.4%

that of the Kevlar tanks used in the gaseous storage system. A comparison of cryogenic and gaseous storage masses, as adapted from Kohout for a 20 kW_e system, is shown in Fig. 5.4.

5.4.2 GASEOUS DRIERS

As the hydrogen and oxygen streams leave the electrolysis unit, they contain a small amount of water vapor that was not completely electrolyzed. This water vapor must be removed before the gases are liquified so that the water does not freeze and block the flow of reactants.

After electrolysis, the gases give off most of their heat through a heat exchanger and then enter a cold trap (~ 275 K) where 99.9% of the water vapor condenses out of the reactant flow [11]. Waste heat is radiated to space. The remaining 0.1% of the water vapor is removed by a sorption drier, where a rotor built up of corrugated sheets impregnated with a hygroscopic salt absorbs the water vapor by molecular forces. This water vapor is then regenerated in the final quarter turn of the rotor and channeled back to the cold trap to begin the drying process again (see Fig. 5.5).

The mass and power requirement of the gaseous driers scale according to the mass flow rate through the system. However, the use of finned composite heat pipe radiators (see section 4.0), instead of the pumped-loop radiators described in the reference, significantly reduces the mass of the drier system. Each drier (one per 25 kW_e unit) has a daytime energy requirement of 0.3 kW_e and a mass of 28 kg.

5.4.3 LIQUEFACTION UNITS

The reactants are converted to a cryogenic fluid through a series of compressions and expansions. A reversed Brayton refrigeration cycle was chosen over Stirling, Vuilleumier and

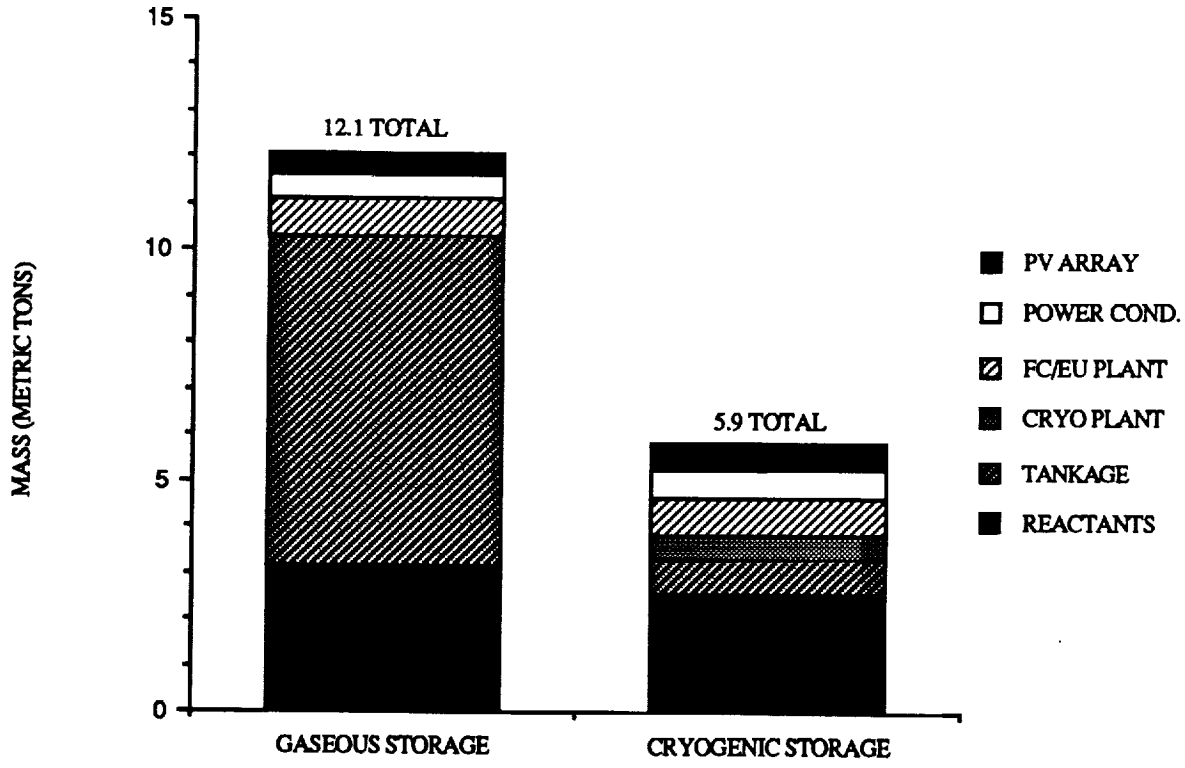

Fig. 5.4. Comparison of Cryogenic vs. Gaseous Reactant Storage for a 20 kW_e System [2].

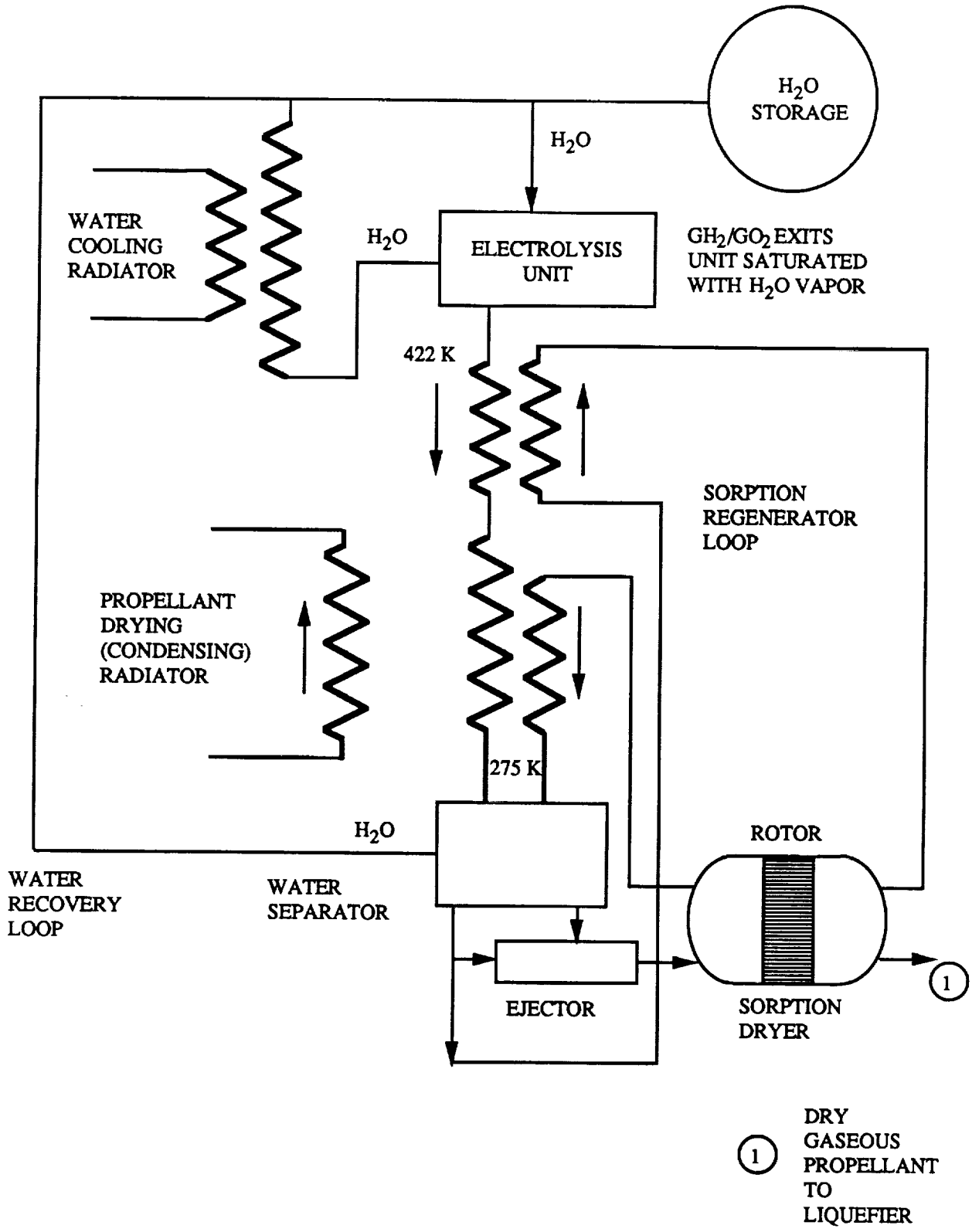

Fig. 5.5. Gaseous Driers [11].

other cycles because it has a lower mass and volume at the refrigeration capacity under consideration [11].

As shown in Fig. 5.6, the gas is first compressed (1 to 2) and then cooled through an inter-cooler (2 to 3). The gas is compressed again (3 to 4) and cooled in an after-cooler (4 to 5). This high pressure gas is cooled in the main heat exchanger (5 to 6) and expanded to a lower-than-boiling temperature (6 to 7). This low temperature fluid is used as the heat sink in the main heat exchanger which warms the fluid slightly, but its final state remains liquid. The hydrogen must undergo an additional expansion/cooling cycle due to its lower boiling temperature. As with the driers, waste heat is radiated to space.

As in the case of the driers, the mass and power requirement of the liquefaction units scale according to the mass flow rate through the system. Again, the use of finned composite heat pipe radiators greatly reduces the liquefier mass. Each H_2 liquefaction unit (one per 25 kW_e unit) has a daytime energy requirement of 3.88 kW_e and a mass of 428 kg. Each O_2 unit has a daytime energy requirement of 1.84 kW_e and a mass of 136 kg.

5.5 STORAGE OPTIONS

A number of different methods for storing the reactants and products for the fuel cell system exist. The option that is currently used for satellites, high-pressure gaseous storage, has already been shown to be much more massive than cryogenic storage for the long lunar night, and therefore eliminated.

A more exotic possibility for storing hydrogen is worthy of some discussion. Hydrogen's extremely low boiling point (20 K) makes it difficult to render liquid, especially under vacuum conditions where heat rejection at low temperature is difficult. Interestingly, it is possible to pack hydrogen atoms into the lattice gaps of certain metals so effectively that the

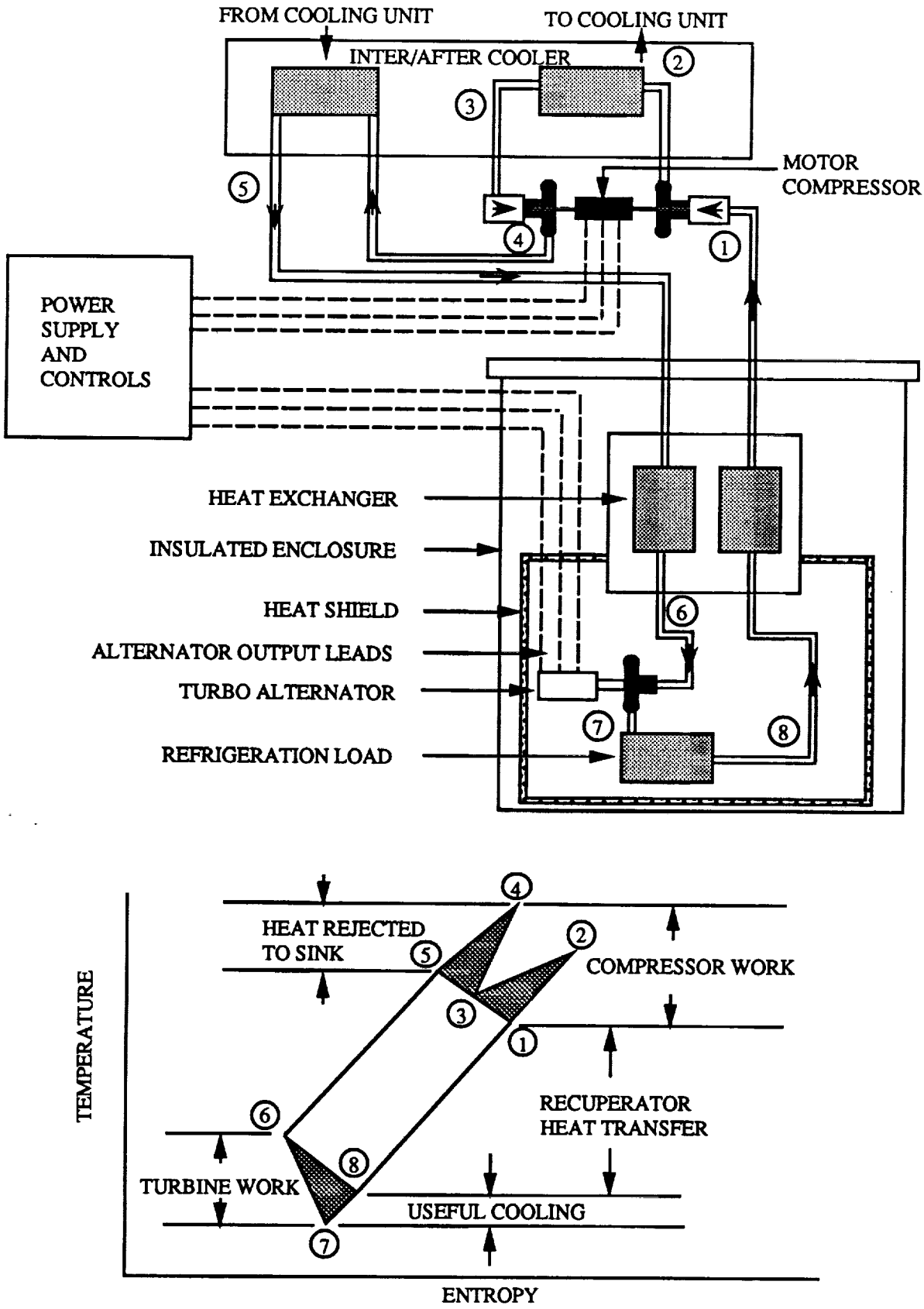

Fig. 5.6. Reversed Brayton Liquefaction Cycle [11].

volume density of hydrogen in the metal exceeds that of liquid hydrogen! Titanium metal absorbs hydrogen reversibly at room temperature to form TiH_2, releasing it again at red heat [12]. A large block of titanium metal sponge could be used at room temperature to absorb hydrogen for storage, and heated to release the gas, without use of a refrigeration system or high-pressure tankage. If the entire body of metal can be converted to TiH_2, each ton of hydrogen would require 22.5 tons of titanium to contain it. This mass is prohibitive if it must be shipped from Earth, but the lunar regolith is rich in titanium-bearing minerals, and with the proper refining equipment, titanium could be produced in bulk locally, making titanium storage of hydrogen more attractive. This study, however, assumes no use of local materials, so titanium storage is not appropriate for the present work. As it turns out, there is a much more attractive option for storing reactants, which will be discussed below.

5.5.1 REACTANT STORAGE TANKS

As discussed earlier, Kohout has shown that storing the reactants as cryogenic liquids greatly reduces the energy storage system mass [2]. However, this mass can be reduced even further by using the propellant tanks of an LEV for reactant storage. These tanks are designed to store H_2 and O_2 as liquids and will have already been delivered to the moon with their own structural support.

In a conceptual report from Martin Marietta, the lunar transit and excursion vehicles (LTV and LEV) will undergo a series of unmanned flight tests from Space Station Freedom [5]. On the fourth and final test flight, an LEV will be loaded with cargo and remain on the moon as the LTV returns to Space Station Freedom. This LEV will provide the reactant tankage for the 50 kW_e energy storage system.

An LEV lands with two H_2 and two O_2 tanks as shown in Fig. 5.7. Each H_2 tank and O_2 tank is capable of storing 1.44 tons of hydrogen and 8.68 tons of oxygen, respectively.

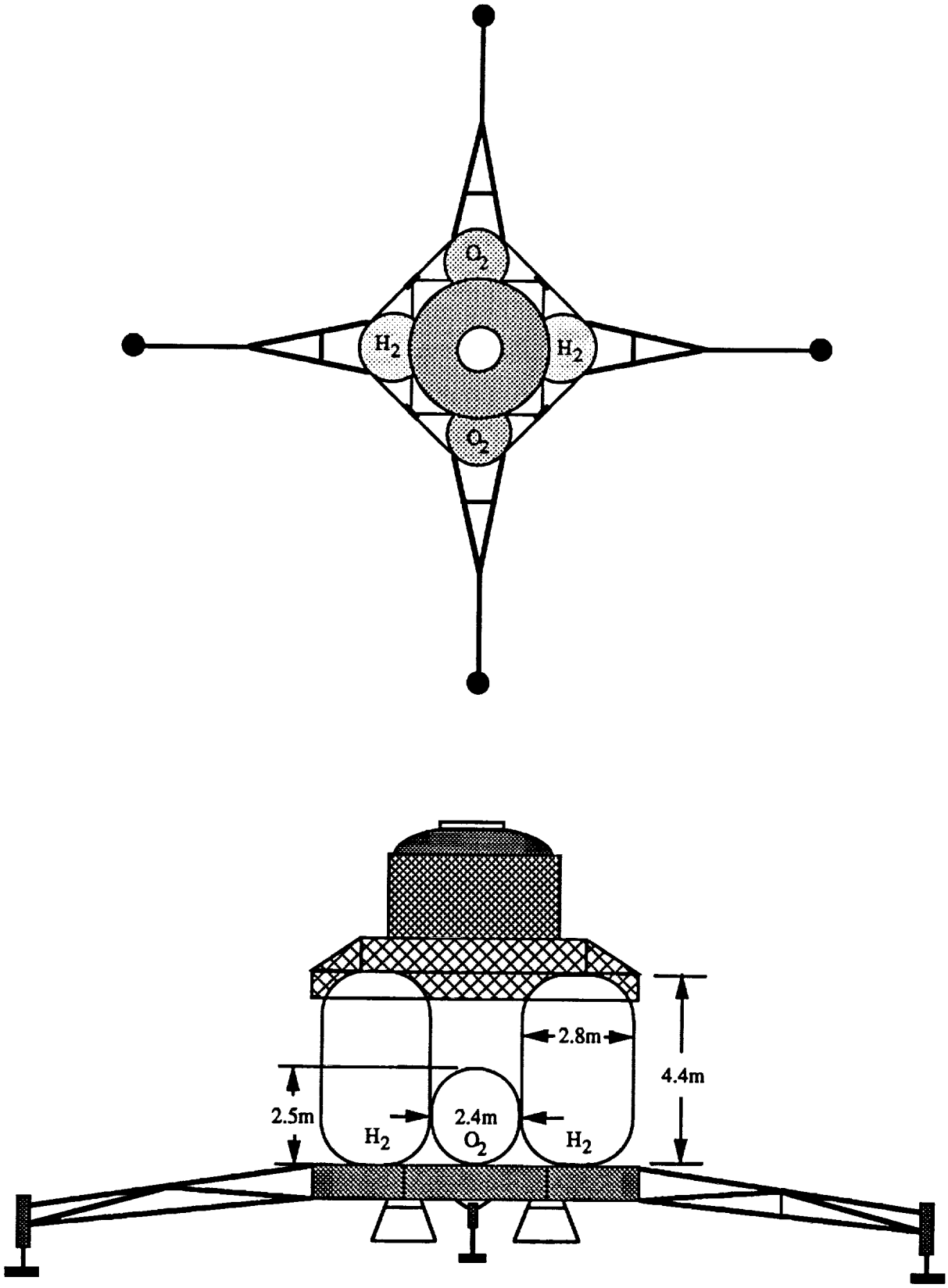

Fig. 5.7. Lunar Excursion Vehicle Propellant Tanks [5].

For the 50 kW_e nighttime power requirement, these tanks will be less than half full (396 kg H_2 and 3166 kg O_2). Should more storage be required as the lunar base activities at night are increased, up to two additional 25 kW_e units can be added to each lander, giving 100 kW_e of night power. The remaining capacity in the 50 kW_e case can be used to store additional reactants for times of peak energy consumption or for use in primary fuel cells on lunar rovers or spacecraft, as suggested by Kohout [2].

5.5.2 WATER STORAGE TANKS

In addition to the LEV tanks, tanks are needed to store the water formed in the fuel cell until the water can be electrolyzed in the daytime. The same tanks that were used to transport the the reactants (in the form of water) from earth can be used. These tanks will have 110% of the volume required by the water to account for possible freezing during transportation. Once the energy storage system is engaged, there will be a constant influx of warm water from the fuel cell during the lunar night, and the water is not expected to freeze. The tanks are made from filament-wound Kevlar/epoxy, and the mass is found to be 148.1 kg by scaling from Kohout's system using the square-cube rule.

5.6 ENERGY STORAGE SUMMARY

Storing the reactants as cryogenic liquids greatly reduces the overall energy storage system mass. Utilizing the propellant tanks from an LEV, the Boeing tandem cell and the finned composite heat pipe radiators further increases the overall system performance. The current alkaline fuel cell was selected over the high-temperature MSOFC for its higher efficiency and lower overall system mass, as well as reduced complexity.

5.6.1 SYSTEM PERFORMANCE

The daytime power requirement for each 25 kW_e unit is listed in Table 5.3 below. (In order to calculate an energy storage system efficiency, power transmission inefficiencies are not included; they are included in section 6.3.) Unit mass is shown in Table 5.4.

The shadowing of the solar collector arrays creates an effective lunar night longer than the day, forcing the electrolyzer to work harder to process the reactants in the shortened time. This means that even if the fuel cells had a round trip efficiency of 100% (electric energy in equal to electric energy out), the power input during the day must be greater than the power output at night. Shading interference creates an effective efficiency of 93.5 % regardless of the electrolyzer selected, and this inefficiency is considered in calculating the power input to the fuel cell.

Table 5.3: 25 kW_e Unit Power Requirements - Daytime

Electrolyzer	48.6 kW_e
H_2, O_2 driers	0.3 kW_e
H_2 liquefaction unit	3.9 kW_e
O_2 liquefaction unit	1.8 kW_e
Unit total	54.6 kW_e
Energy Storage System Efficiency	**45.8%**

Table 5.4: 25 kW_e Unit Mass Summary

Electrolyzer & Fuel Cell	374 kg
Mechanical Ancillaries	338 kg
Fuel Cell Radiators	17 kg
Reactants	
H_2	395 kg
O_2	3,165 kg
Drier units	28 kg
Liquefaction units	
H_2	428 kg
O_2	136 kg
Tanks (effective mass)	
$H_2 + O_2$ *	0 kg
Water	138 kg
Unit Mass	**5,019 kg**

*LEV propellant tanks

In order to have an energy density to compare with other energy storage systems, we must include the mass of the power source. For the Boeing tandem cell (including structures), an additional 1750 kg must be added, giving an energy density of 1550 Wh/kg, compared to current state-of-the art of 500 Wh/kg and future projections of 1000 Wh/kg [4].

5.7 NOMENCLATURE

LeRC	(NASA) Lewis Research Center
LEV	Lunar Excursion Vehicle
LTV	Lunar Transit Vehicle
MSOFC	Monolithic Solid Oxide Fuel Cell
PV	Photovoltaic (Array)

5.8 REFERENCES

1. Weast, R.C., Ed., CRC Handbook of Chemistry and Physics, 63rd ed., CRC Press, Boca Raton, Florida, 1982.

2. Kohout, L. L., "Cryogenic Reactant Storage for Lunar Base Regenerative Fuel Cells," NASA TM 011980, NASA Lewis Research Center, June 1989.

3. McPheeters, C. C., et al., "Recent Advances in Monolithic Solid Oxide Fuel Cell Development," Paper No. 889207, 23rd IECEC, 1988.

4. O'Donnell, P., Deputy Branch Chief, Electrochemical Technology Branch, NASA Lewis Research Center, Private Communication, May, 1990.

5. Mitchell, P., "Lunar/Mars Outpost: Interim Review #1", MCR 89-7505, Martin Marietta Company, 1989.

6. Hoberecht, M.A. et. al., "Design Considerations For a 10-kW Integrated Hydrogen-Oxygen Regenerative Fuel Cell System," Advanced Energy Systems-Their Role in Our Future (19th IECEC), Vol. 1, American Nuclear Society, LaGrange Park, IL,1984, pp. 240-246.

7. Minh, N. Q., Allied-Signal Aerospace Company, AiResearch Los Angeles Division, Materials Engineering, Private Communication, February-March, 1990.

8. Trimble K. A., "The Gas Industry Solid Oxide Fuel Cell Program," Paper No. 889044, 23rd IECEC, 1988.

9. Minh, N. Q., "Forming and Processing of Monolithic Solid Oxide Fuel Cells," Allied-Signal Aerospace Company, AiResearch Los Angeles Division, Materials Engineering, Preprint, 1989.

10. Dees, D.W., Argonne National Laboratory, Private Communication, March, 1990.

11. Bock, E.H., and Fisher, J.G., "In-Space Propellant Processing Using Water Delivered as Shuttle Contingency Payload," AIAA Paper 78-941, July 1978.

12. Livanov, V.A., et al. Hydrogen in Titanium, Israel Program for Scientific Translations Ltd., Jerusalem, 1965.

6.0 POWER TRANSMISSION AND CONDITIONING

Dave Gillespie
John Iacometti
Stan Love

6.1 TRANSMISSION LINES

This section deals with the problem of converting electrical power from the photovoltaic arrays or dynamic cycle engines to different forms for transmission and for use in the fuel cell/electrolysis unit. For the purpose of this study, it was assumed that electric power would have to be transmitted over distances on the order of 100 m. This distance was chosen to provide a buffer zone between the dust-sensitive solar collectors and the activity around the base, while keeping the power generation site within easy walking distance of the habitat. A number of different methods for transmitting power were inspected briefly: wires, microwave beaming, and batteries which would be physically transported between a charging depot and the site of power consumption. The latter two options can be dismissed immediately on the grounds that they are inefficient, needlessly complex, and probably much more massive than transmission cables.

6.1.1 CHOICE OF CONDUCTOR

Choosing the appropriate metal for the wires is fairly straightforward. If the distance for transmission is given, metals can be compared by finding the mass of cable necessary to conduct electricity with the same amount of resistance. The resistance is proportional to the resistivity divided by the cross-sectional area of the wire; the mass of the cable at fixed length is proportional to the same area times the density of material. Different metals can be compared

on the basis of conductivity per unit mass (see Table 6.1). The two metals used most often for commercial power grids on Earth are aluminum and copper [1]; the metal with the best conductivity is silver.

Table 6.1: Conductor Properties [2, 3].

Metal	Conductivity $(\Omega\text{-m})^{-1}$	Density (kg/m^3)	Conductivity per unit mass $(m^2/\Omega\text{-kg})$
Al	3.77×10^7	2,650	14,240
Cu	5.99×10^7	8,960	6,683
Ag	6.29×10^7	10,500	5,990

Inspection of the above table shows that when the mass of the cable is an important consideration, aluminum is the metal of choice because its low density more than makes up for its relatively mediocre conductivity.

6.1.2 VOLTAGE, RESISTANCE, AND FREQUENCY CONSIDERATIONS

The present study calls for the power supply system to be modularized for easy shipping and to eliminate the possibility of single-point failures. The preliminary transmission problem was worked for four 250 kW_e lines, for a total capacity of 1 MW_e. There are a number of tradeoffs between the size of the conductor, the losses in the cable, and the voltage and current used at a given power. If the conductor is made too thin, its resistance is high, and more power is lost in transmission. In extreme cases, resistive heating may melt the line. The conductor must be kept reasonably small, though, or it will weigh too much. Using a high voltage and a low current will keep resistive losses lower at a given power, but voltages cannot be made arbitrarily high for numerous practical reasons.

Kurtz [1] lists the following standards for electrical power transmission on Earth:

1) 1000 V/mi., or 600 V/km;

2) 250 kW_e aluminum line should be about 2-gage cable;

3) Standard voltages used on Earth are 2200, 6600, and 13,200 V.

This study will use the above rules as a starting point because good documentation exists on them, and because the equipment for utilizing them has already been developed and is in ready supply on Earth. Note, however, that these basics were developed for transmission across distances several orders of magnitude larger than that considered in this study. Section 6.4 details the differences in transmission brought about by short distances and the need to minimize mass.

Insulated cable might be preferred as a safety measure. The choice of insulating material would be dependent on the design lifetime of the transmission line. It may not be possible to use common Earth insulators on the Moon because some materials may be broken down by ultraviolet sunlight or exposure to hard vacuum and extremes of temperature. Whatever material is chosen, it must be flexible enough to allow the cable to be wound on spools for transport, and as lightweight as possible to cut down on the mass that must be shipped to the Moon. For the purposes of this work, cables will be uninsulated to reduce the transmission system mass and to decrease the likelihood of arcing (see subsection 6.1.3).

The resistivity of aluminum is somewhat temperature dependent, with larger resistance (and therefore less efficient transmission) at higher temperatures, so it may be advantageous to provide the cable with a sun shield, or perhaps bury it to keep it cool. Burying the cable would also be a good safety measure, since it is not insulated and accidentally contacting it could prove hazardous to astronauts.

Since the power lost in the line is I^2R, where I is the current in the line and R is the resistance of the cable (proportional to its length) and VI, the product of the line voltage and current, is fixed by the power requirement, it is clear that minimizing I keeps resistive losses

down. Therefore, 13200 V would be chosen as the potential difference between the ends of the cable for long distance transmission, although a higher value could be used. If the transmission distance is short, though, the added mass and complication of the equipment needed to change voltage outweighs the comparatively small resistive losses. A detailed discussion of the tradeoff between high and low voltage transmission for different distances is given in Section 6.4.

In practice, power is transmitted as AC rather than DC to allow the voltage to be adjusted at various places in the grid with transformers. The frequency of the AC can have important effects on line losses, beyond those caused by simple resistance, which should not be ignored.

The most straightforward loss mechanism occurs when the length of the cable becomes comparable to or longer than the wavelength of the electrical signal in the wire [4]. If there is more than one wave in the line, the flow of electrons becomes nonuniform, resulting in power loss in the cable. To check what frequency range this effect inhabits for a cable of given length, the relationship:

$$f = \frac{c}{L} \tag{6.1}$$

is used, where L is the length of the cable, f the frequency in cycles per second, and c is the speed of the signal (for most practical purposes the speed of light). If f is comfortably lower than c/L, there is less than one wave in the line and the losses will be at a minimum. Using 1000 m as an upper limit for L, the f at which there is one wave in the line is about 300 kHz. To safely ignore all such losses, our transmission frequency should be 30 kHz or less.

Another possible mode of loss in the cable occurs if the transmission frequency is such that the skin depth (distance in from the surface of a conductor at which the electric field has dropped to 1/e of maximum) in the material is much less than the line radius. If the skin depth is too small, the wave travels along the surface of the conductor, thus decreasing its effective

cross-sectional area and increasing its resistance. The skin depth of a wave of frequency f in a conductive medium of conductivity σ and permeability μ is given by [2]:

$$d = \frac{1}{\sqrt{\pi f \sigma \mu}} \tag{6.2}$$

Inserting the values appropriate for our 2-gage aluminum conductor, we arrive at a skin depth:

$$d = 8.20 \text{ cm} \times \frac{1}{\sqrt{f}} \tag{6.3}$$

If d is to be greater than the radius of the conductor (3.3 mm for the standard 2-gage cable,) f must be less than 630 Hz. It should be noted, however, that it is unlikely that the conductor will be a solid cylinder, but rather a bundle of much smaller wires bound together into a thick cable. The advantages of such an arrangement are twofold. First, it allows the cable to be much more flexible (and therefore easier to ship and work with) than if it were a solid bar; and second, it means that the current flows in wires of small radius, decreasing skin depth losses and allowing a higher transmission frequency. Making the conductor into a bundle of small wires has no effect on resistive losses, which care only about the total cross-section of conducting material. If the bundle contains, for instance, 100 small strands, the diameter of each will be about 1/10 of the total conductor diameter, and the allowable skin depth decreases accordingly. The result is a 100-fold increase in the maximum allowable transmission frequency, well into the realm where wave losses become crippling.

Despite the large allowable range in transmission frequencies, it would probably be best to transmit at 50 or 60 Hz. These frequencies are safely below any wave loss or skin depth effects, and there is a wealth of off-the-shelf equipment and practical experience in dealing with

power transmission at these frequencies. In addition, the solar dynamic engines produce their power in this range, allowing transmission without changing the frequency in that case.

6.1.3 ARCING

In the presence of ionizing radiation and outgassed materials in a space environment, electrical systems can experience arcing, in which the very tenuous plasma surrounding electrical components breaks down, allowing current to arc from one place to another. This short-circuiting interrupts the flow of power and can damage equipment. Arcing is an important consideration in designing electrical systems for use in low Earth orbit (LEO), where the Earth's atmosphere can contribute to the plasma in which breakdown occurs. The lunar environment has a far lower gas density than LEO, but arcing should be considered in the design of the system, particularly in terms of spacing the transmission lines.

Under perfect vacuum conditions, electrons can tunnel out of the surface of a conductor and generate spontaneous arcs [5]. This phenomenon is predicted to occur in the presence of heat (1000 K) and electric fields greater than 10 MV/m. At room temperature, the arc threshold approaches 10 GV/m. Given the voltages used in this system, such fields will not be present. In laboratory experiments (in which, it should be noted, the ambient gas density far exceeded that at the Moon's surface) at room temperature, aluminum electrodes exhibited breakdown at fields of 200 MV/m. Assuming two 13.2 kV cables with currents exactly out of phase (the case in which the greatest electric field exists between them) are laid next to each other, arcing could be expected at a separation of 0.13 mm or less. In actual practice, though, small dents and rough areas on the surface of the wires can lead to greatly enhanced local electric fields, thus lowering the arcing potential. Also, if the wires or anything in their immediate neighborhood emit enough gas to raise the local number density of charged particles, arcing could occur at much greater separations. Such extensive outgassing is unlikely, and would dissipate rapidly in the current Lunar environment.

A different treatment of the arcing problem can be arrived at using data on insulators that might be used to cover these wires. Breakdown for typical insulators is expected at field strengths of about 5 MV/m [5]. Note that arcing is easier to achieve for insulated cables than for uninsulated ones, a somewhat surprising result, and another justification for leaving the wires uninsulated. Breakdown field strength could be achieved by laying two out of phase 13.2 kV (the worst case for long-distance transmission) cables a distance of 5 mm apart. For short range transmission of AC power, where the potential is only 200 V, breakdown occurs at a separation of only 0.08 mm for out of phase lines. For DC transmission, the potential in neighboring cables is always the same, so no arcing will occur. Again, this calculation assumes that the lines are subject to current lunar near-vacuum conditions. A more detailed calculation would require knowledge of the insulator's outgassing rate, and possibly also the mean free path and ionization time of the emitted material. Because of the extreme thinness of the current lunar atmosphere, it appears that arcing or breakdown of insulating coatings can be easily avoided with separations between the cables of a few centimeters.

6.2 POWER CONDITIONING

The storage and transmission of energy require different types of power. For transmission at reasonable voltage, the current must be alternating, at or below a few thousand Hz as discussed above. For storage, the current must be direct, at 200 volts in the proposed configuration. This design does not forbid construction of cells of different voltages, though, so 200 volts is not a hard requirement. The photovoltaic panels in this study produce direct current at 200 volts, which is ideal for the proposed electrolysis units, but not for long-distance transmission. The solar dynamic engines considered in this study produce alternating current at 50 Hz and can be fitted with generators yielding their output at 200 volts. This power must be converted to DC for storage, and to higher voltage (13,200 V as discussed above) for long-

range transmission. At short distances, 200 V will suffice for transmission of power from either generation scheme. Converting between DC and AC is accomplished with an inverter. Estimates of mass and efficiency for typical inverters are 0.272 kg/kW$_e$ and 96.5% to 98% respectively [6]. For this report, 97.5% efficiency will be assumed. It is assumed that the base will use AC at the same voltage and frequency as the rest of the power grid. A 14 kg inverter will be required to convert the 50 kW$_e$ nighttime output of the fuel cells into AC for the base.

Transformers are also needed for various stages of power conditioning. Transformer mass and efficiency are estimated to be 0.91 kg/kW$_e$ and 98.5% respectively [7]. Because a power transformer is built around a heavy iron core, with a minor amount of the total material contained in the windings about the core, it is assumed that the mass does not scale strongly with the voltage change or frequency, but is most strongly dependent on the power that will flow through it.

Given the above inefficiencies in power conditioners, one can calculate the actual rate of energy flow through each stage of the system in order to provide 1 MW$_e$ to the user during the daylight hours, and 50 kW$_e$ during the night. The masses required for various stages of power conditioning can be estimated once the power load is known. A diagram of the power conditioning and transmission system is shown in Fig. 6.1 for the solar photovoltaic system, for both long and short range transmission. An analogous diagram for solar dynamic generation is given in Fig. 6.2.

6.3 TRANSMISSION OPTIMIZATION

Because mass is such an important consideration when designing a power distribution system for any space application, it is prudent to look closely at optimizing the mass of the

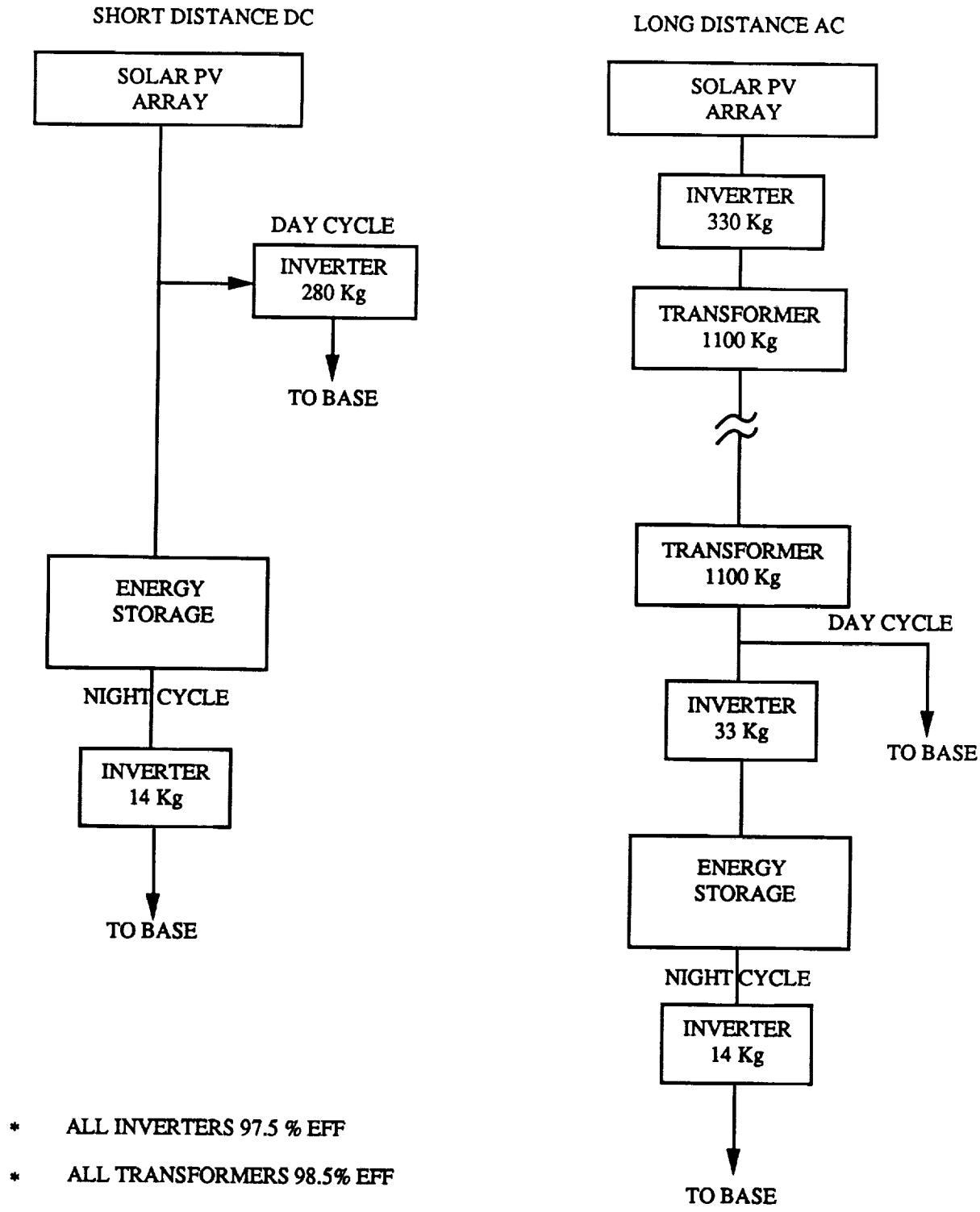

Fig. 6.1. Solar Photovoltaic Power Transmission.

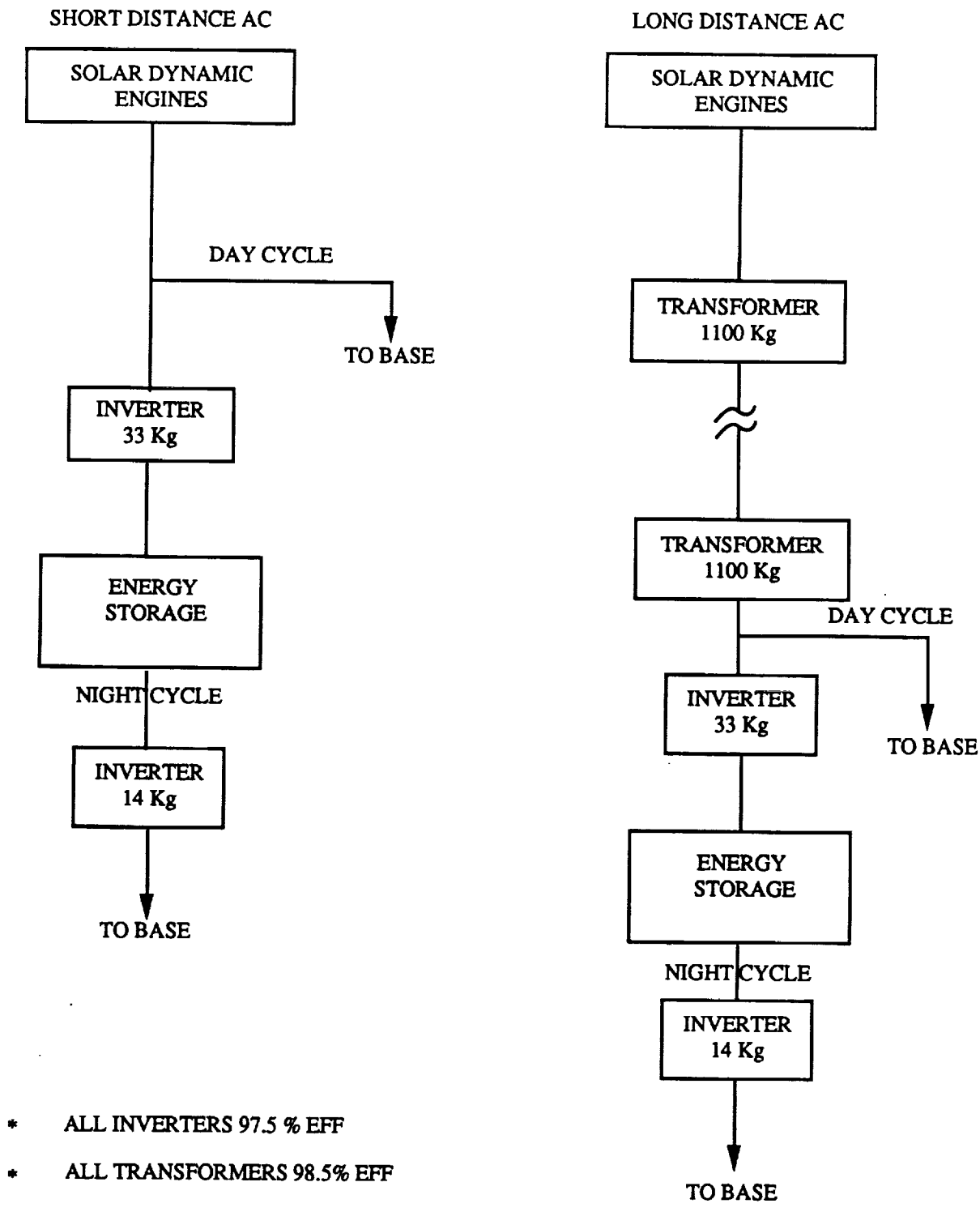

Fig. 6.2. Solar Dynamic Power Transmission.

entire network, not just the cables and conditioners. One could choose an extremely thin and lightweight cable to carry the power load and thus make the transmission system mass very small indeed, but such a thin cable will have large resistive losses and require additional power generation system capability (and therefore mass) to compensate. Likewise, a thick cable may be more mass-costly than additional PV panel sets. This subsection will describe how the mass of the total system can be optimized by choosing the proper value of the transmission inefficiency. It will also quantify the difference between the "long distance" and "short distance" transmission that have been referred to in the previous subsections.

Given values of the voltage and current to be transmitted (the product of which is the power load in the line) and the efficiency at which one wishes to transmit it, the resistance of the line can be computed:

$$R = \frac{(1-\eta)\,P}{\eta\,V^2} \tag{6.4}$$

The resistance can be combined with the cable length and the resistivity and density of the conductor to yield an expression for the mass of the cable:

$$m_{cable} = \rho\,\frac{P\,L^2}{\sigma\,V^2}\left(\frac{\eta}{1-\eta}\right) \tag{6.5}$$

The inefficiency in power transmission has a direct effect upon the mass of the generating system, which must compensate for losses in transmission and conditioning to keep the required power available to the user. An expression for the total mass of the power generation, transmission, and conditioning hardware is given in Eq. 6.6.

$$m_{total} = m_{cable} + m_{cond} + \frac{P\,\mu_{pv}}{\eta} \tag{6.6}$$

The specific mass of the photovoltaic generation system, μ_{pv} , is 16.1 kg/kW$_e$, including structures (see Sections 2.5 and 7.2.5). In the case of transmission without boosting the voltage, the cable mass is found using the 200 V potential difference supplied by the photovoltaic arrays, and the conditioning equipment has a total mass of 280 kg. For AC transmission at 13,200 V, the conditioners have a total mass of 2563 kg. Given all the above information, it is possible to calculate the line efficiency which best balances line mass against the additional generation system mass required to compensate for a light line's increased power losses.

$$\frac{d(m_{total})}{d\eta} = \rho \frac{P L^2}{\sigma V^2} \left(\frac{1}{(1-\eta)^2}\right) - \frac{P \mu_{PV}}{\eta^2} = 0 \qquad (6.7)$$

For long distance AC transmission, the voltage is so large that the first term can be neglected for short distances. This leads to an optimum efficiency of 100%. For DC transmission, this equation must be solved for η for different distances. Assuming the optimum efficiency for each distance, the total generation and distribution system mass can be computed as a function of distance. For the solar photovoltaic energy source, the results are shown in Fig. 6.3. The optimum line efficiency for this system is 96.8%, as shown by the shallow minimum in the combined mass curve in Fig. 6.4. Note that the large mass of the power conditioning for the high-voltage AC transmission case represents a substantial increase in the total system mass at short distances, but beyond about 200 m the inefficiency of transmitting at low voltage becomes crippling. Beyond 200 m, the transmission distance is "long," at least in terms of the power conditioning required. At distances slightly beyond 200 m, it might still be advantageous to use a more massive system without power conditioning, to avoid the added complication and maintenance of the power conditioning machinery. Since the power generation site in this study is assumed to be only 100 m from the

energy storage facility and the base, it is best to transmit at low voltage. For the solar dynamic system, which has a large specific mass than the solar photovoltaic option, the distance at which it becomes more mass-conservative to use high voltage transmission is shifted toward slightly smaller values.

6.4 POWER TRANSMISSION AND CONDITIONING SUMMARY

Optimization of the power conditioning and transmission system is closely tied to the specifics of the system used to generate the power. For the short (100 m) transmission distances used in this study, a simple power distribution system that operates at the voltage generated by the solar cells or dynamic engines requires less mass than a more complicated arrangement that uses high voltage in the lines. Aluminum cables are used, and the only power conditioning required is an inverter between the solar array and the user, plus a smaller inverter downstream of the fuel cells for nighttime power. The power conditioning mass is roughly 300 kg, and the optimized cable mass for solar photovoltaic power generation is 650 kg. The total power conditioning and transmission mass is thus 950 kg. Note, however, that a distance of only 500 m between the solar arrays and the base would require a much more complicated system to transmit the power efficiently. Since the transmission is accomplished at only 200 volts, arcing is not a concern at all.

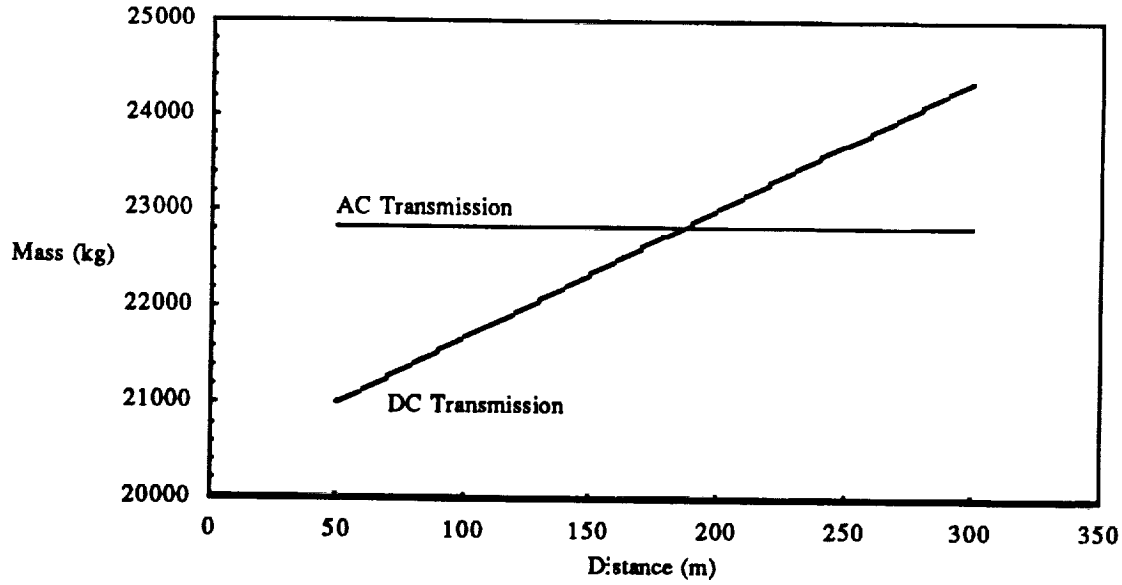

Fig. 6.3. AC vs DC Transmission, Solar Photovoltaic Energy Source.

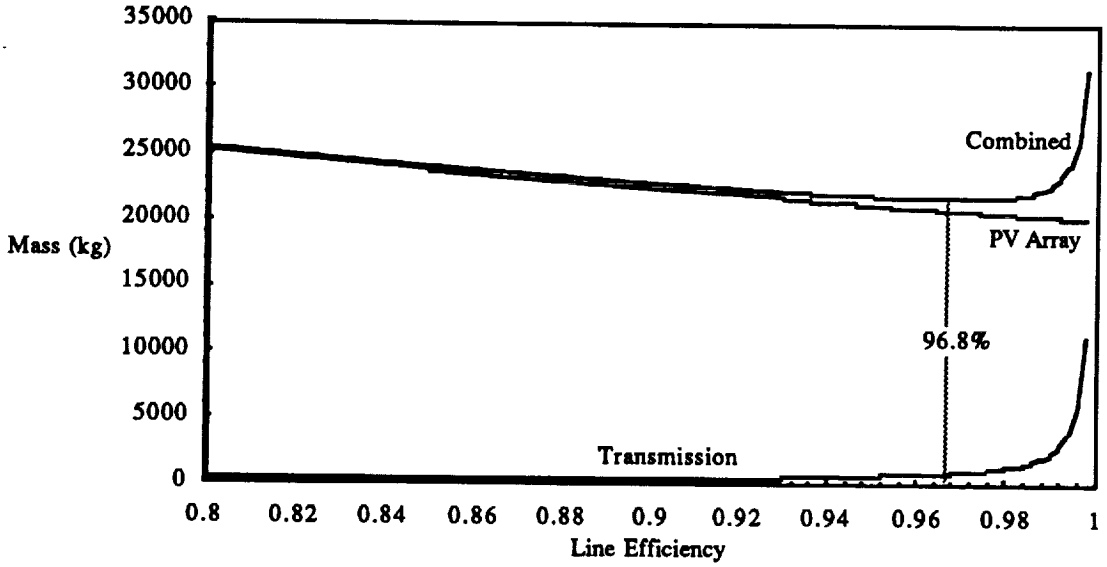

Fig. 6.4. Optimum Line Efficiency at a Distance of 100 m.

6.4 NOMENCLATURE

A	cross-sectional area of conductor
c	speed of light, 3.00×10^8 m/s
d	skin depth
f	transmission frequency, Hz
I	current
L	length of cable
m	mass
P	power in cable
R	resistance
V	voltage
η	transmission efficiency
μ	magnetic permeability
μ_{PV}	photovoltaic specific mass
ρ	conductor material density
σ	electrical conductivity

6.5 REFERENCES

1. Kurtz, E. The Lineman's Handbook, McGraw Hill Book Company, New York, 1928.

2. Griffiths, D.J., Introduction to Electrodynamics, Prentice-Hall, Inc., Englewood Cliffs, N.J., 1981.

3. Weast, R.C., Ed., CRC Handbook of Chemistry and Physics, 63rd ed., CRC Press, Boca Raton, Florida, 1982.

4. Skilling, H.H., Electric Transmission Lines, McGraw Hill Book Company, New York, 1951.

5. Lafferty, J.M., ed., Vacuum Arcs: Theory and Application, John Wiley and Sons, Inc., New York, 1980.

6. Dickerson, A., California Polytechnic Institute, Pomona, Private Communication, February, 1990.

7. Calloway, T.M., "Comparison of Designs for Photovoltaic Power Conditioners," Sandia National Labs, 1986.

7.0 STRUCTURAL DESIGNS

Sam Alhadeff
Brian Adams
John Nelson

7.1 INTRODUCTION

The lunar solar power station will require various types of structural support These structural components will include advanced composite materials, high strength metals , and concrete fabricated from lunar materials. Common to all structures is the requirement of designing for low gravity effects and the harsh lunar environment (including intense solar radiation and rough terrain). The report consists of four major design sections which support the lunar power station:

1) Solar Photovoltaic Cells
2) Solar Dynamic Power Conversion
3) Thermal Management
4) Lunar Concrete

Each section contains its own structural design criteria necessary to support it and the methods required to build it.

Designs must take into consideration the restrictions of the size of the Shuttle C payload bay (25 m x 4.6 m Dia.) and mass capacity (71 metric tons). Pre-assembly on earth of certain structural members of each section will be the most cost effective method to support mass minimization. All composite truss members will be fabricated on earth as well as the other composite components of the solar array support structure and heat pipe radiator support structure. In addition, the members must be designed for ease of handling and assembly in the lunar environment. Each section has its own specific assembly requirements and it was assumed that much of the assembly would be done by astronauts (not robots).

The components of each section will be transported to low earth orbit (LEO) by the Shuttle-C. From there they will be transferred to an orbital transfer vehicle (OTV) for trans-lunar injection (TLI). From lunar orbit they will be transferred to a lunar excursion vehicle (LEV) and ferried to the lunar surface. Upon arrival, most of the structures will be unloaded automatically by the LEV. Those that are not unloaded will remain in the vehicle to be unloaded manually or with a light crane (presumed available).

Another important design criterion was to achieve as much intra-system compatibility as possible within each of the major design sections. In particular, the design of truss members which can be used in more than one area of a structural system will make it easier to inter-change truss members. With fewer types of members, a scheme of marking each type (such as color-coding) will be less complex, decreasing assembly time.

7.2 SOLAR PHOTOVOLTAICS STRUCTURAL DESIGN

7.2.1 ARRAY SIZING

An overall view of an individual solar array is shown Fig. 7.1. There are two 3 m x 12.5 m panels per array allowing the array to provide a 75 m^2 area to be covered with solar cells. Approximately 3750 m^2 of the Boeing high efficiency solar cells or 4875 m^2 of the TRW cells are needed to generate the power requirements of the lunar base. With this design, 50 individual arrays (65 for the TRW cells) will be used to achieve this total area.

The array is designed to be easily assembled and handled by astronauts. The components are designed in segments so that they can be packed compactly in the Shuttle-C cargo bay. The truss members and nodes will be stowed in canisters for easy removal on the lunar surface. The width of the arrays allows them to be easily accessible for repairs and maintenance since the entire optical surface can be reached by astronauts without assistance from large equipment.

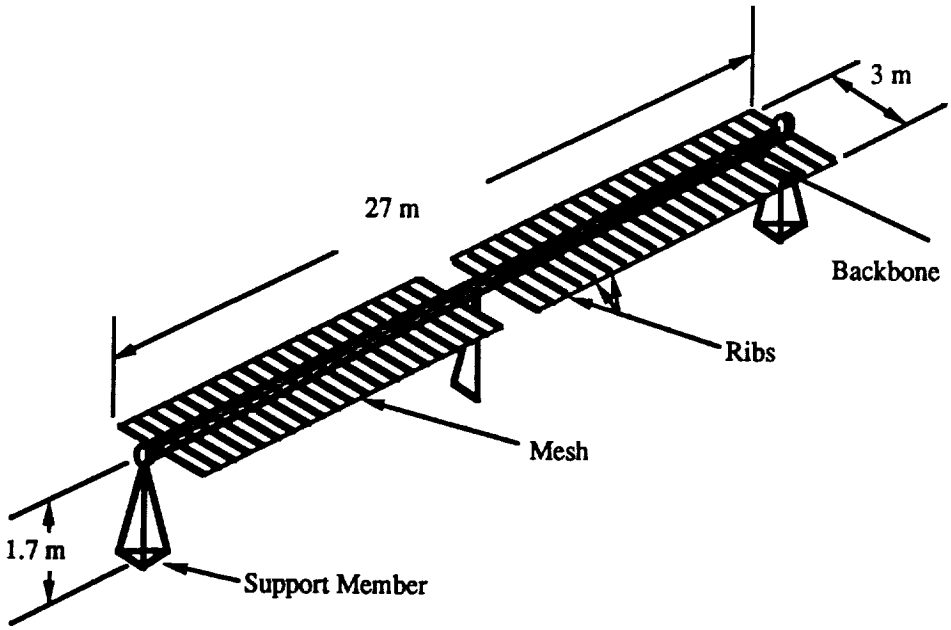

Fig. 7.1: Solar Array Structure.

7.2.2 SOLAR ARRAY STRUCTURE

Detailed views of the array can be seen in Figs. 7.1 and 7.2. Primary design considerations were that the structure be simple, efficient and maintainable. The "backbone and rib" structure, as illustrated in Figs. 7.3 and 7.4 was chosen because it best suited these needs. Little assembly time will be required, and it is lightweight and easy to repair. Each rib is mounted through the backbone using pin connections and a coarse wire mesh is attached to the top of the ribs, extending the entire length of the array. The cells themselves are attached to this mesh. The ribs and mesh allow quick visual inspection of connections and easy access if repairs or replacement is needed. (A box truss structure support was also considered for this design but proved to be unattractive due to the much greater structural mass required for the many members and joints (nodes)). The present design carries the approximately 2.5 kg/m^2 load of solar cells using a minimum of structural mass and allows efficient transport, as described above. The backbone of the structure carries the load of the cells, the mesh, and the 42 ribs. The honeycomb structure of the cell housings is not inherently stiff enough to support the weight of the cells over a distance greater than a few cell lengths. With ribs located every 0.6 m (15 cells per rib), and a tight mesh attached to the top, the cells will be supported with negligible deflection. The wire mesh also allows the cells to radiate waste heat through their base directly to the surroundings.

7.2.3 ARRAY COMPONENTS AND THEORY

The central beam ('backbone') that provides the primary support measures 25 m in length. It is a 15.24 cm square box beam with walls 0.316 cm thick. The box-beam was chosen for its high strength to mass ratio and was designed so that the moment of inertia of the cross section will never approach a critical value as it might with an I or L beam. The beam is composed of 15 plies of graphite/epoxy (Gr/E) with the qualities described in Appendix A. In addition, a localized paddup region of 5 additional plies is used in areas of high stress concentration. This addition increases the mass by only 2.5 kg per array and decreases the

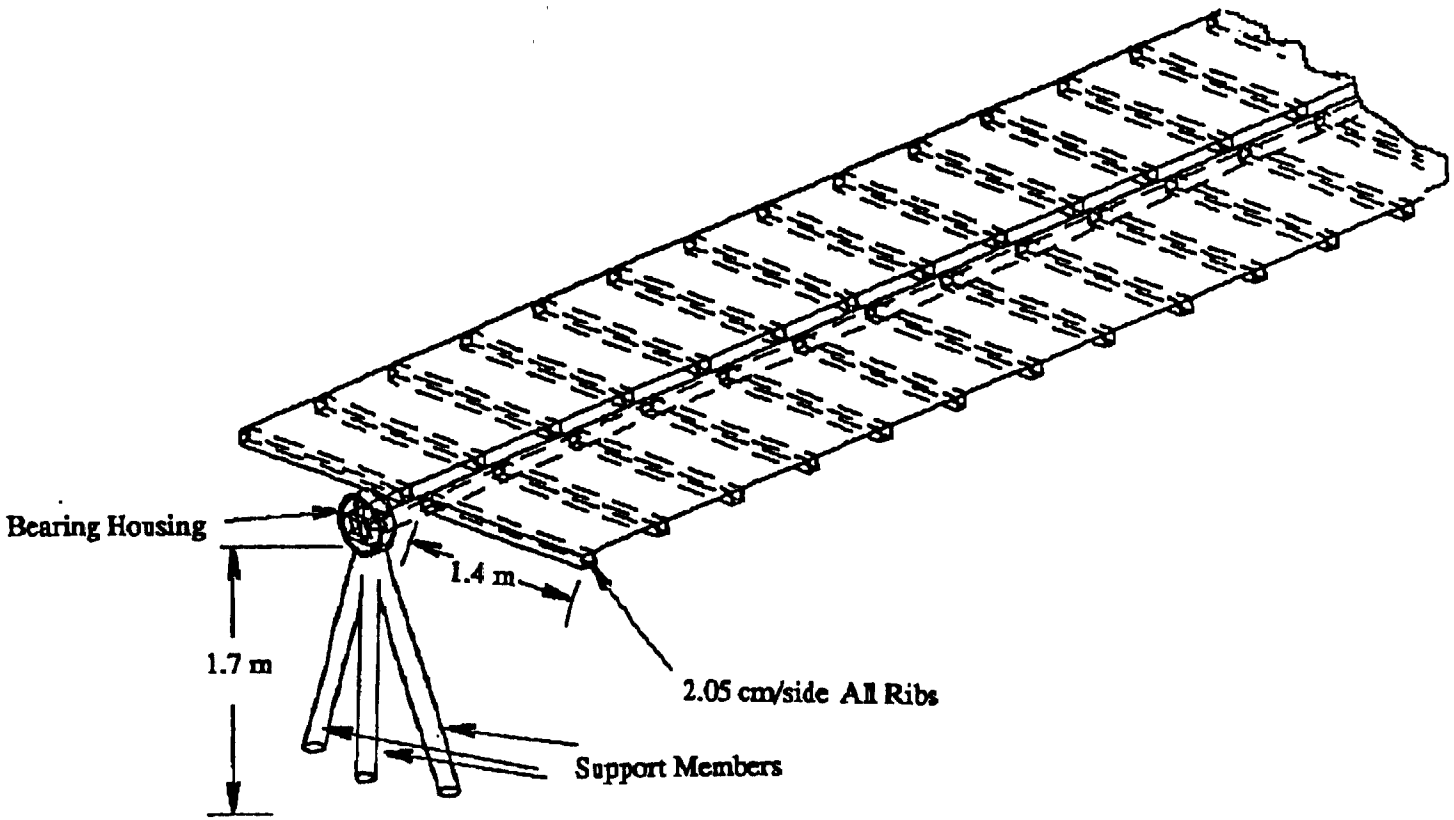

Fig. 7.2. Solar Array End Supports

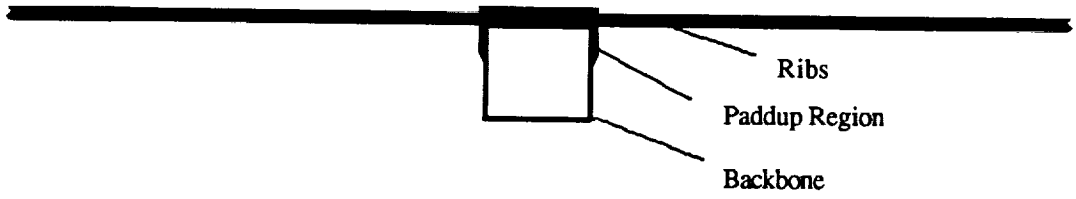

Fig. 7.3: Array Ribs Attached to Backbone

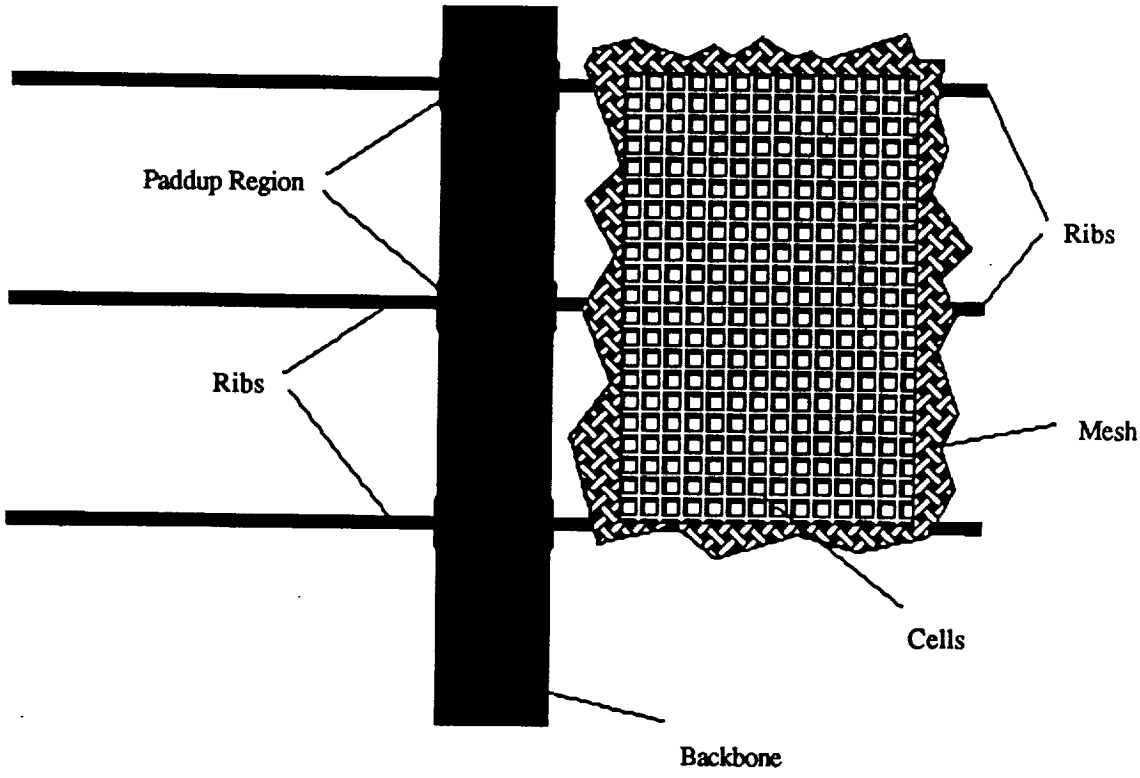

Fig. 7.4: Wire Mesh With Solar Cells Attached.

maximum stress on the beam walls by 20% (the area supporting the load increases, so the stress decreases).

Both the beam and the ribs were designed using linear elastic beam bending theory to produce as little deflection as possible. The moment of inertia of the beam's cross section is given by:

$$I = \frac{b_{out}^4 - b_{in}^4}{12} \tag{7.1}$$

where b_{out} and b_{in} are the outer and inner dimensions of the box beam, respectively. The deflection at the halfway point between the central and end support is given by:

$$U = \frac{P_x L^4}{384EI} \tag{7.2}$$

(assuming fixed ends) where P_x is the load per unit length supported by the box beam, L is its length, and E and I are the modulus of elasticity and moment of inertia, respectively.

Since the Shuttle-C has a payload bay length of 25 m, additional 1.1 m extensions will be placed over the ends of each 'backbone' in order to extend the length to 27 m. This is necessary so that the beam can be supported on its ends by the two primary bearing housings, and in the center by an intermediate bearing housing. These extensions will be fabricated of the same material as the backbone, so that no additional stresses due to incompatible coefficients of thermal expansion (CTE) will be introduced.

The ribs are hollow, square, Gr/E rods measuring 2.54 cm per side, and approximately 1.42 m in length. Each rib contains 5 lb. (5 lb. per ft^3) Nomex honeycomb core to increase its stiffness. The use of Gr/E and core allows each rod to have a mass of only 0.545 kg (based on the 11 ply composite laminate and the mass of the core). The ribs were analyzed as cantilever beams using beam bending theory. The deflection at the end of each rib is given by:

$$U = \frac{P_x L^4}{8EI} \tag{7.3}$$

The maximum deflection at the free end of each rib was designed to be 1.27 cm, less than one percent of the length of the rib. The moment of inertia of a rod's cross section is given by Eq. 7.1. Although the deflection analysis resulted in a very small moment of inertia, we used additional plies (which increases I) to protect against local crippling. Each rib will contain two holes which will allow spring driven pins to lock it into place within the backbone. Array structural member dimensions are listed in Table 7.1.

Table 7.1 Array Structural Members Dimensions

Array Member	Area (m^2)	Length (m)	Mass (kg)	# of members
Box Beam	1.89E-3	26	70	1
Array Ribs	2.20E-4	3	1.2	42

7.2.4 ARRAY SUPPORTS

The support structure for the arrays was designed to minimize mass and to permit easy assembly and installation. The truss support design can be seen in Fig. 7.2. The benefit of this design is that it avoids the usual problems caused by anchoring on the lunar surface (the depth of solid bedrock, small pits, etc.). Due to the almost complete absence of seismic activity and other natural forces, structural reinforcements in anticipation of these events are unnecessary. The tetrahedral end supports are designed to support the bulk of the array load and to provide ample stability in the lateral directions without the aid of guy wires or complicated anchoring. The central support of the central beam decreases the moment of inertia required to support the load carried, reducing the mass of this component.

All three supports will have small pads on the bottom of the supports. These footings will provide additional stability and prevent the trusses from settling unevenly in the lunar regolith. The pads can be fabricated from lunar concrete if it is available for use.

The supports provide a 0.2 m clearance between the array and the lunar surface when it is oriented vertically, so that it may rotate a full 360° if required. Mounted on top of the end

and central supports will be a circular bearing (through which the 'backbone' will fit) to allow the array to rotate.

7.2.5 SUPPORT COMPONENTS AND ANALYSIS

The support trusses will consist of composite members. Each member will be composed of 9 plies of Gr/E and 2 plies of fiberglass (for corrosion protection against the titanium node connectors), which will be fabricated into a tube. This layup was determined using Fig. A.1 (Appendix A). Using tubes instead of solid members will reduce the mass required to support the given loads. Due to the high strength of the Gr/E material, the truss members will never approach critical buckling load [Eq. 7.4]. Although the number of plies of graphite used is greater than required for the critical load, it is necessary so that the members will not be fragile and susceptible to damage. The critical buckling load for a member is given by:

$$P_{cr} = \frac{\pi^2 EI}{L^2} \tag{7.4}$$

The moment of inertia I, of a tube's cross section is given by:

$$I = \frac{R_o^4 - R_i^4}{4\pi} \tag{7.5}$$

where E is the modulus of elasticity of the composite, and R_o and R_i are the outer and inner radii of the tube, respectively. These equations depict the buckling behavior for pinned truss members. This truss will be assembled using a NASA EVA erectable truss joint design [1]. Titanium nodes will be used because of their strength and competitive weight. A breakdown of truss dimensions by size and mass is shown in Table 7.2.

Table 7.2 Array Support Members Dimensions

Member Type	Area (m^2)	Length (m)	Mass (kg)	# of members	Total Mass Per Array (kg)
1	1.23E-3	1.8	3.1	8	25
2	1.23E-3	1.2	2.07	1	2
3	1.23E-3	1.74	1.74	6	11

An estimated load of 2.5 kg/m^2 was used to calculate the weight of the solar cells (lunar gravity). This gives a total load of 187.5 kg per array. The structural mass of this system is approximately 200 kg per array (including the mass of the bearings and truss nodes).

7.2.6 ASSEMBLY

The support trusses will first be assembled and placed in the proper locations. Then the bearings will be mounted on top of them and the extensions will be fitted on to the ends of the "backbone". Next the "backbone" will be placed in the bearings and the ribs will be inserted. Then the wire mesh and solar cells will be attached to the top of the ribs . The tracking motor and wiring will be attached after all structures are securely in place. Table 7.3 lists total structural massed for one solar array.

Table 7.3 Total Structural Mass For One Solar Array

Member Type	Total Mass Per Array (kg)
Box Beam	70
Ribs	50
Support Members	38
Bearings and Nodes (Approx.)	45
TOTAL MASS	203

7.3 SOLAR DYNAMIC POWER CONVERSION STRUCTURAL DESIGN

The design for the solar collector for the Brayton engines consists of a central duct for the working fluid, a parabolic concentrating trough, a framework for the trough, and trusses to support the entire structure (see Figs. 7.5 and 7.6). The overall dimensions of this design were driven by the dimensions of the parabolic trough, which is described by the equation:

$$y = \frac{x^2}{4} \tag{7.6}$$

with the origin of coordinates at the apex of the parabola. Approximately 110 m of solar collector is required per engine. This length is divided into 5 m segments, and the structural design is based on this length. Five meters was chosen since the reflecting panels, (four around the perimeter of the parabolic support structure), are subject to unstable bending while being lifted and placed in position within the support framework.. The truss structure design framework was designed to place the mass centroid of the combination (concentrators and truss structure) one meter above the apex. This allows for rotation to occur about this point while keeping the fluid pipe stationary at the focal point of the parabolic concentrators.

7.3.1 FLUID DUCT

The central duct is to be constructed from UDI MET 700 [see section 3.4.1]. It must retain its strength at a maximum temperature of 1150° K, with an internal pressure of 5.1 MPa over a period of several years in order to have reasonable maintenance characteristics. For these purposes it was determined that a thickness of 2 mm for a 5 cm diameter duct would support these conditions [Eq. 7.7]..

$$\sigma_x = \frac{PD}{2t} \tag{7.7}$$

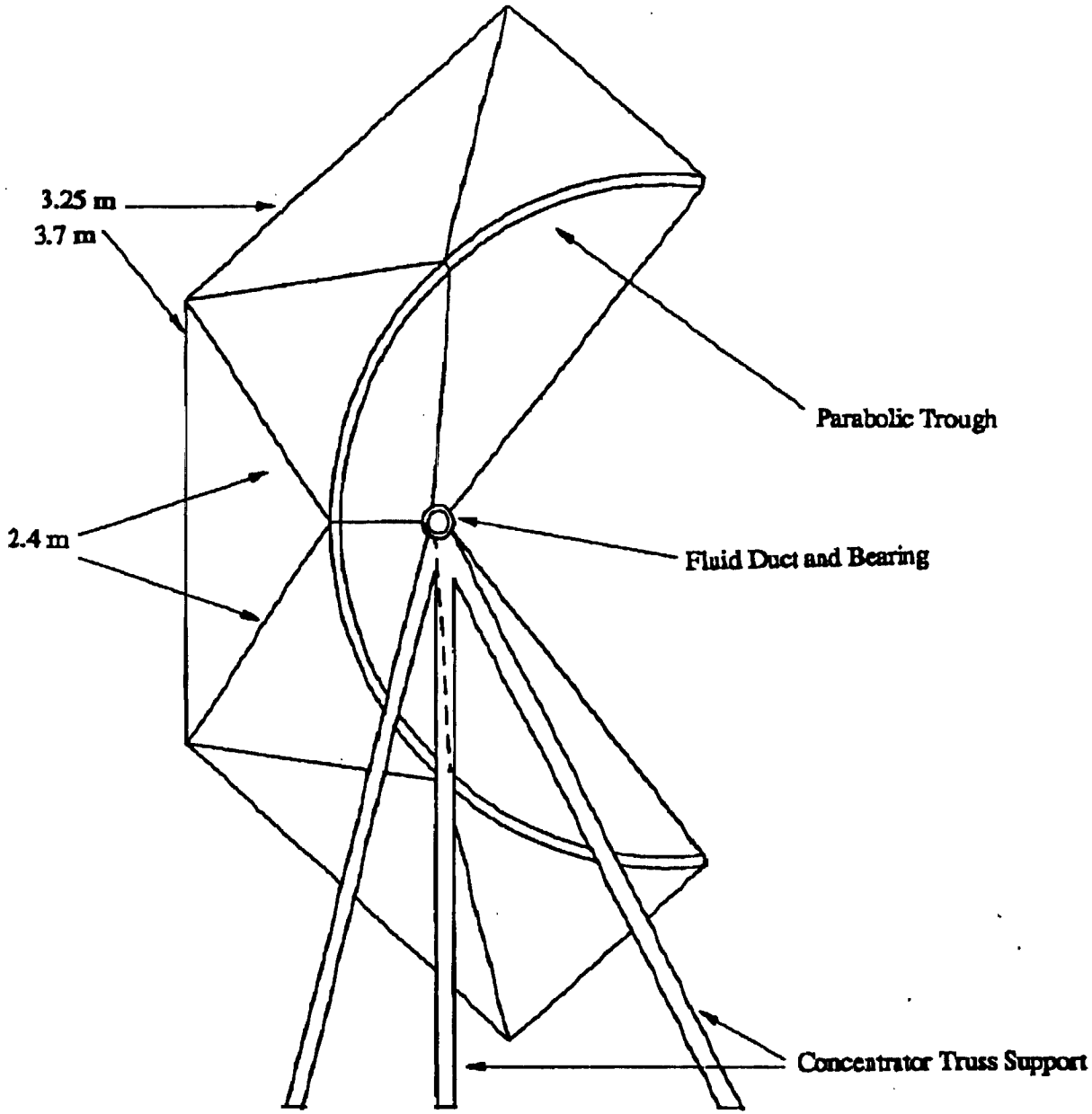

Fig. 7.5. End View of Solar Dynamic Trough Collector

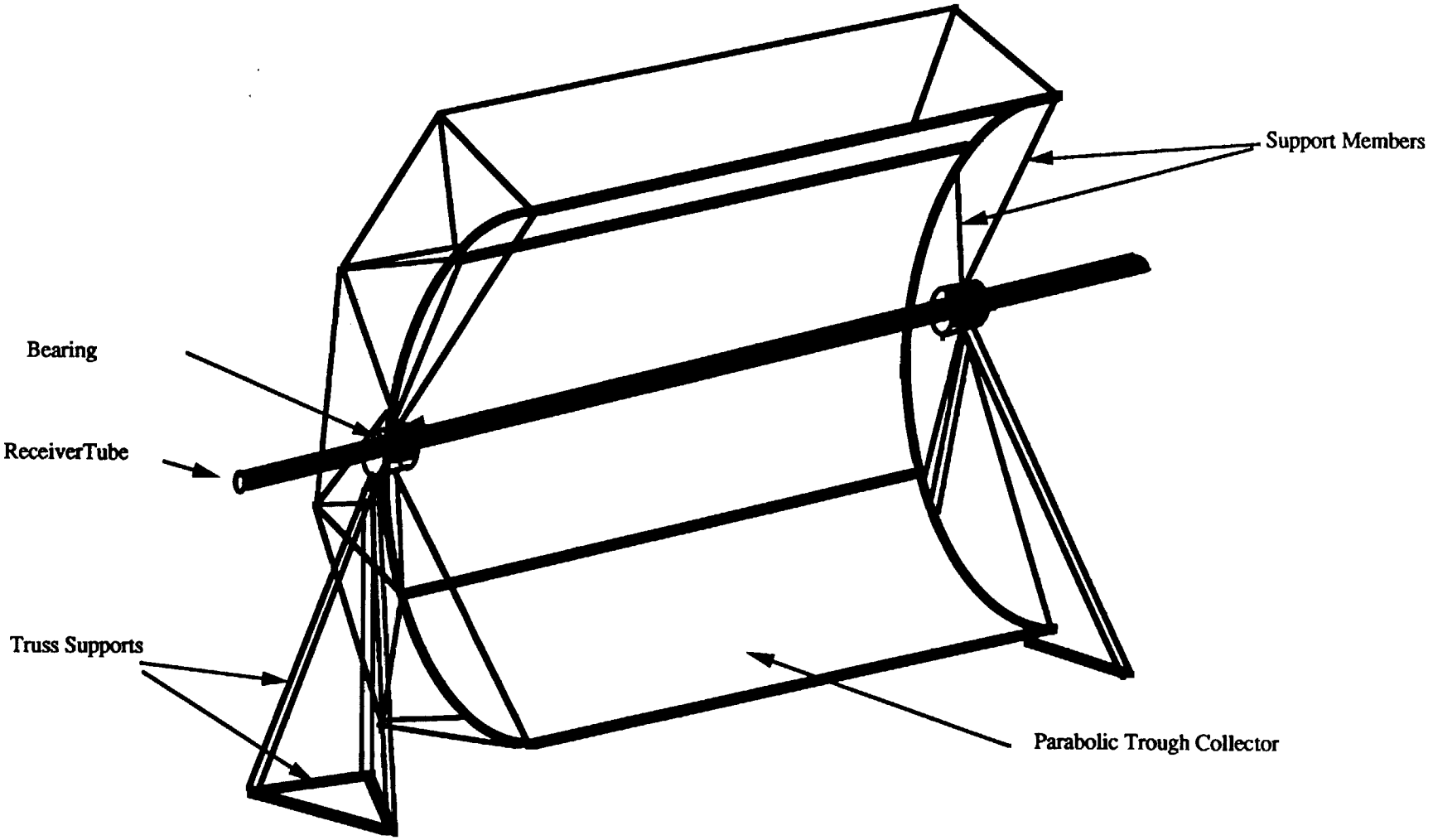

Fig. 7.6: Isometric View Of Solar Trough Collector.

In the above equation, σ_x is the hoop stress on the material (or creep stress, in the case of high temperature applications), P is the internal pressure, D is the duct inner diameter, and t is the duct thickness. The duct is supported approximately every 5.4 m by trusses similar to those used in the solar cells structural design systems. At the location of the supports, bearings allow the concentrator around the duct while the duct remains stationary.

7.3.2 CONCENTRATOR

The parabolic concentrating trough itself is made of a thin sheet of polished aluminum over a Gr/E sandwich construction backing. Each segment is divided into four panels which will be individually attached to the framework rib and cross-members running behind each edge of the panel. Since the reflecting panels will have a small space between them (within each 5 m segment), and since there is a gap between each segment for support structure (a region in which the fluid temperature may drop slightly), two additional 5 m segments will be added to the solar collector for each engine. This implies a total length of 120 m per engine (two 60 m units) or, 24 five meter segments.

7.3.3 CONCENTRATOR TRUSS FRAMEWORK

The framework for the concentrator will consist of two Gr/E ribs, each made from 20 plies, which will have the same dimensions (curve) as the concentrating dish. These are connected to each other by 5 m truss members at each of the five panel edge regions. To provide further structural rigidity, four triangular truss sections are attached to the rear of each rib, one opposite each of the panels. These truss sections will be connected with each of the neighboring sections, as well as the equivalent sections on the other rib by means of Gr/E truss members. The framework will also include members connecting each of the nodes with the bearing around the duct , allowing the dish to rotate freely.

7.3.4 SUPPORT TRUSSES

The supporting trusses will be of two types. At each end of a 60 m unit there will be tetrahedral trusses similar to those described in section 7.2.5 but with a base to apex height of 4.7 m. These will require a clearance of 1.1 m between the collar and the edge of the collector trough. Between the 5 m segments of solar collector trough, a triangular truss will be used. These will have a clearance of 0.2 m between the supports and the edge of the collector. Truss member dimensions can be found in table 7.4. The mass per unit length (m) for each of the truss members listed is 1.72 kg/m.

Table 7.4 Member Lengths For 60 m Unit Of Solar Collector

Member Length (m)	Number Of Members
5.0	136
4.2	4
4.1	44
3.7	24
3.3	11
3.25	48
2.8	6
2.4	196
2.1	44
1.5	2
1.0	22
Rib	36

7.4 STRUCTURAL SUPPORT FOR HEAT PIPE RADIATORS

The design concept for support of the heat pipe radiators (one of the options to provide heat rejection from the Brayton cycle power system) is shown in Figs. 7.7 to 7.9. Although many different approaches could have been used to provide structural support, simplicity was designated as the overriding criterion for this design. Simplicity ensures rapid, easy

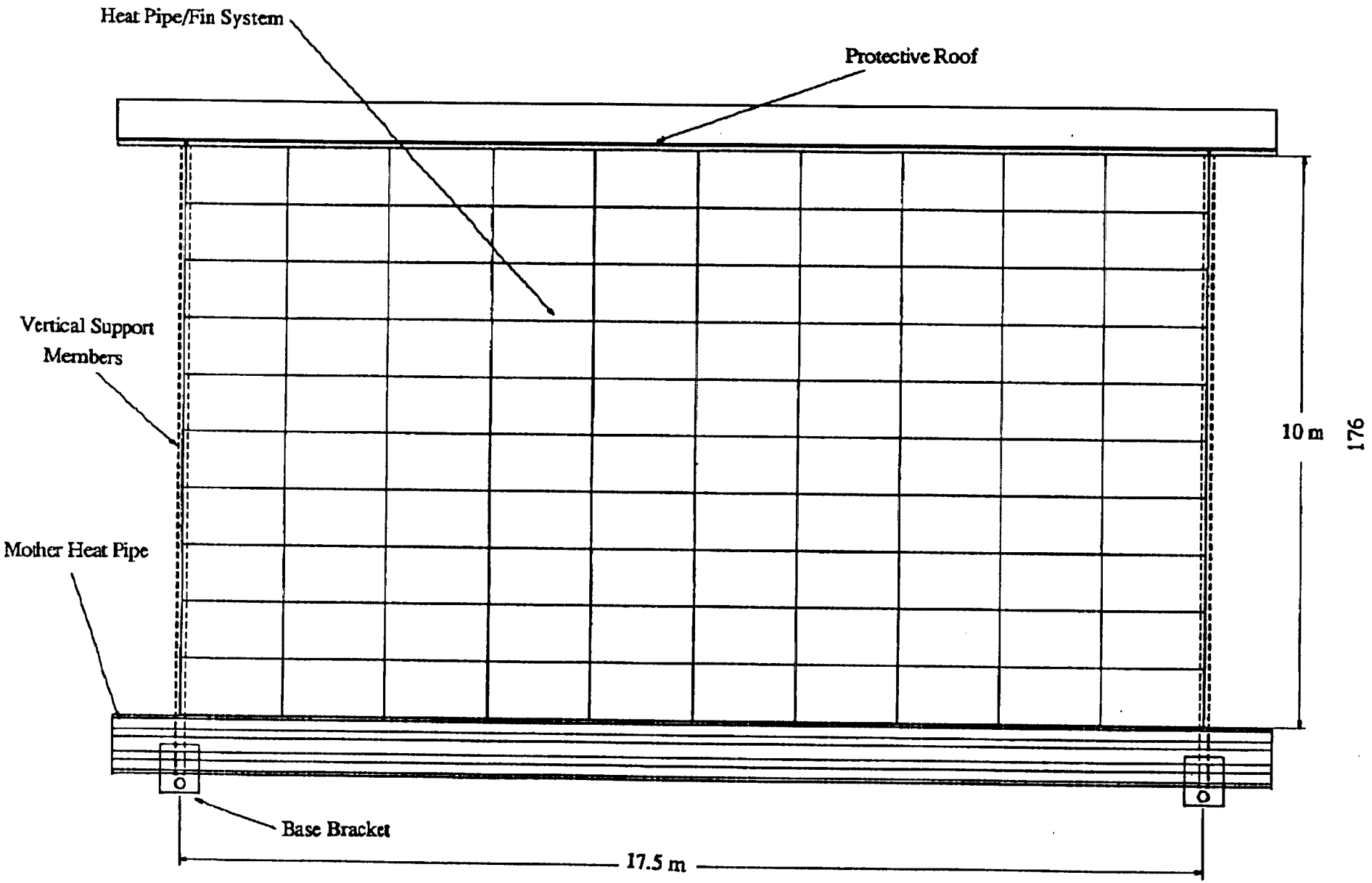

Fig. 7.7. Front View Of Heat Pipe Radiator

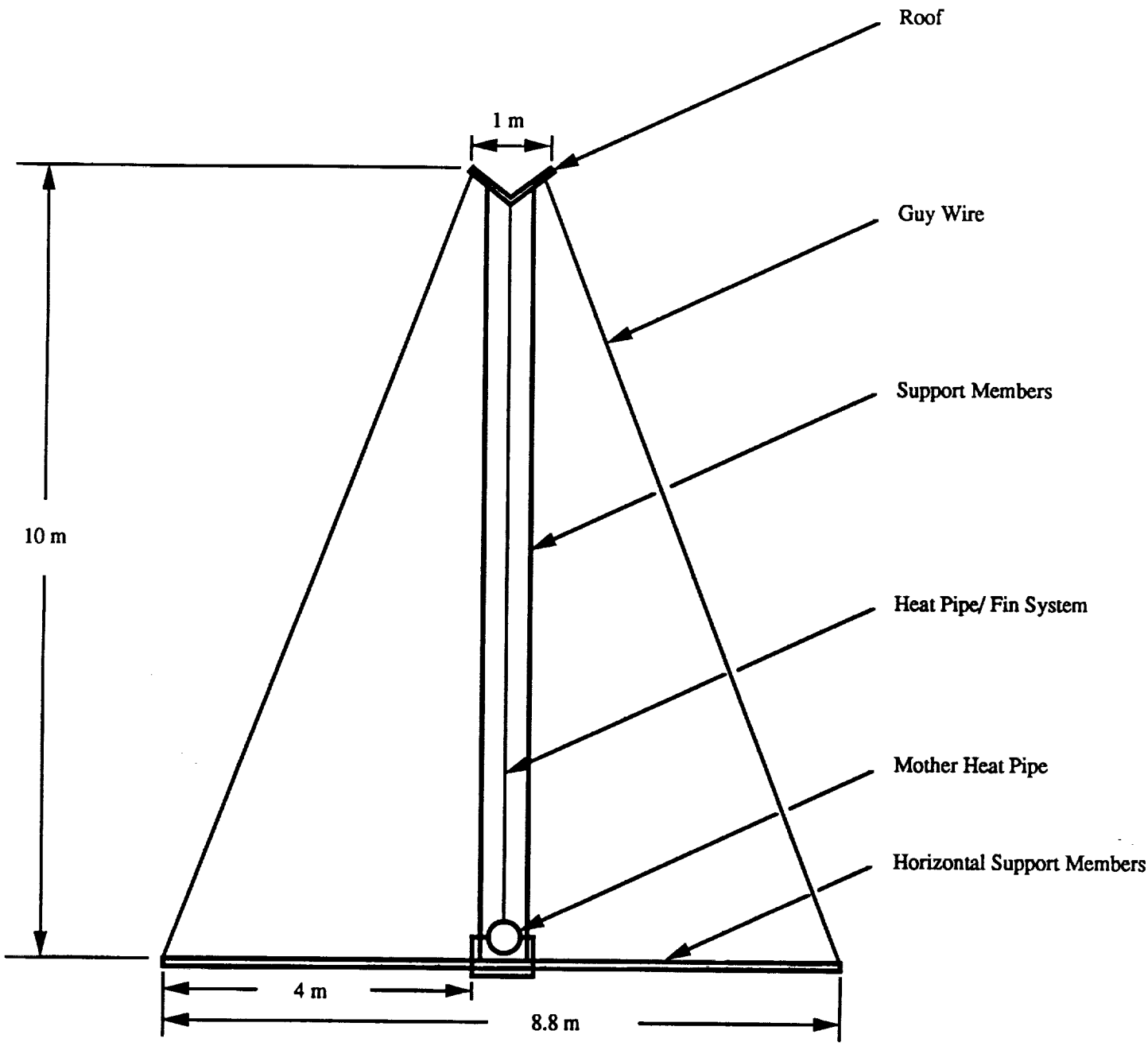

Fig. 7.8: End View of Heat Pipe Radiator.

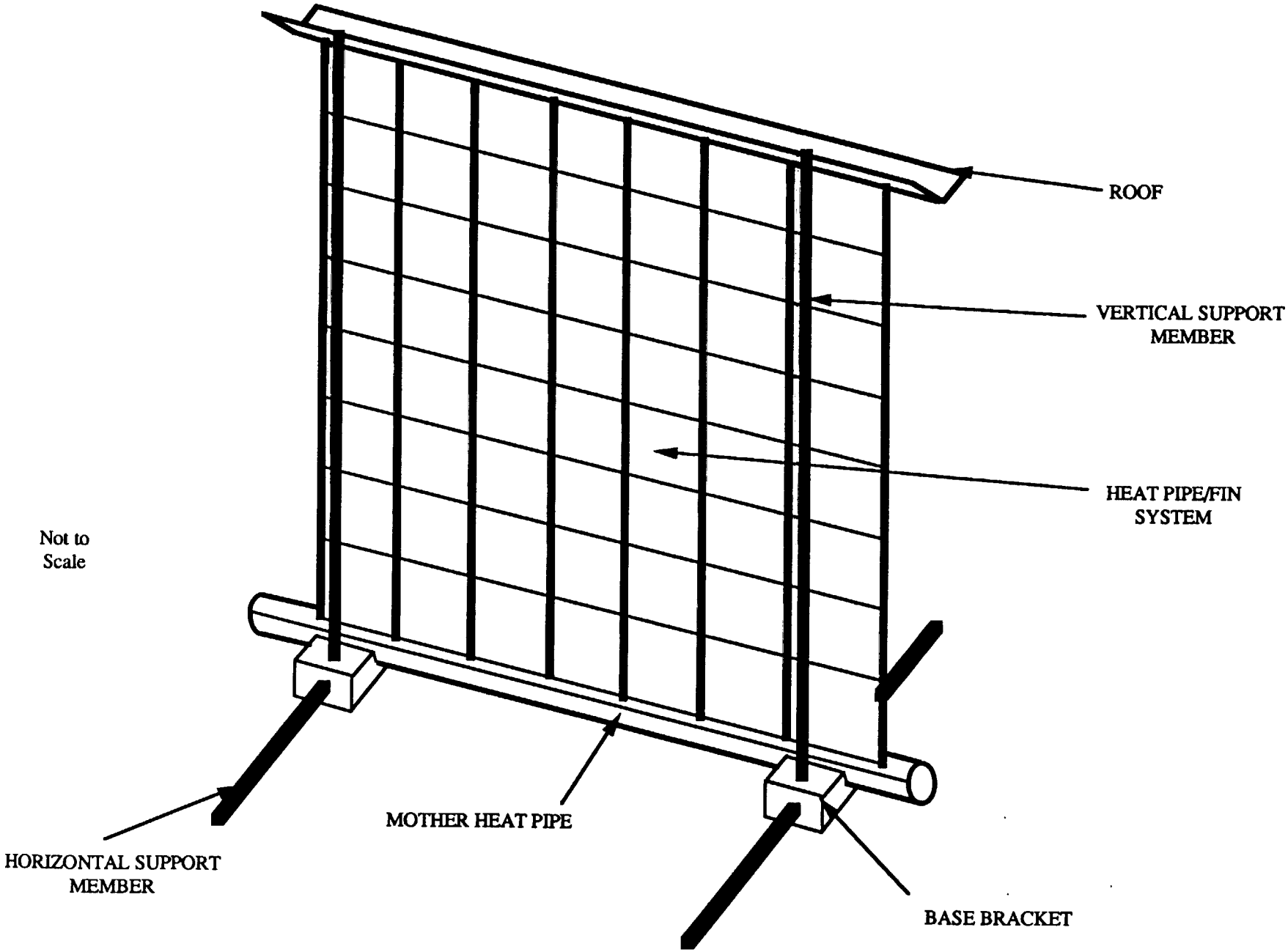

Fig. 7.9: Isometric View of Heat Pipe Radiator.

construction, which may be readily performed by astronauts with bulky gloves and limited mobility. Simplicity also provides a system that is less prone to component failure, thereby decreasing its maintenance (time to replace broken fins or heat pipes) and increasing its ultimate life span. These two motivations become even more significant in light of the fact that thermal management requires a radiator length of 69.6 m and a height of 10 m for heat rejection from each of the Brayton engines. With such a large area requirement, ease of construction and maintenance becomes more important.

7.4.1 LOADS AND COMPONENT DESIGN

Four types of support members are required: a flat plate to serve as a protective roof (against direct solar radiation) and to offer support for the vertical heat pipes, vertical members to support the roof, horizontal members that prevent the possibility of tip-over of the radiator, and support brackets that serve as a base for the mother heat pipe (MHP). Each of these members are constructed from the same Gr/E composite common to all structural designs (see Appendix A).

To supply resistance against bending of the MHP, support brackets are located every 17.5 m along the span of the radiator. This was determined as the minimum spacing required to prevent more than 1 cm deflection of the MHP at any point along its span [Eq. 7.2]. Thus, eight support brackets are required to furnish support for the heat pipes for each engine. The composite roof plate is 1 m wide to furnish solar shading for the small heat pipes and fins. Given this configuration, the loads on various members can be determined.

7.4.2. PROTECTIVE ROOF

The roof plate must exhibit adequate strength and rigidity to support its own weight and provide support for the heat pipes. In order to meet this load requirement, it was determined that a 1.27 cm honeycomb core between two layers of Gr/E composite 11 layers thick will be

utilized. This combination was decided upon by approximating the problem as beam bending (a beam 1 m wide and 10 m long). Using the equations:

$$\sigma_{xx} = - \frac{M_x y}{I_x} \tag{7.8}$$

$$I_x = \frac{bh^3}{12} \tag{7.9}$$

where σ_{xx} is the tensile stress in the member, M_x is the moment about the x-axis, y is the distance from central axis, I_x is the moment of inertia of the beam, and b and h are the width and height of the beam, respectively, the maximum stress that the composite fibers will carry was calculated to be 3.52×10^6 Pa (510 psi). This is much less than the critical tensile load the fibers can support. The roof lends structural support to the small vertical heat pipes by providing holes for each of the heat pipes to fit up into. This prevents the heat pipes from bending and makes the entire array stable to small lateral loads. Additional holes will be required in each of the four corners of the roof to allow the support legs to go through and support it. Holes will also be required to connect the guy wires to the roof. The composite roof plate will be coated with the protective coating described in Appendix A.

7.4.3 VERTICAL SUPPORT MEMBERS

The members used as "legs" to support the roof structure will be 5.08 cm in diameter in order to make them easily handleable by astronauts in gloves and to comply with NASA standards [2]. They will be fabricated from the same 11 ply Gr/E composite common to the entire design. Fabricated on to one end of each member is a paddup ring on which the roof rests and which transfers the weight of the roof to the member. At the other end of the rod there is a male screw fitting that is screwed into the support bracket. Each rod is 10.1 m in

height. The critical buckling load for these members, given by Eq. 7.4 , was found to be 1555 N, whereas the load actually supported is approximately only 35 N.

7.4.4 BASE BRACKET

The bracket serving as a base for the MHP is constructed as a solid Gr/E foundation. This is necessary in order to provide a means of support for the vertical rods and horizontal rods which are placed inside this structure. The inside of the vertical support holes are configured to a female screw-type casting, to accept the vertical rods described above. Although the use of this design means that the MHP will be elevated 15 cm from the lunar surface, this does not pose a problem. The MHP is designed to prevent bending between brackets, easily supporting itself, the heat pipes, and the weight of the working fluid. Furthermore, access to the entire surface of the heat exchanger will make it easier and faster to detect and stop leaks.

7.4.5 HORIZONTAL SUPPORT MEMBERS

The horizontal tubes that serve to prevent overturning of the radiator are also 5.08 cm in diameter and composed of 11 ply Gr/E composite [2]. The radiator resists overturning since its weight reacts to lateral loads through the moment arm created by this member. The horizontal tube is 8.8 m long, and fitted through the hole along the base of the bracket. This allows 4 m of the tube to protrude from each side of the bracket. In this way, the radiator will be inherently stable, and safe against any accidental lateral load. The ends of each tube are supplied with holes through which a clip is attached to connect the guy wires from the roof. Should a lateral load occur, the guy wires on the same side as the load will come under tension and force the load to be distributed to the horizontal support members on the opposite side, not on to the heat pipes. The guy wires will be 1 mm steel wires as a preliminary design concept.

7.4.6 ASSEMBLY PROCEDURE

As stated previously, the most important factor in this structural design is the requirement for simplicity. It is noted that ease of construction of any major design component in a moon based facility is an extremely important factor in determining the feasibility of such a facility. Incorporating this notion, the structural components of this radiator system are easily assembled by gloved astronauts.

The initial step is to lay out the brackets every 17.5 m . After laying the MHP between the brackets and fitting the vertical heat pipes and support legs into their respective holes, the horizontal members may be installed. This is accomplished by simply slipping the tube through the hole until a pin locks it in place. Then the roof is raised above the vertical support legs, with the guy wires already attached (and dangling as it is lifted). As one astronaut raises the roof with a light crane, others may be fitting the heat pipes and support legs into their respective holes. All that remains to do is snap the guy wires into the horizontal stabilizers, and the process is complete. Table 7.5 lists component masses for a 17.5 m section of the HPR.

Table 7.5 Component Masses For 17.5 m Section Of Heat Pipe Radiator

Component	Mass (kg)
Roof	151
Vertical Support Members	23
Horizontal Support Members	5
Brackets (2)	248
TOTAL	427

7.5 LIQUID DROPLET RADIATOR STRUCTURAL DESIGN

The LDR is an alternative waste heat radiator considered here for the dynamic cycle option. It is the largest structural design for the lunar power station. It stands 42 m tall and 15 m wide (see Fig.7.10). The primary design requirement was that the structure be quickly and easily erectable. Many of the major design features were adopted from a previous University

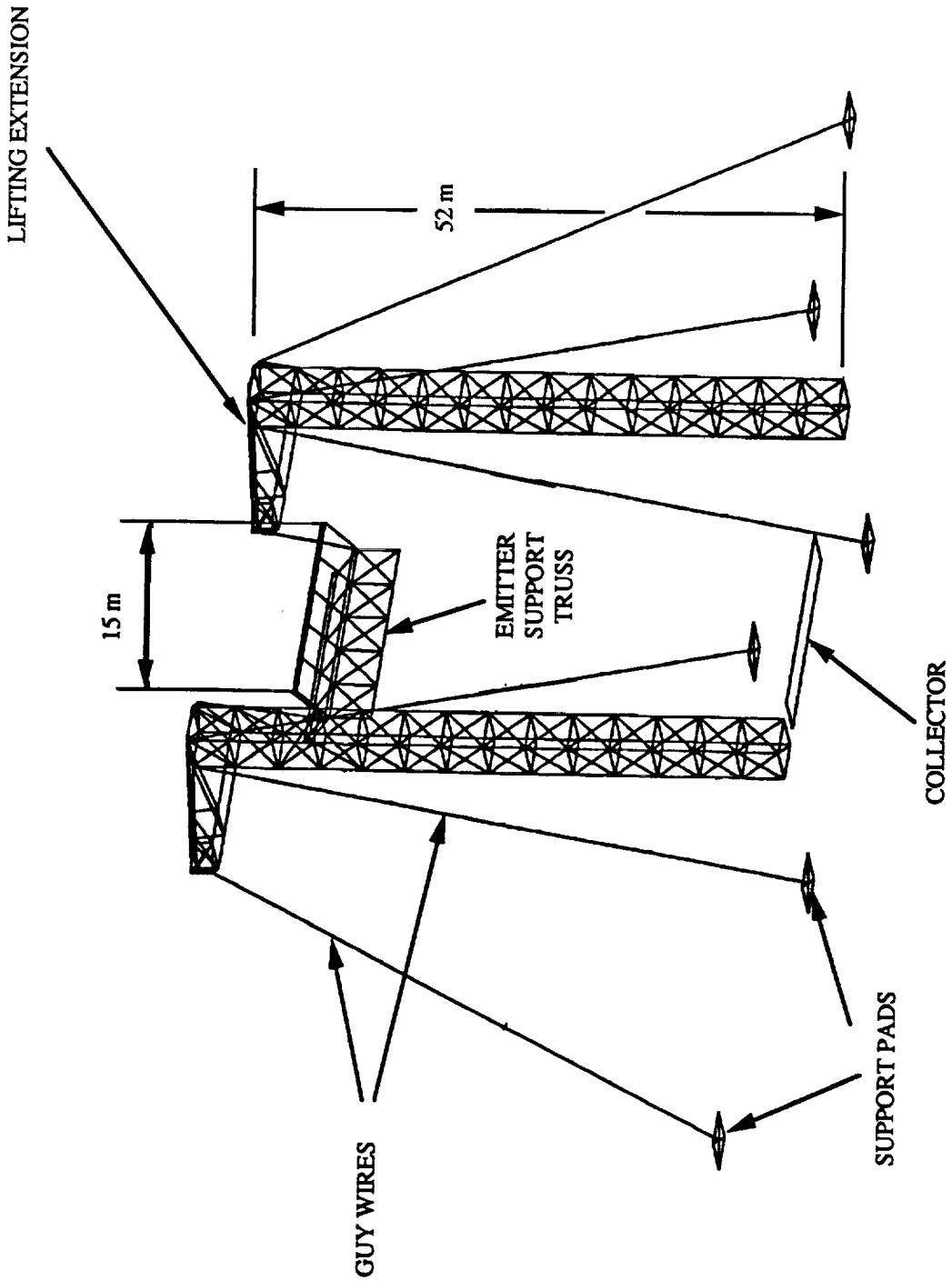

Fig. 7.10: Liquid Droplet Radiator Structure.

of Washington study on nuclear power for a lunar base [3]. The structure consists of four major elements: 1) erectable masts, 2) cable-pulley inter-tie system, 3) emitter longitudinal support truss, and 4) droplet collector.

7.5.1 ERECTABLE MASTS

Each mast consists of 12 4 m x 4 m box trusses [3]. On each lateral face of each box is an additional diagonal member to provide redundancy, and these diagonal members are skewed on parallel faces (Fig. 7.10). The loads on the structure consist of the dead weights of the various components, and the tension in the guy wires. The lunar weight per unit length of the emitter manifold varies linearly from 22 N/m at the inlet to 5 N/m at the opposite end. There may also be a transient load associated with the ejection of fluid from the emitter, and the sudden removal of the same during shut-down of an emitter segment. This load is quite small and was represented by a distributed force of 2 N/m over the length of the emitter. The guy wires are tensioned to 100 N each to provide lateral stability. The joints were analyzed as pinned connections (assuming titanium or some other high strength nodes) and under these conditions the configuration was determined to have the highest specific strength (compared to other configurations such as an additional redundant member on each face of each box truss). The analysis was carried out by a finite element program [4].

Each box is erected one at a time within a framework surrounded by four hydraulic jacks. When each box is complete it is raised 4 m by the jacks, allowing the next one to be erected beneath it [3]. In this way, the entire mast can be constructed on the ground quickly and with little effort. The erecting framework and hydraulic jacks are then moved to the other locations and the rest of the masts are deployed. Table 7.6 lists truss member lengths for one mast.

Table 7.6 Member Lengths For LDR Mast

Member Length (m)	Number of Members
5.7	53
5.1	3
4.9	1
4.6	2
4.3	2
4.2	2
4.0	108
3.9	2
3.4	2
3.3	2
2.9	2
2.2	2
2.0	1
1.8	2

7.5.2 CABLE-PULLEY INTER-TIE SYSTEM

On top of each mast a lifting extension truss is fixed (see Fig. 7.10). This must be assembled as the first unit to be raised, with each box truss erected beneath it. Attached to each side of the lifting extension are an emitter support bracket and a cable-pulley inter-tie system used to hoist the emitter and emitter support truss. When the emitter support truss is erected and in place between two masts, it is fixed to a cable and hoisted to the support brackets by an electric winch. Once the support truss is locked into place, the winches are turned off but remain permanently fixed at the base of each mast for future use.

7.5.3 EMITTER LONGITUDINAL SUPPORT TRUSS

The emitter longitudinal support structure was designed as a plane truss, and was modeled as a two-dimensional structure. The truss consists of 2 m horizontal and vertical members with diagonal members placed in between . This configuration yields the lowest specific mass and is very stiff in bending. The emitter is mounted mechanically to the bottom

of the truss before raising it, and the flexible feed line is attached and allowed to hang freely as it is raised. Table 7.7 lists member lengths for the LDR emitter support truss.

Table 7.7 Member Lengths For LDR Emitter Support Truss

Member Length (m)	Number of Members
2.0	25
2.8	8

The mass per unit length (m) for each of the truss members listed in both tables above is approximately 1.72 kg/m. The total length of members for an entire LDR (two masts and an emitter truss) is 1692 m. This implies a mass per system of approximately 3010 kg (including nodes and sunscreen).

7.5.4 DROPLET COLLECTOR

The liquid droplet collector is assembled in sections directly below the emitter as the final component of the LDR support structure. The fluid is pumped out at one end of the collector back to the dynamic cycle's waste heat exchanger and is there pumped back to the LDR's emitter to repeat the cycle.

7.6 LUNAR CONCRETE FOR LUNAR BASE USE

Lunar concrete provides a method for producing large, structurally sound building blocks for the purposes of fabricating foundations for dynamically unstable systems, and modular units with which to assemble habitable structures. When a permanent lunar base is eventually built on the moon, the formation of building material from in-situ resources will require reduced mass transport from earth (a predominant driving factor behind project

modifications). Below is an outline of a proposed method of production of lunar concrete on the lunar surface based on a study by Shimizu Corp. of Japan [5]. Lunar concrete provides the Brayton cycle and truss foundation platforms and anchor pads for guy wires.

7.6.1 ANALYSIS OF LUNAR CONCRETE PRODUCTION METHOD

Shimizu Corp. has examined the influence of the low acceleration of gravity and the vacuum environment on the moon on concrete production. The analysis of the influence of the low acceleration of gravity indicated that as the acceleration of gravity increases, the amount of bleeding (mass reduction due to water loss), and the density and compressive strength increase. A relationship between compressive strength and the acceleration of gravity was determined and it was predicted that the compressive strength of specimens under the influence of one-sixth Earth gravity is 90% of those under one Earth gravity. It is therefore believed that the low acceleration of gravity on the moon will not seriously affect the quality of the concrete.

The results of the test of the influence of the vacuum environment indicated that if concrete in the process of hardening is exposed to a vacuum, the measured strengths are significantly lower than those of companion specimens cured in air. A pre-curing period (the time difference between mixing the concrete and exposing it to the vacuum) will be required before the concrete can be exposed to the vacuum environment. A period of 11 hours resulted in a compressive strength ratio of 89.2% (vacuum/non-vacuum) whereas a zero pre-curing period resulted in a ratio of only 35%.

To minimize the mass of water , the water to cement (W/C) ratio can be as low as 25%, and still provide the compressive strength necessary to withstand the loads generated by the dynamic power cycle engines. At a water to cement ratio of 25%, the compressive strength is approximately 12 MPa [5]. Table 7.8 below lists W/C vs. unit weight and compressive strength.

Table 7.8 Water To Cement Ratio vs. Physical Properties

(W/C) (%)	Unit Weight (kg/m^3)	Compressive Strength (MPa)
35	2070	16.6
50	2080	20.8
65	2080	23.9

Note that the unit weight does not change appreciably. A low W/C ratio will provide a more than adequate material strength while keeping the mass of water that must be transported to a minimum. Eventually, when oxygen is produced on the moon, concrete can be produced entirely from lunar resources plus a supply of hydrogen which can be trickled off propellant tanks.

The following is an outline for the production method for lunar concrete.

1. Frozen water or cement paste is crushed to small particles in an airtight chamber. Powdered ice is produced by spraying water or cement paste inside a cold chamber or onto the surface of a cold metallic pan supplied for this purpose.

2. Cement, aggregate, and powdered ice are mixed at low temperature in a vacuum. Since all the materials are solid particles, a uniform concrete mixture is easily produced. In addition, the concrete mix can be transported in a vacuum because the vapor pressure of ice at a low temperature is very low.

3. The concrete mixture at a low temperature is transported and placed in the prescribed location. The temperature of the concrete should not be excessively raised when the concrete mixture is transported and put in place.

4. After casting, the concrete is covered with airtight material and is thawed with applied energy from outside. Simultaneously, the concrete is compacted with applied vibration and pressure. Microwaves are being considered as outside energy. The concrete is covered with airtight material for thawing and to prevention evaporation.

5. The concrete is used as a structural material after having been cured for the predetermined period. A heat insulator is used to enclose the concrete during curing in order to control the minimum and maximum temperatures of the concrete. After the concrete hardens, the airtight material is removed and the concrete is exposed to a vacuum.

The power required to thaw the inhomogeneous concrete mixture has not yet been precisely determined, but it is thought to be approximately 144 W/m^2, or, 44 kW for the entire operation.

7.6.2 DESIGNS FOR CONCRETE STRUCTURES

Each Brayton engine will have a mass of approximately 800 kg. If each is supported by four legs, then a support pad under each must provide a reactive force of 327 N, or, for a solid leg of 5 cm diameter, approximately 0.1613 MPa. A slab of concrete 30 cm x 30 cm x 10 cm under each leg should provide adequate support, while keeping the engine from working its way into the regolith under prolonged vibration (although this is almost negligible).

Similarly, a circular slab underneath each truss support for the solar photovoltaic arrays and solar collectors will provide a more stable surface on which to place the joints. Each tetrahedral truss configuration for the solar arrays must support one third of the weight of a 12.5 m x 3 m array. This has a mass of approximately 90 kg, or a lunar weight of 109 N. A slab of 1.2 m diameter and 0.3 m thickness provides the necessary surface area over which to disperse the weight. If necessary, steel or tungsten cables can be imbeded near the upper surface during production to pre-stress the concrete and assure that no portion is under tension. Similar slabs can lie beneath the support trusses for the solar collector, and be used to anchor the support lines for the LDR.

The volume of concrete required for these applications is on the order of 300 m^3. The cement and water required for this have a combined mass of approximately 152 metric tons. Unfortunately, if cement and water must be transported from the earth to produce this while using lunar regolith as aggregate, the operation could be costly. Cement simply weighs too much per unit volume to compete directly with lighter materials such as solid composite Gr/E.

7.7 NOMENCLATURE

b_{in}	inner radius of box beam
b_{out}	outer dimension of box beam
CTE	coefficient of thermal expansion
D	diameter
E	modulus of elasticity
Gr/E	graphite/epoxy composite
I	moment of inertia
LEO	low earth orbit
LEV	lunar excursion vehicle
OTV	orbital transfer vehicle
P	pressure
P_{cr}	critical buckling load of a structural member
P_x	load per unit length
R_i	inner radius
R_o	outer radius
t	thickness
TLI	trans-lunar injection
U	deflection of beam
W/C	water to cement ratio
σ_x	hoop stress
σ_{xx}	tensile stress

7.8 REFERENCES

1. Heard, W., Bush, H., and Watson, J., "Space Truss Construction Studies," ASCE SPACE 88 Engineering, Construction, & Operations In Space Conference, August, 1988.

2. Watson, J. J., et. al., "Results Of EVA/Mobile Transporter Space Station Truss Assembly Tests," NASA TM-100661, Langley Research Center, 1988.

3. Trueblood, B., Pressentin, R., and Bruckner, A. P., "Multi-Megawatt Nuclear Power System for Lunar Base Applications," Space Nuclear Power Systems 1987, M. S. El-Genk and M. D. Hover (eds.), Orbit Book Company, Malabar, FL, 1988.

4. Zienkeiwicz, O.C., The Finite Element Method, McGraw-Hill Book Co. (UK) Ltd., Maidenhead, England, 1985.

5. Namba, H., et. al., "Concrete Production Method For Construction Of Lunar Bases," Academic Papers Regarding Concrete On The Moon, Shimizu Corporation, Tokyo, Japan, 1990.

8.0 EMERGENCY BACKUP POWER SYSTEM

David Carlile
Matt Jardin

8.1 INTRODUCTION

Although a high degree of redundancy is built into the main power system, the possibilty for complete system failure still exists. In the event of such a rare failure, a highly reliable backup power source must be available to permit the base personnel time to evacuate. Several types of energy storage devices exist, and one must be chosen which provides a high degree of reliability while keeping system mass to a minimum. Once the type of energy storage is determined, it must be configured into a working backup power unit including any necessary electrical support equipment. Whenever possible, off-the-shelf components known to have high degrees of reliability are to be used.

8.2 ENERGY STORAGE SYSTEMS

Since the backup power system must be able to operate during both the lunar day and night, and may remain dormant for long periods of time, some type of long duration energy storage system must be used. The most reliable energy storage systems are passive, such as fuel cells and batteries.

Fuel cells have excellent energy densities [1] as seen in Table 8.1, and have proven their reliability in many space applications. The biggest problem with their use is that over long periods of time, they may experience substantial loss of the working fuels due to boil-off when left in a charged state. Battery technology is the oldest and most thoroughly tested power

storage method, and also has a long history of reliability in space systems. One drawback to using batteries instead of fuel cells, however, is that battery energy densities are relatively low [2] (see Table 8.2) which tends to make the backup power system mass prohibitively large. Batteries are extremely reliable, however, and can be left unused for long periods of time, whereas fuel cells cannot. For these reasons, batteries are to be used for the lunar power backup design in this study. It should be kept in mind that this may not necessarily be the decision of the designers of the lunar base, and that these designers may opt for a slightly less reliable system in the interest of reducing system mass to acceptable levels.

Table 8.1: Fuel Cell Energy Densities.

Type	Energy Density (W-hr/kg)
Alkaline/Bromine	3,000
Acid Electrolyte	2,000

Table 8.2: Battery Options.

Material	Type	Energy Density (W-hr/kg)	Depth of Discharge (%)
Lithium Thionyl	Primary	600	100
Sodium Sulfur	Secondary	800	75
Silver Zinc	Secondary	110	35
Nickel Hydrogen	Secondary	55	80
Nickel Cadmium	Secondary	35	20

There are two main categories of batteries; primary batteries which can be used only once, and secondary, or rechargeable batteries. Primaries are generally more energy dense and therefore lighter than secondaries, but they can only be used once before they must be replaced.

Secondaries can be used many times, but are more massive and may require a small current for charge maintenance.

Since the emergency backup system is being designed to handle only the worst case scenario in which the main power system shuts down and forces a base evacuation, primary or secondary batteries both work equally well. Since the base would hopefully be reoccupied and repaired soon after the failure, secondary batteries would be advantageous because the same backup system could remain in use without requiring that a new system be launched from Earth. However, if a primary system is available with a much higher energy density than a secondary system, it might be possible that several primary systems would have less mass than one of the secondary systems. In this case, it would be advantageous to use a disposable primary system.

To illustrate the differences between the two types of batteries, current state of the art examples of both types are presented here. One of the most promising primary batteries is the lithium thionyl cell. These cells are presently being developed for space applications and feature very high energy storage densities. They may someday provide a light, high energy backup system for the Moon, but at the present, they have many reliability problems, including a tendency to explode [3]. A promising secondary battey is the sodium sulfur cell. It features energy densities even higher than the lithium thionyls, with the advantage of rechargeability. They do, however, make use of very thin, brittle ceramic components, and operate at very high temperatures, which creates difficult operational problems.

The two previous cells mentioned are still highly experimental may not be ready for use in the timeframe of the present lunar base concept. Among the remaining battery types, existing primary and secondary cells have similar energy densities. In this case, secondary batteries offer the benefit of rechargeablity, and are, therefore, to be used for emergency power backup. The most likely candidates for the backup system are nickel cadmium, silver zinc, and nickel hydrogen batteries. Nickel cadmium is the oldest of these cells, and is used extensively

in aerospace applications. It has been proven reliable, but happens to have the lowest energy density of the three types, and, therefore, is not used here. The silver zinc batteries have a much higher energy density, but can only be discharged to 35% of their total capacity to avoid permanently damaging the cells. Nickel hydrogen batteries have just over half the energy density of the silver zinc batteries but can be discharged to as much as 80% before significant damage occurs [4]. When these numbers are compared, the available energies are nearly equal, negating the density advantage of the silver zinc cells.

Since there is no net energy density gained by using silver zinc batteries, nickel hydrogen batteries are proposed for the lunar power backup application. This is primarily because nickel hydrogen cells are in wide use in the aerospace industry, and by the time the lunar base becomes operational, the reliability of nickel hydrogen cells will be well proven. A current application of these cells is in the Space Station Freedom (SSF) energy storage system design which is to supply power for the station during the eclipse portion of Earth orbit [5]. As it turns out, several modifications can be made to the existing power storage system design for SSF, which adapt it well for use as an emergency backup power source for a lunar base. The space station is to become operational by the late 1990's, between five and fifteen years before the lunar base is scheduled to come on-line, and therefore the nickel hydrogen storage system will be well tested for reliability, which is an extremely important factor in power backup design.

8.3 SPACE STATION FREEDOM STORAGE SYSTEM

Space Station Freedom is powered by the sun through the use of solar cells during the sunlit portion of its orbit. A battery storage system using nickel hydrogen batteries provides power during the shaded portion of its orbit. This system can easily be adapted for use on the

Moon as a backup power system, and by doing so, a substantial savings in development time, resources, and money may be achieved. The SSF system described below is illustrated in Figure 8.1.

The energy storage system is comprised of modular units called utility plates which function both as structural members to which the batteries and charge/discharge units are attached, and as heat transfer fluid junction boxes through which the coolant fluid flows. The batteries and electrical equipment are designed in modular units called Orbital Replacement Units (ORU's) which are connected to the utility plates. Utility plates can be added in any desired number to add more total stored power to the system. In addition to the utitlity plates, a radiator is necessary to reject the waste heat generated during battery discharge, and power switching. Also, in the SSF design, a structural member called the Integrated Equipment Assembly (IEA) is used as a frame to which the utility plates are held together as a unit. In order to reduce mass for use on the Moon, an IEA is not used as it is not be necessary to keep the utility plates so rigidly connected. In the sections that follow, some components from the SSF design to be used in the emergency lunar backup power system are described along with the modifications necessary to adapt the components to their new application.

8.3.1 BATTERY ORBITAL REPLACEMENT UNIT

The battery ORU, shown in Figure 8.2, is designed to be easily replaceable by astronauts. That constraint, coupled with a nominal voltage requirement of 95 volts results in a battery module consisting of two battery ORU's connected in series. One benefit of the ORU design is that if significant advances are made in battery technology by the time the lunar base is built, the new batteries may easily be incorporated into the existing modular design. In the current design, one battery ORU is comprised of 38 nickel hydrogen cells providing 1.25 volts each for a total series potential of 47.5 volts. Each of the 38 cells is mounted in an aluminum sleeve which provides a heat transfer path to the utility plate heat transfer system described in

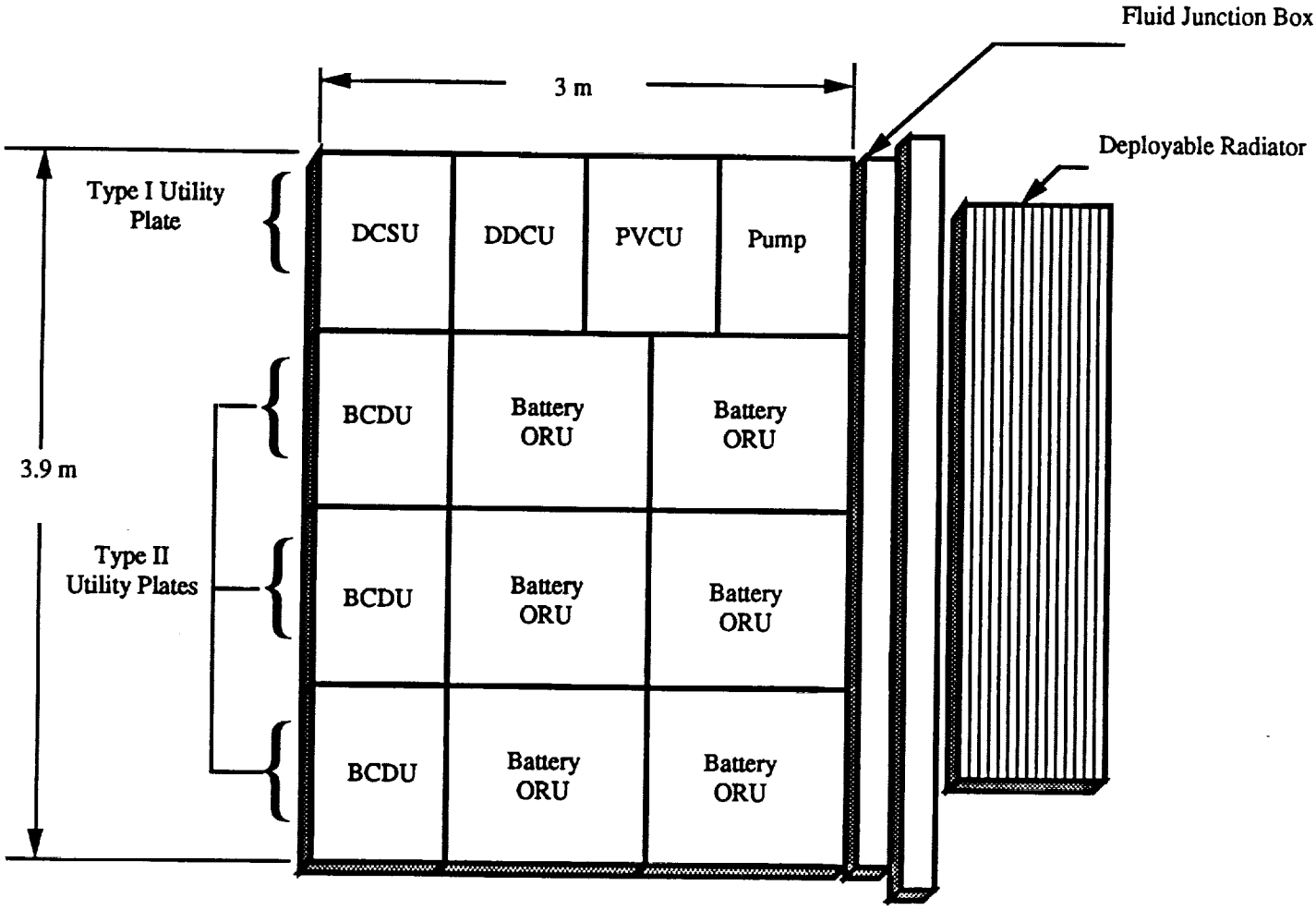

Fig. 8.1: Space Station Freedom Energy Storage System.

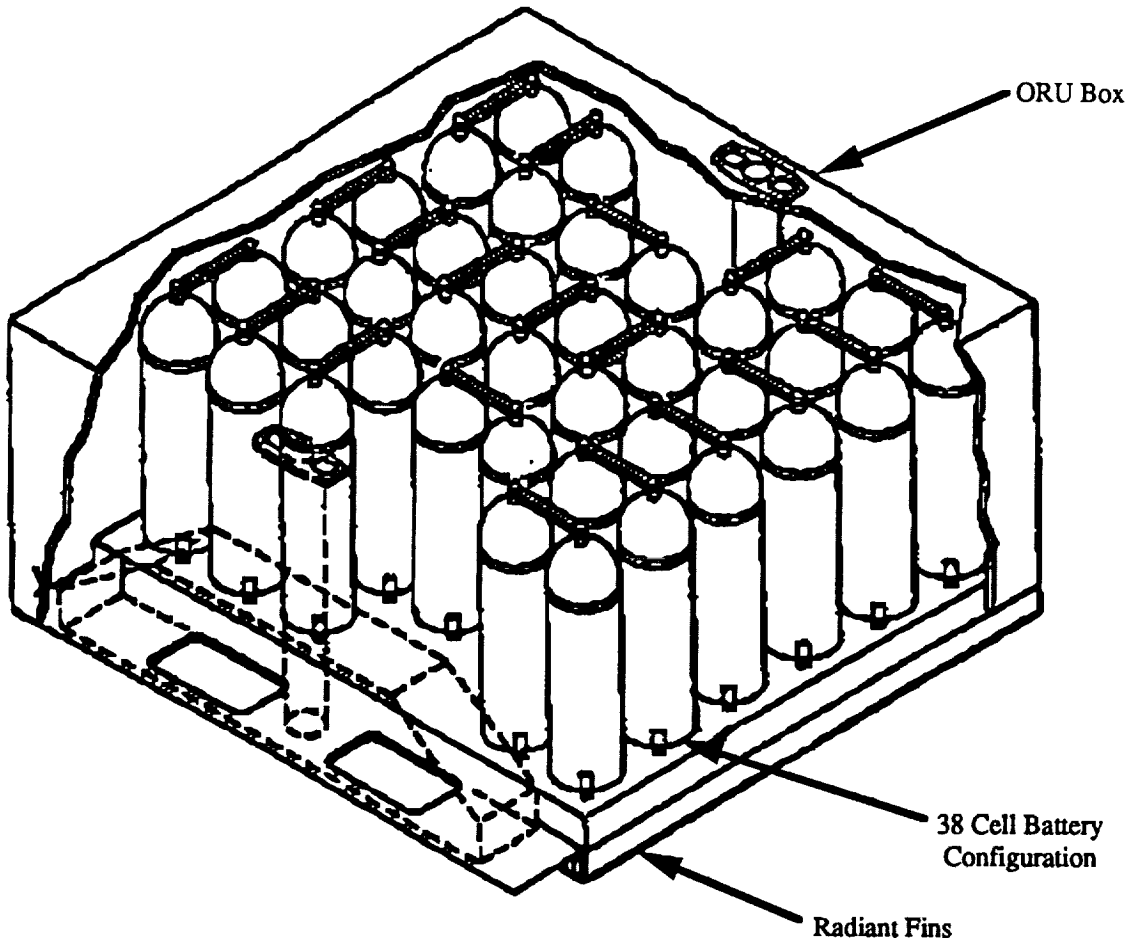

Fig. 8.2: Space Station Battery ORU Assembly

Section 8.3.3. Since the battery ORU design is modular, it does not need any modification for use in the lunar backup power system.

8.3.2 ELECTRICAL EQUIPMENT

The lunar backup energy storage system does not require nearly as much electrical equipment as the SSF energy storage design. The SSF design currently requires three separate types of electrical equipment Orbital Replacement Units (ORU's) to perform electronic operations as well as to provide switching between various input photovoltaic arrays. These are the Battery Charge/Discharge Unit (BCDU), the Direct Current Switching Unit (DCSU), and the DC-DC Conversion Unit (DDCU). The lunar backup energy storage system only needs a unit equivalent to the SSF battery charge/discharge unit along with some power switching electronics. For mass and size estimation, a hybrid ORU called the Electrical Equipment Unit (EEU) is created. The EEU required for emergency backup power is assumed to have the same mass and spatial dimensions as a BCDU from the space station. This is only an approximation, but is fairly well justified due to the reduced requirements of the lunar emergency backup power supply.

8.3.3 THERMAL CONTROL SYSTEM

Due to inefficiencies in the batteries and related electric equipment, some waste heat is generated. To prevent heating damage to the energy storage components, and to keep the batteries operating at their optimum temperature of about 280 K, the anhydrous ammonia pumped loop thermal control system (TCS) from the space station is modified for incorporation into the backup system. It retains the basic elements of the space station power storage TCS but is reduced in size to reflect the lower heat rejection demands in the lunar system.

There are four basic components in the TCS; the utility plates, the fluid junction box, the pump ORU, and the radiator. The utility plates provide structural support for the battery

boxes as well as for the various electrical equipment boxes and contain fins and coolant tubes which carry waste heat away from these components. The fluid junction box provides a physical connection for fluid lines between the utility plates and the pump ORU, with a coolant reservoir, a pump for moving the ammonia through the system, and related control devices. The radiator consists of several large aluminum honeycomb matrix panels through which two coolant flow channels run delivering heat to the panels. The surface is coated with high emissivity, low absorptivity silver teflon and radiates this heat into space.

As seen in figure 8.1, the SSF design has two types of utility plates. On Utility Plate Type I, the dc-dc converter, direct current switching unit, Photovoltaic (PV) controller, and TCS pump ORUs are attached. For the lunar power backup system, the PV controller is obviously not necessary, and the dc-dc converter and direct current switching unit are combined with the Battery Charge/Dischare Units which are located along with the batteries on Utility Plate Type II. This leaves the pump ORU alone on its utility plate, which is not a very efficient use of space. For this reason, and since the entire TCS is being reduced in size, this utility plate is deleted from the system, and the pump unit is included in an enlarged version of what is called the Fluid Junction Box. The Type II Utility Plates are not altered for use in the lunar backup system and are henceforth referred to as Utility Plates (UP).

The Fluid Junction Box is altered from its standard configuration to include various components of the pump ORU. In addition to the fluid interconnect lines, valves, and manifolds, a downsized ammonia coolant reservoir , a pump sized to the new system and all related control equipment and electronics is incorporated into the lunar power backup system.

The radiator design is not altered to any great extent for use on the moon but is only be reduced in size by deleting panels not necessary to meet reduced heat rejection demands. Each of the space station radiators is designed to reject 9 kW under nominal charge/discharge conditions. Trickle charge maintenance requires significantly less thermal management than

this. This rejection capability keeps the ammonia coolant at 260 K while keeping the batteries and electrical components at or below 280 K as required for optimum battery operation.

Since a radiator on the Moon will be under gravitational conditions, a support post and cables may be necessary to keep the radiator supported. Additionally, some reflective shielding may be necessary to reduce the view factor between the sun and the radiator, and between the lunar surface and the radiator. The support structure and reflective shielding are not expected to add significantly to the system mass.

8.4 LUNAR EMERGENCY POWER BACKUP SYSTEM

For flexibility of the lunar base design, the emergency power backup system is designed in a modular fashion. A collection of relevant information on mass, power output, and size for the space station power storage system, compiled from Ref. 5 is presented in Table 8.3. From the information in Table 8.3, it is determined that a unit consisting of two batteries can supply 1.5 kW per person to two people for approximately 3.5 hours. This takes into account the parasitic power required by all of the electrical components as well as the power required by the astronauts. For the complete lunar power backup system, four of these two-person units are connected in parallel to provide backup for eight persons, the nominal number of occupants for the lunar power system in this report. The 1.5 kW power output is chosen based on information from Ref. 6. A time of 3.5 hours should be sufficient for personnel to evacuate the base, but adjustments may be necessary once lunar base systems operations are better defined.

Many of the components from the space station are designed to function as part of a larger unit, and therefore are reduced for use in the smaller lunar power backup system. For example, the space station Fluid Junction Box is designed to provide the coolant fluid interface between four utility plates whereas the lunar backup system only has two utility plates. In these cases, mass, parasitic power, and thermal dissipation requirements for the reduced

number of components are estimated by assuming that proportional cuts can be made in the existing equipment. In the Fluid Junction Box example, the mass of the new component is estimated to be half of the equivalent space station component's mass.

Table 8.3: SSF Energy Storage System Data.

Component	Mass (kg)	Parasitic Power (kW)	Energy (kWh)	Size (m)
Battery ORU	145.5	-	3	0.91 x 0.97 x 0.43
BCDU	76.0	0.14	-	0.71 x 0.97 x 0.30
Utility Plate	136.0	-	-	3.20 x 0.97 x 0.15
TCS Pump ORU	72.0	0.25	-	0.71 x 0.97 x 0.30
Fluid Junction Box	42.0	-	-	3.90 x 0.25 x 0.20
Radiator	598.0	-	-	3.60 x 2.00 x 13.7

The radiator from the SSF design is quite large, and is designed to reject 9kW under nominal space station operational conditions. Thermal dissipation requirements for the smaller lunar power backup are determined by summing up the dissipation requirements of the reduced components along with the expected thermal output of the batteries assuming an electrical efficiency of 84% in the batteries[2].

The resulting component characteristics for use in the lunar power backup system are presented in Table 8.4. It must be kept in mind that these values are only approximations based upon size reductions of a similar, but larger system. Figure 8.3 is a schematic diagram showing the configuration of the lunar backup power system after the revisions are made to the SSF system.

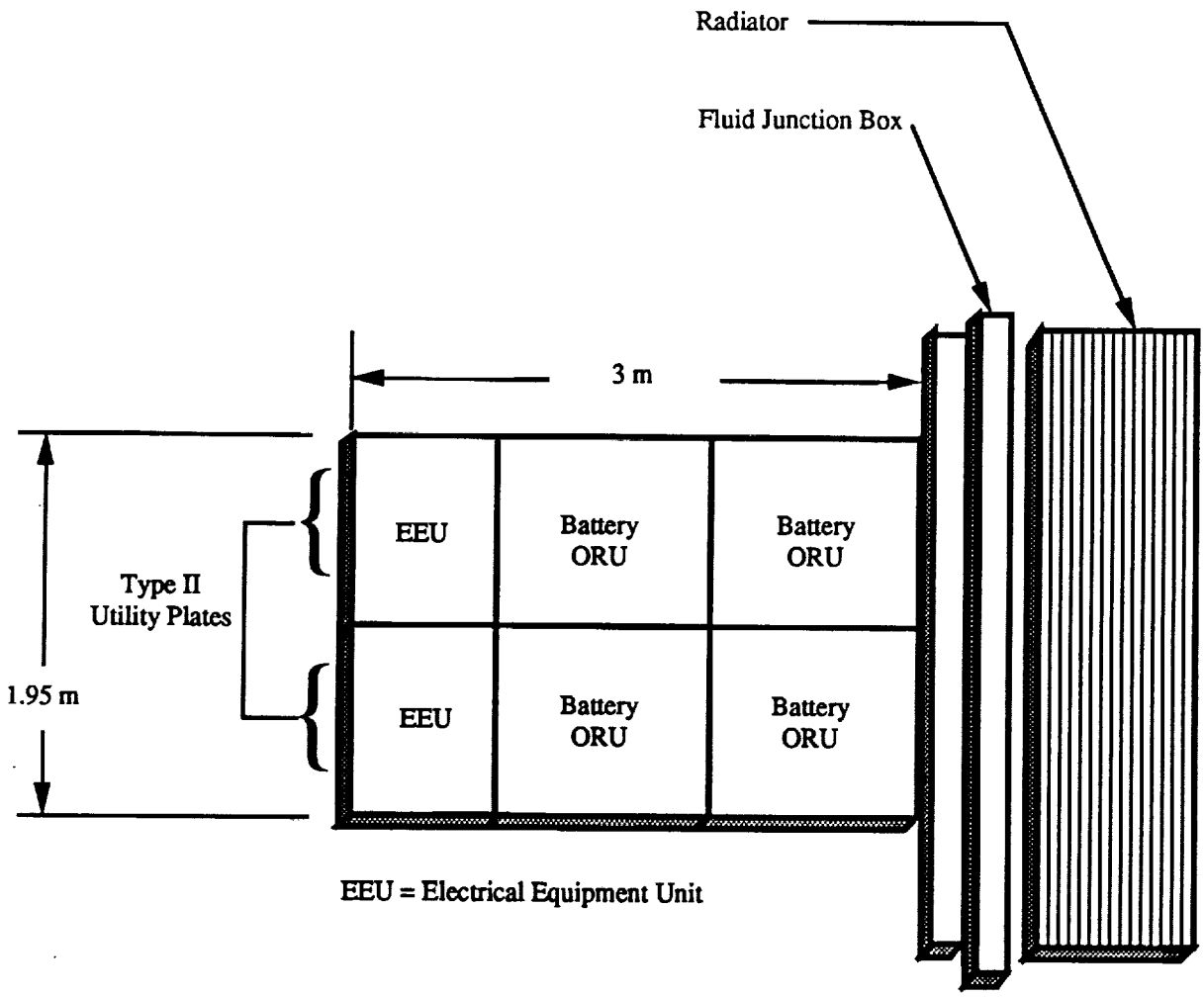

Fig. 8.3: Lunar Emergency Power System Configuration.

Table 8.4: Lunar Emergency Backup Power System Components.

Component	Mass (kg)	Parasitic Power (kW)	Energy (kWh)	Quantity
Battery ORU	145.5	-	3	4
EEU	76	0.140	-	2
Utility Plate	136	-	-	2
TCS Pump ORU	36	0.125	-	1
Fluid Junction Box	21	-	-	1
Radiator	125	-	-	1

8.5 CONCLUSION

In the event of a catastrophic failure of the main power system which has been designed in this report, a backup power system would necessarily have to be available to allow sufficient time for the base occupants to evacuate. Several methods of energy storage have been researched, with the final choice being a modified version of the nickel hydrogen energy storage system from the Space Station Freedom. The final system design is modular, which allows backup capability to be added in units which supply 1.5 kW per person for two base occupants for a duration of 3.5 hours. The mass of this system is quite large relative to the main power supply, an inherent problem with battery storage. Additionally, some of the benefits which were to be gained by using the SSF energy storage system no longer exist since so many modifications must be made in order to reduce mass. This backup power system is very reliable, but the cost in overall increased system mass may be too large to justify its use. As a recommendation for future studies, a rigorous probability analysis should be performed to determine exactly how much more reliable a battery system is than a fuel cell system, and perhaps redundant configurations of the fuel cell energy storage system from Section 5 of this report should be looked into in more detail.

8.6 REFERENCES

1. Kohout, L. L., "Cryogenic Reactant Storage for Lunar Base Regenerative Fuel Cells," NASA TM 011980, NASA Lewis Research Center, June 1989.

2. "Prospects for Advanced Storage Battery Technologies," SAND-84-0769C, Sandia National Labs., Albequerque, NM, Nov. 1984.

3. Subbarao, S., Halpert, G., and Stein, I., "Safety Considerations of Lithium-Thionyl Chloride Cells," NASA-CR-180129, Jet Propulsion Lab, Pasadena, CA, June 1986.

4. Beauchamp, R., and Sindorf, J., "Nickel Hydrogen Battery Development: Final Report," SAND-88-7100, Sandia National Labs., Albequerque, NM, Aug., 1988.

5. "Power System Description Document," RI/RD88-633, Rockwell International Corp., Rocketdyne Division, Canoga Park, CA, Feb. 1990.

6. Brandhorst, H., "Challenges for Future Space Power Systems," NASA-TM-102063, NASA Lewis Research Center, Cleveland, OH, Oct. 1989.

9.0 CONCLUSION

David Carlile
Matt Jardin

For each subsystem in this report, several competing ideas were examined in order to determine the best ones for use in a megawatt scale solar power generation system. The most ideal subsystems for this application were determined in a study of the various efficiency, practicality, and suitability tradeoffs between the different ideas.

In the area of solar photovoltaic power generating systems, the advanced new tandem GaAs/GaSb cell arrays are recommended over more conventional GaAs cells due to the higher power density exhibited by this type of cell, leading to a lower overall system.mass. In the comparison of solar dynamic power generation systems, the Brayton cycle was found to have several advantages over the Stirling cycle in this particular application. Brayton engines proved to be more compact, less complex, and better understood due to their wide use in terrestrial applications. Thermal management is a key issue for dynamic cycle systems, and will be provided to the Brayton cyle by the heat pipe radiator (HPR) system. The HPR system slightly outperformed the liquid droplet radiator (LDR) system also examined in this report, and HPR technology is better developed. The LDR may provide better performance values in microgravity environments some day, but some dust and gravity related problems arise when trying to adapt the LDR for use on the lunar surface.

From Table 9.1, a mass comparison of the preferred photovoltaic and dynamic power generation systems, the specific power of the photovoltaic array system is shown to be nearly four times greater than that of the Brayton cycle system studied in this report. An additional benefit of the photovoltaic array system is that it is largely passive with no moving parts except those involved in solar tracking. It also does not require a separate thermal control system, making it far less massive and complex than the Brayton cycle system. The only possible

drawback to using the photovoltaic arrays is that they require about 5 acres of land area on the lunar surface, although this is not an unreasonable amount of space. It is actually a very small amount of land when compared to the amount required by some nuclear systems, such as that presented in the 1986 University of Washington NASA/USRA report, which may render large sections of the lunar surface uninhabitable for centuries.

Table 9.1: Comparison of Solar Power Systems.

	Photovoltaic Arrays	Brayton Cycle
Photovoltaic Array Mass	9,150 kg	-
Structural Mass (PV)	10,150 kg	-
HPR Brayton Engines (5)	-	2985 kg
Solar Collector (5)	-	54,525 kg
Radiator (HPR) (5)	-	17,450 kg
Total Power Supplied	1,190 kW	1,250 kW
Total Specific Power	**61.7 W/kg**	**16.7 W/kg**

Obviously, the solar cells produce no power during the lunar night, and since energy storage systems for the lunar night are so incredibly massive when compared with daytime power systems, reducing the nighttime power output is highly recommended. In this system, 50 kW was chosen as the nominal nighttime power output in order to greatly reduce overall system mass while still providing enough power for essential operations as well as some scientific experimentation. This power storage will be provided by a state of the art alkaline fuel cell system using hydrogen and oxygen reactants. For large scale power storage, the standard fuel cell system turned out to be less massive than the advanced monolithic solid-oxide fuel cell system which was examined as an alternative. The monolithic cells had a higher energy density, but a lower round trip chemical to electric efficiency than the alkaline cells. This led to the interesting result that the monolithic cells may be a better choice for small scale

power systems (such as satellites), but for large scale energy storage, the alkaline system requires fewer reactants and is therefore less massive.

This nighttime power storage system will require the storage of large amounts of fuel cell reactants. It was shown that a large mass savings can be obtained by storing the reactants as cryogenic liquids rather than as gases even after consideration of the extra power and equipment needed to liquify the reactant gases. A further reduction in mass comes from the use of existing cryogenic tanks from a spent lunar excursion vehicle assumed already to be present on the moon. Although these innovations reduce the mass of the energy storage system considerably over conventional systems, the mass required to store enough energy to supply 50 kW of power for use during the lunar night is still nearly half of the mass required to supply 1 MW during the lunar day. This provides the reason behind nighttime power reduction as stated in this report, and suggests that careful scheduling of lunar operations may avoid this problem while reducing the overall system mass.

The nickel hydrogen energy storage system designed for Space Station Freedom (SSF) has been modified to provide emergency backup power for the lunar base. The choice was made based upon the idea that the modified SSF system will be extremely reliable, and can be developed at low cost. This system is quite massive, however, so the recommendation is to examine alternative systems which may provide much higher energy densities with close to the same degree of reliability as a battery system. One possible alternative is to configure the nighttime energy storage system in a more redundant fashion. This would greatly improve the power backup capability, and might approach the same degree of reliability as the nickel hydrogen battery system.

The final system configuration is comprised of a GaAs/GaSb photovoltaic array system providing 1 MW during the day, an alkaline fuel cell storage system with cryogenically stored reactants providing 50 kW during the night, power transmission equipment, and a nickel hydrogen emergency battery backup system capable of supplying 8 astronauts with 1.5 kW

each for up to 3.5 hours. The mass breakdown, as well as the total power system mass are given in Table 9.2.

Table 9.2: Final Power System Configuration Mass.

Subsystem	Mass (kg)
GaAs/GaSb Photovoltaic Power System	19,300
Energy Storage System	10,040
Power Transmission	950
Backup Power	4,760
TOTAL POWER SYSTEM MASS	**35,050**

The megawatt solar power system examined in this report demonstrates that with new advances in solar photovoltaic conversion cells, and in energy storage methods, solar power is feasible for use on the Moon. The main disadvantage to employing a solar power system is that energy needs to be stored for use during the lunar night which greatly increases overall system mass, but as mentioned above, clever operations planning may circumvent the need for continuous high power production. This is a mission planning problem, however, and was not discussed in detail in this report.

Due to the technological and political barriers to using nuclear power systems, the fact that a solar power system may provide similar power densities, if configured properly, makes it an attractive alternative. A system such as the one developed in this report could be utilized within the context of current plans for the resumption of manned flights to the Moon to provide a clean and non-hazardous power source for large scale lunar surface operations.

APPENDIX A: COMPOSITE MATERIALS

Composite materials are used for many of the support members in the structural designs in this study. All of these members are fabricated from AS4-3502 graphite/epoxy laminate. The motivation for this selection was based on the strength to mass ratio and extremely low coefficient of thermal expansion (CTE) of this material. Both the strength and CTE of this composite are markedly superior to those of aluminum alloys.

The layup of this material is the same for all uses referenced in this report. Fig. A1 shows the stiffness modulus vs. percentage of fibers in certain orientations. Based on the loads to be supported and the results shown in this figure, the following layup was chosen: 70% of the plies used consist of graphite tape and are arranged in the 0 degree orientation (meaning the axial direction of the member). The remaining 30% of the plies are made of graphite fabric and are oriented in the $\pm$ 45 degree direction. Each ply of this composite has a thickness of 0.015 cm and an areal mass of 0.229 kg/m^2. Young's Modulus for this layup is 8.62E10 N/m^2 [1].

Although graphite/epoxy has competitive properties, problems with composite materials can exist when used for space applications. Severe thermal stresses may be encountered as one side of a member is exposed to the sun and the other is shaded. This thermal cycling over long periods of use may cause the formation of microcracks in the composite. It has also been shown that composite materials' strength properties can degrade with long exposure to radiation if unprotected. In order to combat these effects, a protective coating is applied to all composite members. In a study conducted by Tompkins, et. al., [2] it was demonstrated that anodized aluminum foil has been found to protect against radiation while reducing the temperature gradients without a severe increase in weight penalty. Anodizing offers a wide range of absorptivity and emissivity and, therefore, a wide range of temperature extremes. Chromic acid anodized aluminum foil provides excellent adhesion to graphite/epoxy tubes and

exhibits stable optical properties when subjected to a simulated low earth orbit environment. Since a lunar based application would encounter similar extremes, with the exception of atomic oxygen exposure, these results may be applied to composites that will be used in structures on the moon. Because of the advanced state of development and ease of application of chromic acid anodized aluminum foil, it was selected for use on the structural members of the lunar power station.

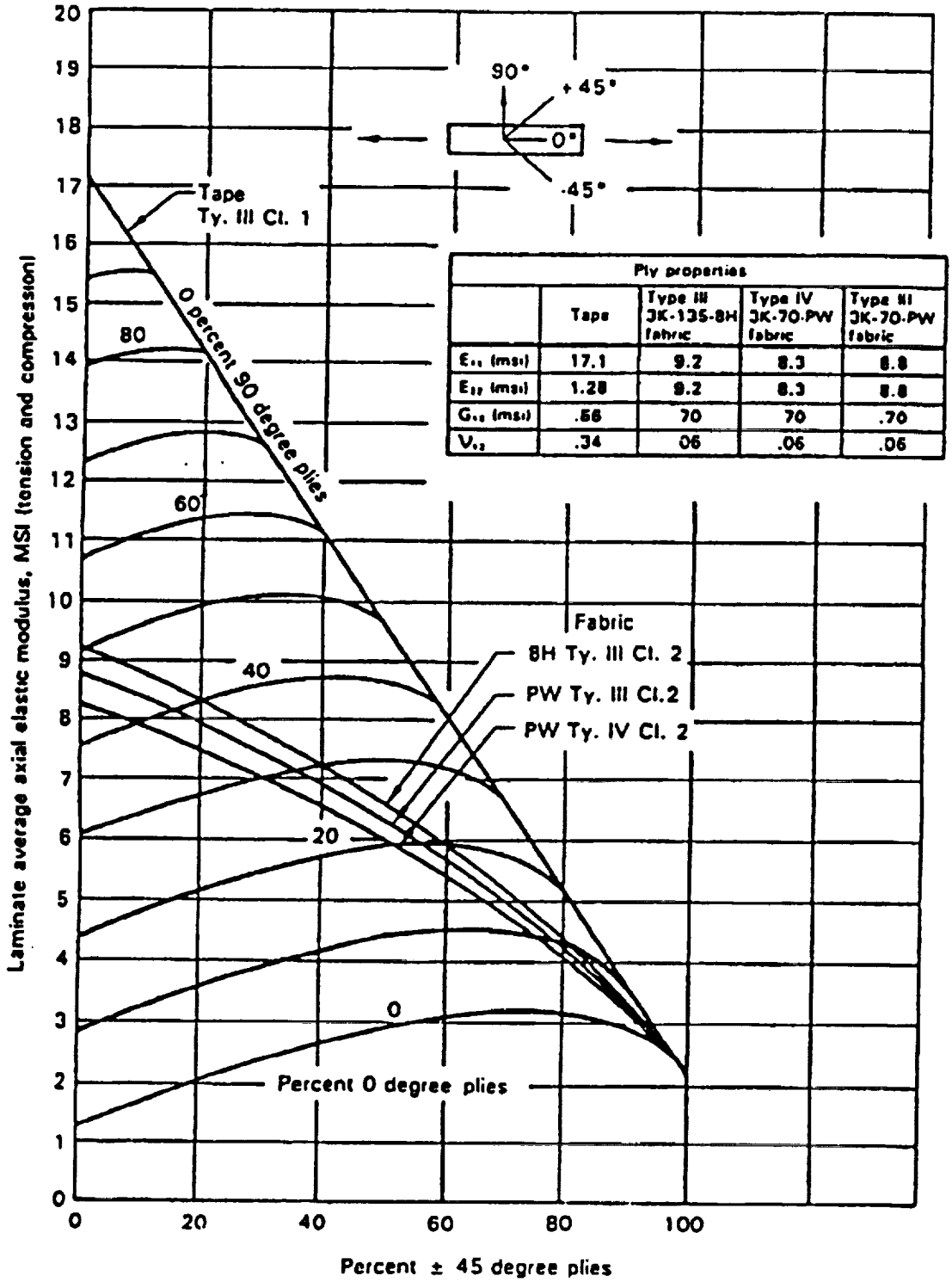

Fig. A.1: Average Axial Elastic Modulus [1].

A.1 REFERENCES

1. Advanced Design Handbook, Boeing Military Airplane Company, B-2 Division, 1988 (Rev. F), p. 3.1-5.

2. Tompkins, S.S., et. al., "Response Of Composite Materials To The Space Station Orbit Environment," Space Station Symposium AIAA (NASA), Williamsburg, VA, 1988.